

# **Climate change projections for the Northwest Atlantic from six CMIP5 Earth System Models**

John W. Loder and Augustine van der Baaren

Ocean and Ecosystem Sciences Division,  
Fisheries and Oceans Canada  
Bedford Institute of Oceanography  
P.O. Box 1006  
Dartmouth, Nova Scotia  
Canada B2Y 4A2

2013

**Canadian Technical Report of  
Hydrography and Ocean Sciences 286**



Fisheries and Oceans  
Canada

Pêches et Océans  
Canada

**Canada**

## **Canadian Technical Report of Hydrography and Ocean Sciences**

Technical reports contain scientific and technical information of a type that represents a contribution to existing knowledge but which is not normally found in the primary literature. The subject matter is generally related to programs and interests of the Oceans and Science sectors of Fisheries and Oceans Canada.

Technical reports may be cited as full publications. The correct citation appears above the abstract of each report. Each report is abstracted in the data base *Aquatic Sciences and Fisheries Abstracts*.

Technical reports are produced regionally but are numbered nationally. Requests for individual reports will be filled by the issuing establishment listed on the front cover and title page.

Regional and headquarters establishments of Ocean Science and Surveys ceased publication of their various report series as of December 1981. A complete listing of these publications and the last number issued under each title are published in the *Canadian Journal of Fisheries and Aquatic Sciences*, Volume 38: Index to Publications 1981. The current series began with Report Number 1 in January 1982.

## **Rapport technique canadien sur l'hydrographie et les sciences océaniques**

Les rapports techniques contiennent des renseignements scientifiques et techniques qui constituent une contribution aux connaissances actuelles mais que l'on ne trouve pas normalement dans les revues scientifiques. Le sujet est généralement rattaché aux programmes et intérêts des secteurs des Océans et des Sciences de Pêches et Océans Canada.

Les rapports techniques peuvent être cités comme des publications à part entière. Le titre exact figure au-dessus du résumé de chaque rapport. Les rapports techniques sont résumés dans la base de données *Résumés des sciences aquatiques et halieutiques*.

Les rapports techniques sont produits à l'échelon régional, mais numérotés à l'échelon national. Les demandes de rapports seront satisfaites par l'établissement auteur dont le nom figure sur la couverture et la page de titre.

Les établissements de l'ancien secteur des Sciences et Levés océaniques dans les régions et à l'administration centrale ont cessé de publier leurs diverses séries de rapports en décembre 1981. Vous trouverez dans l'index des publications du volume 38 du *Journal canadien des sciences halieutiques et aquatiques*, la liste de ces publications ainsi que le dernier numéro paru dans chaque catégorie. La nouvelle série a commencé avec la publication du rapport numéro 1 en janvier 1982.



**Canadian Technical Report of  
Hydrography and Ocean Sciences 286**

**2013**

**Climate change projections for the Northwest Atlantic from six CMIP5  
Earth System Models**

**by**

**John W. Loder and Augustine van der Baaren**

**Science Branch  
Maritimes Region  
Fisheries and Oceans Canada**

**Bedford Institute of Oceanography  
P. O. Box 1006  
Dartmouth, Nova Scotia  
Canada B2Y 4A2**

© Her Majesty the Queen in Right of Canada, 2013

Cat. No. Fs 97-18/286E    ISSN 0711-6764 (print version)

Cat. No. Fs 97-18/286E-PDF    ISSN 1488-5417 (on-line version)

Correct Citation for this publication:

Loder, J.W. and A. van der Baaren. 2013. Climate change projections for the Northwest Atlantic from six CMIP5 Earth System Models. Can. Tech.. Rep. Hydrogr. Ocean. Sci. 286: xiv + 112 p.

## TABLE OF CONTENTS

Table of Contents .....	iii
List of Figures .....	iv
List of Tables .....	xii
Abstract .....	xiii
Résumé.....	xiv
Section 1: Introduction.....	1
Section 2: Methodology .....	3
2a. Models, Simulations and Fields .....	3
2b. Comparison with Observations .....	6
2c. Projected Changes .....	8
Section 3: Surface Air Temperature (TAS) .....	11
3a. Comparison with Observations at Selected Meteorological Locations .....	11
3b. Spatial Distribution of Projected TAS Climate Changes in Six ESMs .....	14
3c. Temporal Variability of Projected TAS Climate Changes in ESMs.....	18
Section 4: Sea Ice Concentration (SIC) .....	23
4a. Comparison with Observed Spatial Distributions .....	23
4b. Spatial Distribution of Projected SIC Climate Changes in Six ESMs.....	25
Section 5: Surface Ocean Temperature (TOS) .....	31
5a. Comparison with Observed Spatial Distributions and Temporal Variability .....	31
5b. Spatial Distribution of Projected TOS Climate Changes in Six ESMs .....	37
5c. Temporal Variability of Projected TOS Climate Changes in ESMs.....	41
5d. Estimates of TOS Changes from Six ESMs at Representative Locations .....	46
Section 6: Surface Ocean Salinity (SOS).....	49
6a. Comparison with Observed Spatial Distributions and Temporal Variability .....	49
6b. Spatial Distribution of Projected SOS Climate Changes in Six ESMs.....	54
6c. Temporal Variability of Projected SOS Climate Changes in ESMs.....	58
Section 7: Cross-Basin Structure of Ocean Temperature and Salinity .....	63
7a. Comparison with Observations .....	63
7b. Projected Climate Changes .....	65
Section 8: Ocean Mixed Layer Depth (OML-max).....	69
Section 9: Sea Surface Height (SSH).....	71
Section 10: Summary, Discussion and Conclusions .....	75
Acknowledgements.....	79
References .....	80

## **TABLE OF CONTENTS (continued)**

Appendix A: Additional Displays of Surface Air Temperature (TAS) .....	87
Appendix B: Additional Displays of Sea Ice Concentration (SIC) .....	93
Appendix C: Additional Displays of Surface Ocean Temperature (TOS) .....	94
Appendix D: Additional Displays of Surface Ocean Salinity (SOS) .....	99
Appendix E: Additional Displays of Subsurface Ocean Temperature and Salinity .....	104
Appendix F: Additional Displays of Sea Surface Height (SSH) .....	111

## LIST OF FIGURES

<b>Figure 2-1</b> The uniform 2°x2° grid to which the 2-d (horizontal) data fields from the six ESMs were interpolated and provided by J. Christian of DFO-IOS. ....	4
<b>Figure 2-2</b> Map showing locations of the three sections (Baffin Bay; AR7W or LSSS across the Labrador Shelf/Slope/Sea; and AtlNW or SSSR across the Scotian Shelf/Slope/Rise) used for displays of subsurface temperature and salinity (blue lines); the five model sites where temporal variability in TOS and SOS is examined (red squares); and the two coastal observation sites (Prince 5 or P5, and Station 27 or S27; green dots) that are not co-located with the model sites. ....	5
<b>Figure 2-3</b> Map showing locations of the meteorological observation sites where temporal variability in TAS is examined. ....	7
<b>Figure 2-4</b> Maps showing “Off-Shelf” (or “Offshore”; left) and “Shelf” (right) sites at which projected TOS changes are presented in Section 5d. ....	9
<b>Figure 3-1</b> Annual cycles of the bi-decadal monthly means of TAS for 1986-2005 at six sites from observations (AHCCD; red) and from CanESM2 (run 1, and ensemble mean of five runs) and GFDL-ESM2M (run 1) (see Fig. 2-3 for locations). The error bars on each side of the observational means indicate the standard deviations of the individual-year means about the bi-decadal means. ....	11
<b>Figure 3-2a</b> Annual cycles of the bi-decadal monthly means of TAS for 1986-2005 at six sites from observations (AHCCD; red) and from interpolated data for run 1 of all six ESMs (see Fig. 2-3 for locations). ....	12
<b>Figure 3-2b</b> Annual cycles of the bi-decadal monthly TAS means for 1986-2005 at six sites from observations (AHCCD; red), and of the ensemble-mean bi-decadal monthly values from the six ESMs (Fig. 3-2a) with the inter-model standard deviations indicated by the error bars on each side of the ensemble means. ....	12
<b>Figure 3-3</b> Time series of observed (AHCCD) and model annual means of TAS for CanESM2 (ensemble mean and run 1) and GFDL (run 1) for 1950-2005 at six sites (see Fig. 2-3 for locations). ....	14
<b>Figure 3-4</b> Climate changes in bi-decadal TAS for Canada from 1986-2005 to 2046-2065 from six ESMs for RCP8.5 in a) February and b) August. Data interpolated to the common grid were used. ....	15
<b>Figure 3-5</b> Mean, standard deviation, and spread of climate changes in bi-decadal TAS between 1986-2005 and 2046-2065 from RCP4.5 and RCP8.5 in a) February and b) August, computed from the ensemble of six ESMs using interpolated data (Fig. 3-4). The white contours are the 0, 5 and 10°C isotherms. ....	17
<b>Figure 3-6</b> Ensemble mean of the changes in bi-decadal mean TAS from 1986-2005 to 2046-2065 for RCP8.5, from six ESMs for twelve months: a) January – June and b) July – December. ....	18
<b>Figure 3-7</b> Ensemble-mean model annual cycles of bi-decadal monthly TAS at nine stations for 1986-2005 (Historical) and 2046-2065 (RCP4.5 and RCP8.5), from run 1 from six ESMs	

using interpolated data (see Fig. 2-3 for locations). The inter-model standard deviations are indicated by the error bars.....	19
<b>Figure 3-8a</b> Climate changes in bi-decadal monthly TAS means from 1986-2005 to 2046-2065 for RCP8.5 at the same nine locations as in Figure 3-7, for each of the six ESMs using interpolated data. ....	20
<b>Figure 3-8b</b> Ensemble means, and inter-model standard deviations, of the climate changes in bi-decadal monthly TAS means shown in Figure 3-8a. ....	20
<b>Figure 3-9</b> Time series plots of annual means of TAS from the CanESM2 ensemble mean of five runs and from GFDL-ESM2M run 1 for RCP4.5 and RCP8.5 for 2006-2100, for the same nine locations as in Figures 3-7 and 3-8. ....	22
<b>Figure 4-1</b> Comparison of SIC in a) March and b) September from interpolated data from the Historical simulation of each of six ESMs, the ensemble mean of the data from the six ESMs, and the HadISST1 dataset for the NWA and Eastern Arctic for 1986-2005. The differences in the apparent land areas (white, except for northeast corner) in the different models partly reflect their native grids but are also affected by the 2°x2° common interpolation grid.....	24
<b>Figure 4-2</b> Bi-decadal mean SIC distributions in February for a) 1986-2005 from the Historical simulations, and b) 2046-2065 from the RCP8.5 simulations from the six ESMs. Data interpolated to the common 2°x2° grid (Fig. 2-1) were used. The differences in the apparent land areas (white, except for northeast corner) in the different models reflect a combination of their native grids and the interpolation grid.....	26
<b>Figure 4-3</b> Bi-decadal mean SIC distributions in May for a) 1986-2005 from the Historical simulations, and b) 2046-2065 from the RCP8.5 simulations from the six ESMs (see Fig. 4-2 for details). ....	27
<b>Figure 4-4</b> Climate changes in bi-decadal monthly mean SIC from 1986-2005 in the Historical simulations to 2046-2065 in the RCP8.5 simulations from the six ESMs for a) February and b) May (see Fig. 4-2 for details). ....	28
<b>Figure 4-5</b> Ensemble mean bi-decadal monthly SIC for January (left), March (middle) and May (right) for 1986-2005 from Historical simulations (upper) and 2046-2065 from the RCP8.5 simulations (lower), from the six ESMs using interpolated data.....	29
<b>Figure 4-6</b> Ensemble-mean climate change in bi-decadal monthly SIC (percentage) for January (left), March (middle) and May (right) for RCP4.5 (upper) and RCP8.5 (lower), using interpolated data.....	30
<b>Figure 5-1</b> Observed surface temperature climatologies for 1946-2005 (top right panels; from I. Yashayaev) and TOS fields (interpolated to a common grid) for the NWA from the Historical simulations (1986-2005) from the six ESMs in a) February and b) August. ....	32
<b>Figure 5-2</b> Model and observed annual cycles of TOS for 1986-2005 at four DFO observational sites: Labrador Sea (Bravo), Grand Bank (Station 27), Gulf of Maine (Prince 5) and Scotian Shelf (Emerald Basin) (see Fig. 2-2 for locations). Model cycles are shown for run 1 and the ensemble mean from CanESM2, and for run 1 from GFDL-ESM. ....	34

<b>Figure 5-3a</b> Model and observed annual cycles of TOS for 1986-2005 at the same four sites as in Figure 5-2. Model cycles (based on interpolated data) are shown for each of the six ESMs.....	35
<b>Figure 5-3b</b> Ensemble-mean model (over the six ESMs) and observed annual cycles of TOS for 1986-2005 at same four sites as in Figure 5-2. The inter-model standard deviations are indicated by the error bars on each side of the ensemble means. ....	35
<b>Figure 5-4</b> Comparison of model annual mean time series of TOS at four sites with observations for 1950-2012. Model data are for run 1 from GFDL-ESM and five runs from CanESM2, for the concatenated Historical and RCP8.5 simulations. Observed time series are for the ocean surface at three sites, but for the 16-150m interval at Bravo. The long-term annual-mean surface temperature at Bravo is $\sim 1^{\circ}\text{C}$ higher than that over the 16-150m interval, so the actual observed TOS values are generally intermediate between those from CanESM2 and GFDL-ESM2M in Figure 5-2. ....	36
<b>Figure 5-5</b> Bi-decadal monthly TOS change fields from 1986-2005 to 2046-2065 for the NWA for RCP8.5 from interpolated data from the six ESMs for a) February and b) August. The white contour is the $0^{\circ}\text{C}$ isotherm. ....	38
<b>Figure 5-6</b> Mean, standard deviation, and spread of bi-decadal TOS changes for the NWA for RCP4.5 and RCP8.5 in a) February and b) August, computed from the ensemble mean change of the six ESMs (e.g. Fig. 5-5 for RCP8.5). The white contour in the “mean” panels is the $0^{\circ}\text{C}$ isotherm. ....	39
<b>Figure 5-7</b> Changes in bi-decadal monthly TOS from 1986-2005 to 2046-2065 for the NWA, from the ensemble mean of interpolated data from the six ESMs for RCP8.5, for the twelve months of the year.....	40
<b>Figure 5-8a</b> Annual cycles of TOS for Historical (1986-2005) and RCP8.5 (2046-2065) at four sites (Bravo, GB, Gulf of St. Lawrence or GSL, and SS) for the CanESM2 ensemble-mean of all runs and GFDL-ESM2M run 1 (see Fig. 2-2 for locations). ....	42
<b>Figure 5-8b</b> Changes in bi-decadal monthly mean TOS from 1986-2005 (Historical) to 2046-2065 (RCP8.5) at the four sites in Figure 5-8 for five runs of CanESM2 and run 1 of GFDL-ESM2M. ....	42
<b>Figure 5-9a</b> Ensemble-mean annual cycles (with standard deviations) of TOS from the Historical simulations for 1986-2005, and from the RCP4.5 and RCP8.5 simulations for 2046-2065, at nine sites for the ensemble of six ESMs. Five of the sites are the same as in Figures 5-2 or 5-8, while the locations of the other sites are shown in Figure 2-4. ....	43
<b>Figure 5-9b</b> Changes in bi-decadal monthly mean TOS from 1986-2005 (Historical) to 2046-2065 (RCP8.5) at the nine sites in Figure 5-9a, in run 1 from the six ESMs. ....	44
<b>Figure 5-9c</b> Ensemble means, and inter-model standard deviations, of the climate changes in bi-decadal monthly mean TOS shown in Figure 5-9b. ....	44
<b>Figure 5-10</b> Time series of annual means of TOS from CanESM2 (five runs) and GFDL-ESM2M (run 1) for 1950-2100 at the same four sites as in Figure 5-4 (Bravo, GB, SS and GoM).....	45

- Figure 6-1** Comparison of observed surface salinity climatologies for 1946-2005 (top right panels; from I. Yashayaev) with interpolated SOS fields for 1986-2005 from the Historical simulations from the six ESMs in a) February and b) August.....50
- Figure 6-2** Model (two ESMs) and observed annual cycles of SOS for 1986-2005 at the same four sites (Bravo, GB, SS and GoM) as in Section 5a (see Fig. 2-2 for locations). Model cycles are shown for run 1 and the ensemble mean from CanESM2, and for run 1 from GFDL-ESM2M. ....51
- Figure 6-3a** Model (six ESMs) and observed annual cycles of SOS for 1985-2005 at the same four sites (Bravo, GB, SS and GoM) as in Figure 6-2. Model cycles are shown for each of the six ESMs, using interpolated data.....52
- Figure 6-3b** Ensemble-mean model (over the six ESMs in Fig. 6-3a) and observed annual cycles of SOS for 1986-2005 at the same sites as in Figure 6-2. The inter-model standard deviations are indicated by the error bars on each side of the ensemble means.....52
- Figure 6-4** Comparison of model annual mean time series of SOS at four sites with observations for 1950-2012 (see Fig. 2-2 for locations). Model data are for run 1 from GFDL-ESM2M and five runs from CanESM2, from the concatenated Historical and RCP8.5 simulations. Observed time series are for the ocean surface at three sites, but for the 16-150m interval at Bravo.....53
- Figure 6-5** Bi-decadal monthly SOS climate change fields from 1986-2005 to 2046-2065 for the NWA for RCP8.5 for a) February and b) August, using interpolated data from the six ESMs. The white contour is the 0 psu isohaline.....55
- Figure 6-6** Mean, standard deviation, and spread of climate changes in bi-decadal SOS from 1986-2005 to 2046-06 for RCP4.5 and RCP8.5 in a) February and b) August, computed from the ensemble of the changes from the six ESMs (Fig. 6-5). The white contour is the 0 psu isohaline.....56
- Figure 6-7** Changes in bi-decadal monthly SOS from 1986-2005 to 2046-2065 for RCP8.5 for the twelve months of the year, from the ensemble mean of the change fields from interpolated data from the six ESMs.....57
- Figure 6-8a** Annual cycles for Historical (1986-2005) and RCP8.5 (2046-2065) at four sites (Bravo, GB, GSL and SS) for the CanESM2 ensemble-mean of all runs and GFDL-ESM2M run 1 (see Fig. 2-2 for locations).....58
- Figure 6-8b** Changes in bi-decadal monthly mean SOS from 1986-2005 (Historical) to 2046-2065 (RCP8.5) at the four sites in Figure 6-8a for five runs of CanESM2 and 1 run of GFDL-ESM2M.....59
- Figure 6-9a** Ensemble-mean annual cycles (with standard deviations) of SOS from the Historical simulations for 1986-2005, and from the RCP4.5 and RCP8.5 simulations for 2046-2065, at nine sites for the ensemble of the six ESMs. Five of the sites are the same as in Figures 6-2 or 6-8, while the locations of the other sites are shown in Figure 2-4.....60
- Figure 6-9b** Changes in bi-decadal monthly mean SOS from 1986-2005 (Historical) to 2046-2065 (RCP4.5) at the nine sites in Figure 9-6a, in run 1 from 6 ESMs.....60



<b>Figure 6-9c</b> Ensemble means, and inter-model standard deviations, of the climate changes in bi-decadal monthly mean SOS shown in Figure 6-9b.....	61
<b>Figure 6-10</b> Time series of annual means of SOS from CanESM2 (five runs) and GFDL-ESM2M (run 1) for 1950-2100 at the same four sites as in Figure 6-4 (Bravo, GB, SS and GoM).....	62
<b>Figure 7-1</b> Comparison of decadal mean (1996-2005) ocean temperature across the LSSS section from five ESMs, with observations from the AR7W line (courtesy of I. Yashayaev). .....	64
<b>Figure 7-2</b> Comparison of decadal mean (1996-2005) ocean salinity across the LSSS section from five ESMs, with observations on the AR7W line (courtesy of I. Yashayaev). .....	64
<b>Figure 7-3</b> Changes in bi-decadal mean potential temperature from 1986-2005 in the Historical simulations to 2046-2065 in the RCP8.5 simulations of five ESMs, on sections across a) Baffin Bay, b) the LSSS and c) the SSSR (NW Atlantic). .....	65, 66
<b>Figure 7-4</b> Changes in bi-decadal mean salinity from 1986-2005 in the Historical simulations to 2046-2065 in the RCP8.5 simulations of five ESMs, on sections across the a) Baffin Bay, b) the LSSS and c) the SSSR (NW Atlantic). .....	67, 68
<b>Figure 8-1</b> Bi-decadal mean fields of OML-max in February from four ESMs for a) 1986-2005 from their Historical simulations and b) 2046-2065 from their RCP8.5 simulations.....	69
<b>Figure 8-2</b> Projected change in bi-decadal mean OML-max in February from four ESMs from 1986-2005 (Historical simulations) to 2046-2065 (RCP8.5 simulations). .....	70
<b>Figure 9-1</b> Bi-decadal monthly mean adjusted SSH (zos + zosga) for Canada for a) February and b) August, from CanESM2 and GFDL-ESM2M for 1986-2005 from their Historical simulations (left panels) and for 2046-2065 from their RCP8.5 simulations (right panels). ..	72
<b>Figure 9-2</b> Changes in bi-decadal mean adjusted SSH (zos + zosga) for Canada for February (left) and August (right) from CanESM2 (upper) and GFDL-ESM2M (lower), from 1986-2005 using the models' Historical simulations to 2046-2065 using their RCP8.5 simulations. ....	73
<b>Figure 9-3</b> Changes in bi-decadal mean adjusted SSH (zos + zosga) from 1986-2005 to 2046-2065 in February (left) and August (right), for the NWA from CanESM2 (upper row) and GFDL-ESM2M (lower row), for a) RCP4.5 and b) RCP8.5. ....	74
<b>Figure A-1</b> Annual cycles computed from bi-decadal monthly means for TAS from Historical (1986-2005; row 1) and RCP8.5 (2046-2065; row 2) data for Mont-Joli, St. John's and Bravo, for five runs from CanESM2 and run 1 from GFDL-ESM2M (see Fig. 2-3 for site locations). .....	87
<b>Figure A-2</b> Time series of annual means of TAS for Historical and RCP8.5 data for 1900-2100 at the same three sites as in Figure A-1, for five runs of CanESM2 and run 1 of GFDL-ESM2M. ....	88
<b>Figure A-3</b> Bi-decadal February TAS means for Canada using interpolated data from six ESMs, for a) 1986-2005 from their Historical simulations and b) 2046-2065 from their simulations for RCP8.5. ....	89

<b>Figure A-4</b> Bi-decadal August TAS means for Canada using interpolated data from six ESMs, for a) 1986-2005 from their Historical simulations and b) 2046-2065 from their simulations for RCP8.5. ....	90
<b>Figure A-5</b> Minimum (left), mean (middle), and maximum (right) TAS <u>changes</u> for Canada from 1986-2005 to 2046-2065 in a) February and b) August, from the ensemble of six ESMs for each of RCP4.5 and RCP8.5. The white contours are the 0, 5 and 10 °C isotherms. ....	91
<b>Figure A-6</b> Bi-decadal annual cycles of TAS at the same nine stations as in Figure 3-7, for Historical (1986-2005) and RCP8.5 (2046-2065) from the CanESM2 ensemble of five runs and from run 1 of GFDL-ESM2M (see Fig. 2-3 for locations). ....	92
<b>Figure A-7</b> Annual cycle of climate changes in bi-decadal monthly TAS from 1986-2005 to 2046-2065 at the same nine locations as in Figure 3-6, for five runs of CanESM2 and 1 run of GFDL-ESM2M for RCP8.5. ....	92
<b>Figure B-1</b> Bi-decadal mean SIC in a) January and b) May for 1986-2005, from the Historical simulations with the six ESMs, the observational HadISST1 dataset (upper right panels), and the ensemble mean of the ESMs (lower right panels). ....	93
<b>Figure C-1</b> Bi-decadal mean TOS for the NWA in a) February and b) August in 2046-2065 from the six ESMs for RCP8.5, using data interpolated to the common grid. ....	95
<b>Figure C-2</b> Climate changes in bi-decadal mean TOS in a) February and b) August from 1986-2005 to 2046-2065 for the waters surrounding Canada from the six ESMs for RCP8.5, using data interpolated to the common grid. ....	96
<b>Figure C-3</b> Statistics (ensemble mean, standard deviation, and spread) of climate changes in bi-decadal mean TOS from 1986-2005 to 2046-2065 for the waters surrounding Canada in a) February and b) August, for RCP4.5 (upper rows) and RCP8.5 (lower rows) using interpolated data from the six ESMs. ....	97
<b>Figure C-4</b> Statistics (ensemble minimum, mean and maximum) of climate changes in bi-decadal monthly TOS from 1986-2005 to 2046-2065 for the NWA in a) February and b) August, for RCP4.5 (upper rows) and RCP8.5 (lower rows) using interpolated data from the six ESMs. The white contours are the -2, -1, 0, +1 and +2 °C isotherms. ....	98
<b>Figure D-1</b> Bi-decadal mean SOS for the NWA in a) February and b) August in 2046-2065 from the six ESMs for RCP8.5, using data interpolated to the common grid. ....	100
<b>Figure D-2</b> Climate changes in bi-decadal mean SOS in a) February and b) August from 1986-2005 to 2046-2065 for the waters surrounding Canada for RCP8.5, using interpolated data from the six ESMs. ....	101
<b>Figure D-3</b> Statistics (ensemble mean, standard deviation, and spread) of climate changes in bi-decadal mean SOS from 1986-2005 to 2046-2065 for the waters surrounding Canada in a) February and b) August, for RCP4.5 (upper rows) and RCP8.5 (lower rows) using interpolated data from the six ESMs. ....	102
<b>Figure D-4</b> Statistics (ensemble minimum, mean and maximum) of climate changes in bi-decadal monthly SOS from 1986-2005 to 2046-2065 for the NWA in a) February and b)	

August, for RCP4.5 (upper rows) and RCP8.5 (lower rows) using interpolated data from the six ESMs. The white contours are the -1, 0 and +1 isohalines..	103
<b>Figure E-1</b> Bi-decadal mean temperature across the Baffin Bay section from five AR5 models for a) 1986-2005 from their Historical simulations and b) 2046-2065 from their RCP8.5 simulations.	105
<b>Figure E-2</b> Bi-decadal mean temperature across the LSSS section from five AR5 models for a) 1986-2005 from their Historical simulations and b) 2046-2065 from their RCP8.5 simulations.	106
<b>Figure E-3</b> Bi-decadal mean temperature across the SSSR section from five AR5 models for a) 1986-2005 from their Historical simulations and b) 2046-2065 from their RCP8.5 simulations.	107
<b>Figure E-4</b> Bi-decadal mean salinity across the Baffin Bay section from five AR5 models for a) 1986-2005 from their Historical simulations and b) 2046-2065 from their RCP8.5 simulations.	108
<b>Figure E-5</b> Bi-decadal mean salinity across the LSSS section from five AR5 models for a) 1986-2005 from their Historical simulations and b) 2046-2065 from their RCP8.5 simulations.	109
<b>Figure E-6</b> Bi-decadal mean salinity across the SSSR section from five AR5 models for a) 1986-2005 from their Historical simulations and b) 2046-2065 from their RCP8.5 simulations.	110
<b>Figure F-1:</b> Bi-decadal monthly mean zos in the NWA from CanESM2 (top row) and GDFL-ESM2M (bottom row) for 1986-2005 from their Historical simulations and 2046-2065 from their RCP8.5 simulations for a) February and b) August.	111
<b>Figure F-2</b> Climate changes in bi-decadal monthly zos in the NWA from CanESM2 (top row) and GDFL-ESM2M (bottom row) from Historical 1986-2005 to RCP8.5 2046-2065 simulation data, for February (left column) and August (right column)..	112

## LIST OF TABLES

<b>Table 5-1a</b> “Shelf” sites in the Atlantic LAB with statistics of the projected surface temperature changes between 1986-2005 and 2046-2065 from the six AR5 ESMs and two RCPs (12-model ensemble) for each of February and August. Changes at the sites have been estimated from bilinear interpolation from adjacent grid points. The spread is the difference between the minimum value for RCP4.5 and the maximum value for RCP8.5 (it should be noted that, in a few cases, the actual spread is greater than given here since the minimum change can occur in an RCP8.5 member or the maximum in an RCP4.5 member). See Figure 2-4 for site locations .....	47
<b>Table 5-1b</b> “Off-Shelf” sites in the Atlantic LAB with same statistics as in Table 5-1a. See Figure 2-4 for site locations .....	47

## **Abstract**

Loder, J.W. and A. van der Baaren. 2013. Climate change projections for the Northwest Atlantic from six CMIP5 Earth System Models. *Can. Tech.. Rep. Hydrogr. Ocean. Sci.* 286: xiv + 112 p.

Selected variables for the Northwest Atlantic Large Aquatic Basin (LAB) are examined in the Historical and future (RCP4.5 and RCP8.5) simulations of six Earth System Models (ESMs) being considered in Phase 5 of the Climate Model Intercomparison Project (CMIP5). The variables are air temperature, sea ice concentration, surface and subsurface ocean temperature and salinity, ocean mixed layer depth, and sea surface height. Comparison of the Historical simulations with observational data indicates that the models provide a good qualitative representation of most of the large-scale climatological atmospheric and ocean features in the NW Atlantic LAB (e.g. annual cycles and spatial gradients). However, the models have a poor representation of the detailed structure of some important ocean and ice features, such that caution needs to be used in the application of their projected future changes. Monthly “climate change” fields between the bi-decades 1986-2005 and 2046-2065 are described, using ensemble statistics of the changes across the six ESMs. The results point to warmer air temperatures everywhere and surface ocean temperatures in most areas, reduced sea ice extent and, in most areas, reduced surface salinities and mixed layer depths, and increased sea surface height. However, the magnitudes of the inter-model differences in the projected changes are comparable to those of the ensemble-mean changes in many cases, such that robust quantitative projections are generally not possible.

## Résumé

Loder, J.W. et A. van der Baaren. 2013. Climate change projections for the Northwest Atlantic from six CMIP5 Earth System Models. *Rapp. tech. can. hydrogr. sci. océan.* 286: xiv + 112 p.

Des variables précises propres au Grand bassin aquatique du nord-ouest de l'Atlantique sont examinées à l'aide des résultats historiques et des prévisions obtenus (profils représentatifs d'évolution de concentration [RCP] RCP 4,5 et RCP 8,5) par simulations de modèles du système terrestre exécutées selon la phase 5 du projet de comparaison de modèles climatiques (CMIP5). Les variables sont les suivantes : la température de l'air, la concentration de la glace de mer, la température et la salinité à la surface et sous la surface de l'océan, la profondeur de la couche de mélange océanique et la hauteur de la surface de la mer. Les données du modèle issues de simulations historiques offrent une bonne représentation qualitative de la plupart des caractéristiques climatologiques à grande échelle de ces variables dans la région (p. ex. les cycles annuels et les gradients spatiaux); cela dit, elles représentent mal la structure détaillée de certaines caractéristiques importantes de l'océan et de la glace. Par conséquent, l'application des prévisions de changements climatiques doit être effectuée avec circonspection. Les différences entre les périodes de 20 ans qui s'étendent de 1986 à 2005 et de 2046 à 2065 offrent des indications grossières des changements climatiques prévus selon les variables examinées sur une échelle temporelle d'un demi-siècle. En général, les statistiques propres aux changements tendent à indiquer des températures de l'air plus chaudes à l'échelle globale, une réduction de l'étendue de la glace de mer et, dans la plupart des régions, des températures océaniques plus chaudes à la surface, une réduction des salinités à la surface, une réduction des profondeurs des couches de mélange et une augmentation de la hauteur de la surface de la mer. Dans bon nombre de cas, l'ampleur des différences entre les modèles en ce qui concerne les changements prévus est toutefois comparable à celle des changements généraux moyens; il est donc impossible d'établir des prévisions quantitatives certaines.

## Section 1 Introduction

As part of its Aquatic Climate Change Adaptation Services Program (ACCASP), Fisheries and Oceans Canada (DFO) is conducting assessments of climate change impacts and risks on biological systems and infrastructure within its mandate, specifically for four Large Aquatic Basins (LABs). Scientific reviews of climate change trends and projections, and of associated impacts, vulnerabilities and opportunities, are being prepared for each LAB, drawing on the growing climate change science literature including focussed DFO studies for the LABs.

For the Atlantic LAB, a Canadian Science Advisory Secretariat (CSAS) Special Response Process is being carried out (DFO 2013a) and a summary technical report on observed trends and future projections (Loder et al. 2013) is being prepared. The trends and projections (T&P) summary report is drawing on input from a number of more detailed scientific reports on particular aspects of climate change related to the Atlantic LAB. The present report is one of these, intended to be used in conjunction with other climate change information from the Northwest (NW) Atlantic. It also provides input on the Baffin Bay region to the CSAS assessment (DFO 2013b) and T&P summary report (Steiner et al. 2013) for the Arctic LAB.

The Fourth Assessment Report (AR4; Solomon et al. 2007) of the Intergovernmental Panel on Climate Change (IPCC), together with supporting and follow-up assessments and studies, provides a broad foundation for future climate change projections, particularly on large scales. However, a new wave of assessments and studies based on updated observations and new knowledge and models is now appearing in the literature. These more recent studies provide the basis for the upcoming Fifth Assessment Report (AR5) of the IPCC, planned for release in late 2013. Climate change projections in AR5 are expected to rely more heavily on climate models available through Phase 5 of the Coupled Model Intercomparison Project (CMIP5, <http://cmip-pcmdi.llnl.gov/cmip5/>; Taylor et al. 2012) of the World Climate Research Programme, than on those from CMIP3<sup>1</sup> used in AR4 and subsequent regional climate modelling. Hence, the primary purpose of our report is to carry out an initial examination of the CMIP5 simulations and projections for key variables relevant to the Atlantic LAB in particular, for consideration in the Atlantic T&P summary report. Focus is on the “50-Year” time scale of interest to ACCASP (DFO 2013a) using the “long-term” simulations that are available from CMIP5, since the CMIP5 “near-term” simulations (that would be appropriate for the ACCASP “Decadal” time scale) are considered to be more exploratory (Taylor et al. 2012) and their analysis is much less advanced.

While comprehensive evaluations of the CMIP5 models have been underway for some time, and some papers have appeared in the literature (e.g. Andrews et al. 2012; Cheng et al. 2013; Diffenbaugh and Giorgi 2012; Harvey et al. 2012; Mizuta 2012; Sillmann et al. 2013a,b; Stroeve et al. 2012; Wang and Overland 2012; Yin 2012) with many others being submitted, studies with rigorous evaluations of these models are generally not yet available. A pragmatic approach has been adopted in this study, involving the use of readily-available fields from a subset of the more advanced models from some of the world’s premier climate modelling centres. Specifically, we used data from six Earth System Models (ESMs) which have a more sophisticated atmosphere-

---

<sup>1</sup> CMIP3 refers to Phase 3 of the Climate Model Intercomparison Project of the Program for Climate Model Diagnosis and Intercomparison (PCMDI; [http://www-pcmdi.llnl.gov/ipcc/about\\_ipcc.php](http://www-pcmdi.llnl.gov/ipcc/about_ipcc.php)). CMIP5 refers to Phase 5.

ocean-terrestrial carbon cycle than the Atmosphere-Ocean General Circulation Models (AOGCMs) used in CMIP3 and by many groups in CMIP5. Interpolated (to a common grid) and averaged fields for the horizontal distributions of key variables from these six AR5 ESMs were generously provided by James Christian of DFO's Institute of Ocean Sciences (IOS) who has co-lead the preparation of the T&P summary report for the Pacific LAB (Christian and Foreman 2013), which used these same interpolated fields. Other fields were generously provided by Diane Lavoie of DFO's Maurice Lamontagne Institute (MLI) who has led the preparation of complementary reports on biogeochemical and physical variables in subareas of the Atlantic and Arctic LABs using fields from the same ESMs (Lavoie et al. 2013a,b).

The ESMs used in this report were chosen because of their inclusion of (and DFO's interest in) the ocean carbon cycle, and the availability of the model fields at the time when this study was initiated. These models are not necessarily more advanced than other more recently-available ESMs, nor other CMIP5 (or CMIP3) AOGCMs in their representation of the regional atmosphere-ice-ocean coupling of physical variables (e.g. heat, freshwater, momentum), particularly in specific geographic areas such as the Eastern Arctic and NWA. Thus, these models should be considered to be a subset of the 30-40 AOGCMs and ESMs being used in AR5, and not necessarily the "best" models for representing the Atlantic LAB. An important, but limited (due to time constraints), aspect of this report is the exploratory comparison of most variables with readily-available observations to provide an indication of the extent to which the ESMs capture the salient features of observed spatial and temporal variability relevant to the Atlantic LAB.

The report is organized by variable. After a brief description of the methodology in Section 2, displays and results are presented for Surface Air Temperature (TAS) and Sea Ice Concentration (SIC) in Sections 3 and 4, respectively. Displays and results are then presented for Surface Ocean Temperature (TOS; also commonly referred to as Sea Surface Temperature or SST) and Surface Ocean Salinity (SOS; also commonly referred to as Sea Surface Salinity or SSS) in Sections 5 and 6, respectively, and for subsurface ocean temperature and salinity on selected vertical sections in Section 7. Next, the report has brief presentations on maximum Ocean Mixed Layer (OML-max) depth and Sea Surface Height (SSH) in Sections 8 and 9, respectively. The report concludes with a summary commentary in Section 10. Supplementary displays for key variables are provided in Appendices A-F.



## Section 2 Methodology

### 2a Models, Simulations and Fields

The six Earth System Models (ESMs) whose long-term simulations were used to produce this report are:

- **CanESM2**: the second generation of the Canadian ESM developed and run by the Centre for Climate Change Modelling and Analysis (CCCMA) of Environment Canada (e.g. Arora et al. 2011; <http://www.cccma.ec.gc.ca/data/cgcm4/CanESM2/index.shtml>), with an atmospheric grid size of  $\sim 2.8^\circ$  and an ocean grid size of  $\sim 1.4^\circ \times 1^\circ$ ;
- **GFDL-ESM2M**: an ESM in which the vertical coordinate is based on depth, developed and run by the Geophysical Fluid Dynamics Laboratory (GFDL) of the United States National Oceanic and Atmospheric Administration (e.g. Dunne et al. 2012; <http://www.gfdl.noaa.gov/earth-system-model>), with an atmospheric grid size of  $\sim 2^\circ \times 2.5^\circ$  and an ocean grid size of  $\sim 1^\circ \times 1^\circ$ ;
- **HadGEM2-ES**: the ESM used by the United Kingdom's Met Office Hadley Centre with its Hadley Global Environment Model 2 (e.g. Booth et al. 2012; <https://verc.enes.org/models/earthsystem-models/hadgem2-es>), with an atmospheric grid size of  $1.875^\circ \times 1.25^\circ$  at mid-latitudes and an ocean grid size of  $\sim 1^\circ \times 1^\circ$ ;
- **IPSL-CM5A-LR**: the Low Resolution (LR) version of the Coupled Model 5A of the ESM of France's Institut Pierre Simon Laplace (e.g. Marti et al. 2010; Dufresne et al. 2013; <https://verc.enes.org/models/earthsystem-models/ipslesm>), with an atmospheric grid size of  $\sim 1.9^\circ \times 3.8^\circ$  and an ocean grid of  $\sim 2^\circ \times 2^\circ$ ;
- **MIROC-ESM**: the ESM of the Model for Interdisciplinary Research on Climate (MIROC) developed by Japanese organizations (e.g. Watanabe et al. 2011; <http://www.geosci-model-dev-discuss.net/4/1063/2011/gmdd-4-1063-2011.html>), with an atmospheric grid size of  $\sim 2.8^\circ$  and an ocean grid size of  $\sim 1.4^\circ \times 1^\circ$ ;
- **MPI-ESM-LR**: the Low Resolution (LR) version of the ESM used by Germany's Max Planck Institute of Meteorology (e.g. Brovkin et al. 2012; <http://www.mpimet.mpg.de/en/science/models/mipi-esm.html>), with an atmospheric grid size of  $\sim 1.9^\circ$  and an ocean grid size of  $\sim 1.6^\circ$ ;

These ESMs are essentially AOGCMs with newly-added carbon system components. As indicated in the Introduction, the models were chosen for this study because they include the carbon cycle and are being examined for other DFO regions.

The simulations considered are the Historical model runs from  $\sim 1850$  to 2005, and the forced runs for Representative Concentration Pathways (RCPs) 4.5 and 8.5 from 2006 to 2100 (Moss et al. 2010; Taylor et al. 2011, 2012). These RCPs were chosen to provide a rough indication of the range of potential future atmospheric greenhouse gas (GHG) concentrations based on recent emissions and current discussions about future emissions (Peters et al. 2013). For the 50-Year time scale of primary focus here, the future radiative forcing associated with these RCPs is

roughly in the range of that for SRES<sup>2</sup> scenarios B2 to A1FI used in AR4 (although this depends on the time scale) (Rogelj et al. 2012).

The primary fields examined here are time-averaged (bi-decadal and monthly) two-dimensional (2-d) horizontal fields from run (or “member”) 1<sup>3</sup> of the above six ESMs interpolated onto a common 2° x 2° grid (Figure 2-1), provided by J. Christian of DFO IOS. The key benefit of using these “interpolated” fields is that further time averaging or differencing of the fields from the different models is greatly facilitated by the common grid (instead of dealing with each model’s native grid). The disadvantages include the general (but relatively small) spatial smoothing of the fields, the loss of resolution of the ice and ocean fields in the vicinity of land-ocean boundaries, and some artificial features in the statistics of the variables at some coastal sites due to the mismatch between the common and native model grids.

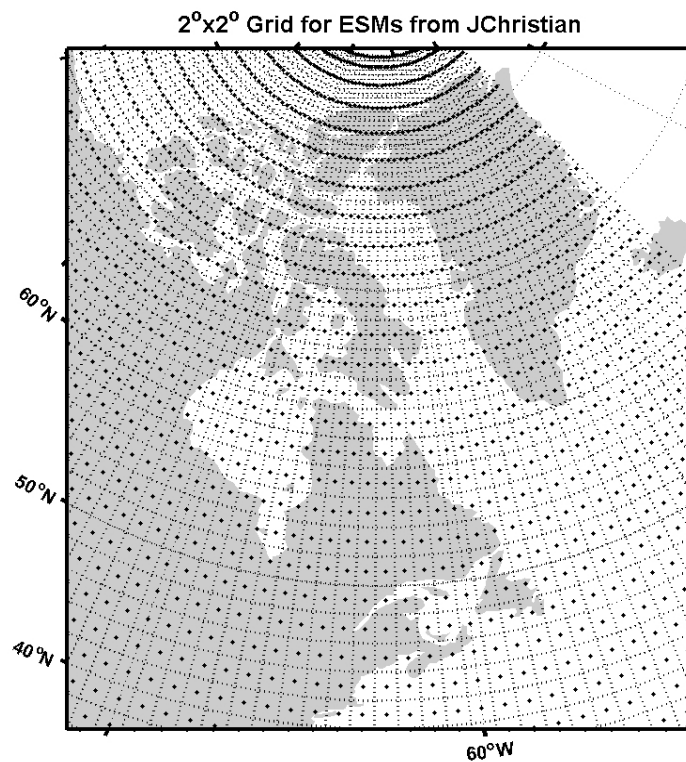


**Figure 2-1** The uniform 2°x2° grid to which the 2-d (horizontal) data fields from the six ESMs were interpolated and provided by J. Christian of DFO-IOS.

The temporal resolution of the interpolated fields is the monthly mean over selected bi-decadal periods. The specific periods are 1966-1985, 1986-2005, 2006-2025, 2026-2045, 2046-2065 and 2066-2085. The 20-year (bi-decadal) mean for a particular month and period was computed as the arithmetic mean of the annual monthly means during the period.

<sup>2</sup> SRES refers to the Special Report on Emissions Scenarios (Nakićenović et al., 2000)

<sup>3</sup> Run 1 refers to the first of several runs that are usually carried out using the same model and forcing, but with different initializations. More technically, it is also referred to as run r1i1p1.

The variables for which we consider the interpolated bi-decadal horizontal fields are Air Temperature (TAS), Sea Ice Concentration (SIC), Surface Ocean Temperature (TOS or SST), Surface Ocean Salinity (SOS or SSS), and the maximum Ocean Mixed Layer depth (OML-max) (see Taylor 2012 for more detail on these variables). TAS is included because it is one of the primary Earth System variables that is changing with increasing GHGs and it has a strong influence on upper-ocean climate. SIC is also changing due to anthropogenic GHG emissions, and it is a key factor in physical and chemical fluxes between the atmosphere and ocean in the Atlantic and Arctic LABs. TOS and SOS are indicators of heat/temperature and freshwater/salinity in the upper ocean, and OML-max in February provides an indication of the vertical extent of water mass modification and ocean ventilation due to wintertime atmospheric forcing.

In addition to the surface variables, we examine the vertical and cross-basin distribution of ocean temperature and salinity for selected sections (Figure 2-2) across Baffin Bay, the Labrador Shelf/Slope/Sea (LSSS or AR7W), and the Scotian Shelf/Slope/Rise (SSSR or AtlNW) – the same as those used in Lavoie et al. (2013a,b). Three-dimensional (3-d) annual-mean data from run 1 of five<sup>4</sup> of the ESMs on their native grids were interpolated to a set of points constituting each section, and averaged over the same bi-decadal periods as used for the surface fields.



**Figure 2-2** Map showing locations of the three sections (Baffin Bay; AR7W or LSSS across the Labrador Shelf/Slope/Sea; and AtlNW or SSSR across the Scotian Shelf/Slope/Rise) used for displays of subsurface temperature and salinity (blue lines); the five model sites where temporal variability in TOS and SOS is examined (red squares); and the two coastal observation sites (Prince 5 or P5, and Station 27 or S27; green dots) that are not co-located with the model sites.

<sup>4</sup> 3-d annual-mean fields from the 6<sup>th</sup> ESM were not readily available at the time of the analysis.

Finally, selected variables were examined in more detail for the EC CanESM2 and NOAA GFDL-ESM2M models, using monthly mean data on their native grids. The monthly data were downloaded directly from the CCCMA and GFDL data portals. We computed annual-mean time series and bi-decadal means and annual cycles of TAS, TOS and SOS for the Historical and future RCP scenarios from five different runs (and an ensemble mean of the 5 runs) of CanESM2, and from run 1 of GFDL-ESM. The computations with the five-member CanESM2 ensemble allowed a brief examination of inter-run (or inter-member) variability, for comparison with inter-model variability using run 1 from the six ESMs. We also computed bi-decadal monthly means of SSH from CanESM2 (ensemble mean of 5 runs) and GFDL-ESM2M (run 1) for the same scenarios.

The ensemble mean of the bi-decadal monthly values (means or climate changes) from individual models or runs was computed by arithmetic averaging over the N members of the ensemble, and the inter-model standard deviation was computed for the individual models about their ensemble mean.

## **2b Comparison with Observations**

The observational realism of climate models is a very important issue and, in many cases, their limited realism is a factor in their value for useful climate change projections, particularly on regional scales. All the models examined here have been developed through the long-term efforts of large organizations, involving simulations of past climate variability (e.g. the Historical simulations discussed here as well as precursor control experiments) and comparisons with observations at some level. However, these comparisons have generally been done for large-scale distributions, such as global or hemispheric means, or on continental scales. Observational validations have generally not been published for the CMIP5 ESMs nor for their earlier CMIP3 versions for the regional scales of the Canadian Arctic Archipelago (CAA), NW Atlantic, and the subbasins of the Atlantic LAB that are important to ACCASP, especially validations of ice and ocean properties. It is therefore important that some consideration be given to how well the spatial and temporal variability of key variables compares with well-known observational features.

With their coarse spatial resolution of coastlines and ocean topography, AOGCMs (including ESMs) are not expected to provide realistic representations of important regional ice and ocean features. Higher-resolution Regional Climate Models (RCMs) have been used over the past decade to dynamically downscale AOGCM atmospheric simulations to “regional” scales of interest such as in the North American Regional Climate Change Assessment Program (NARCCAP; e.g. Bukovsky 2012). The RCMs provide much more realistic representations of atmospheric structure over the land-ocean boundary and large mountain ranges; however, they generally do not have active ice and ocean components so their representation of ice and ocean features remains limited. Ocean biases in AOGCM simulations are generally well-recognized and crude adjustments are made based on observations (but not on ice-ocean dynamics).

The exploratory comparisons of the Historical simulations with observations included here are intended to provide an indication of the realism of the models' representation of some key variables. They are not a rigorous observational comparison or validation.

- For TAS (whose spatial gradient across the land-ocean boundary is recognized to be only coarsely represented in AOGCMs), bi-decadal annual cycles during 1986-2005 in the Historical simulations from the six ESMs are compared with observations from several meteorological stations (Figure 2-3) in the Atlantic LAB using the Adjusted Homogenized Canadian Climate Dataset (AHCCD; Vincent et al. 2012) from Environment Canada (EC). In addition, interannual variability in TAS in the CanESM2 and GFDL-ESM2M Historical simulations is compared with observations.



**Figure 2-3** Map showing locations of the meteorological observation sites where temporal variability in TAS is examined.

- For SIC, the climatological (over 1966-2005) monthly spatial patterns in the ESMs are compared with the observed monthly SIC patterns in an updated version (downloaded from <http://www.metoffice.gov.uk/hadobs/hadisst>) of the HadISST1 dataset (Rayner et al. 2003) for selected months.
- For TOS and SOS, the climatological (over 1966-2005) monthly spatial patterns in the six ESMs are compared with the observed monthly climatologies developed by Igor Yashayaev of DFO's Bedford Institute of Oceanography (BIO) for 1946-2005, for each of February and August. In addition, the 1986-2005 annual cycles in the Historical simulations from the six ESMs and the interannual variability in CanESM2 and GFDL-ESM2M are compared with

observations from DFO's Atlantic Zone Monitoring Program (AZMP<sup>5</sup>) at three sites and from its Atlantic Zone Off-shelf Monitoring Program (AZOMP<sup>6</sup>) at one site. For three of the sites (Bravo in the Labrador Sea, Station 27 on the Grand Bank, and Emerald Basin on the Scotian Shelf), the observations are expected to provide a reasonable representation of broader areas, but the observations (especially salinity) from the Prince 5 site in Passamaquoddy Bay are expected to be significantly affected by local run-off into the Bay.

- For the vertical distributions of subsurface temperature and salinity across the Labrador Sea, the decadal means over 1996-2005 from the five ESMs are compared with observations over the same period from DFO's AZOMP sampling on the AR7W line (courtesy of I. Yashayaev).

These crude comparisons complement those in Lavoie et al. (2013a,b) to provide an indication of the observational realism and limitations of the ESMs in the Atlantic LAB.

Model data for specific stations were interpolated from the four gridpoints that surround the station location using bilinear interpolation, which involved performing a linear interpolation first in the *x*-direction (east) and then in the *y*-direction (north).

Data for the vertical sections were obtained by extracting the gridpoint data from grid cells that were contiguous to the line that joined the two endpoints of the section line, similar to using a nearest neighbour algorithm.

## 2c Projected Changes

The projected climate changes from the ESMs are primarily presented as the differences between the bi-decadal monthly means for 2046-2065 (approximately mid 21<sup>st</sup> century or 40 years from now) from the RCP simulations, and those for 1986-2005 from (the last 2 decades of) the Historical simulation. The 60-year offset between these periods is an approximation to the 50-Year time scale that is of primary interest to ACCASP issues. While the differences from the changes for an exact 50-year time offset are generally well within the inter-model differences, caution nevertheless needs to be used in identifying implications of the specific magnitudes of the projected changes for various reasons. Changes over a decade or two in these simulations are expected to be substantially influenced by decadal-scale variability internal to the model which cannot be assumed to reproduce that in the real world (Taylor et al. 2012). Consequently, projections for the ACCASP "Decadal" time scale are not presented in this report.

There is substantial similarity between the spatial patterns of the projected changes for RCP4.5 and RCP8.5, with those for RCP8.5 generally having larger magnitude. In most cases, the differences between the projected changes for the two RCPs (out to 2046-2065) are less than the differences among the projected changes from the different models. The similarity of the patterns for the two RCPs is not surprising considering that the climate system appears to have

---

<sup>5</sup> Observations provided by Roger Pettipas of DFO-BIO, from DFO's Atlantic Zone Monitoring Program (AZMP): <http://www.bio.gc.ca/science/monitoring-monitorage/azmp-pmza-eng.php>

<sup>6</sup> Observations provided by I. Yashayaev of DFO-BIO, from DFO's Atlantic Zone Off-shelf Monitoring Program (AZOMP): <http://www.bio.gc.ca/science/monitoring-monitorage/azomp-pmzao/azomp-pmzao-eng.php>

some fundamental modes of response to increased radiative forcing from GHGs (e.g. Ishizaki et al. 2012), and the limited differences in magnitude are not surprising considering the “committed” climate change (e.g. Meehl et al. 2007) associated with the increase in radiative forcing to date and that which is expected during the next couple of decades. Only the projected changes for RCP8.5 are presented in most cases in this report. These changes can be considered to be near the high end of those plausible for a wide range of global political and socio-economic responses to increasing GHGs, but they might be the most realistic if GHG emissions are not substantially reduced (e.g. Peters et al. 2013).

It is widely recognized in the climate change science community that, at present and perhaps in the foreseeable future, no single AOGCM or ESM is likely to provide a robust representation of all the important processes in the climate system (e.g. Taylor et al. 2012), especially those affecting regional climate (e.g. Li et al. 2012b). Consequently, IPCC projections are based on the statistics of a growing ensemble of models numbering just over 20 in AR4 and over 30 in AR5. Such an ensemble approach is also needed to represent regional climate change, perhaps even more so. Initial examination of the present model results indicated inadequacies in their representation of key ice and oceanic features in all six ESMs, such that it was beyond the resources of the present study to identify a “best” one for the Atlantic LAB. Consequently, we took an ensemble approach in which ensemble statistics of the change fields from the six ESMs have been computed for the key variables of interest. In this approach, the ensemble means of the change fields from the six models are presented, together with the minimum and maximum changes, and the spread (range) of the changes with their standard deviations from the mean. Our examination of the inter-run variability of TAS, TOS and SOS in the five-member ensemble of CanESM2 simulations indicated that there is little difference in the bi-decadal means (e.g. annual cycles) from the different runs (although significant differences in the interannual to decadal scale variability at specific locations). Consequently, with our focus on the 50-Year time scale, we do not consider the multiple runs from CanESM2 in any detail, but primarily present results from the multi-model (ESM) and multi-run (CanESM2) ensembles.

Ensemble means and statistics of TOS changes at representative sets of “Shelf” and “Offshore” sites (Figure 2-4) are used to provide quantitative estimates of the projected changes between 1986-2005 and 2046-2065 in February and August for areas of particular interest. It should be cautioned that, with the limited number of models considered and the ongoing assessments of the models for reliability, there is some uncertainty in the confidence level for these estimates.

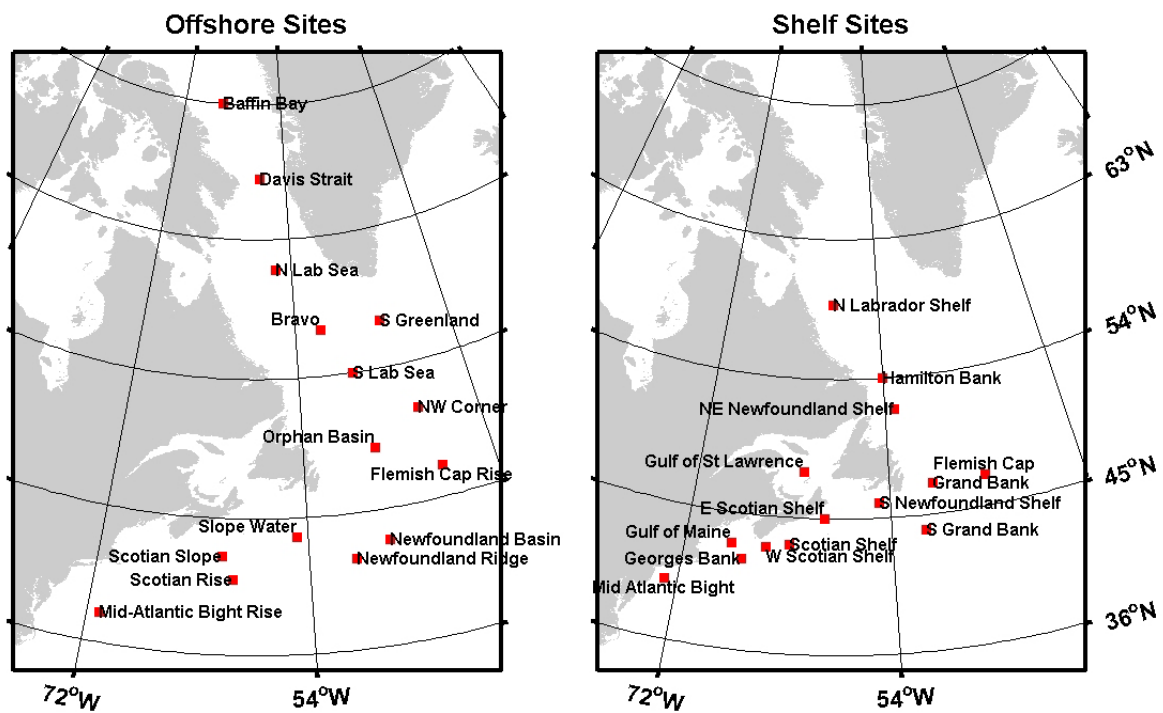


**Figure 2-4** Maps showing “Off-Shelf” (or “Offshore”; left) and “Shelf” (right) sites at which projected TOS changes are presented in Section 5d.



## Section 3 Surface Air Temperature (TAS)

### 3a Comparison with Observations at Selected Meteorological Locations

To provide an indication of the extent to which the annual cycles of TAS in the Historical simulations are in agreement with observed air temperatures, Figure 3-1 compares bi-decadal monthly means for 1986-2005 from the AHCCD at six meteorological stations scattered across the Atlantic LAB with those from two ESMs for the same period – specifically, with the monthly means from run 1 of the CanESM2 and GFDL-ESM2M simulations and from the ensemble mean of the five available CanESM2 runs. There is little difference in the annual cycles in the different CanESM2 runs (Figure A-1 of Appendix A) so the primary comparison here is among observed (red), CanESM2 (blue) and GFDL-ESM2M (green) data.

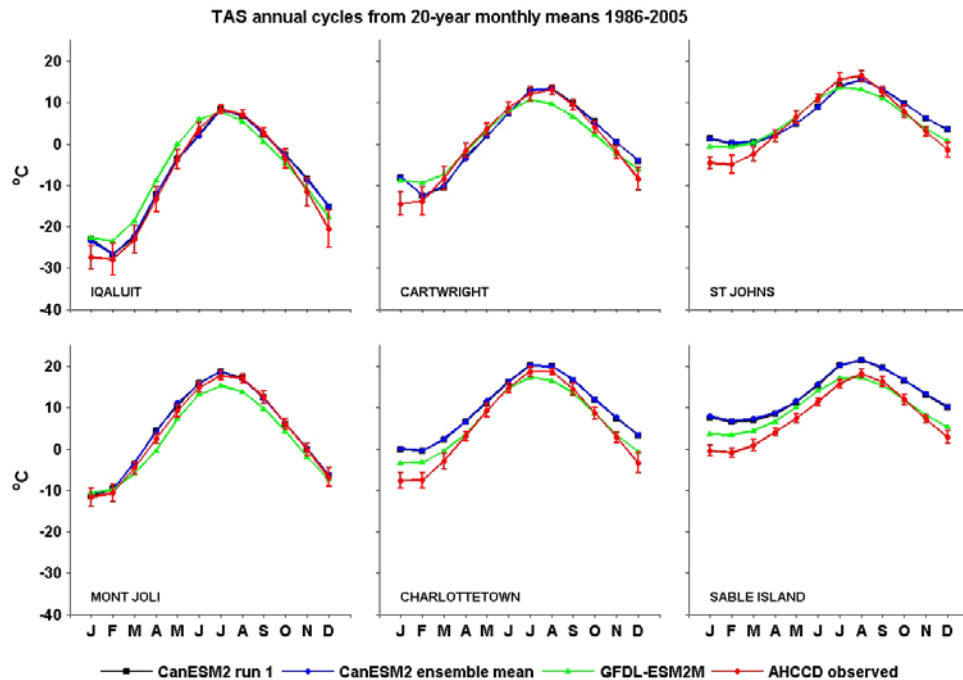


**Figure 3-1** Annual cycles of the bi-decadal monthly means of TAS for 1986-2005 at six sites from observations (AHCCD; red), and from CanESM2 (run 1, and ensemble mean of five runs) and GFDL-ESM2M (run 1) (see Fig. 2-3 for locations). The error bars on each side of the observational means indicate the standard deviations of the individual-year means about the bi-decadal means.

Overall, the annual cycles in TAS in the two ESMs are in approximate agreement with observations with notable exceptions. The agreement is very good (within  $3^{\circ}\text{C}$  in every month) at Mont-Joli which is the furthest inland station. However, it is reduced at the other 5 sites which lie in the land-ocean boundary zone, probably in part due to the smoothed TAS gradients in this zone in the models (because of their limited spatial resolution). Both models show higher winter minimum temperatures (by  $3\text{--}10^{\circ}\text{C}$ ) than observed, including at the offshore Sable Island station where CanESM2 has higher temperatures year-round. However, the models' summer maxima

are within  $3^{\circ}\text{C}$  of those observed at all sites, with the exception of CanESM2 being  $5^{\circ}\text{C}$  too high at Sable Island.

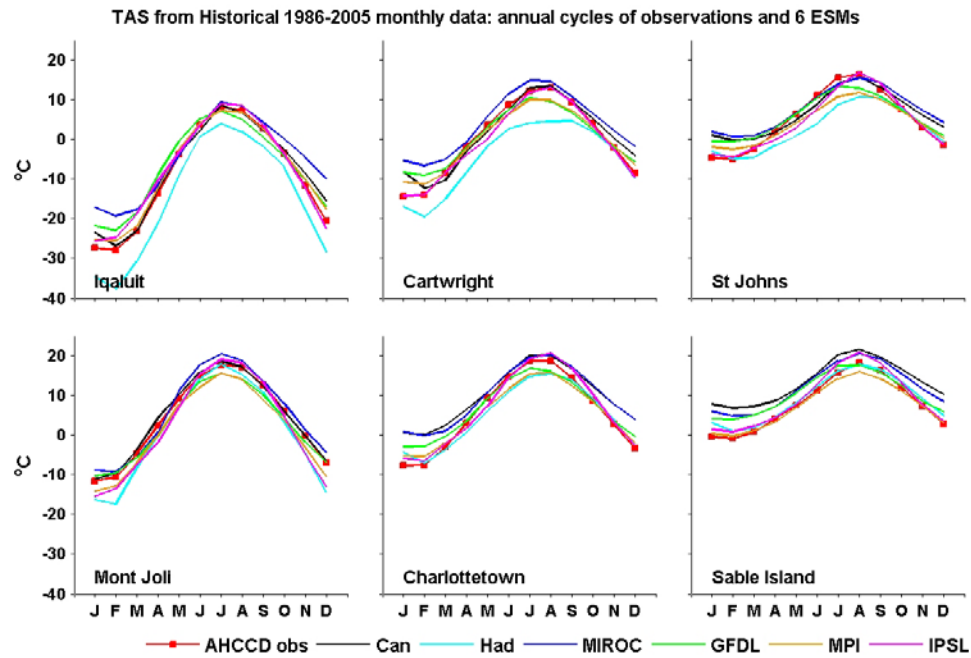


**Figure 3-2a** Annual cycles of the bi-decadal monthly means of TAS for 1986-2005 at six sites from observations (AHCCD; red) and from interpolated data for run 1 of all six ESMs (see Fig. 2-3 for locations).

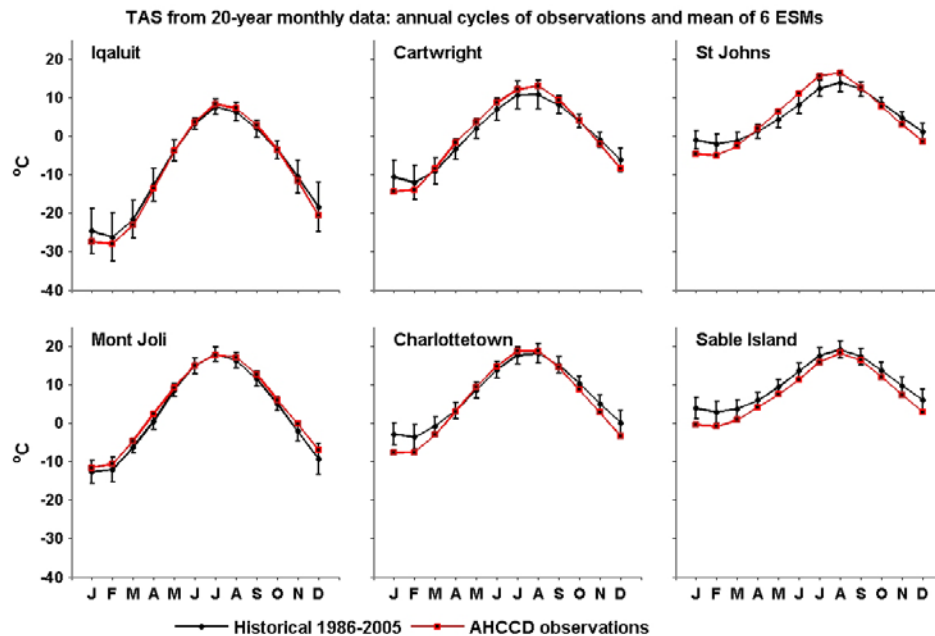


**Figure 3-2b** Annual cycles of the bi-decadal monthly TAS means for 1986-2005 at six sites from observations (AHCCD; red), and of the ensemble-mean bi-decadal monthly values from the six ESMs (Fig. 3-2a) with the inter-model standard deviations indicated by the error bars on each side of the ensemble means.

Figure 3-2a shows a similar comparison between the annual cycles in run 1 of all six ESMs and those in the AHCCD, while Figure 3-2b compares the ensemble-mean annual cycles from these ESM runs with those from the AHCCD. The most striking feature is the spread among the annual cycles in the different ESMs, especially at the two northernmost sites (Iqaluit and Cartwright). MIROC-ESM generally has the warmest TAS and HadGEM2-ES the coolest at all sites but, at the two southernmost ones (Charlottetown and Sable Island), the CanESM2 and MPI-ESM-LR cycles are similar to those in MIROC-ESM and HadGEM2-ES, respectively. The observed annual cycles lie within or near the envelope of the model cycles, and generally within the inter-model standard deviation of the ensemble-mean annual cycles (Figure 3-2b). The observed and model annual cycles are well within the combined observational (interannual; Figure 3-1) and inter-model standard deviations of each other. There are differences of a month in the timing of the annual minima and maxima among the models and between some models and the observations, but there are only small differences in the timing of the extrema in the ensemble-mean and observed annual cycles.

To examine the extent to which the interannual and lower-frequency variability in the Historical simulations from two of these ESMs agrees with observations, Figure 3-3 provides a comparison of the time series of annual means for the same six meteorological stations for 1950-2005. Figure A-2 (Appendix A) shows the time series for individual CanESM2 runs for 1900-2005. With the zoomed TAS scales in these plots (compared to those in the annual-cycle plots), differences in the long-term (annual) means are more apparent. The CanESM2 means are increasingly larger than the observed means and larger than the GFDL-ESM2M means as one proceeds south among the four southernmost sites. There are notable high-frequency (supra-decadal) differences between the ensemble-mean and run-1 time series from CanESM2, the run-1 time series from GFDL-ESM2M, and the observations. This is consistent with the expectation that a particular Historical simulation is unlikely to reproduce deterministically the observed interannual-to-decadal-scale TAS variability in a region (partly because it is not initialized with information representing this variability and partly because it may not resolve the dynamics of regional modes of coupled atmosphere-ice-ocean variability) (e.g. Taylor et al. 2012).

On the other hand, there is some similarity in the positive long-term trends in the models and observations at all sites, with the values for all time series in Figure 3-3 being in the 0.06-0.3 °C/decade range (except for a smaller observed value at Iqaluit). This reflects the occurrence of global warming over land across the LAB, consistent with Trenberth et al. (2007). However, there are differences of order 0.1 °C/decade in the trends among the models and runs at each site, reflecting variability among the individual-model/-run trends that is comparable to the overall mean trend. There is a marked discrepancy between the models' and observed trends at Iqaluit since 1950. There is also an indication that the observed cooling from the 1980s to 1990s at Iqaluit, and to a lesser extent at Cartwright and St. John's, is not reproduced by the models. These results indicate that there is qualitative agreement between the models and observations in the long-term trends for TAS but there is important decadal-scale variability not resolved by these six ESMs.

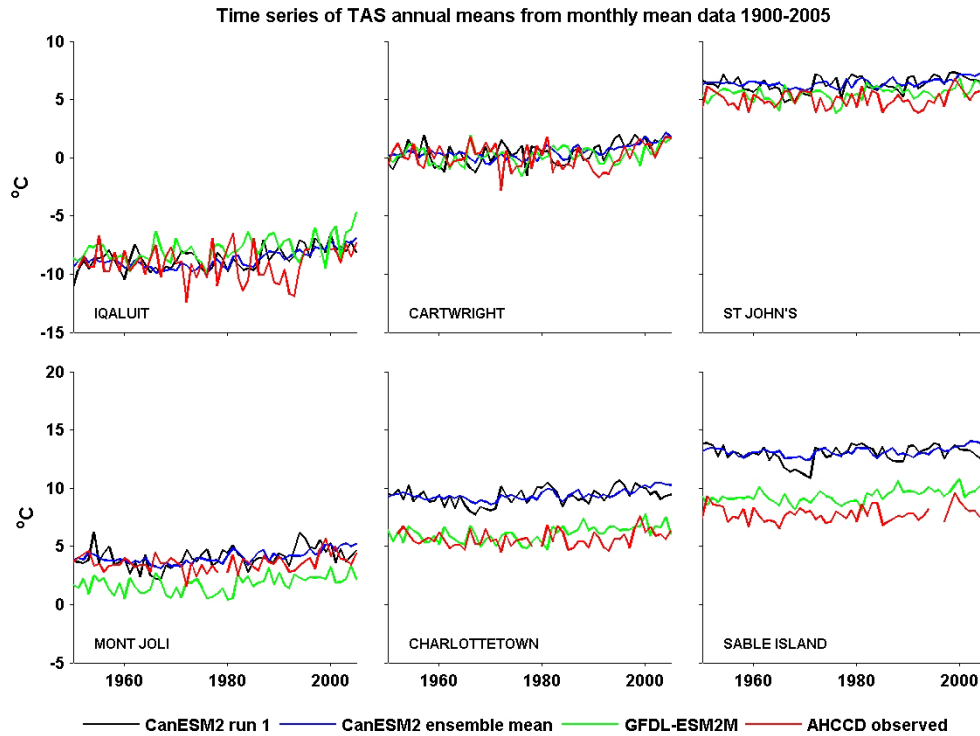


**Figure 3-3** Time series of observed (AHCCD) and model annual means of TAS for CanESM2 (ensemble mean and run 1) and GFDL (run 1) for 1950-2005 at six sites (see Fig. 2-3 for locations).

### 3b Spatial Distribution of Projected TAS Climate Changes in Six ESMs

In this subsection, we focus on the projected climate changes in TAS from the six ESMs and their spatial structure. We consider a Canada-wide domain in order to place the changes over the Atlantic LAB in a larger-scale context and to provide input to the ACCASP reviews for other LABs. The large-scale patterns described below are similar to those in Diffenbaugh and Giorgi's (2012) global-scale examination of a CMIP5 ensemble of 20 models and seasonal changes between 1986-2005 and 2080-2099. However, the magnitudes of the changes differ.

Figure 3-4 shows the projected changes in bi-decadal mean TAS between 1986-2005 and 2046-2065 from each of the six ESMs for RCP8.5, for February and August taken to represent the winter minimum and summer maximum, respectively. The actual bi-decadal mean distributions for these months are shown in Appendix A (Figure A-3, Figure A-4). The appendix figures demonstrate the strong seasonality and latitudinal gradient of TAS over North America, as well as the northwest-southeast (land-ocean) gradient zone over the Atlantic LAB. Of particular note in these latter displays is the southeastward extension of the area of cold winter air (so-called "Arctic amplification"; e.g. Serreze and Barry 2011) over the central Canadian Arctic towards the Atlantic LAB, and the northeastward extension of the mid-latitude area of warm summer continental air towards the southern part of the LAB.

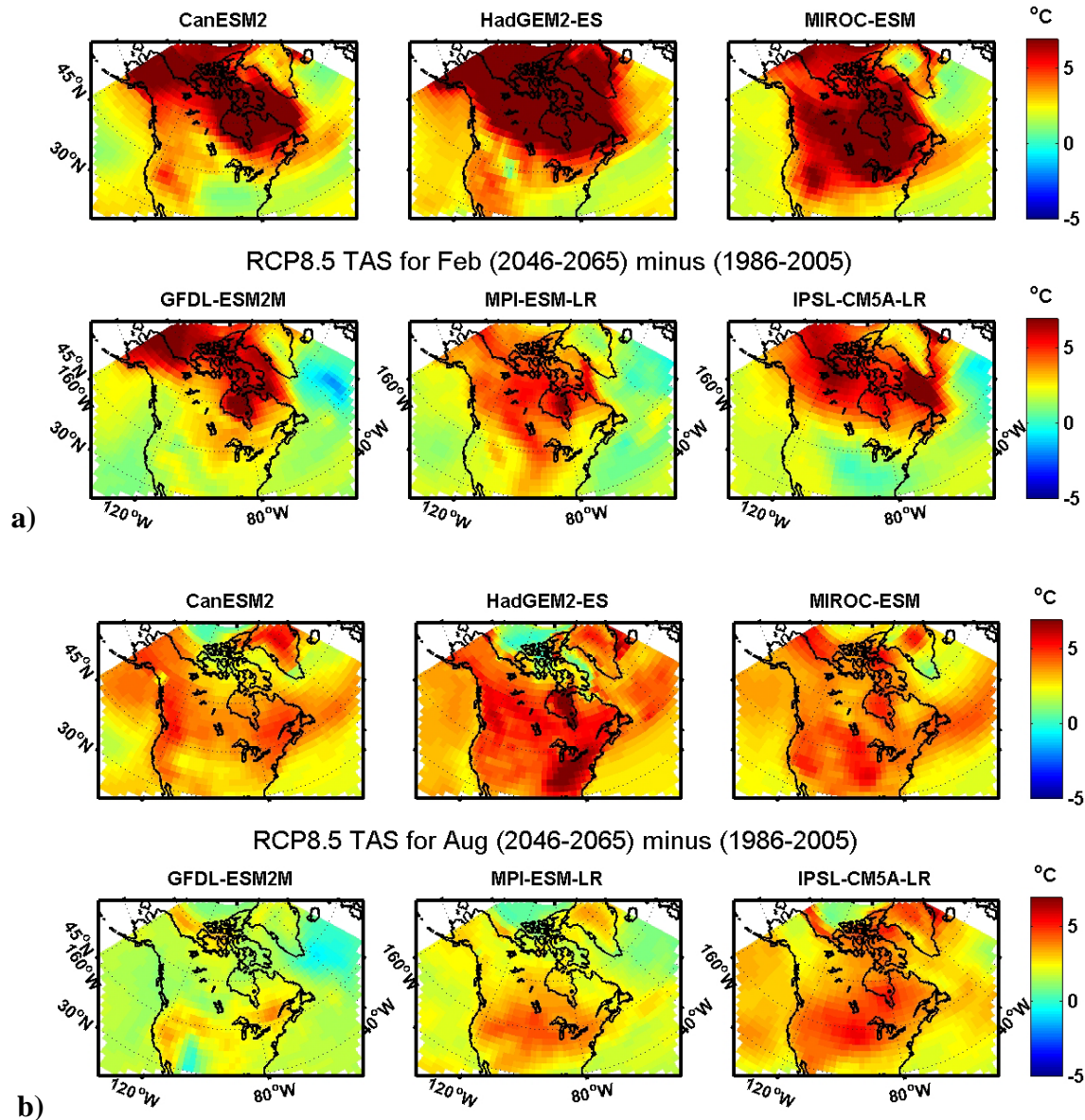


**Figure 3-4** Climate changes in bi-decadal TAS for Canada from 1986-2005 to 2046-2065 from six ESMs for RCP8.5 in a) February and b) August. Data interpolated to the common grid were used.

The winter change pattern in all six ESMs shows a broad maximum of Arctic amplification over northern central Canada that was also described in AR4, but with substantial variations in its extent, shape, and magnitude in each of the CMIP5 models (Figure 3-4a). The size of these variations, about a factor of two in magnitude and spatial extent, is somewhat remarkable and points to the uncertainty in climate change projections. For the Atlantic LAB, some models show the largest changes extending southeastward from northern central Canada while others show the largest changes over the northern Labrador Sea and/or Hudson Bay (pointing to a possible sea ice influence). In some models there is a suggestion of a tail of larger changes extending eastward from the continent across the southern part of the Atlantic LAB, and of an area of reduced change in the northern North Atlantic south of Greenland that is consistent with

IPCC AR4 projections (Meehl et al. 2007). In two models, there are notable areas of winter cooling southeast of Greenland from 1986-2005 to 2046-2065.

The summer change pattern in all six ESMs (Figure 3-4b) shows some indication of a broad maximum at mid-latitudes over the North American continent that is, again, similar to AR4 projections, but again with substantial variations in extent, shape, and magnitude in the different models (by about a factor of two or more). A clear feature in five models is the eastward extension across the Maritimes, Newfoundland, and the Grand Bank of a zonal band of larger changes that is somewhat more pronounced than in winter. There are areas of cooling or limited warming south of Greenland in two models that extend into the Labrador Sea.

The ensemble statistics for these February and August TAS change fields are presented in Figure 3-5 for each of RCP4.5 and RCP8.5. It can be seen that the patterns for RCP4.5 are very similar to those for RCP8.5 (for the mean, standard deviation and spread<sup>7</sup>), with the magnitude of the mean changes for RCP4.5 being ~60-80% of those for RCP8.5. It is also apparent from Figure 3-5 that, over a large portion of the domain (including much of the Atlantic LAB), the spread of the change estimates from the different models is comparable to or exceeds the ensemble mean of the changes, particularly in winter. This again points to uncertainty in regional climate change projections. However, in general the standard deviation is substantially smaller than the mean, such that a confidence interval based on two standard deviations should point to changes that are significantly different from zero in most areas.

From Figure 3-5a, the projected ensemble-mean change for TAS in February for RCP8.5 is greater than 3°C over almost all of Canada and its adjacent waters. The projected change exceeds 5°C north of 50-55°N and peaks at 10°C over Hudson Bay. Over the Atlantic LAB, the (ensemble-mean) changes range from about 2-3°C in the south and east to 6-8°C in the north. In August (Figure 3-5b), the changes range from ~4°C in southern Canada to ~1°C over the Arctic Ocean, with changes over the Atlantic LAB in the 2-3°C range. To illustrate the differences in the projected changes from the different models, Figure A-5 (Appendix A) shows the minimum and maximum (as well as mean) change at each grid point from each model, pointing to a large range of values. It should be emphasized, however, that these estimates are based on an ensemble of only six of the >30 models under consideration in IPCC AR5.

The ensemble-mean change pattern for RCP8.5 for all 12 months (Figure 3-6) provides more detail on the seasonal evolution of the TAS change pattern over the year. The winter area of maximum change expands southward from northern Baffin Bay in October to Newfoundland in February, and retreats by May. The zonal band of maximum change extends eastward past Newfoundland all year, with peak extent and magnitude in summer and fall and minimal extent in winter and spring. The zonal band is also reported by Li et al. (2012a).

---

<sup>7</sup> The “spread”, sometimes called the range, refers to the difference between the maximum and minimum values in the ensemble.



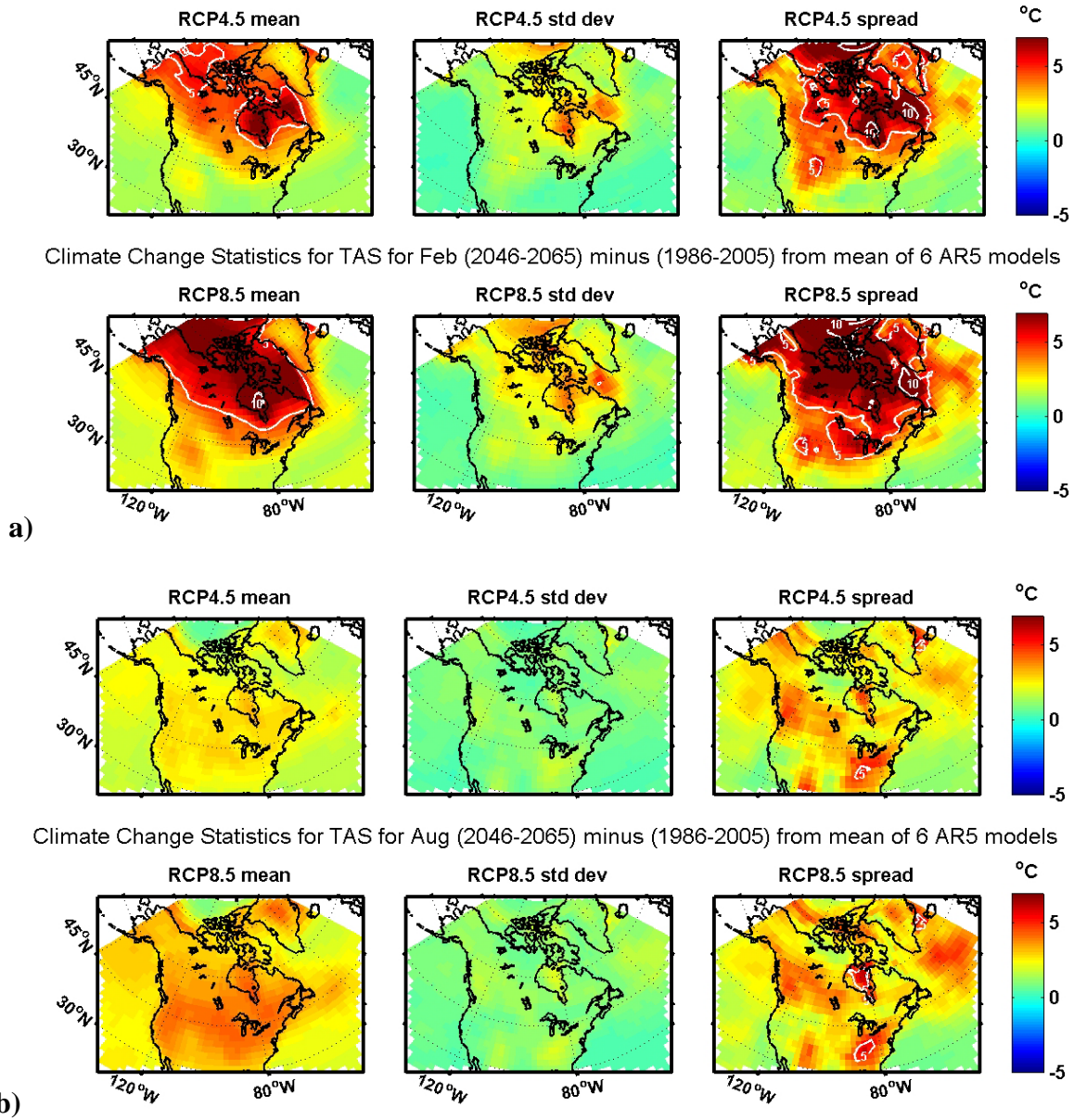


**Figure 3-5** Mean, standard deviation, and spread of climate changes in bi-decadal TAS between 1986-2005 and 2046-2065 from RCP4.5 and RCP8.5 in a) February and b) August, computed from the ensemble of six ESMs using interpolated data (Fig. 3-4). The white contours are the 0, 5 and 10 °C isotherms.

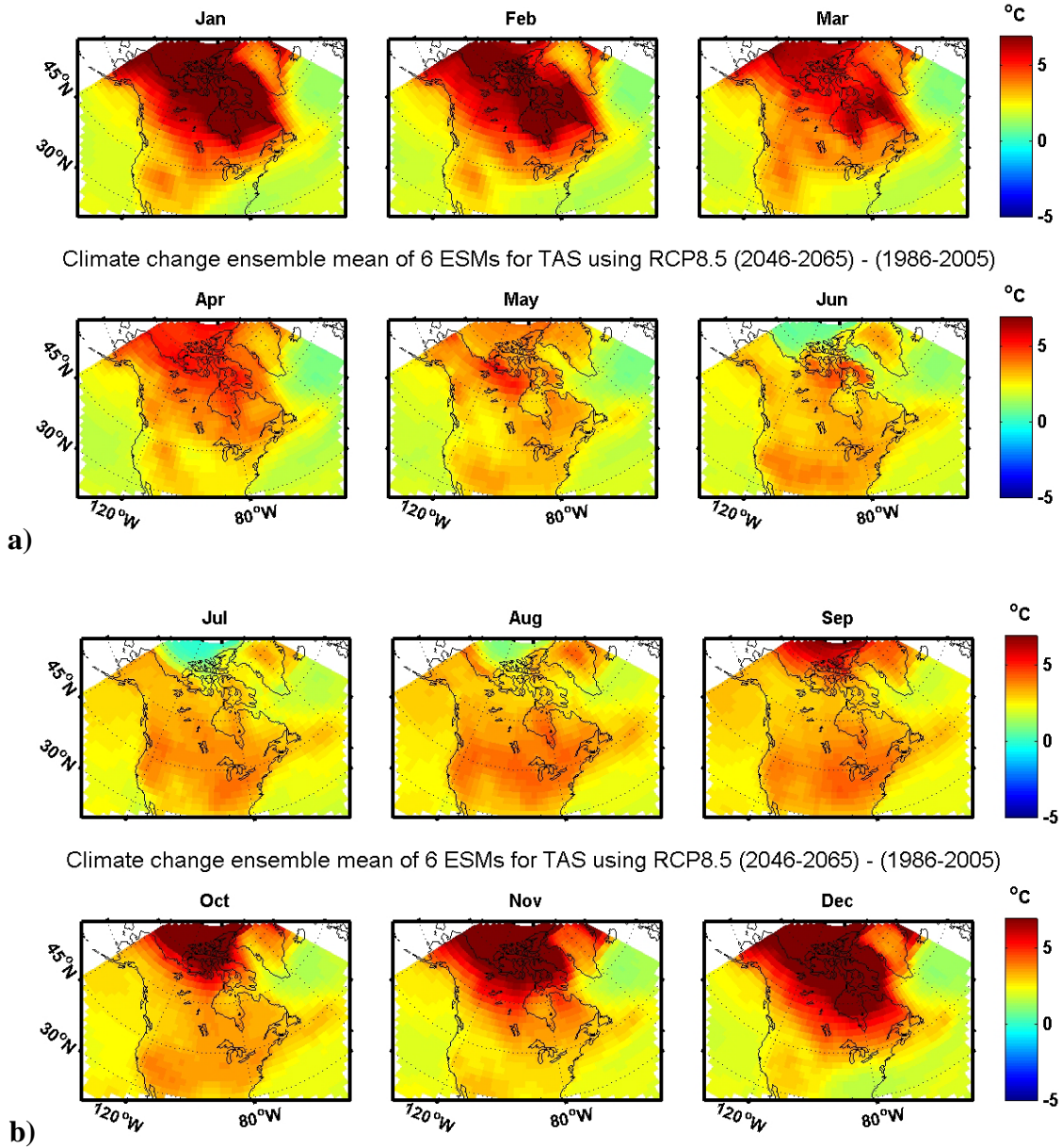


**Figure 3-6** Ensemble mean of the changes in bi-decadal mean TAS from 1986-2005 to 2046-2065 for RCP8.5, from six ESMs for twelve months: a) January – June and b) July – December.

### 3c Temporal Variability of Projected TAS Climate Changes in ESMs

To follow-up on the time variability of TAS discussed in Section 3a, this subsection presents the future time variations at nine stations from the 6 ESMs. The annual cycles for the monthly means for 1986-2005 from the Historical simulations, and for 2046-2065 from the RCP8.5 simulations, are shown in Figure 3-7 for the ensemble mean of the six ESMs and in Figure A-6 for the ensemble mean of the five CanESM2 runs and for run 1 from GFDL-ESM2M. The monthly climate changes in TAS at these sites are shown in Figure 3-8 for run 1 from the 6 ESMs and in Figure A-7 for the five CanESM2 runs.



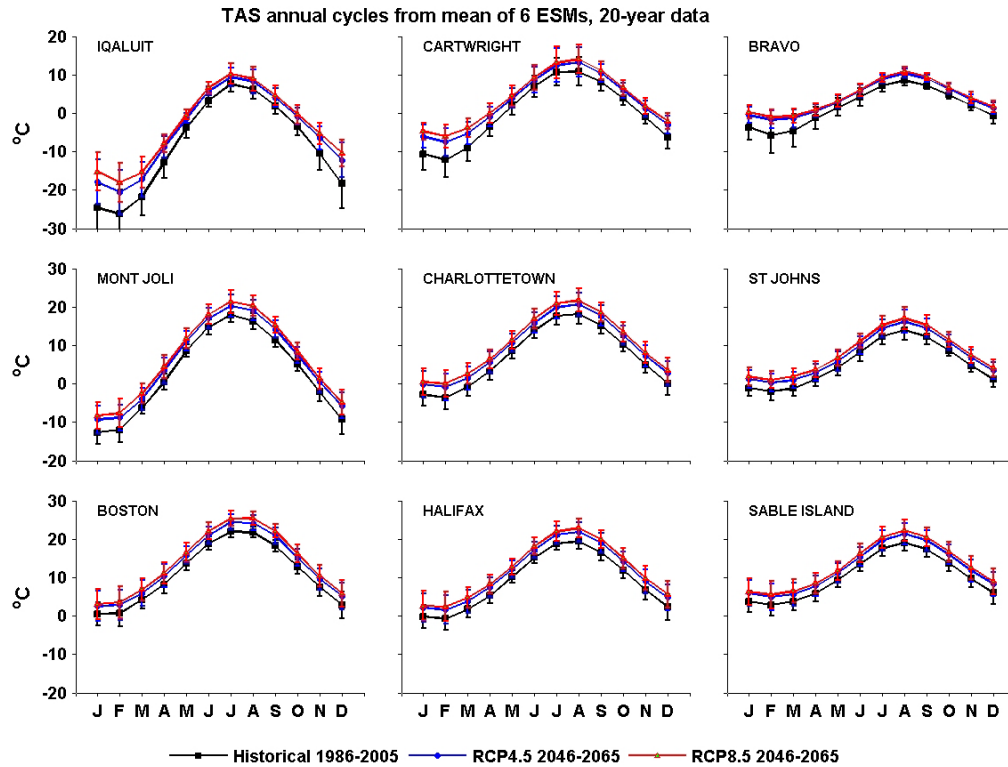


**Figure 3-7** Ensemble-mean model annual cycles of bi-decadal monthly TAS at nine stations for 1986-2005 (Historical) and 2046-2065 (RCP4.5 and RCP8.5), from run 1 from six ESMs using interpolated data (see Fig. 2-3 for locations). The inter-model standard deviations are indicated by the error bars.

The future bi-decadal ensemble means are larger than the Historical ones at all sites and in all months for both RCPs (Figure 3-7), and the changes for RCP8.5 are larger than those for RCP4.5. However, the changes in the ensemble-means are within the inter-model standard deviations in all cases. The future bi-decadal means for RCP8.5 are also larger than the Historical ones at all sites and in all months, in each of CanESM2 and GFDL-ESM2M (Figure A-6).

For the six southernmost sites (south of 50°N), the changes for RCP8.5 are approximately the same year-round although the inter-model differences are comparable in magnitude to the ensemble-mean changes (Figure 3-8a). There is some indication of weak winter and summer maxima, reflecting the different winter and summer distributions (e.g. Figure 3-5), but the seasonal variation in the ensemble means is much less than the inter-model standard deviations (Figure 3-8b). The changes in GFDL-ESM2M (~1.5-3°C) are only about one-half the magnitude of those in CanESM2 (~3-5°C), and the differences in the changes among the different CanESM2 runs are relatively small (Figure A-7).

In contrast to the southern sites, there is an apparent seasonal variation in the changes at the three northernmost sites, with largest magnitudes in February and weak minima in May and September (Figure 3-8a). The seasonal differences exceed the inter-model standard deviations at Iqaluit and Cartwright but not at Bravo (Figure 3-8b).

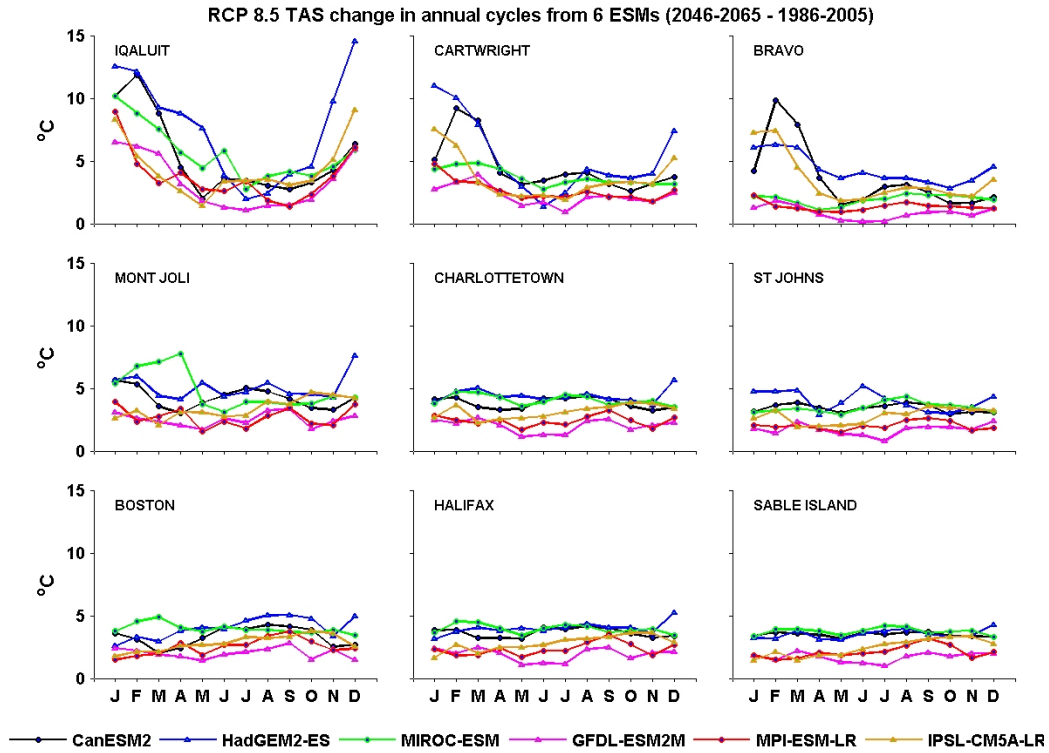


**Figure 3-8a** Climate changes in bi-decadal monthly TAS means from 1986-2005 to 2046-2065 for RCP8.5 at the same nine locations as in Figure 3-7, for each of the six ESMs using interpolated data.

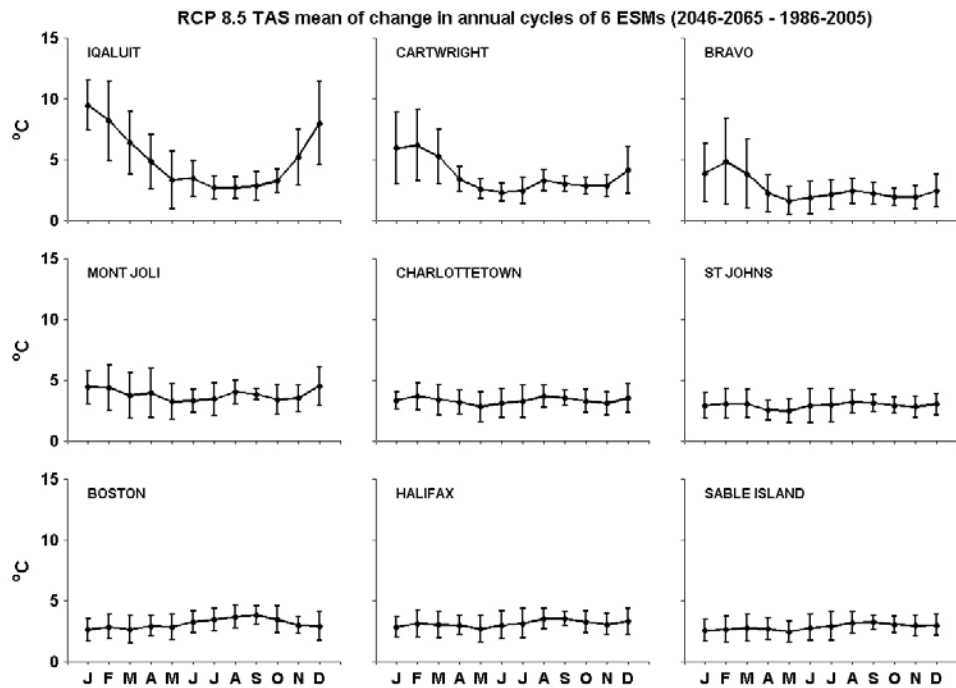


**Figure 3-8b** Ensemble means, and inter-model standard deviations, of the climate changes in bi-decadal monthly TAS means shown in Figure 3-8a.

There is also greater inter-model variability in the projected winter changes at the northern sites than in the changes at the southern sites (Figure 3-8). For example, the changes from GFDL-ESM2M are only about one-half the magnitude of those from CanESM2 at Iqaluit and Cartwright (Figure A-7) while, at Bravo, the GFDL-ESM2M changes are a smaller fraction of the CanESM2 ones (with little change at Bravo in May, June and July). While the estimated changes at these northern (or any of the) stations in these models may not be reliable, it is worth noting their magnitudes. The projected winter changes are in the range of 5-12°C at Iqaluit, 3-10°C at Cartwright and 2-10°C at Bravo. The magnitudes of the summer-fall changes at these northern stations are similar to those at the southern stations, namely in the 2-4°C range except for changes of <1°C in GFDL-ESM2M at Bravo in summer.

From a mathematical perspective, one would regard the changes in the bi-decadal monthly TAS values at the southern stations in Figures 3-7 and 3-8 to be largely changes in the annual mean rather than changes in the annual “cycle”, with the changes at the northern sites comprising changes in both the means and annual cycles (if cycle is taken to refer to the changes in relation to the annual means).

The projected future evolution of the annual means of TAS at the same nine meteorological stations is shown in time series from 2006-2100 in Figure 3-9, for RCP4.5 and RCP8.5 from CanESM2 (ensemble mean of 5 runs) and GFDL-ESM2M (run 1). Consistent with Figure 3-7 (but less apparent there), the annual means at the start of these future simulations are higher in CanESM2 than in GFDL-ESM2M for all sites except Bravo. It is also apparent that the warming in CanESM2 is greater than in GFDL-ESM2M over the 21<sup>st</sup> century, and that there is little difference between the TAS increases for RCP4.5 and RCP8.5 (for a particular model and site) before 2040. The differences in the TAS increases between the two RCPs grow substantially after about 2060. This is consistent with the design of RCP4.5 to have little increase in radiative forcing in the latter part of this century. The trends for RCP8.5 from the CanESM2 ensemble range from 6°C/century at the southern sites to 10°C/century at Iqaluit, while those from GFDL-ESM2M range from 1°C/century at Bravo to 3°C/century at Sable Island in the south and 5°C/century at Iqaluit in the north.

The supra-decadal variability is markedly different in the two models, and also somewhat different for the two RCPs (for a particular model). More decadal-scale variability is apparent for GFDL-ESM2M than for CanESM2, with a variation of about 5°C over 20 years in the GFDL-ESM2M TAS time series at Bravo (Figure 3-9). The origin and reliability of this and other interannual-to-decadal scale variability are unclear, together with the reliability of the magnitude of the long-term trend in these models (as well as in the other ESMs). Note from Figures 3-4 and 3-8 that, while CanESM2 has one of the larger TAS increases over the Atlantic LAB and GFDL-ESM2M has one of the smaller increases, it is not clear that these two models are the extreme cases. For example, HadGEM2-ES has a larger overall increase (than CanESM2) at the northern sites, and IPSL-CM5A-LR and MPI-ESM-LR have smaller increases than GFDL-ESM2M at the northern sites in some months.

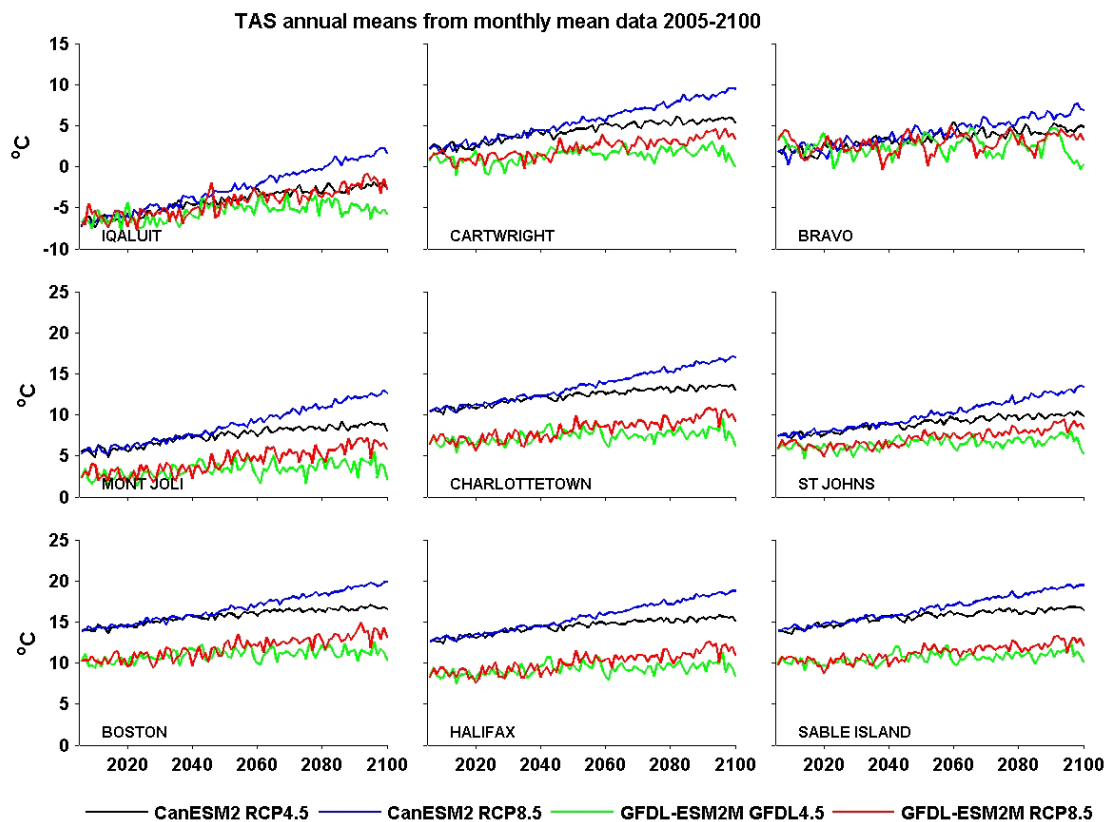


**Figure 3-9** Time series plots of annual means of TAS from the CanESM2 ensemble mean of five runs and from GFDL-ESM2M run 1 for RCP4.5 and RCP8.5 for 2006-2100, for the same nine locations as in Figures 3-7 and 3-8.

## **Section 4    Sea Ice Concentration (SIC)**

In this section we present a brief examination of the distributions of one metric of sea ice variability in the six ESMs, namely SIC expressed as a percentage. The goal is more to obtain an indication of the realism of the representation of sea ice variability in the models affecting air-sea interactions and ocean properties, than to obtain specific projections for SIC changes. Numerous studies of sea ice variability in the Arctic using the CMIP5 models are underway with particular focus on the observed and expected reductions in summer ice cover and volume, and some papers have been published (e.g. Stroeve et al. 2012; Wang and Overland 2012; Overland and Wang 2013). However, limited attention has been given to the representation of sea ice variability in the NW Atlantic (NWA) in CMIP3 and CMIP5 models.

### **4a      Comparison with Observed Spatial Distributions**

To compare the seasonal evolution of ice cover in the Historical simulations from the six ESMs to observations, we choose a domain that includes the Eastern Arctic as well as the NW Atlantic, and use the updated HadISST1 interpolated observational dataset for ice concentration (e.g. Rayner et al. 2003). We present model results averaged for the 1986-2005 bi-decadal period to represent the longer period back to the 1950s for which the HadISST1 data are shown. The reader is referred to Tivy et al. (2011) and Peterson and Pettipas (2013) for further information on sea ice variability in the Atlantic LAB.

Figure 4-1 shows the bi-decadal monthly SIC distributions from the six ESMs, their ensemble mean, and the HadISST1 observations for March and September – months that indicate the seasonal extremes of sea ice in the Arctic. On a broad scale, all models show the large seasonal change in the latitudinal extent of sea ice in the region. Sea ice extends south to about 50°N in March and retreats to the vicinity of northern Baffin Bay and the Canadian Arctic Archipelago (CAA) in September. However, if one looks in more detail at the spatial pattern and seasonal timing of sea ice cover between Baffin Bay (BB) and the Gulf of St. Lawrence (GSL), significant differences among the models and between the models and observations are apparent. This is also seen in the corresponding ESM and observed distributions for January and May shown in Figure B-1 (Appendix B).

From an ocean climate change perspective for the Atlantic LAB, four sub-areas where sea ice is of distinct importance can be identified:

- Baffin Bay (BB) which is ice-covered most of the year but ice-free in late summer and early fall;
- the Labrador Shelf and Northeast Newfoundland Shelf (NENS) where there is varying seasonal ice cover in winter and spring primarily related to advection by the Labrador Current;
- the off-shelf Labrador Sea which is generally ice-free but where the offshore extension of ice cover in winter can have strong influences on the formation/ventilation of water masses to intermediate depths (1000-2500m), affecting the entire subpolar gyre; and
- the Gulf of St. Lawrence (GSL) where there is local ice formation in winter resulting in a varying winter-spring ice cover.

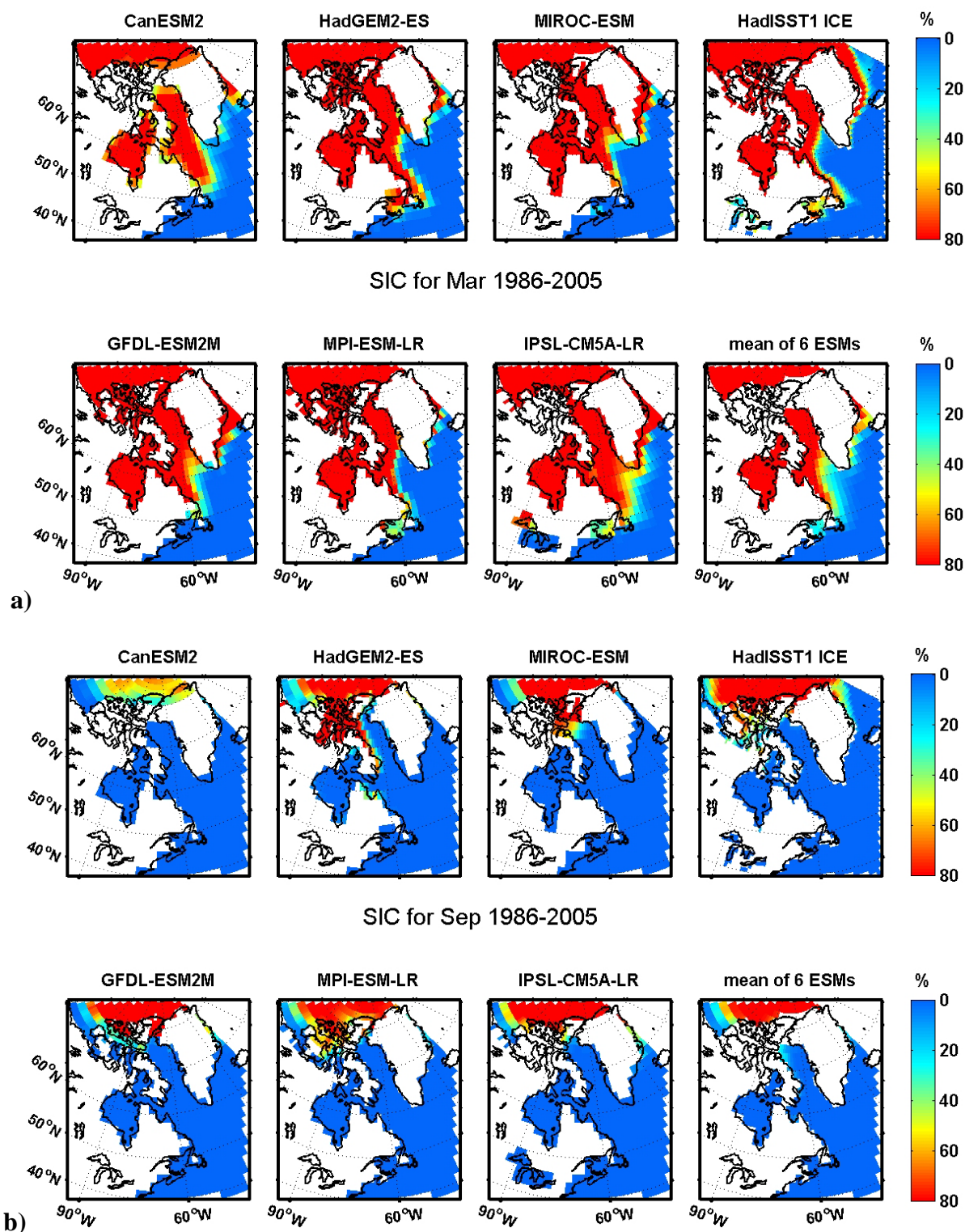


**Figure 4-1** Comparison of SIC in a) March and b) September from interpolated data from the Historical simulation of each of six ESMs, the ensemble mean of the data from the six ESMs, and the HadISST1 dataset for the NWA and Eastern Arctic for 1986-2005. The differences in the apparent land areas (white, except for northeast corner) in the different models partly reflect their native grids but are also affected by the  $2^\circ \times 2^\circ$  common interpolation grid.

Clear features among the SIC fields from the ESMs (Figure 4-1 and Figure B-1) are substantial inter-model variability in the timing and occurrence of SIC in these sub-areas, and a general lack of reproduction of the observed spatial structure on the scales of importance to these sub-areas by any of the models. For example, only three of the models have winter ice cover occurring in the GSL as observed; all the models have greater March ice cover in the Labrador Sea than observed (some by a substantial amount); and the springtime extension of ice cover to the Grand Bank is not reproduced in any models. This lack of agreement is actually not surprising considering the relatively coarse spatial resolution of the ice and ocean models in the region compared to the scales of important ocean features such as the straits connecting the Arctic and NW Atlantic oceans and the width of the Labrador Current. Because some of the models (e.g. CanESM2) have limited (if any) ocean transport through the CAA, a realistic representation of the ocean climate in BB should probably not be expected.

#### **4b Spatial Distribution of Projected SIC Climate Changes in Six ESMs**

Although the ESMs may not resolve the regional details of SIC variability, it is nevertheless useful to examine the projected broad-scale changes, both for implications for sea ice itself and for the interpretation of changes in other variables such as TOS. In this subsection we examine the projected changes for two seasons in which sea ice is of particular importance to the Atlantic LAB – winter (represented by February) because of ice cover in the GSL and deep convection in the Labrador Sea, and spring (represented by May) because of sea ice extending down the Labrador Shelf to the Grand Bank.

Figures 4-2 and 4-3 show the bi-decadal distributions of SIC for February and May, respectively, in the six ESMs for 1986-2005 from the Historical simulations and for 2046-2065 from the RCP8.5 simulations. While the SIC patterns differ in the different models, there is a clear reduction in the equatorward extent of sea ice in both seasons in all the models for the future. The details of this can be seen better in the corresponding SIC change fields presented in Figure 4-4. While the exact locations and spatial extent of the areas of SIC reduction, as well as the magnitude of the reductions, vary from model to model, there are areas where SIC reduction is more than 20% in all models and in both months. The exception is HadGEM2-ES in May when the changes within the Atlantic LAB are smaller. This points to a consistent tendency for a reduced equatorward extent of sea ice in the Atlantic LAB on the 50-Year time scale, even though the details of the timing and location from particular models may not be reliable.

The bi-decadal ensemble mean SIC fields in January, March and May for 1986-2005 (from the Historical simulations) and for 2046-2065 (from the RCP8.5 simulations) are shown in Figure 4-5, indicating the overall winter-spring evolution of SIC in the ESMs. The corresponding projected change fields are shown in Figure 4-6, for both RCP4.5 and RCP8.5. As expected, the areas and magnitudes of the changes are smaller for RCP4.5. The general feature of reduced sea ice concentration in the Atlantic LAB is consistent with observations of an overall decline in sea ice extent in the LAB over the past half century (e.g. Henry 2011; Tivy et al. 2011; Cavalieri and Parkinson 2012; Peterson and Pettipas 2013).



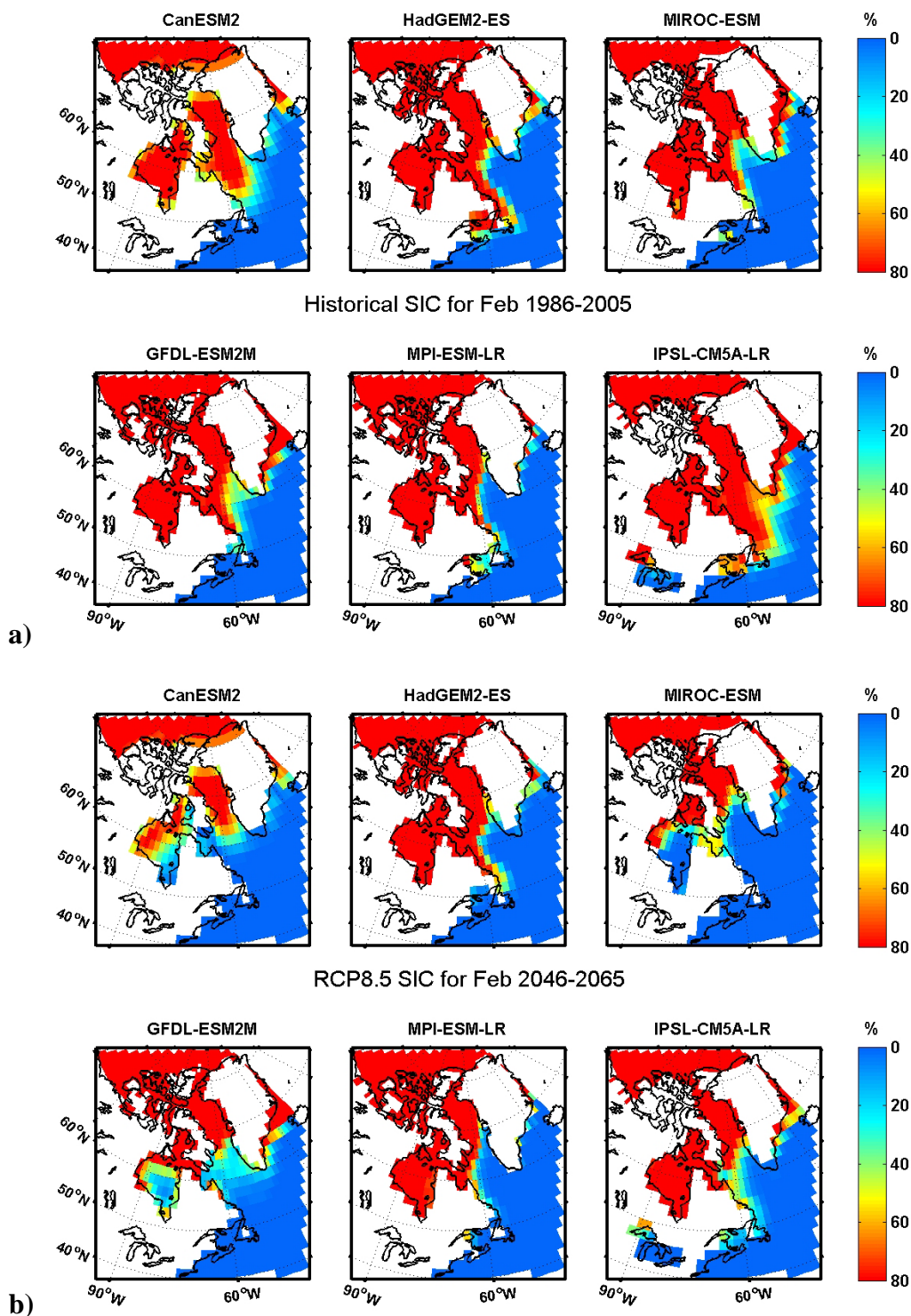


**Figure 4-2** Bi-decadal mean SIC distributions in February for a) 1986-2005 from the Historical simulations, and b) 2046-2065 from the RCP8.5 simulations from the six ESMs. Data interpolated to the common  $2^{\circ} \times 2^{\circ}$  grid (Fig. 2-1) were used. The differences in the apparent land areas (white, except for northeast corner) in the different models reflect a combination of their native grids and the interpolation grid.



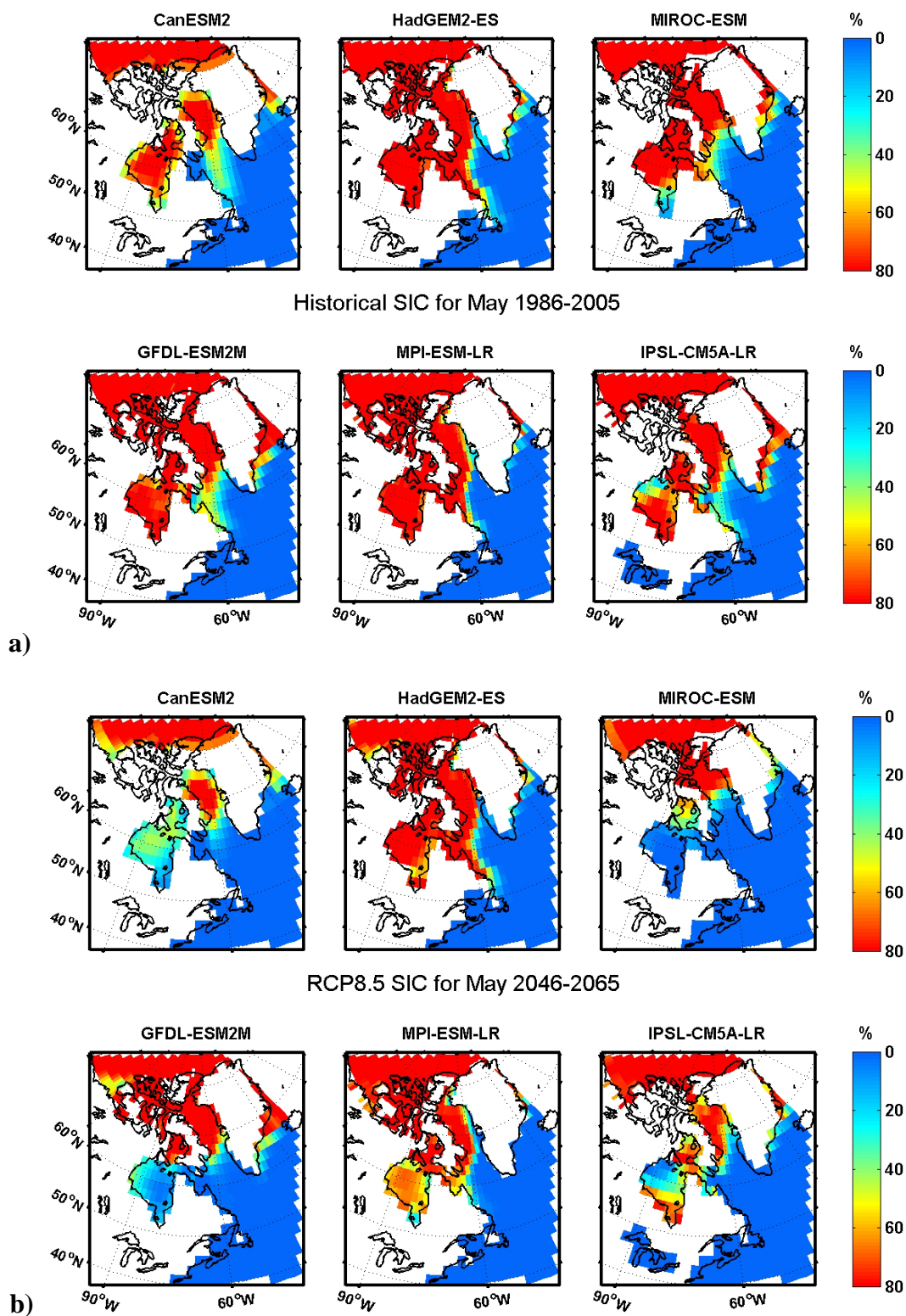


**Figure 4-3** Bi-decadal mean SIC distributions in May for a) 1986-2005 from the Historical simulations, and b) 2046-2065 from the RCP8.5 simulations from the six ESMs (see Fig. 4-2 for details).

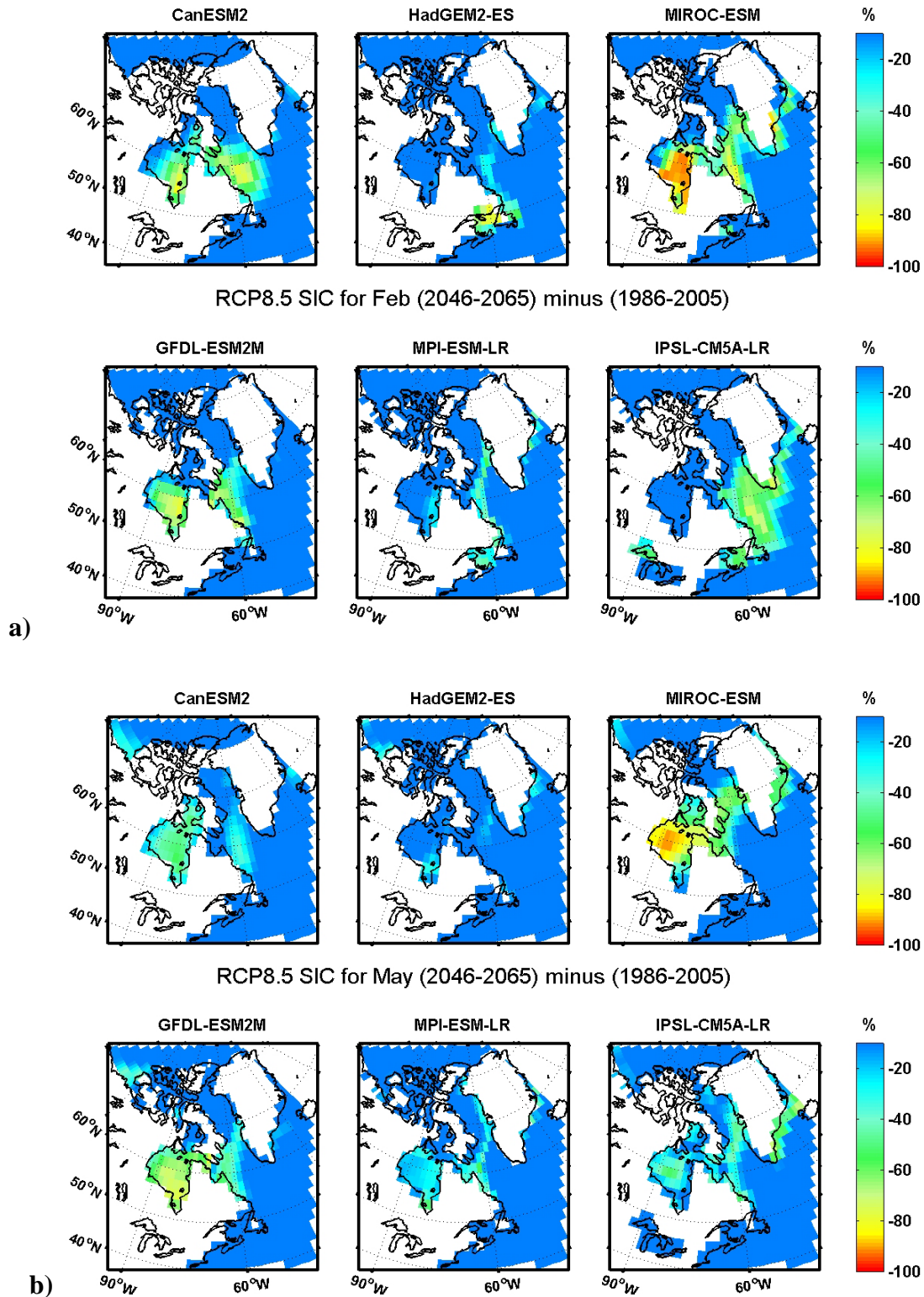


**Figure 4-4** Climate changes in bi-decadal monthly mean SIC from 1986-2005 in the Historical simulations to 2046-2065 in the RCP8.5 simulations from the six ESMs for a) February and b) May (see Fig. 4-2 for details).

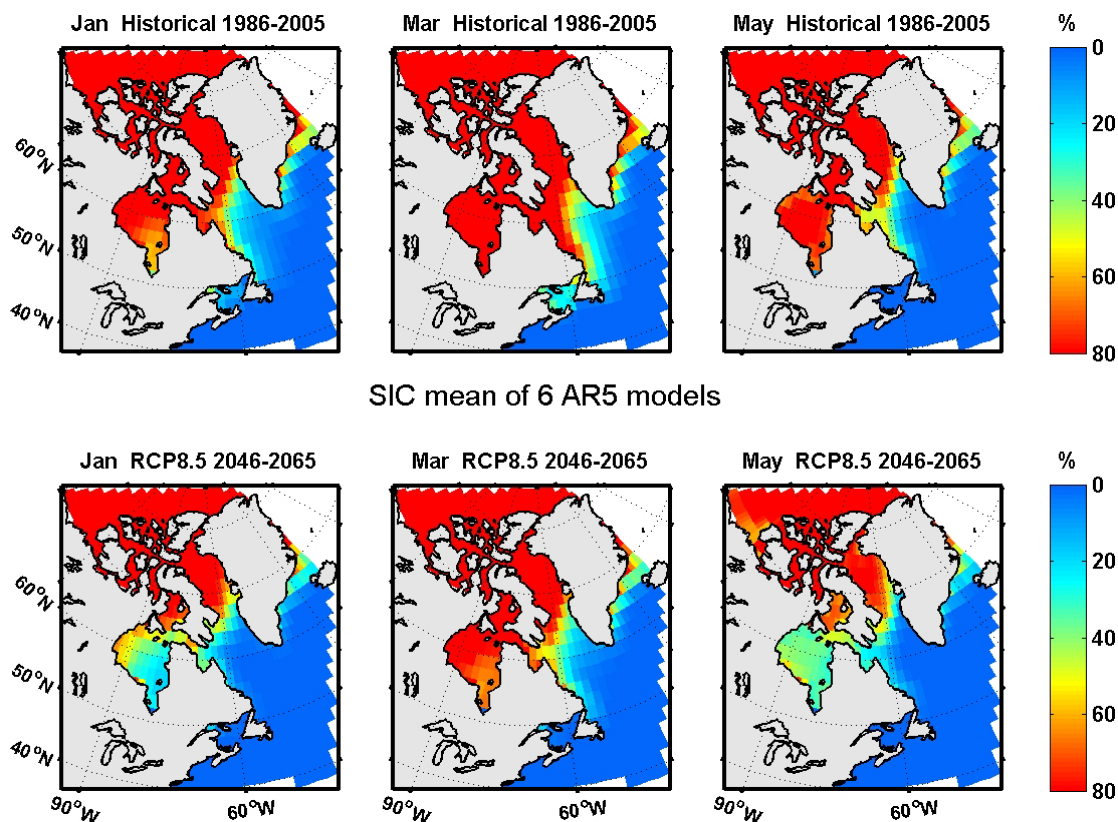


**Figure 4-5** Ensemble mean bi-decadal monthly SIC for January (left), March (middle) and May (right) for 1986-2005 from Historical simulations (upper) and 2046-2065 from the RCP8.5 simulations (lower), from the six ESMs using interpolated data.

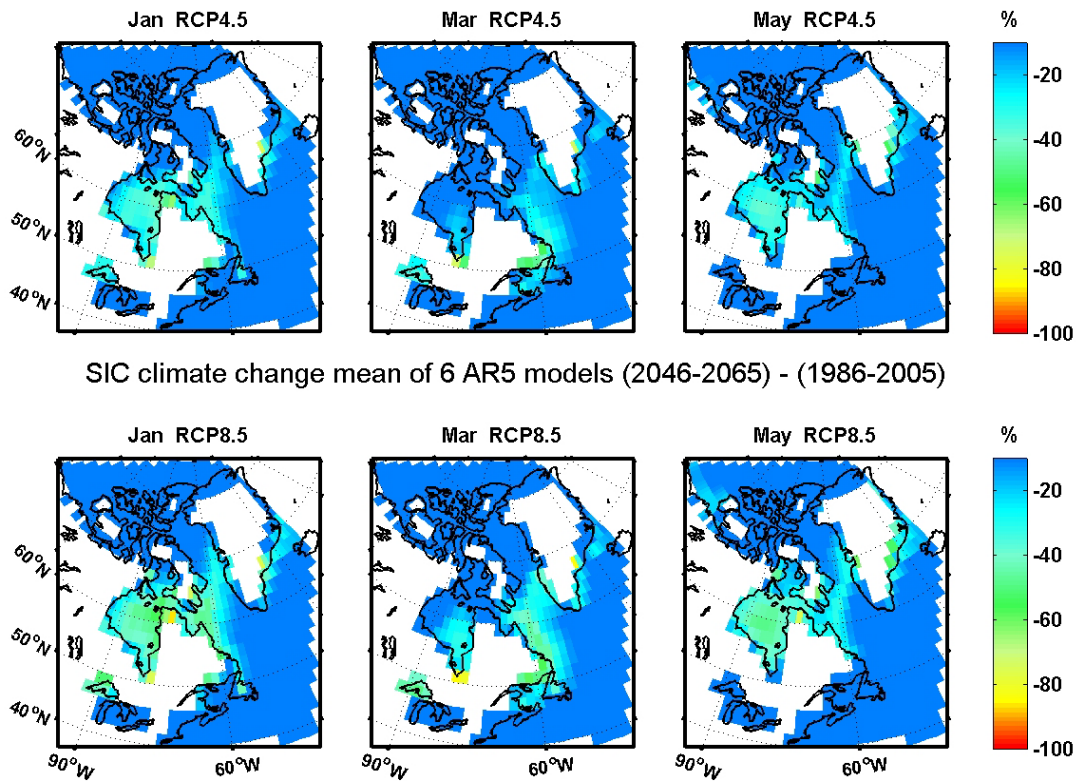


**Figure 4-6** Ensemble-mean climate change from 1986-2005 to 2046-2065 in bi-decadal monthly SIC (percentage) for January (left), March (middle) and May (right) for RCP4.5 (upper) and RCP8.5 (lower), using interpolated data.

## 5 Surface Ocean Temperature (TOS or SST)

In this section we examine the spatial and temporal variability of TOS<sup>8</sup> (essentially Sea Surface Temperature or SST) in the ESMs, focussing on the Atlantic LAB and starting with an exploratory comparison with observations. Complementary displays of TOS change patterns for a larger “Canada” domain which includes Canadian Arctic and Pacific waters are presented in Appendix C.

TOS fields for February and August are presented to represent model results for winter and summer, respectively. Considering that the observed surface mixed layer depth is typically 50-200m in the NW Atlantic (NWA) in winter, and that average (spatially) winter mixed layer depths in the five ESMs examined by Lavoie et al. (2013a) are greater than 100m, the February surface temperature (TOS) fields and changes should be representative of at least the upper 50m. In contrast, because the observed and modelled surface mixed layer depths in summer are typically 10-20m, the August fields and changes presented here should be considered as representative of the upper 10m or so, with the temperatures and climate changes averaged over the upper 50m expected to be lower and smaller, respectively.

### 5a Comparison with Observed Spatial Distributions and Temporal Variability

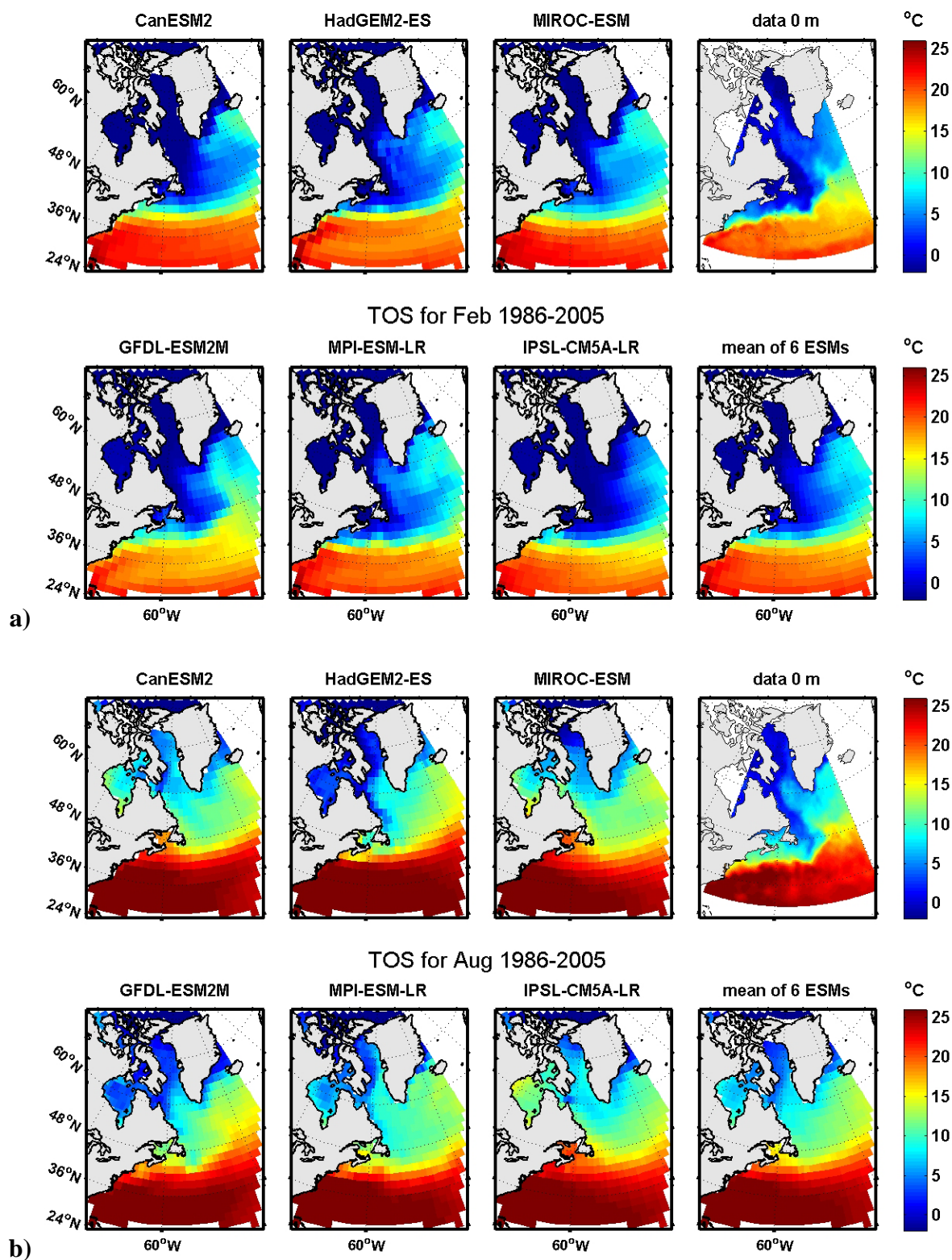
Figure 5-1 shows the bi-decadal mean distributions of TOS for the six ESMs for February and August during the Historical 1986-2005 period, together with the observed climatologies (1946-2005) obtained from I. Yashayaev of DFO-BIO. There is qualitative similarity between the models and observed fields in the seasonal change ( $\sim 10\text{-}15^{\circ}\text{C}$ ) from winter to summer, and in the large-scale contrast ( $\sim 20\text{-}25^{\circ}\text{C}$ ) of subpolar and subtropical waters in the NWA. However, there are noticeable differences among the models and observations in the spatial structure of the important subpolar-subtropical water boundary. In particular, the separation position of the Gulf Stream (GS) from the shelf edge is too far north in all the models compared to the observed position near Cape Hatteras, and the North Atlantic Current (NAC) does not extend far enough north to the northeast of Flemish Cap (in the so-called Northwest Corner) in the model data. This results in subtropical water extending too far north to the west of the Grand Bank and not far enough north to the northeast of Flemish Cap (see Figure 2-4 for locations). This can alternatively be described as subpolar water not extending far enough equatorward on the Atlantic shelf/slope, and extending too far eastward in the offshore north of Flemish Pass. The present ESMs’ difficulty in reproducing the positions of the GS and NAC is not surprising considering the typical  $1\text{-}2^{\circ}$  grid size in their ocean models and previous high-resolution ocean model studies of this problem (e.g. Bryan et al. 2007).

Together with the differences in the winter-spring SIC distributions between the models and observations, and with the differences in surface salinity discussed in the next section, the TOS fields raise serious questions about the realism of the spatial structure of the subpolar and subtropical gyres in the Atlantic LAB in the ESMs, similar to deficiencies previously identified in AR4 models (de Jong et al. 2009; Loder et al. 2011).

---

<sup>8</sup> Temperature of the Ocean Surface (TOS) is the variable name used in CMIP5. We refer to it as Surface Ocean Temperature or TOS. From an observational perspective, it is often referred to as Sea Surface Temperature or SST.

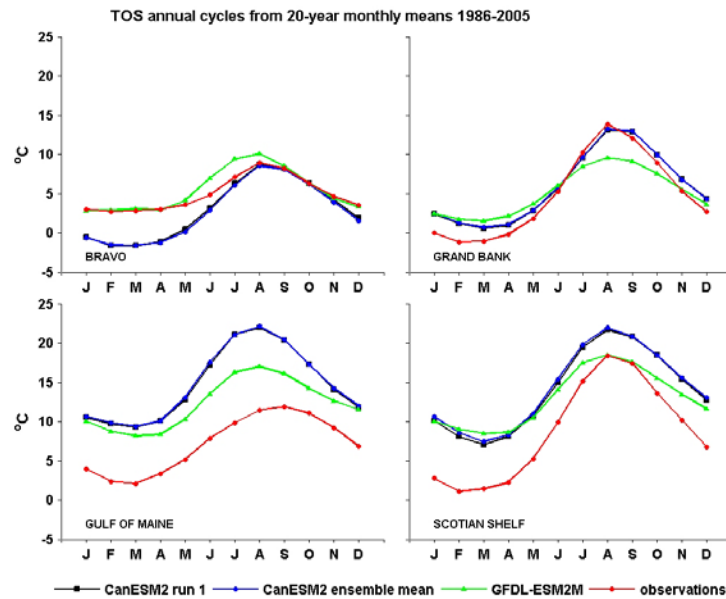




**Figure 5-1** Observed surface temperature climatologies for 1946-2005 (top right panels; from I. Yashayaev) and TOS fields (interpolated to a common grid) for the NWA from the Historical simulations (1986-2005) from the six ESMs in a) February and b) August.

Figures 5-2 and 5-3 compare the temporal variability in TOS in the ESM Historical simulations, with observed surface temperature annual cycles and interannual time series from DFO's Atlantic monitoring programs. The four sites with the longest observational records are used: OWS Bravo in the Labrador Sea, Station 27 on the Grand Bank (GB) off St. John's, Emerald Basin on the Scotian Shelf (SS) off Halifax, and Prince 5 in Passamaquoddy Bay adjoining the Gulf of Maine (GoM). It should be noted that the model position used for the GoM is only an approximation to the coastal Prince 5 site such that some differences in the means are expected.

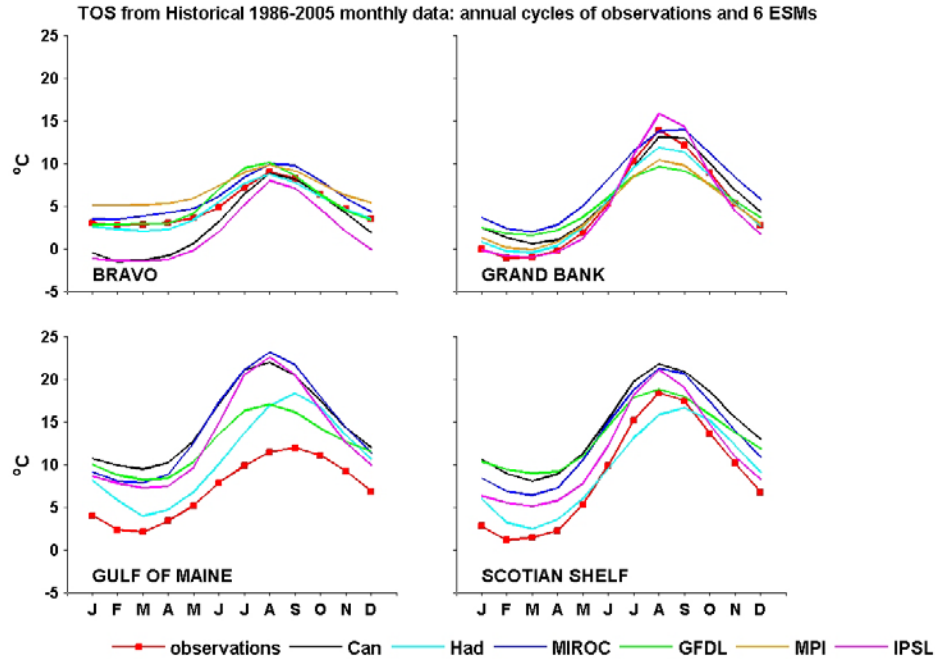
We start with an observational comparison of the bi-decadal annual cycles from run 1 of the CanESM2 and GFDL-ESM2M simulations and from the ensemble mean of the five available CanESM2 runs (Figure 5-2). The CanESM2 annual cycles for run 1 and its ensemble mean are essentially the same, and there is qualitative agreement among the annual cycles in both models and those observed. However, there are significant quantitative differences among the means and cycles from the two models and those observed at all 4 sites. The bi-decadal mean in both models is 4-8°C warmer than that observed in the GoM and SS (consistent with the northward extension of the subtropical gyre in Figure 5-1), but similar to that observed on the GB (differences of 0.3-1.1°C). At Bravo, the GFDL-ESM2M mean is similar to that observed while the CanESM2 mean is smaller than observed by ~2°C. The amplitude of the annual cycle in GFDL-ESM2M is smaller than observed at all 4 sites, while that in CanESM2 is larger than observed at Bravo and in the GoM, but smaller than observed on the GB and SS. There is approximate agreement among the phases but there are still differences in some cases.



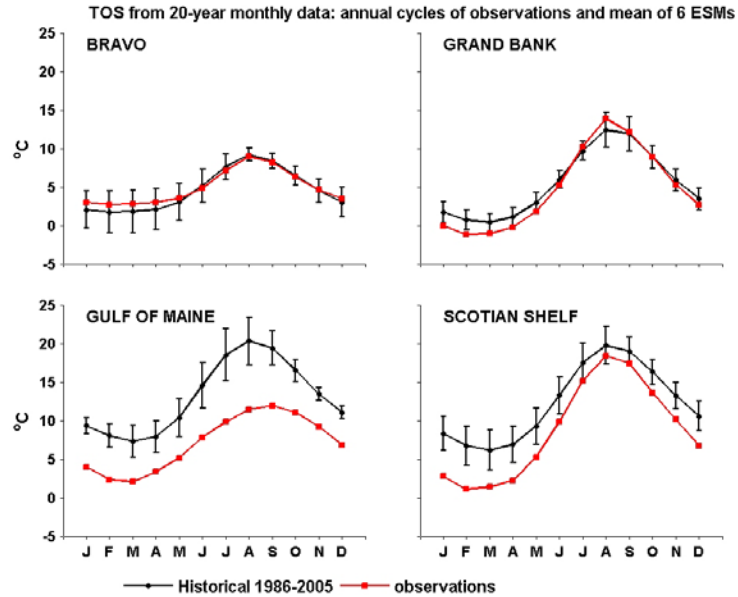
**Figure 5-2** Model and observed annual cycles of TOS for 1986-2005 at four DFO observational sites: Labrador Sea (Bravo), Grand Bank (Station 27), Gulf of Maine (Prince 5) and Scotian Shelf (Emerald Basin) (see Fig. 2-2 for locations). Model cycles are shown for run 1 and the ensemble mean from CanESM2, and for run 1 from GFDL-ESM.

Figure 5-3a shows a similar comparison of annual cycles for run 1 of each of the six ESMs and the observations, while Figure 5-3b compares the ensemble-mean annual cycles from these ESM runs with the observations. At Bravo, three other ESMs have means and annual cycles similar to

those of GFDL-ESM2M and observed, while those in IPSL-CM5A-LR are similar to those in CanESM2 (with lower winter values than observed) (Figure 5-3a). On the GB, the amplitude of the annual cycle is smaller than observed in five of the ESMs and slightly larger in one, with winter TOS in the models higher than observed and summer TOS generally lower than observed.



**Figure 5-3a** Model and observed annual cycles of TOS for 1986-2005 at the same four sites as in Figure 5-2. Model cycles (based on interpolated data) are shown for each of the six ESMs.



**Figure 5-3b** Ensemble-mean model (over the six ESMs) and observed annual cycles of TOS for 1986-2005 at the same four sites as in Figure 5-2. The inter-model standard deviations are indicated by the error bars on each side of the ensemble means.



On the SS and in the GoM, the model TOS is higher than observed at all sites and in all months, except for HadGEM2-ES and GFDL-ESM2M on the SS in summer. The observed climatology in Figure 5-1 indicates that the offshore gradient in TOS probably contributes to the model-vs-observation differences in the GoM. However, the different spatial patterns between the models and observations in that same figure suggest that the northward displacement of subtropical water in the ESMs is a major factor to the differences at the GoM and SS sites in Figure 5-3a, and possibly also a factor the differences on the GB.

The ensemble-mean (bi-decadal) monthly TOS values are within, or close to being within, the inter-model standard deviations from the observed monthly means in all months at the LS and GB sites, and in the summer months at SS site (Figure 5-3b). In contrast, they are substantially more than a standard deviation from the observed means in winter on the SS and in all months in the GoM. However, the implications of these differences are uncertain since the confidence that one can place in the ensemble mean of the ocean fields from the ESMs remains unclear.

Figure 5-4 compares the time series of annual mean TOS in the Historical simulations from two ESMs (CanESM2 and GFDL-ESM2M), with observed annual-mean time series from DFO's Atlantic monitoring programs at the same four sites. The time series clearly show the differences in the long-term means mentioned above, as well as indications that the observed mean is slightly lower than in both models on the GB and has an intermediate value between the models at Bravo. Perhaps the most notable feature is the interannual-to-decadal-scale variability whose amplitude varies between models and among the sites. There is some similarity but also differences among the CanESM2 runs at all four sites, and little similarity between these and those in GFDL-ESM2M and the observed data. The TOS variability in the models is much larger than observed at Bravo, with a predominant multi-decadal variation in GFDL-ESM2M and predominant higher-frequency variability in CanESM2, and no indication in the models of the observed lower values in the late 1980s and early 1990s (Yashayaev 2007). The amplitude of the variability in the models is closer to that observed at the other three sites, but there is no indication in the models of the observed cool periods on the GB in the 1950s, 1970s, and 1990s (e.g. Colbourne et al. 2012), and on the SS and in the GoM in the 1960s (e.g. Petrie and Drinkwater 1993). This is not unexpected, because it would be somewhat surprising if the models were able to reproduce the observed decadal-scale ocean variability in the region (e.g. Bindoff et al. 2007; Palmer et al. 2009; Loder and Wang 2013) without having good representations of the gyre-gyre interactions, and air temperature and sea ice variability.

The magnitudes of the model trends (not shown) show some similarity with the observations, but there is a large variation among the trends from the different CanESM2 runs at all sites except in the GoM, such that the trend from a particular run (like that from GFDL-ESM2M) is probably not reliable. At Bravo, the model trends range from  $-0.1$  to  $+0.2$  °C/decade compared to a trend of  $0.0$  °C/decade in the observations. For the GB, the model trends are in the range  $0.13$ - $0.22$  °C/decade compared to  $0.11$  °C/decade for the observed trend. For the SS and GoM, the model trends are in the ranges  $0.04$ - $0.26$  °C/decade and  $0.18$ - $0.23$  °C/decade, respectively, compared to  $0.09$  °C/decade for the observed trends. Thus, it appears that the model Historical simulations are not able to reproduce the observed TOS trends since 1950 with any quantitative accuracy. It should be noted however that, due to decadal-scale variability, the observed trends are dependent on the period examined such that the observed trends indicated above (for 1950-2011) are generally not the best estimates of long-term trends for climate change applications.

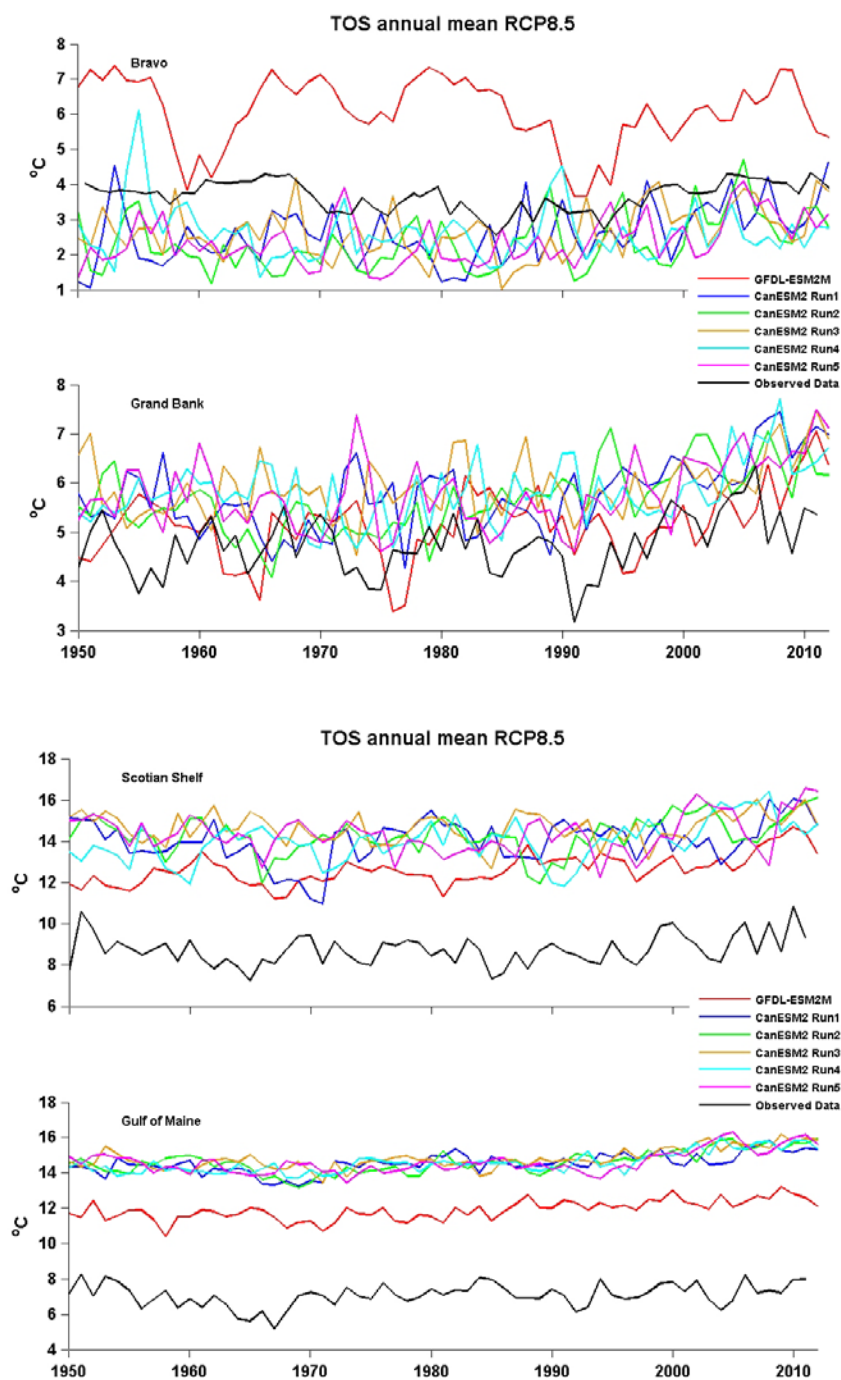


**Figure 5-4** Comparison of model annual mean time series of TOS at four sites with observations for 1950-2012. Model data are for run 1 from GFDL-ESM and five runs from CanESM2, for the concatenated Historical and RCP8.5 simulations. Observed time series are for the ocean surface at three sites, but for the 16-150m interval at Bravo. The long-term annual-mean surface temperature at Bravo is  $\sim 1^{\circ}\text{C}$  higher than that over the 16-150m interval, so the actual observed TOS values are generally intermediate between those from CanESM2 and GFDL-ESM2M in Figure 5-2.

## 5b Spatial Distribution of Projected TOS Climate Changes in Six ESMs

The bi-decadal TOS fields for 2046-2065 from the six ESMs for RCP8.5 are presented in Figure C-1 (Appendix C), using February and August to represent the seasonal variation (analogous to Figure 5-1 above). General warming is apparent, but the TOS climate change fields in Figure 5-5 show the magnitude and spatial pattern better.

Notable features of the change fields in Figure 5-5 include: i) the substantial spatial structure with latitudinal gradients and other features; ii) the differences in the patterns among the models; iii) the presence of areas with cooling instead of warming, particularly in winter; and iv) the greater overall warming in summer than winter. There is an overall tendency for a mid-latitude zonal band of greater warming, with the largest magnitude occurring in summer, extending eastward from the Scotian Shelf/Slope Water region. There is some similarity in this band in three models in winter, and also in a fourth model in summer. Candidate contributors to this band include a poleward expansion (shift) of the subtropical gyre (Gulf Stream) in the models (e.g. Wu et al. 2012), and the band of enhanced TAS warming extending eastward over the region in the models that have the enhanced TOS warming band (Figure 3-4). Alternatively, the enhanced TOS could be contributing to the enhanced TAS. There is also a general tendency for limited warming in sub-Arctic areas (including BB) in winter that is consistent with continued sea ice cover. However, there is a wide variation in the summer changes amongst the models in these areas that is probably related to different sea ice coverage in the models. All the models have an area of cooling or substantially reduced warming southeast of Greenland, similar to that in the AR4 models and often attributed to a reduction in the Atlantic Meridional Overturning Circulation (AMOC) (e.g. Meehl et al. 2007; Drifhout et al. 2012). On the sub-basin (e.g. subpolar, subtropical, and transition zone) and regional (e.g. Labrador Shelf, GB and GSL) scales, there are similarities in the change patterns across most of the models but also differences such that the reliability of the projections from a particular model is unclear.

The ensemble statistics for these TOS change fields are presented in Figure 5-6, for both RCP4.5 and RCP8.5 (analogous to those for TAS in Figure 3-5). For a particular season, there is close similarity in the patterns of the change statistics for the two RCPs, with slightly greater (ensemble-mean) warming for RCP8.5 in February and a larger increase in warming for RCP8.5 in August. The greater warming in August is consistent with much of the spring-summer surface heat input being trapped in the shallow spring-summer mixed layer. The spread of TOS changes among the models is noticeably larger than the magnitude of the changes for the ensemble mean of the models. This is in contrast to the situation for TAS (Figure 3-5) where the spread and the mean had comparable magnitudes. The TOS standard deviations are also larger relative to the ensemble means, with comparable magnitudes in winter. This indicates that the changes for the ensemble mean of the models in February may not be significantly different from zero, in general, if a criterion related to two standard deviations is used. The magnitude of the inter-model differences is further illustrated by the distributions of, and differences between, the ensemble minimum values and ensemble maximum values shown in Figure C-4 (Appendix C). There is a clear indication there that, in spite of the much greater thermal inertia of the ocean, these particular ESMs have greater inter-model differences in their TOS in the NWA than in their TAS. This is consistent with a greater difficulty in representing the overall complexity of factors affecting TOS in the NW Atlantic than those affecting TAS.

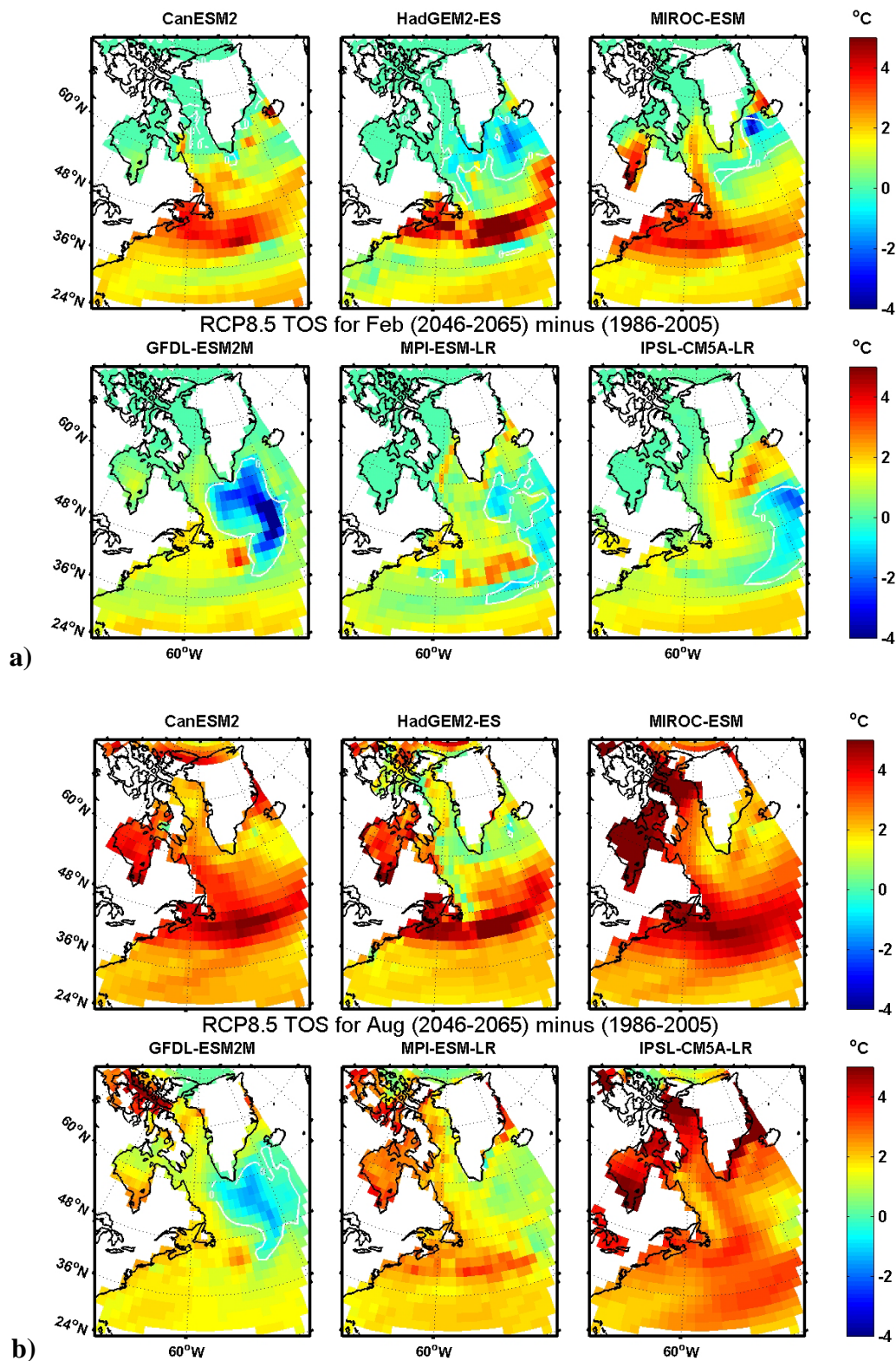


**Figure 5-5** Bi-decadal monthly TOS change fields from 1986-2005 to 2046-2065 for the NWA for RCP8.5 from interpolated data from the six ESMs for a) February and b) August. The white contour is the 0 °C isotherm.



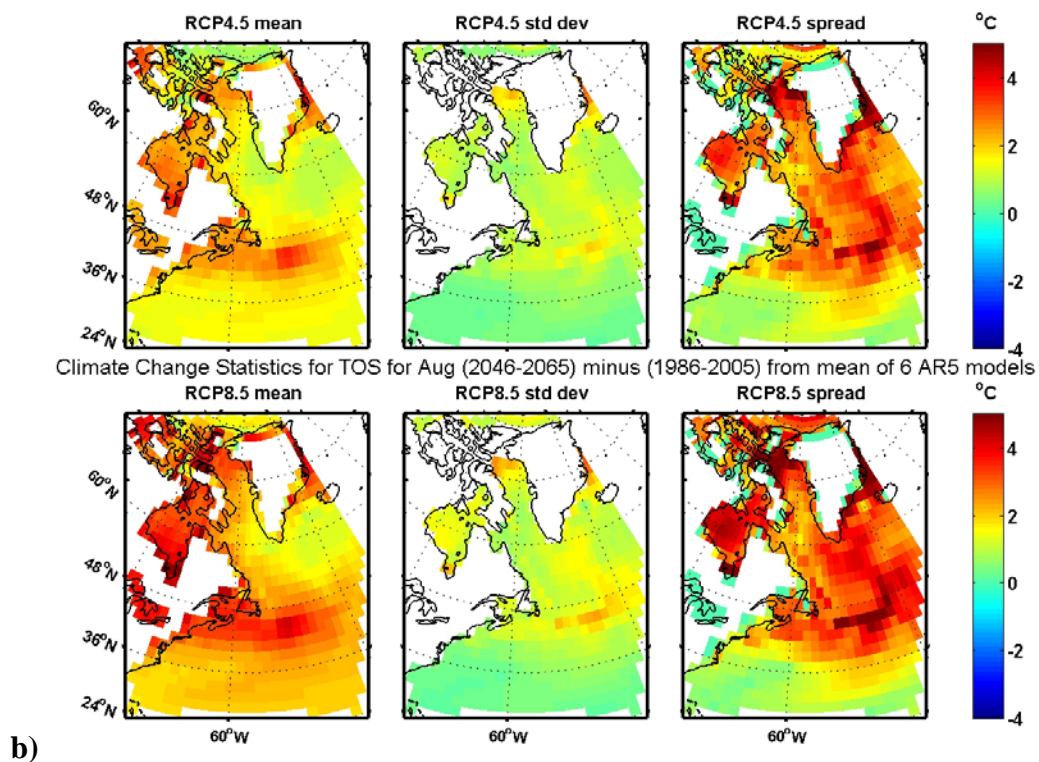
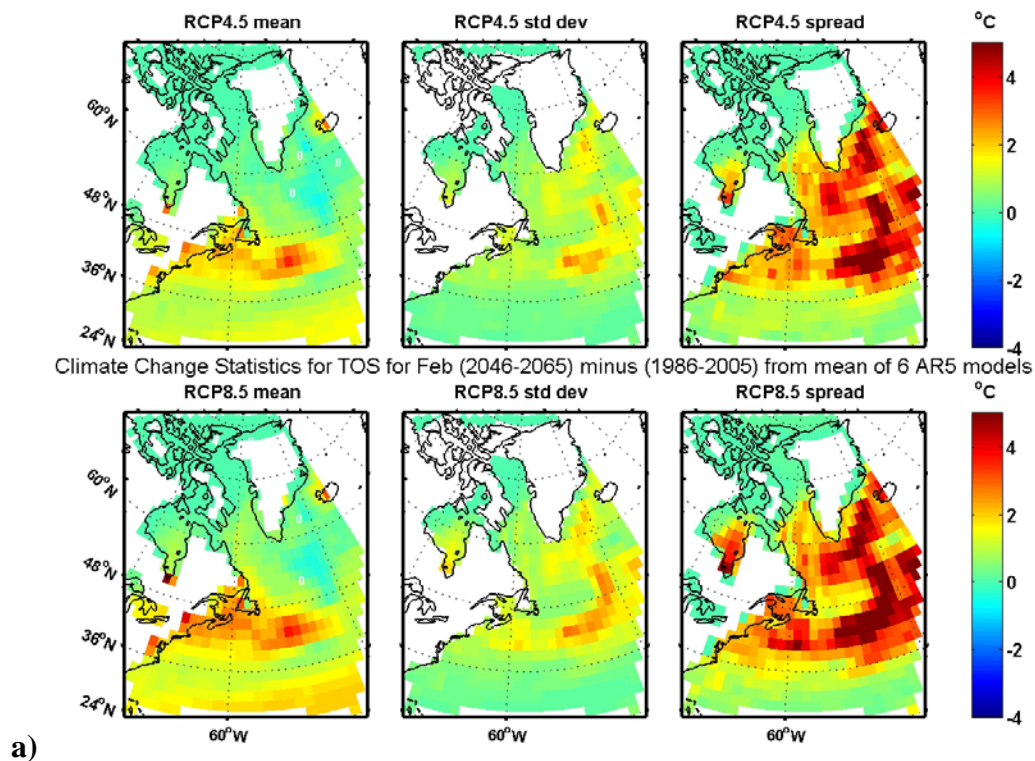


**Figure 5-6** Mean, standard deviation, and spread (maximum minus minimum) of bi-decadal TOS changes for the NWA for RCP4.5 and RCP8.5 in a) February and b) August, computed from the ensemble of bi-decadal change fields from the six ESMs (e.g. Fig. 5-5 for RCP8.5). The white contour in the “mean” panels is the 0°C isotherm.

In spite of the substantial differences among the models, there is nevertheless a smooth seasonal evolution of each model's fields and of the ensemble mean TOS, as illustrated by the monthly ensemble means in Figure 5-7.

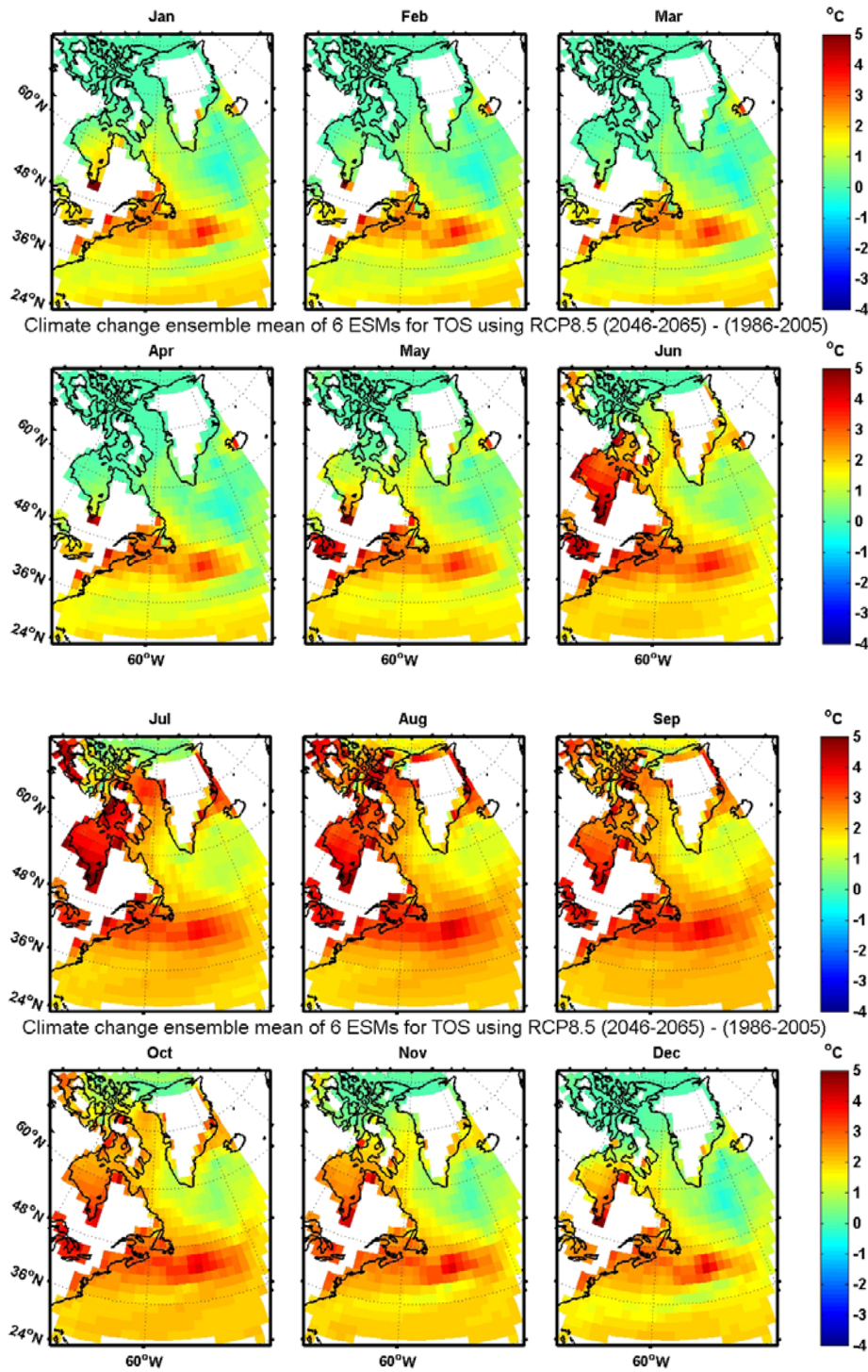


**Figure 5-7** Changes in bi-decadal monthly TOS from 1986-2005 to 2046-2065 for the NWA, from the ensemble mean of interpolated data from the six ESMs for RCP8.5, for the twelve months of the year.

To place these TOS changes in a broader perspective, Figures C-2 and C-3 (Appendix C) show the TOS change and statistics fields for the broader Canada domain. Substantial inter-model differences are apparent in the Arctic and Pacific LABs with the exception of the limited deviation from the freezing temperature in the Arctic in winter. In February, there is a clear indication that the mid-latitude western North Atlantic is a “hot spot” for an enhanced temperature increase (Wu et al. 2012) and the broader NWA a hot spot for variability among the ESMs. In August, there are comparable hot spots in other areas around Canada, particularly in the Arctic LAB.

### **5c Temporal Variability of Projected TOS Climate Changes in ESMs**

The projected future means and annual cycles of TOS for three of the observational sites discussed in Section 5a and for the GSL are presented in Figure 5-8a for 2046-2065 from RCP8.5 and the same two ESMs as in Figure 5-2, together with the means and cycles for 1986-2005 (note that, for the three previous sites, the latter are the same as those used for the observational comparisons in Figure 5-2). TOS increases are projected in all months at the GB, GSL and SS sites, but a decrease in TOS is projected in GFDL-ESM2M in winter at Bravo.

The climate changes in the bi-decadal monthly means for individual runs in CanESM2 and for the GFDL-ESM2M run are presented in Figure 5-8b. There is variability of up to 2 °C among the changes from the different CanESM2 runs which is substantially larger (relative to the magnitude of the change) than for TAS in Figure A-7. The changes in the GSL and on the SS have limited seasonal variations in both models (pointing to a change in the mean rather than annual cycle), but their magnitude in CanESM2 is about twice that of those in GFDL-ESM2M. The variability is more complex at the other two sites where there is a clear seasonal variation in the CanESM2 changes with a maximum in late summer at both sites, and minima in winter and fall at Bravo and on the GB, respectively, consistent with a shallower surface layer in summer. In contrast, there is a limited seasonal variation in the GFDL-ESM2M changes for the GB with magnitudes similar to the GFDL-ESM2M changes in the GSL and on the SS while, at Bravo, the GFDL-ESM2M changes have a seasonal variation with some similarity to those in CanESM2 data from winter to summer (but very different in fall). However, there is a large difference between the annual means of the Bravo changes in CanESM2 and GFDL-ESM2M, with the latter showing a projected decrease in TOS during most of the year and by over 1 °C in winter.

The ensemble bi-decadal means and annual cycles for 1986-2005 from the Historical simulations, and for 2046-2065 from the RCP4.5 and RCP8.5 simulations, of the six ESMs are shown in Figure 5-9a for a total of nine sites, together with the inter-model standard deviations for each ensemble. The ensemble monthly means for the past and future periods for both RCPs lie within their combined inter-model standard deviations of each other for all months and sites, reflecting the modest magnitude of the changes relative to the model uncertainties. The ensemble-mean future TOS values for RCP8.5 are slightly larger than those for RCP4.5, except in winter in BB where there is no TOS increase because of the continued presence of sea ice.

The inter-model and seasonal variability in the climate changes is apparent in the monthly TOS changes for the individual ESMs shown in Figure 5-9b, and in the ensemble means and inter-model standard deviations of the changes in Figure 5-9c.

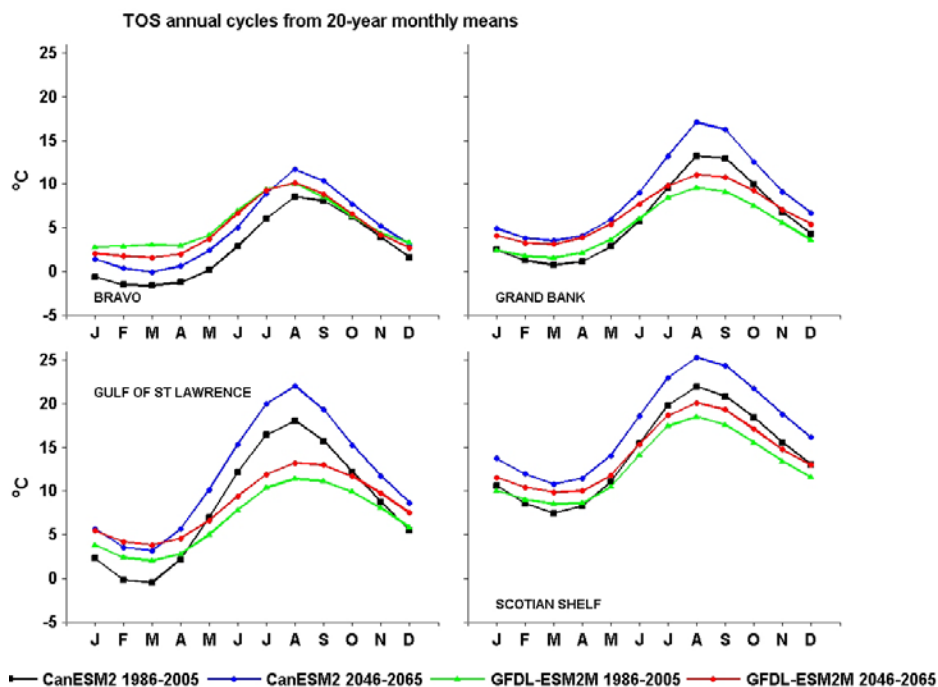


**Figure 5-8a** Annual cycles of TOS for Historical (1986-2005) and RCP8.5 (2046-2065) at four sites (Bravo, GB, Gulf of St. Lawrence or GSL, and SS) for the CanESM2 ensemble-mean of all runs and GFDL-ESM2M run 1 (see Fig. 2-2 for locations).

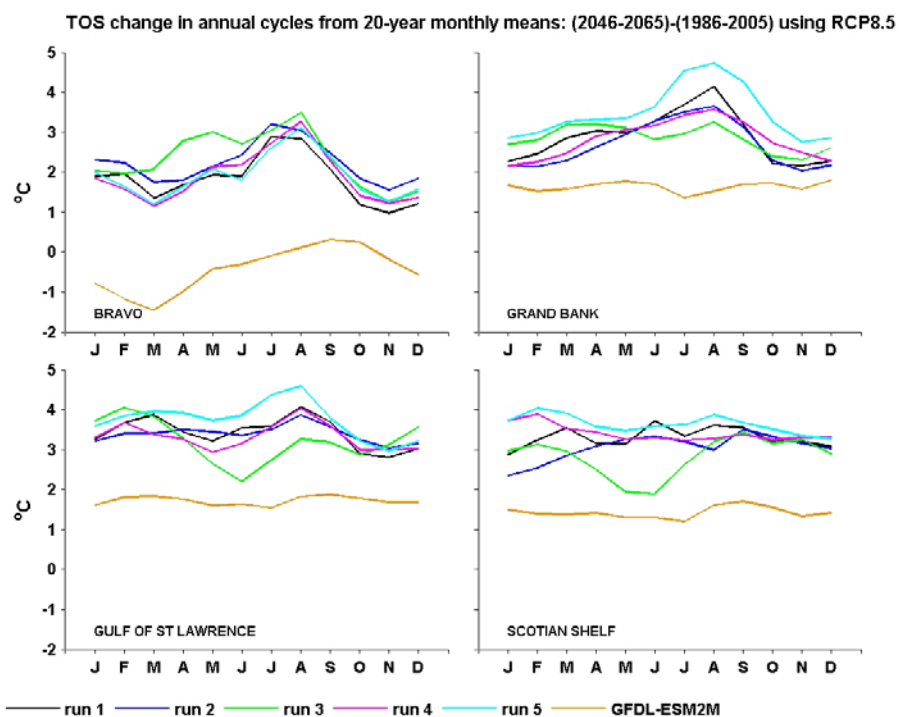


**Figure 5-8b** Changes in bi-decadal monthly mean TOS from 1986-2005 (Historical) to 2046-2065 (RCP8.5) at the four sites in Figure 5-8a for five runs of CanESM2 and run 1 of GFDL-ESM2M



The inter-model spread of the changes (Figure 5-9b) is typically in the 2–4 °C range at most sites, with the notable exceptions of Baffin Bay (BB) where there are no changes in winter, Newfoundland Basin where the spread is 3–6 °C due to a 7 °C increase in HadGEM2-ES, and the Grand Bank (GB) where the spread in winter is <2 °C (probably related to its shallow depths and near-freezing temperatures). This spread is comparable to the ensemble-mean change at most sites, with the exceptions of Bravo where the ensemble mean change is small and BB where there is a predominant seasonal variation in the changes. At most other sites, the seasonal variation in the climate changes differs among the models. At all sites except Bravo, the seasonal variation of the ensemble mean changes is small relative to the inter-model standard deviations (Figure 5-9c). There are however indications in most of the models of larger changes in summer than winter at most of the sites, consistent with the broad-scale difference between the February and August ensemble-mean change fields in Figures 5-5 and 5-6. The projected seasonality in the GSL is qualitatively consistent with that found by Chassé et al. (2013) from their regional ocean model forced by a down-scaled AR4 simulation for SRES A1B.

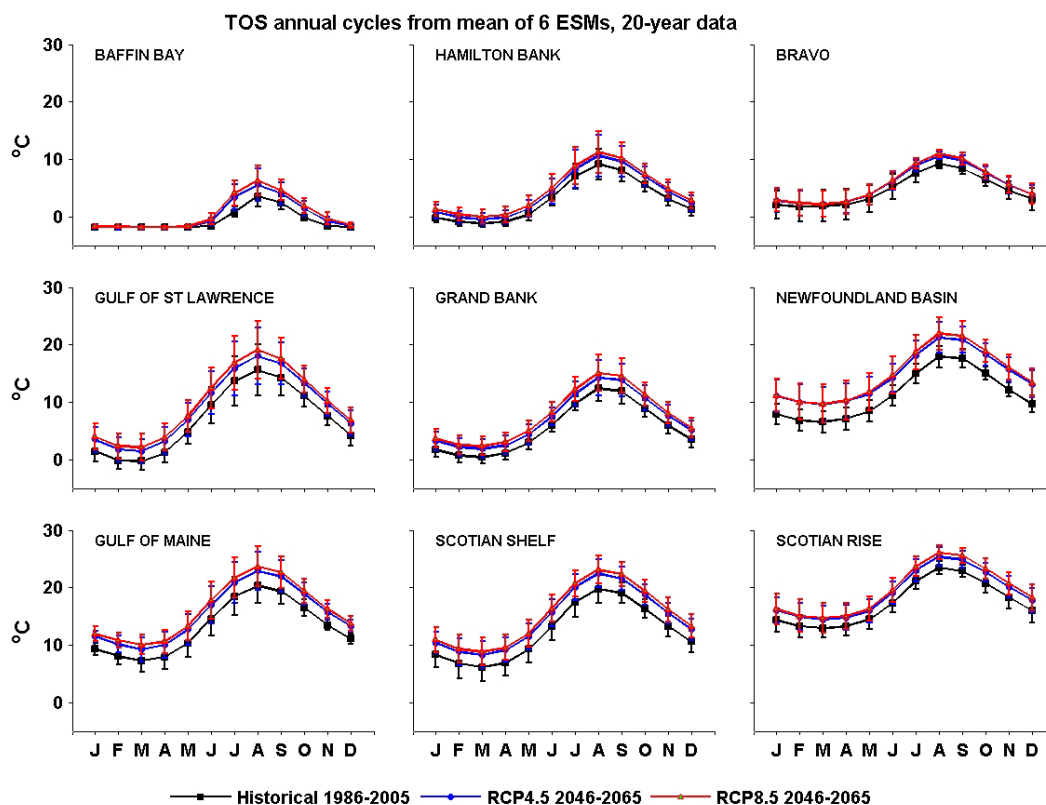


**Figure 5-9a** Ensemble-mean annual cycles (with standard deviations) of TOS from the Historical simulations for 1986–2005, and from the RCP4.5 and RCP8.5 simulations for 2046–2065, at nine sites for the ensemble of six ESMs. Five of the sites are the same as in Figures 5-2 or 5-8, while the locations of the other sites are shown in Figure 2-4.

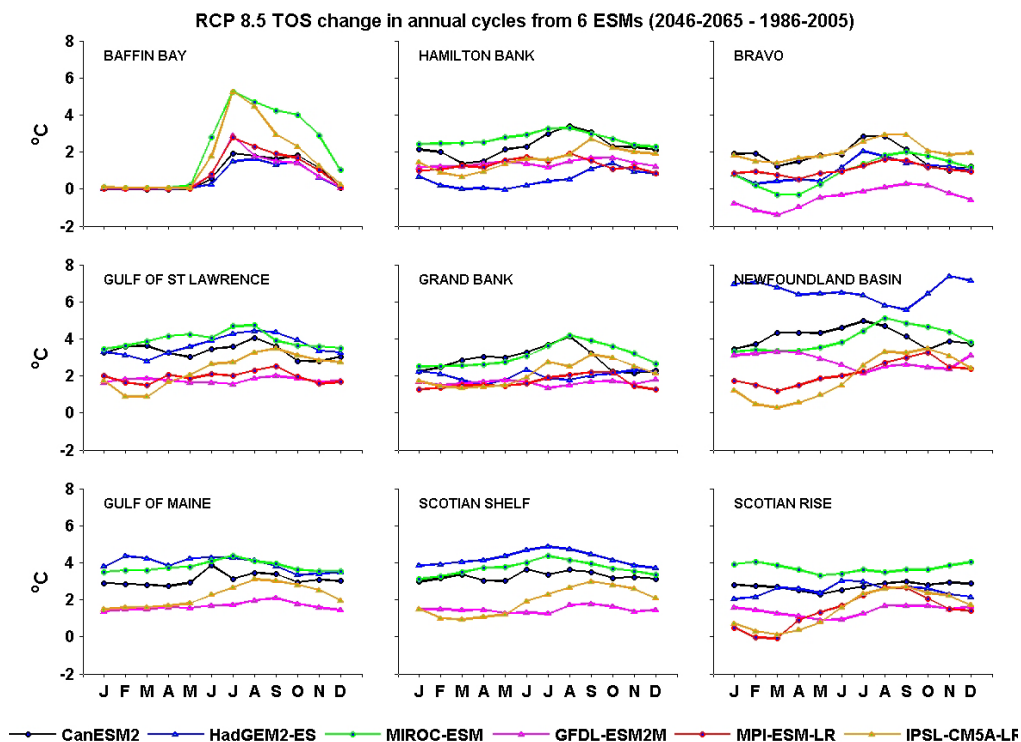


**Figure 5-9b** Changes in bi-decadal monthly mean TOS from 1986-2005 (Historical) to 2046-2065 (RCP8.5) at the nine sites in Figure 5-9a, in run 1 from the six ESMs.

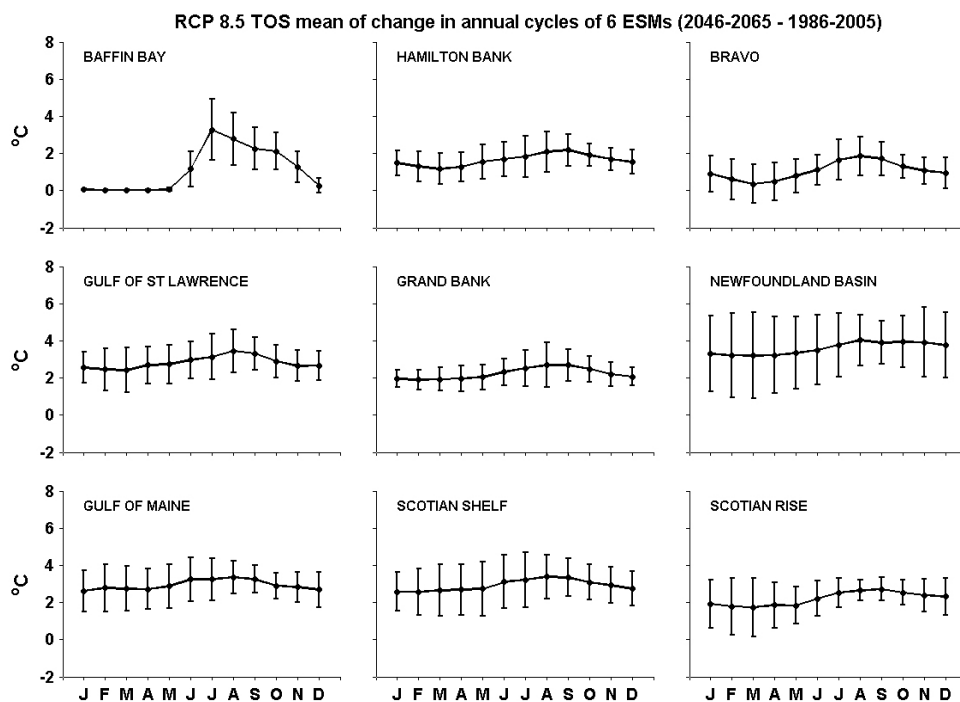


**Figure 5-9c** Ensemble means, and inter-model standard deviations, of the climate changes in bi-decadal monthly mean TOS shown in Figure 5-9b.

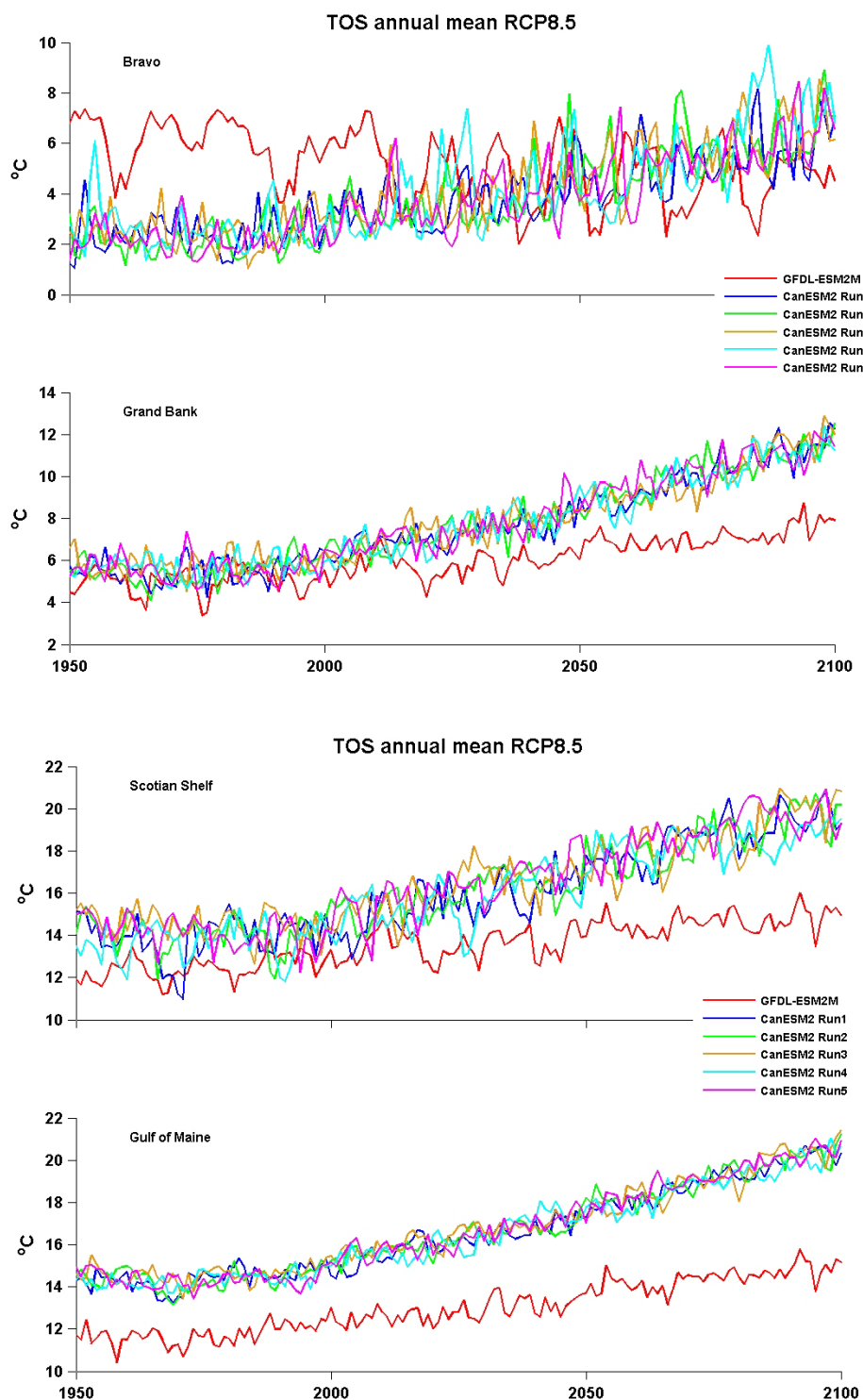


**Figure 5-10** Time series of annual means of TOS from CanESM2 (five runs) and GFDL-ESM2M (run 1) for 1950-2100 at the same four sites as in Figure 5-4 (Bravo, GB, SS and GoM).

The projected future evolution of annual-mean TOS in CanESM2 and GFDL-ESM2M at the four observational sites discussed in Section 5a is shown in Figure 5-10 where time series from both

the Historical simulations (as in Figure 5-4) and RCP8.5 simulations to 2100 are presented. There are clear differences in the future long-term trends from the two models with relatively-monotonic (low-frequency) increases at all four sites in the CanESM2 data and at the three southernmost sites in the GFDL-ESM2M data, but with larger magnitudes in CanESM2. On the other hand, the high-frequency (interannual-to-decadal) variability at the three southern sites has similar magnitude (but different details) in the two models (and among the CanESM2 runs) and does not show a noticeable change in character in the 21<sup>st</sup> century. There are notable differences in the interannual-to-decadal variability, as well as in the long-term trends, in the models at Bravo, with the variability in the GFDL-ESM2M time series changing from predominantly multi-decadal in the 20<sup>th</sup> century to decadal scale in the 21<sup>st</sup> century while the overall trend is negative (decreasing; in contrast to CanESM2 and the other sites). The interannual-to-decadal scale variability in the CanESM2 series has an increasing magnitude in the 21<sup>st</sup> century while the overall trend is positive (increasing). These results reinforce concerns about how well the AOGCMs in AR4 (e.g. de Jong et al. 2009) and in AR5 (because their ocean components generally have similar spatial resolution) deal with atmosphere-ice-ocean coupling in the NWA.

## **5d Estimates of TOS Changes from Six ESMs at Representative Locations**

This subsection provides quantitative estimates of the TOS climate changes at selected locations across the Atlantic LAB, for the ACCASP 50-Year time scale.

One reasonable approach is to compute the spatial average of the change fields over regions or ocean features of interest. Along this line, Lavoie et al. (2013a,b) have computed time series and trend lines for the areal averages of various physical and biogeochemical variables from five of the ESMs used here. Their reports provide results for two large areas within the Atlantic LAB: the Labrador Sea (between 54 and 67°N) and a NW Atlantic (AtlNW) domain (west of 47°W and between 37 and 54°N); and two sub-areas of the Arctic LAB: Baffin Bay and Hudson Bay. They find that, although the average mean temperature over the AtlNW domain differs by up to 3.5°C across the five models, the trends over the next 50 years (2012-2062) are positive in all the models and within a factor of about two in magnitude: 0.2-0.4°C/decade for RCP4.5 and 0.3-0.6°C/decade for RCP8.5. These trends correspond to changes in the range of 1-3°C on the 50-Year scale.

To provide information more specific to oceanographic and/or ecological regions (or subregions) of interest to the Atlantic ACCASP, one could either average over smaller areas or spatially interpolate from neighbouring grid points to particular sites. The latter has been done here following the approach in Sections 5a and 5c. TOS change statistics analogous to those in Figures 5-6 and C-4 are provided in Table 5-1a for ten “Shelf” sites and in Table 5-1b for fifteen “Off-Shelf” sites in the Atlantic LAB (see Figure 2-4 for locations). Shelf sites for which interpolation estimates were available from at least five of the six models are included. The notable difference from the statistics in Figures 5-6 and C-4 is the use here of a 12-member ensemble with two RCPs per model and six ESMs in total (instead of a 6-model ensemble for each of the RCPs as used previously). It should be emphasized that, while two significant figures are provided for the change values, the changes should probably be considered at the level of only one significant figure in any application.

**Table 5-1a** “Shelf” sites in the Atlantic LAB with statistics of the projected TOS changes between 1986-2005 and 2046-2065 from the six ESMs and two RCPs (12-model ensemble) for each of February and August. Changes at the sites have been estimated from bilinear interpolation from adjacent grid points. The spread is the difference between the minimum value for RCP4.5 and the maximum value for RCP8.5 (it should be noted that, in a few cases, the actual spread is greater than given here since the minimum change can occur in an RCP8.5 member or the maximum in an RCP4.5 member). See Figure 2-4 for site locations.

AR5 TOS	February					August			
Shelf Sites	Min	Mean	Max	Spread		Min	Mean	Max	Spread
N Labrador Shelf	0.0	0.4	1.2	1.2		0.7	2.2	3.3	2.5
Hamilton Bank	-0.1	1.1	2.4	2.6		-0.1	1.8	3.4	3.5
NE Nfld Shelf	-0.1	1.2	2.4	2.5		-0.2	1.8	3.7	3.9
Flemish Cap	0.2	1.4	2.4	2.2		0.9	2.7	4.5	3.5
Grand Bank	1.0	1.7	2.5	1.5		0.6	2.3	4.2	3.6
S Grand Bank	0.9	2.0	3.4	2.5		1.2	3.0	4.9	3.7
S Nfld Shelf	0.9	2.0	3.2	2.3		1.1	2.9	4.7	3.6
Gulf St Lawrence	0.5	2.2	3.6	3.1		1.1	2.9	4.7	3.6
E Scotian Shelf	1.1	2.4	4.7	3.6		1.0	3.0	4.8	3.8
Scotian Shelf	0.9	2.3	3.9	3.0		1.2	3.0	4.7	3.5
W Scotian Shelf	1.0	2.3	4.1	3.1		1.4	3.0	4.4	3.0
Georges Bank	0.7	2.0	3.6	2.9		1.3	2.6	3.8	2.5

**Table 5-1b** “Off-Shelf” sites in the Atlantic LAB with the same statistics as in Table 5-1a. See Figure 2-4 for site locations.

AR5 TOS	February					August			
Off-Shelf Sites	Min	Mean	Max	Spread		Min	Mean	Max	Spread
Baffin Bay	0.0	0.0	0.1	0.1		0.8	2.4	4.7	3.9
Davis Strait	0.0	0.3	1.4	1.4		0.7	1.9	3.4	2.7
N Labrador Sea	-0.5	0.4	1.6	2.2		0.1	1.4	2.8	2.6
Bravo (C Lab Sea)	-0.9	0.6	1.9	2.8		0.0	1.6	2.9	3.0
S Greenland	-1.6	0.1	1.9	3.5		-0.7	1.5	2.7	3.4
S Labrador Sea	-1.7	0.7	2.2	3.9		-0.1	1.7	3.3	3.4
Orphan Basin	-0.3	0.9	1.8	2.1		0.5	2.1	3.7	3.1
NW Corner	-0.8	0.7	1.6	2.4		-0.2	1.9	3.1	3.3
Flemish Cap Rise	0.3	1.2	2.5	2.1		0.4	2.6	4.1	3.7
Nfld Basin	1.1	3.2	7.1	6.0		2.1	3.7	5.8	3.7
Nfld Ridge	1.0	2.3	4.0	2.9		1.3	3.0	4.9	3.6
Slope Water	1.2	2.2	3.5	2.3		1.0	3.0	4.6	3.5
Scotian Slope	1.0	2.1	3.5	2.4		1.1	2.7	4.2	3.1
Scotian Rise	0.6	1.7	4.1	3.5		0.9	2.3	3.5	2.6
Mid-Atl Bight Rise	0.3	1.2	2.8	2.4		1.2	1.9	2.8	1.6

In the following discussion, the mean change across both RCPs will tentatively be taken as a “best” rough single estimate of the change on the 50-Year time scale, under the premise that the 60-year time interval exceeding the nominal time scale (thereby tending to make the values in Table 5-1 slight overestimates) should be at least partly offset by the emerging likelihood (e.g. Peters et al. 2013) that future radiative forcing on these time scales will be closer to RCP8.5 than RCP4.5 (such that the values in Table 5-1 will be underestimates).

Considering first the Shelf sites, it could be argued that the ESM simulations suggest that surface temperature increases on the 50-Year time scale in February will be a few tenths of a °C on the Northern Labrador Shelf, roughly 1 °C between the Central Labrador Shelf (Hamilton Bank) and the NE Newfoundland Shelf (NENS) and Flemish Cap, and roughly 2 °C on the GB and shelf areas to the west including the GSL. However, the spread of projected February changes from the different models and concentration scenarios is about 1 °C for the Northern Labrador Shelf, 2 °C for the GB and adjoining regions, and about 3 °C west of the GB and between the Central Labrador Shelf and NENS. Considering that the spread of the projected change exceeds the magnitude of the “rough-estimate” change in all sub-regions, it could alternatively be argued that the use of a single rough estimate is not appropriate and that a rough “change range” should be used instead. For the Shelf sites, the summary statement would then be that the models indicate that the changes in February surface temperature will be in the range of 0-1 °C for the Northern Labrador Shelf, 0-2 °C from the Central Labrador Shelf to Flemish Cap, 1-3 °C for the GB and Southern Newfoundland Shelf, and 1-4 °C for the GSL, SS and areas to the west.

Similarly for August, the best rough estimate of the changes (based on the ESMs) would be 2 °C from the Northern Labrador Shelf to the GB, and 3 °C for Flemish Cap, the GSL, southern GB and areas to the west. Alternatively, it could be stated that the models indicate that the changes in August surface temperature will be in the range of 1-3 °C for the Northern Labrador Shelf; 0-3 °C for the Central Labrador Shelf and NENS; 1-4 °C for the GB, Georges Bank, and Western SS; and 1-5 °C between the GSL, Southern Newfoundland Shelf, and central SS. On the other hand, it could be argued that this level of spatial resolution is excessive (especially considering the cross-shelf gradients apparent in Figure 5-7) and that the most appropriate summary statement is that the models indicate that the changes in August temperatures will be in the 0-4 °C range on the Labrador and Newfoundland Shelves, and in the 1-5 °C range for Flemish Cap, GSL, SS and GoM.

The statistics for the Off-Shelf sites (Table 5-1b) are included here to help interpret the Shelf results. The overall spread of the projected changes is greater for the Off-Shelf sites than the Shelf sites in both winter and summer because some models project cooling (by up to 2 °C) of the subpolar waters south of Greenland and some models project large warming (by up to 7 °C) in the vicinity of the subpolar-subtropical boundary (e.g. Newfoundland Basin). These features, as well as large warming in some northern areas in summer, are apparent in Figures 5-6 and C-4 which also serve as a reminder of the suspect spatial structure in some areas in these models.

## 6 Surface Ocean Salinity (SOS)

In this section we examine the spatial and temporal variability of the SOS (essentially the Sea Surface Salinity or SSS) fields in the ESMs, in an analogous approach to that for the TOS fields in Section 5 (except that we do not provide estimates of the climate changes at particular sites as in Section 5d). Complementary displays are presented in Appendix D.

### 6a Comparison with Observed Spatial Distributions and Temporal Variability

Figure 6-1 shows the bi-decadal mean SOS distributions in the six ESMs for February and August in 1986-2005 from the Historical period, together with the observed climatologies (1946-2005) obtained from I. Yashayaev of DFO-BIO. Similarities in the broad-scale SOS patterns among the different models and observations can be seen, especially for the transition zone from the relatively-fresh sub-Arctic to the subtropical gyre. However, similar to TOS, there are notable differences, both among the models, and with the observations. In particular, high-salinity subtropical water extends too far north on and to the west of the SS in all six ESMs. Low-salinity subpolar water extends too far east on and to the north of the GB in most of the models. In addition, there are differences in the GSL, over the Newfoundland and Labrador Shelves, and around Greenland. The differences in the northward extent of the subtropical gyre reinforce the concerns based on TOS regarding the detailed boundary of the subtropical and subpolar gyres in the ESMs, while the differences in the Labrador Shelf-Sea region reinforce the concerns based on SIC regarding the extent of subArctic melt water in the northern part of the LAB. Nevertheless, considering all the information presently available on these six ESMs, it is not obvious that any one or two of them are outstanding outliers that should be discarded, or that any subset of them is more reliable than the overall set.

Figures 6-2 and 6.3 compare temporal variability in SOS in the ESM Historical simulations, with observed surface salinity from the same monitoring sites considered in Section 5a for TOS. We start again with an observational comparison of the bi-decadal means and annual cycles from run 1 of the CanESM2 and GFDL-ESM2M simulations and from the ensemble mean of the five available CanESM2 runs (Figure 6-2). The CanESM2 annual cycles for run 1 and its ensemble mean are nearly the same (as was the case for TOS) but, in this case, there are qualitative as well as quantitative differences among the model and observed annual cycles in most cases.

The observational comparison for the bi-decadal means and annual cycles from all six ESMs is shown in Figure 6-3a, and that for the ensemble monthly means from the ESMs in Figure 6-3b. Perhaps the most striking feature of the comparison is the substantially larger variability in the mean SOS among the models at the GoM and SS sites in the subpolar-subtropical transition zone, than at the Bravo and GB sites in the subpolar region (Figure 6-3a). This reflects the previously-discussed difficulty in model resolution of the subpolar-subtropical boundary in particular. At Bravo, four of the ESMs are in approximate agreement with the observed SOS, but the SOS in CanESM2 and IPSL-CM5A-LR is low by about 2 psu which is a significant amount from the perspective of the important role of salinity in deep convection in the Labrador Sea (e.g. Yashayaev 2007). The observed means at Bravo are well within the inter-model standard deviations of the ensemble means, but this should be interpreted with caution in view of the sensitivity of deep convection to a combination of atmospheric and oceanographic forcings



(e.g. Yashayaev and Loder 2009). On the GB, the GFDL-ESM2M mean is higher than the observed mean by about 1 psu and the CanESM2 mean higher by about 0.5 psu. All of the

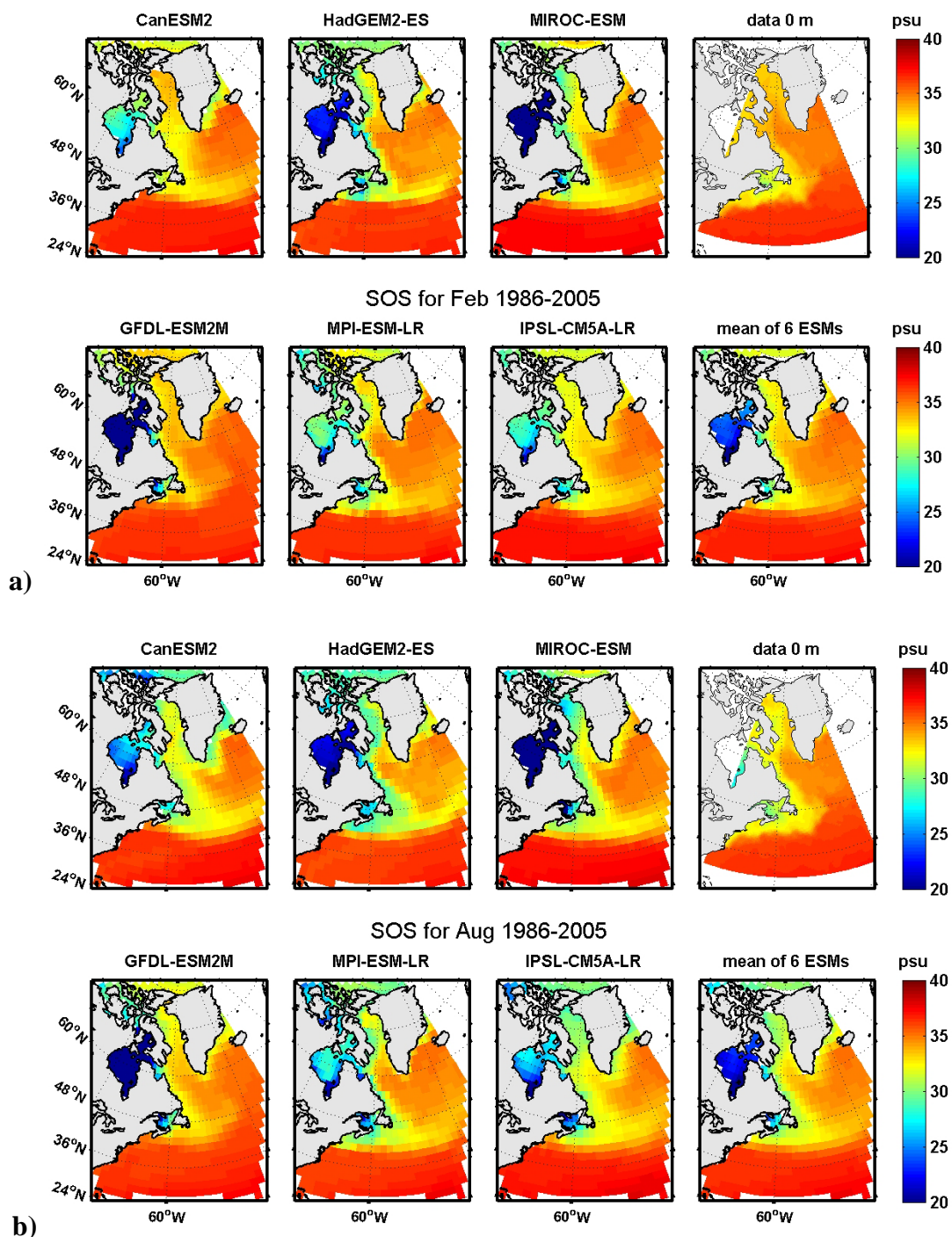


**Figure 6-1** Comparison of observed surface salinity climatologies for 1946-2005 (top right panels; from I. Yashayaev) with interpolated SOS fields for 1986-2005 from the Historical simulations from the six ESMs in a) February and b) August.



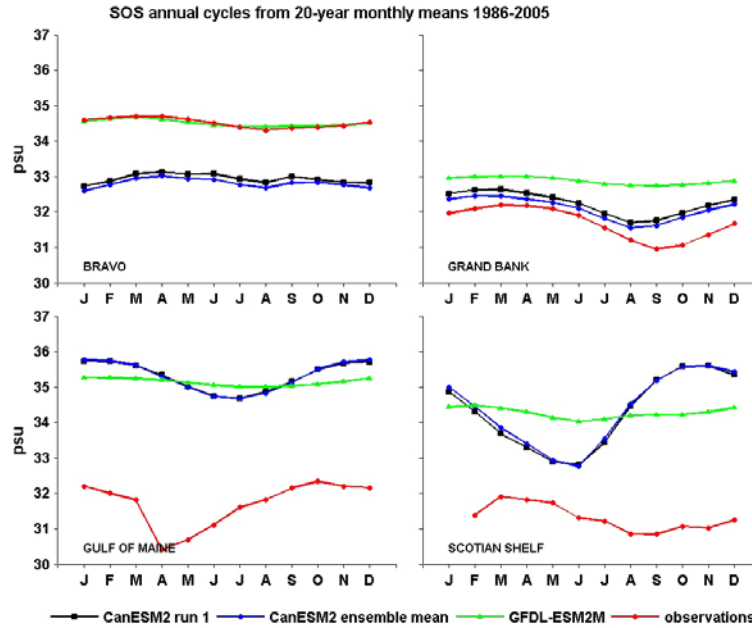


**Figure 6-2** Model (two ESMs) and observed annual cycles of SOS for 1986-2005 at the same four sites (Bravo, GB, SS and GoM) as in Section 5a (see Fig. 2-2 for locations). Model cycles are shown for run 1 and the ensemble mean from CanESM2, and for run 1 from GFDL-ESM2M.

other ESMs have SOS means for the GB lower than that in GFDL-ESM2M by  $<2$  psu, such that the envelope of model annual cycles brackets the observed GB cycle (Figure 6-3a). The model ensemble means for the GB are within the inter-model standard deviation of the observed means in all months, and the model and annual variations are in approximate agreement with higher SOS in winter than in summer (Figure 6-3b).

For the SS and GB sites, both the CanESM2 and GFDL-ESM2M mean SOS values are higher than the observed mean by 3-4 psu, with the GoM difference partly due to the estuarine location of the observational site. The other ESMs have lower mean SOS values at these sites, with those in HadGEM2-ES and MIROC-ESM being lower than or approximating the observed means. The ensemble-mean monthly values are generally within the inter-model standard deviations of the observed monthly means, but this may be misleading due to the large magnitude (2-3 psu) of the standard deviations. The seasonal variation differs among the models and observations at these sites, providing a further indication that it is uncertain whether any of the ESMs have a reliable representation of detailed oceanographic structure in the SS-GoM region.

The time series of the observed SOS annual means, and those from the five CanESM2 runs and run 1 of GFDL-ESM2M, are shown in Figure 6-4. In contrast to the bi-decadal annual cycles, there are pronounced differences among the CanESM2 runs in the interannual-to-decadal variability, with inter-model and inter-annual ranges of about 1 psu and no apparent correlation in the variability across the runs. There is also no apparent correlation between the variability in the CanESM2 and GFDL-ESM2M runs, or between the model and observed time series at the four sites. The long-term trends (not shown) in both the models and observations are weak compared to this variability, consistent with the strong interannual to multi-decadal variability observed in the NWA (Bindoff et al. 2007; Yashayaev 2007; Durack and Wijffels 2010).

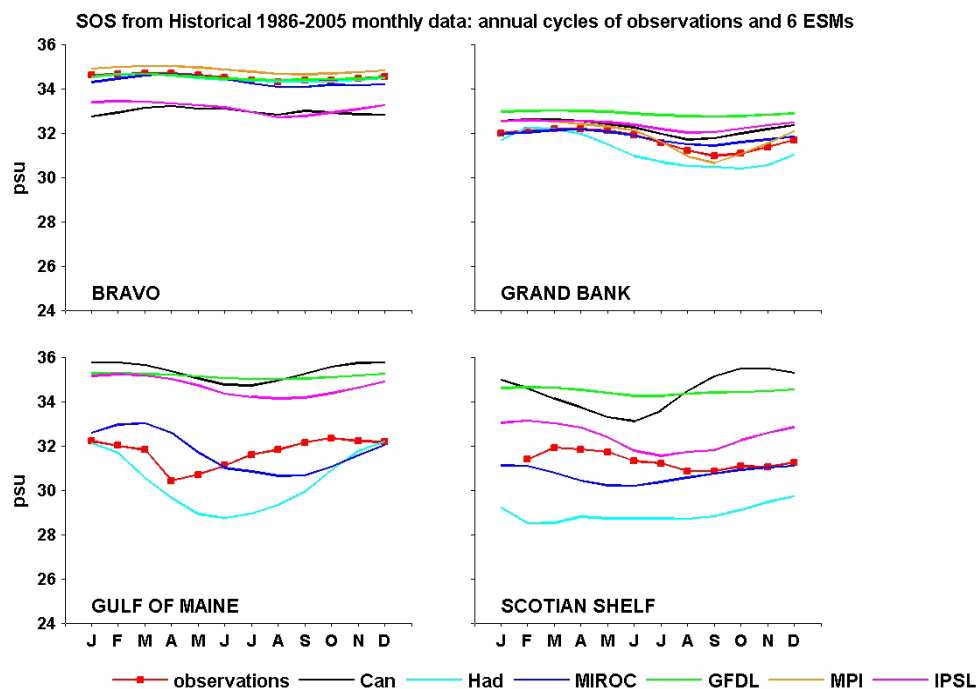


**Figure 6-3a** Model (five ESMs) and observed annual cycles of SOS for 1986-2005 at the same four sites (Bravo, GB, SS and GoM) as in Figure 6-2. Model cycles are shown for each of the six ESMs, using interpolated data.

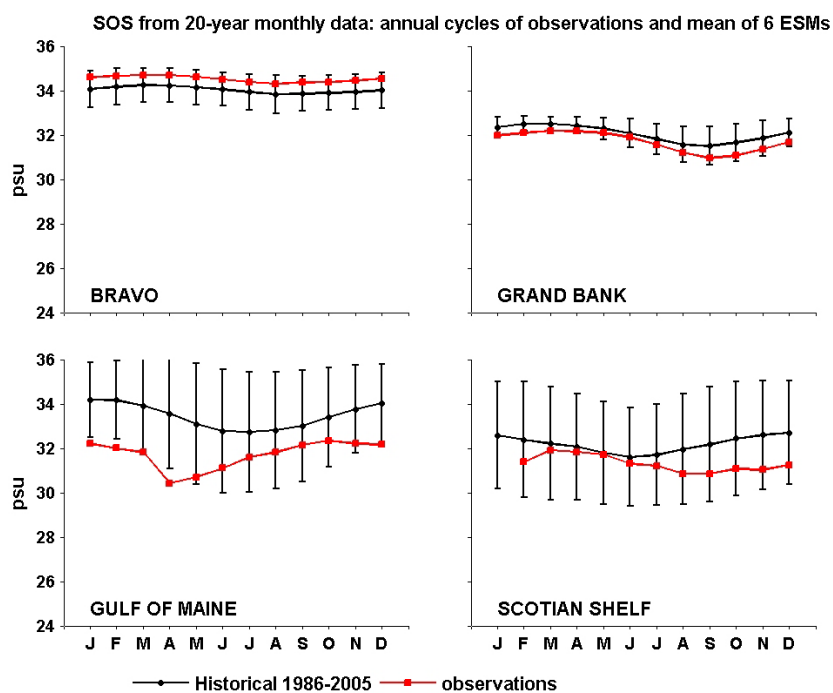


**Figure 6-3b** Ensemble-mean model (over the six ESMs in Fig. 6-3a) and observed annual cycles of SOS for 1986-2005 at the same sites as in Figure 6-2. The inter-model standard deviations are indicated by the error bars on each side of the ensemble means.

Similar to TOS, the spread of the long-term trends from the model runs ( $-0.08$  to  $+0.04$  psu per decade) substantially exceeds the magnitude and variability among the observed trends ( $-0.02$  to  $0.00$  psu per decade) since 1950. Thus, there is little consistency between the models and observations beyond the dominance of interannual-to-decadal scale variability over any trend.

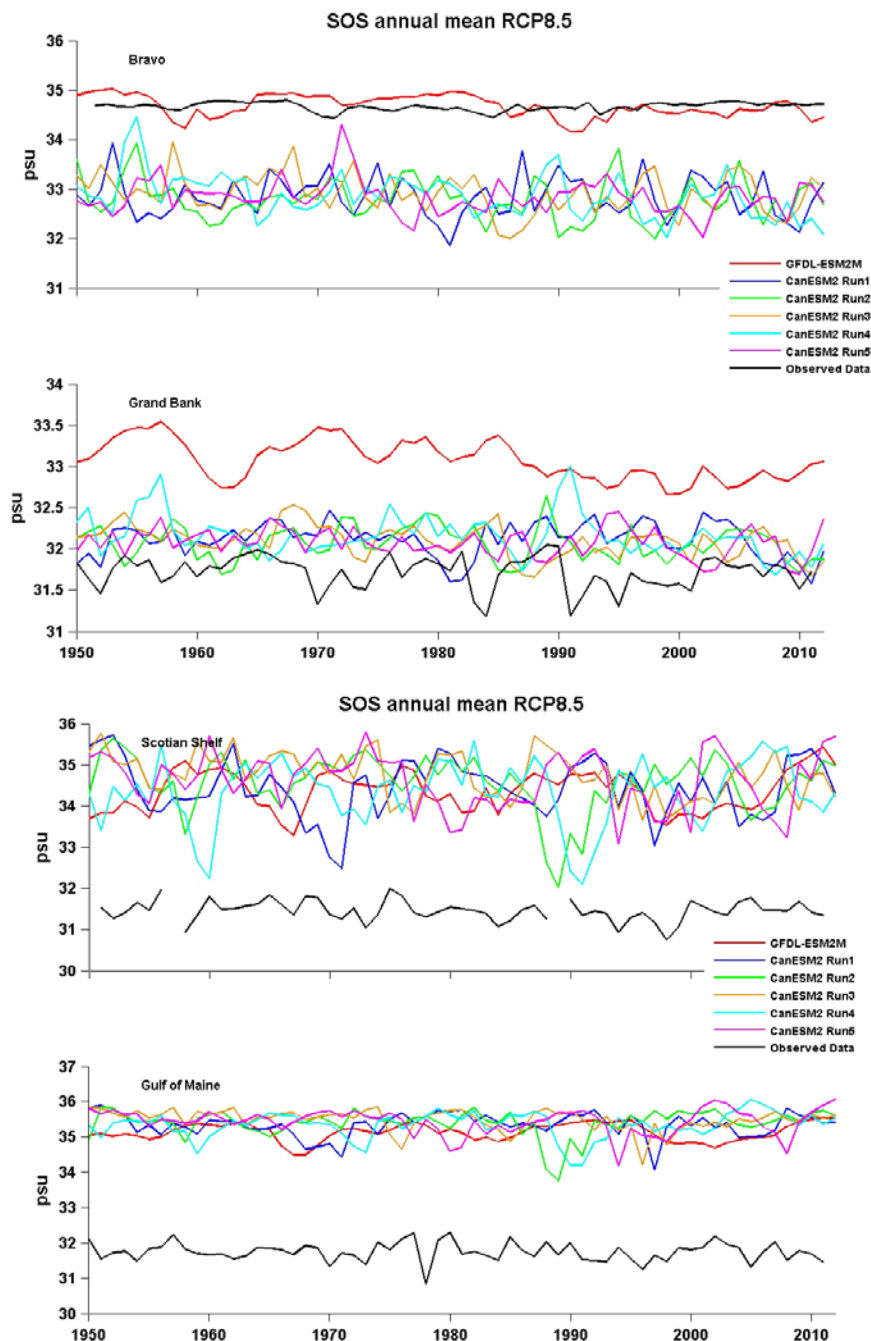


**Figure 6-4** Comparison of model annual mean time series of SOS at four sites with observations for 1950-2012 (see Fig. 2-2 for locations). Model data are for run 1 from GFDL-ESM2M and five runs from CanESM2, from the concatenated Historical and RCP8.5 simulations. Observed time series are for the ocean surface at three sites, but for the 16-150m interval at Bravo.

## 6b Spatial Distribution of Projected SOS Climate Changes in Six ESMs

The bi-decadal mean SOS fields for February and August during 2046-2065 from the ESMs under RCP8.5 are presented in Figure D-1 (Appendix D), analogous to those for 1986-2005 in Figure 6-1. Projected freshening in the subpolar region is clearly apparent but the changes in the southern part of the LAB are less clear. The projected climate changes are best seen in the bi-decadal change fields in Figure 6-5.

A clear broad-scale pattern is apparent, with decreasing SOS in the subpolar region (north of about 40°N) and increasing SOS in the subtropical waters to the south. This pattern is consistent with expectations from the AR4 models (Meehl et al. 2007; Capotondi et al. 2012; Durack et al. 2012) that also show freshening associated with the intensified hydrological cycle and ice melt in the north, and increasing salinity associated with increased evaporation in areas under subtropical influences. The projected decrease in the GSL is at least qualitatively consistent with that found by Chassé et al (2013) using a regional ocean model and down-scaled atmospheric forcing from an AR4 AOGCM for SRES A1B.

However, similar to TOS, substantial differences in the detailed patterns and magnitudes of the changes are apparent (Figure 6-5), particularly in the subpolar gyre region. These inter-model differences are generally larger than the seasonal changes, although these particular months may not represent the seasonal extremes (see Section 6a). The local areas with greatest freshening generally vary among the models and, while the boundary for the sign change (0 psu isohaline) is generally around 40°N, there are notable differences in the details of the boundary in the GM and SS region (which is not well resolved in the models). The larger-scale change fields (Figure D-2) generally show greater freshening in the Arctic than in the NWA (although not everywhere), and reduced freshening in the NE Atlantic with increasing salinity in some cases.

The statistics of the climate changes are presented in Figures 6-6 and D-3 for the NWA and Canada, respectively. The boundary for the latitudinal change in the sign (0 psu isohaline) of the ensemble-mean SOS changes lies around 40°N to the west of the GB but shifts towards 50°N east of the GB. There is an associated zonal band of enhanced inter-model spread extending across the Atlantic in the vicinity of the subtropical-subpolar gyre boundary (or North Atlantic Current), reflecting the models' differences in the representation of this important feature. There is a weak indication that this band is broader in summer than winter, and a stronger indication of greater spread in the projected changes in Baffin Bay and around Greenland in summer than in winter. Figure 6-6 indicates a spread with magnitude in the 1-3 psu range across most of the Atlantic LAB for RCP8.5 in summer. Figure D-4 provides more detail on the spatial structure of the extremes of the projected SOS changes in the present ESMs (but note that many of these details are probably dependent on the particular models used here).

Finally, Figure 6-7 shows the seasonal evolution of the ensemble-mean monthly SOS changes in the six ESMs, confirming the seasonal and inter-seasonal persistence of the features described above. The next subsection discusses the seasonality of the changes further.

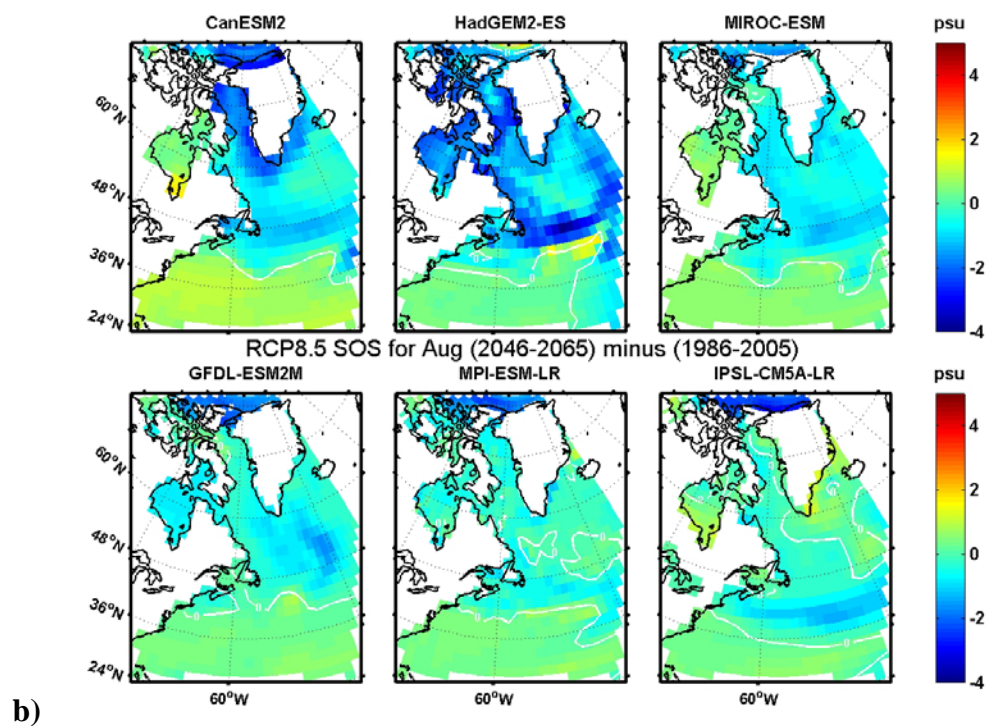
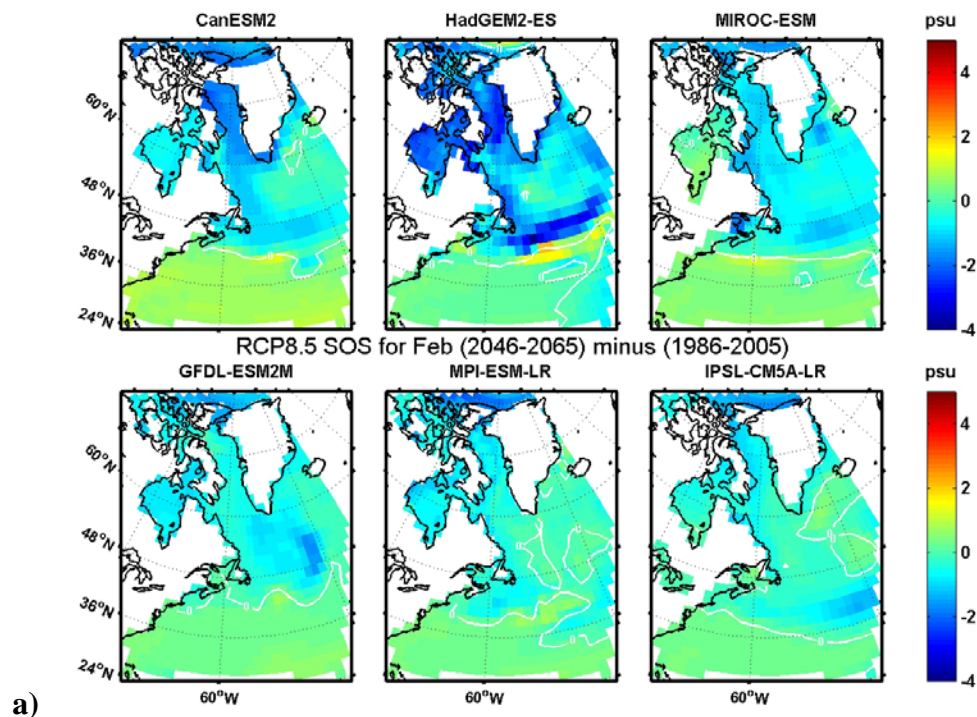


**Figure 6-5** Bi-decadal monthly SOS climate change fields from 1986-2005 to 2046-2065 for the NWA for RCP8.5 for a) February and b) August, using interpolated data from the six ESMs. The white contour is the 0 psu isohaline.



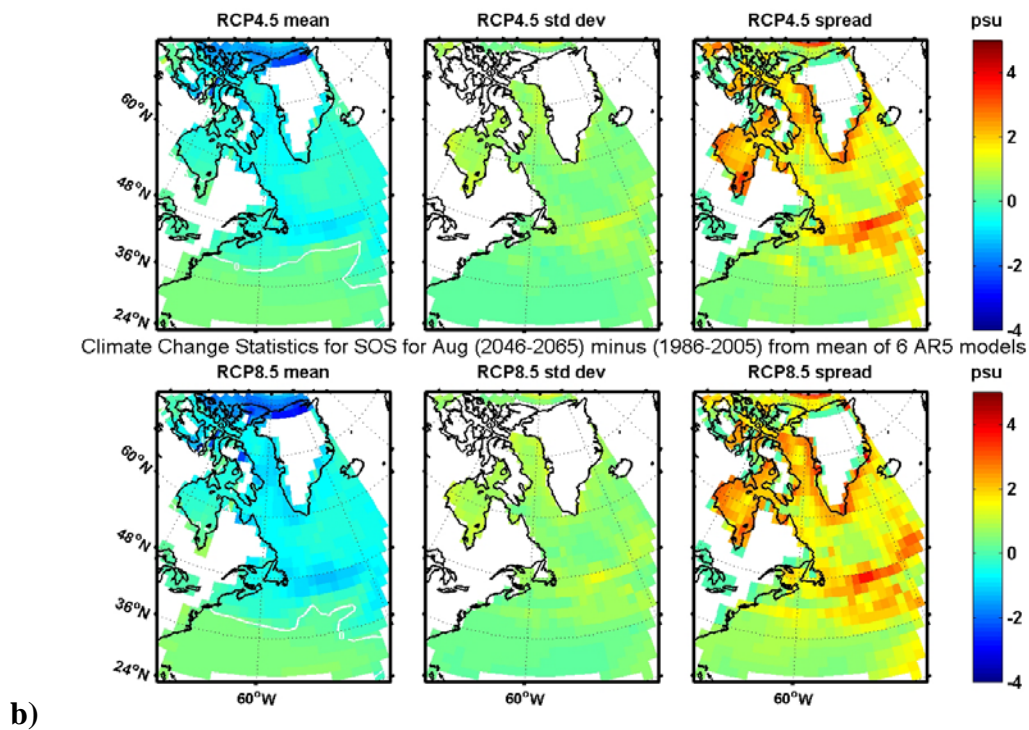
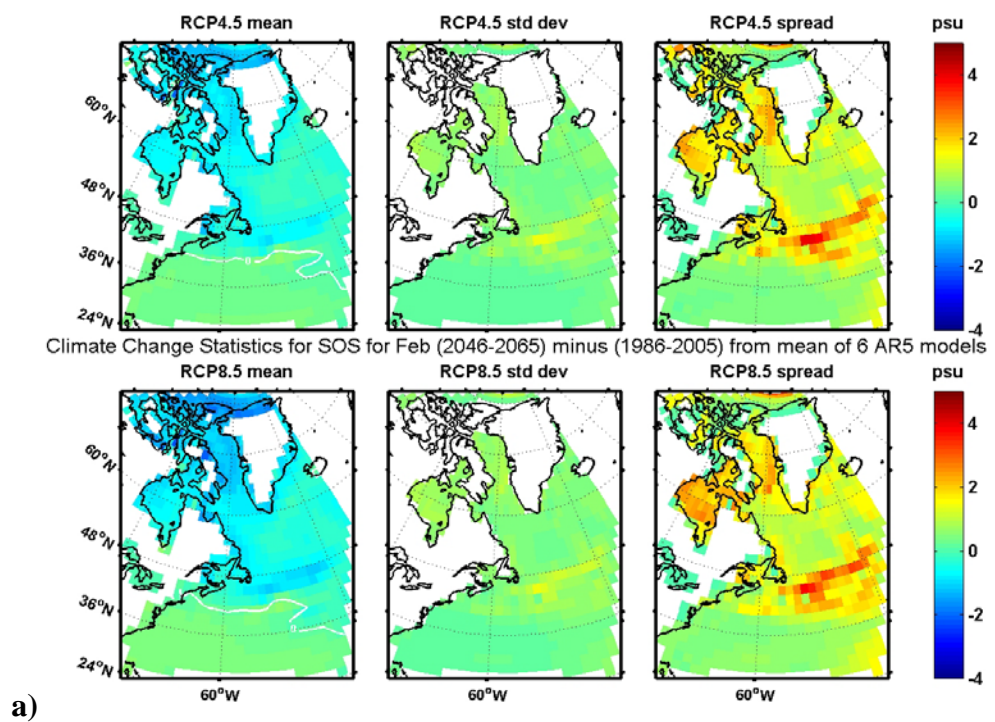


**Figure 6-6** Mean, standard deviation, and spread of climate changes in bi-decadal SOS from 1986-2005 to 2046-2065 for RCP4.5 and RCP8.5 in a) February and b) August, computed from the ensemble of the changes from the six ESMs (Fig. 6-5). The white contour is the 0 psu isohaline.

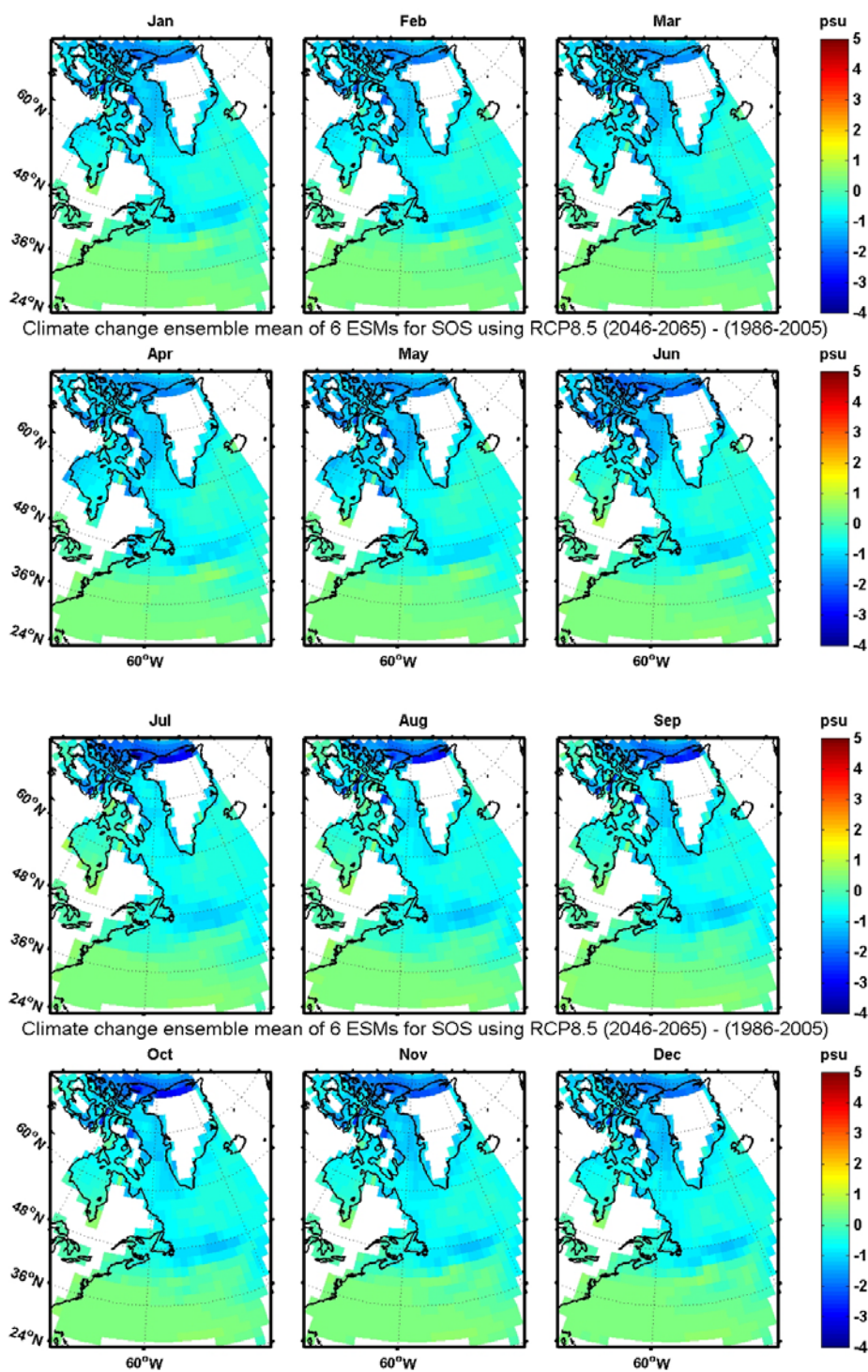


**Figure 6-7** Changes in bi-decadal monthly SOS from 1986-2005 to 2046-2065 for RCP8.5 for the twelve months of the year, from the ensemble mean of the change fields from interpolated data from the six ESMs.



### 6c Temporal Variability of SOS Climate Changes in ESMs

The bi-decadal annual cycles and climate changes of SOS at the four sites discussed for TOS in Section 5c are presented in Figure 6-8 for the Historical (1986-2005) and RCP8.5 (2046-2065) simulations from the same two ESMs as before. For three of the sites, the time series for the 1986-2005 period are the same ones used for the observational comparisons in Figures 6-2 and 6-3, while the GSL site is the same as for TOS in Section 5c.

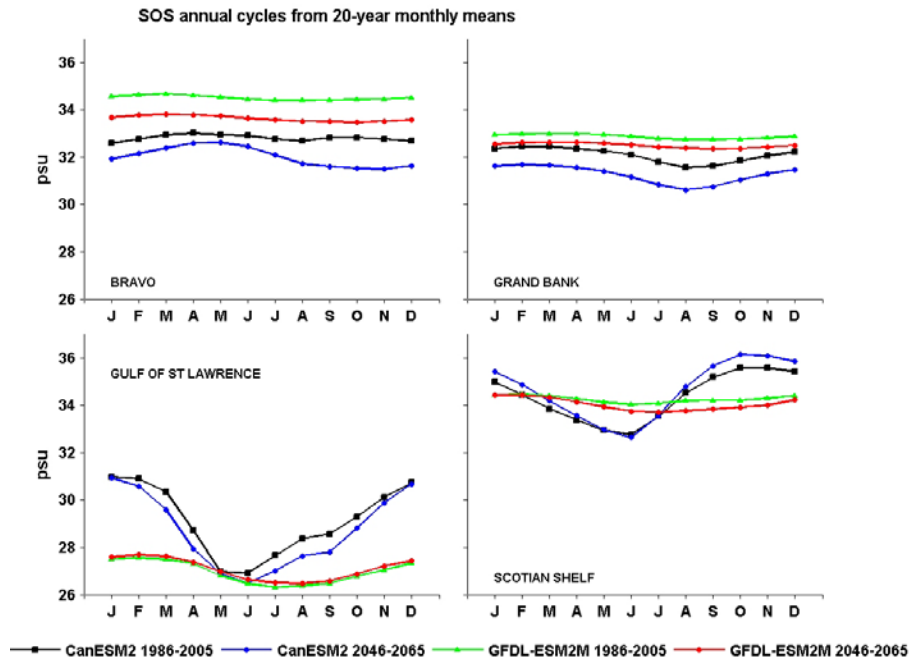


**Figure 6-8a** Annual cycles of SOS for Historical (1986-2005) and RCP8.5 (2046-2065) at four sites (Bravo, GB, GSL and SS) for the CanESM2 ensemble-mean of all runs and GFDL-ESM2M run 1 (see Fig. 2-2 for locations).

As expected from the results in the previous subsection, the ensemble means from the CanESM2 simulations and run 1 of GFDL-ESM2M project a decrease in SOS for all months at the Bravo and GB sites (Figure 6-8a). On the other hand, while the CanESM2 ensemble means also project a small decrease in the GSL in most months and the GFDL-ESM2M means project a small decrease on the SS in most months, the CanESM2 means project a small increase in annual-mean SOS on the SS and the GFDL-ESM2M means project a very small increase in the GSL. There are only small changes projected in the annual cycles, except for the CanESM2 ensemble means at Bravo. It is noteworthy that there is a large difference between the two models' annual cycles in the GSL. The relatively-large CanESM2 annual cycle has a phase and amplitude that more closely agree with observations and are consistent with the GSL outflow's influence on the SS annual cycle as mentioned in Section 6a (e.g. Sutcliffe et al. 1976).

The seasonal variations (Figure. 6-8b) of the SOS changes in the individual CanESM2 runs (and in the GFDL run) reveal substantial differences among the runs and between the models (to the point that the annual cycle from the CanESM2 ensemble means discussed above needs to be used with caution). There are substantial differences in the magnitudes of the changes in the

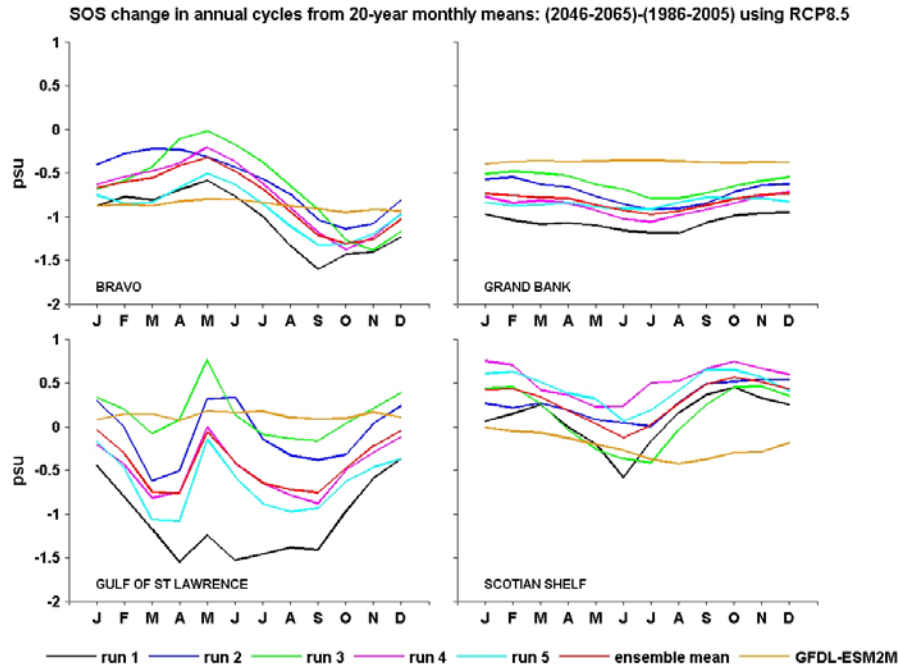


**Figure 6-8b** Changes in bi-decadal monthly mean SOS from 1986-2005 (Historical) to 2046-2065 (RCP8.5) at the four sites in Figure 6-8a for five runs of CanESM2 and run 1 of GFDL-ESM2M.

different CanESM2 runs in the GSL in particular (spread of 1-2 psu depending on season), which probably reflects differences in precipitation changes in the runs (e.g. Chassé et al. 2013). There is nevertheless similarity in the seasonal variation in the different CanESM2 runs, in contrast to relatively small seasonal variations in GFDL-ESM2M (which is inconsistent with observations).

The projected decreases in SOS at Bravo from CanESM2 are generally largest in fall, because of water flowing from the north, and smallest in spring, with differences of a factor of 2-3 in the changes between these seasons (Figure 6-8b). On the GB, the reductions are largest in summer and smallest in winter with a much smaller seasonal change. On the SS, the increase in salinity is largest in winter and smallest in summer (with a salinity decrease in some runs). In the GSL there are indications of larger decreases in early spring and late summer and smaller ones (or even increases in salinity) in winter and late spring.

The ensemble-mean annual cycles from the Historical and two RCP simulations from the six ESMs, together with the inter-model standard deviations, are shown in Figure 6-9a for the same nine sites as in Section 5c. The seasonal variations of the climate changes in the individual ESMs for RCP8.5 are shown in Figure 6-9b, and the ensemble means and inter-model standard deviations of the changes are shown in Figure 6-9c.

The ensemble-mean monthly climate changes are within the inter-model standard deviations in all months at all sites, reflecting the model uncertainty, particularly at the SS and GoM sites (Figure 6-9a). The seasonal variations in the changes are small relative to the inter-model variability, with the most consistent changes across models being in Baffin Bay where there is an enhanced decrease in SOS in May-June followed by a smaller decrease in July-August (Figure 6-9b,c). These changes are probably related to the end of the sea ice season in that area.

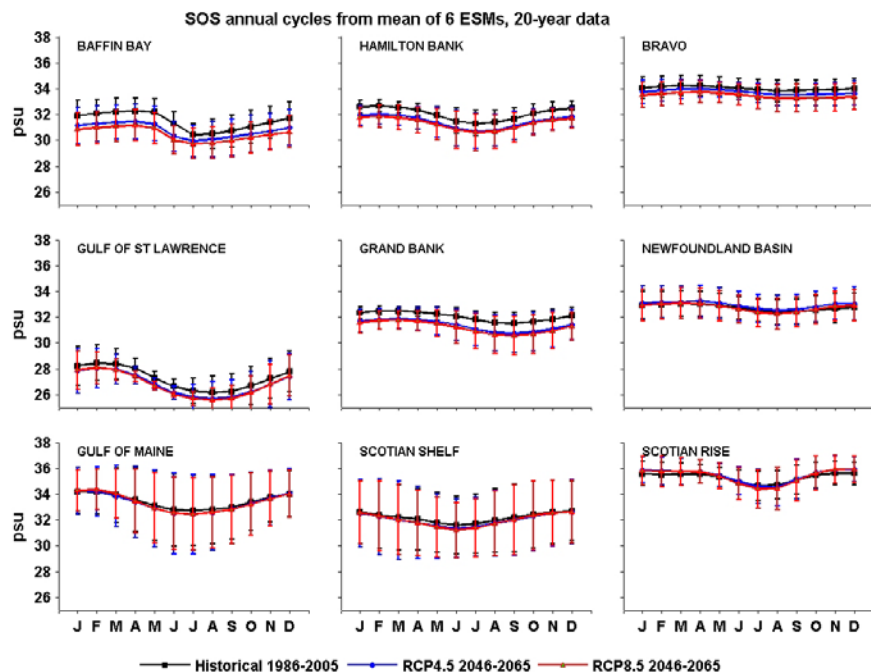


**Figure 6-9a** Ensemble-mean annual cycles (with standard deviations) of SOS from the Historical simulations for 1986-2005, and from the RCP4.5 and RCP8.5 simulations for 2046-2065, at nine sites for the ensemble of the six ESMs. Five of the sites are the same as in Figures 6-2 or 6-8, while the locations of the other sites are shown in Figure 2-4.

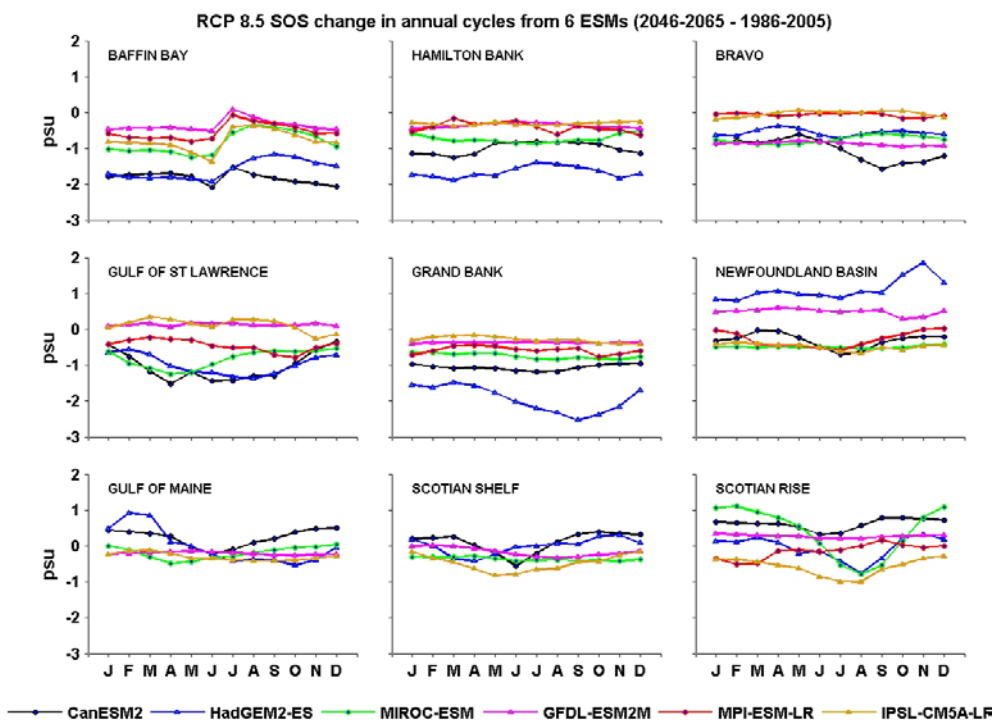


**Figure 6-9b** Changes in bi-decadal monthly mean SOS from 1986-2005 (Historical) to 2046-2065 (RCP8.5) at the nine sites in Figure 6-9a, in run 1 from the six ESMs.

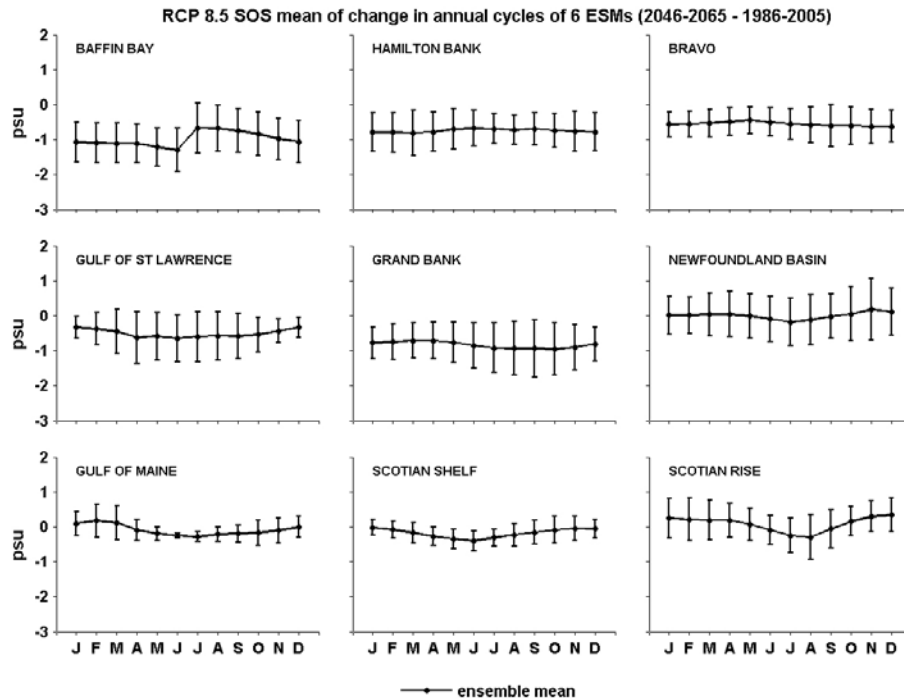


**Figure 6-9c** Ensemble means, and inter-model standard deviations, of the climate changes in bi-decadal monthly mean SOS shown in Figure 6-9b.

The projected future evolution of SOS in CanESM2 and GFDL-ESM2M at the four sites considered in Section 6a is shown in Figure 6-10 where time series of annual mean data from both the Historical (as in Figure 6-4) and RCP8.5 simulations to 2100 are presented. There are clear differences in the nature of the variability at the two northern and two southern sites. At Bravo and on the GB, there are long-term decreases in SOS in both models, consistent with previous model projections (e.g. Meehl et al. 2007; Capotondi et al. 2012). However, GFDL-ESM2M has higher salinities in the Historical simulations (as discussed in Section 6a) and more pronounced decadal variability in the future in contrast to the more pronounced interannual variability in CanESM2. In each model, the range of interannual-to-decadal scale variability is of order 1 psu. Considering the differing future TOS variability in these models discussed earlier, it appears that there are significant differences in the nature of the dynamics affecting ocean properties in the Labrador-Newfoundland region in these two models. It is not obvious that one model is more reliable than the other.

The character of the projected future temporal variability at the two southern sites is markedly different than at the northern sites, with the interannual-to-decadal variability being much larger than the long-term change. On the SS, the SOS variations in the CanESM2 data have a range of about 4 psu and large differences among the runs (Figure 6-10), but the magnitude of the 60-year changes in the ensemble means is only a few tenths of a psu (Figure 6-9). In the GoM, the corresponding range of the SOS variations in CanESM2 runs grows from 1-2 psu in the Historical simulation to about 3 psu in the late 21<sup>st</sup> century, swamping any long-term trend. The range of the interannual-to-decadal variability in the GFDL-ESM2M simulations at these two sites is smaller than in the CanESM2 simulations (but still larger than at the northern sites), with no apparent long-term increase. There is however some indication of a weak negative trend at

the SS and GoM sites in GFDL-ESM2M in the last half of the 21<sup>st</sup> century, but the reliability of both models' representation of the processes controlling the gyre-gyre interactions in this complex transition region remains unclear (as discussed previously).

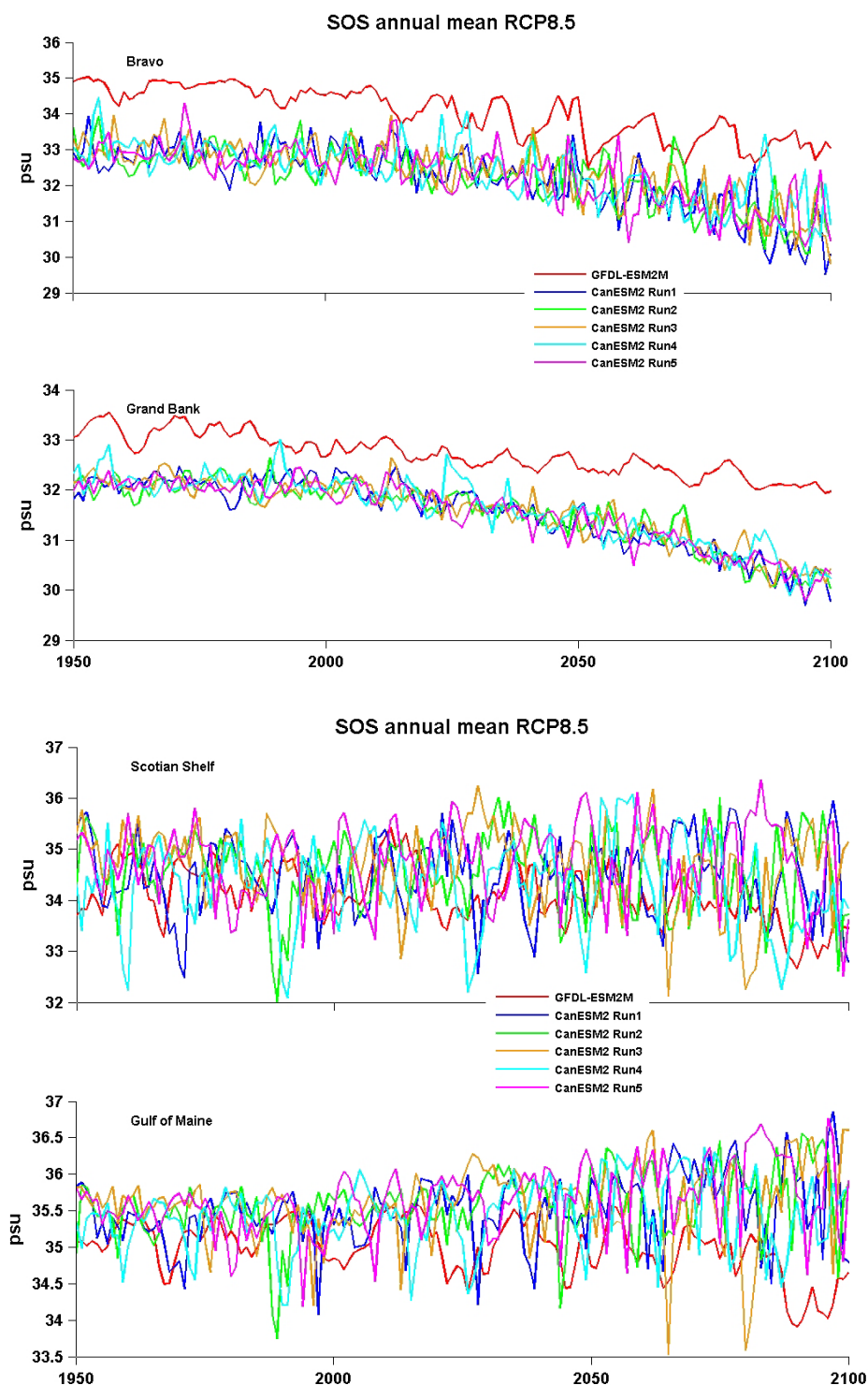


**Figure 6-10** Time series of annual means of SOS from CanESM2 (five runs) and GFDL-ESM2M (run 1) for 1950-2100 at the same four sites as in Figure 6-4 (Bravo, GB, SS and GoM).

## 7 Cross-Basin Structure of Ocean Temperature and Salinity

In this section, we present displays of subsurface temperature and salinity from five of the ESMs on vertical sections across Baffin Bay, the Labrador Shelf/Slope/Sea (LSSS), and the Scotian Shelf/Slope/Rise (SSSR; also referred to as the NW Atlantic or AtlNW in the displays); see Figure 2-2 for locations of the sections. We use annual (rather than monthly) mean data because they were more readily available and involved much smaller 3-d datafiles. Complementary quantitative information on the subsurface temperature and salinity variability is presented in Lavoie et al. (2013a,b) using volume-averages computed from the models for broad areas and vertical intervals.

### 7a Comparison with Observations

We start by comparing the modelled and observed decadal mean temperature (Figure 7-1) and salinity (Figure 7-2) on the AR7W section across the LSSS, choosing the period 1996-2005 which includes Argo data that improves the seasonal coverage. The observational decadal mean fields were provided by I. Yashayaev of DFO-BIO and drew on all available survey (vessels, floats) data from this period; see Yashayaev et al. (2008) and Yashayaev and Loder (2009) for background on the observations. With the 4000-m depth range displayed in these figures, focus here is on the *upper* couple of hundred meters on the Labrador Shelf/Slope, and on the *intermediate* 2000-3000 m and the *bottom* 1000 m in the central Labrador Sea. The displays also provide an indication of the different horizontal resolution in the models, and of the higher resolution in MPI-ESM-LR in particular.

All the models include a crude representation of the relatively cool and fresh (subArctic) water over the Labrador Shelf, but the IPSL-CM5a-LR model has this layer extending too far (and deep) across the Labrador Sea, and the CanESM2 and HadGEM2-ES models have indications of overly warm and salty water extending onto the shelf at depth. The offshore intermediate-layer water is too warm and salty in all of the models, but by significantly varying amounts. CanESM2 and MPI-ESM-LR have the largest overestimates of temperature, while CanESM2 overestimates salinity the most. This points to a poor representation of the Labrador Sea Water (LSW) that is formed in this region by wintertime convection (Yashayaev 2007), reminiscent of de Jong et al.'s (2009) findings for AR4 models. CanESM2 has the closest bottom temperature to that observed (Denmark Strait Overflow Water - DSOW), with three other models showing decreasing temperature (as observed) as the bottom is approached. CanESM2 and MPI-ESM-LR have the closest bottom salinity to that observed although none of the models have the observed near-bottom layer of slightly saltier Iceland-Scotland Overflow Water (ISOW) overlying the DSOW (e.g. Yashayaev 2007).

It is difficult to infer the depth of the winter mixed layers (from atmospherically-forced deep convection) in these annual mean fields, so discussion of this is deferred to the next section.

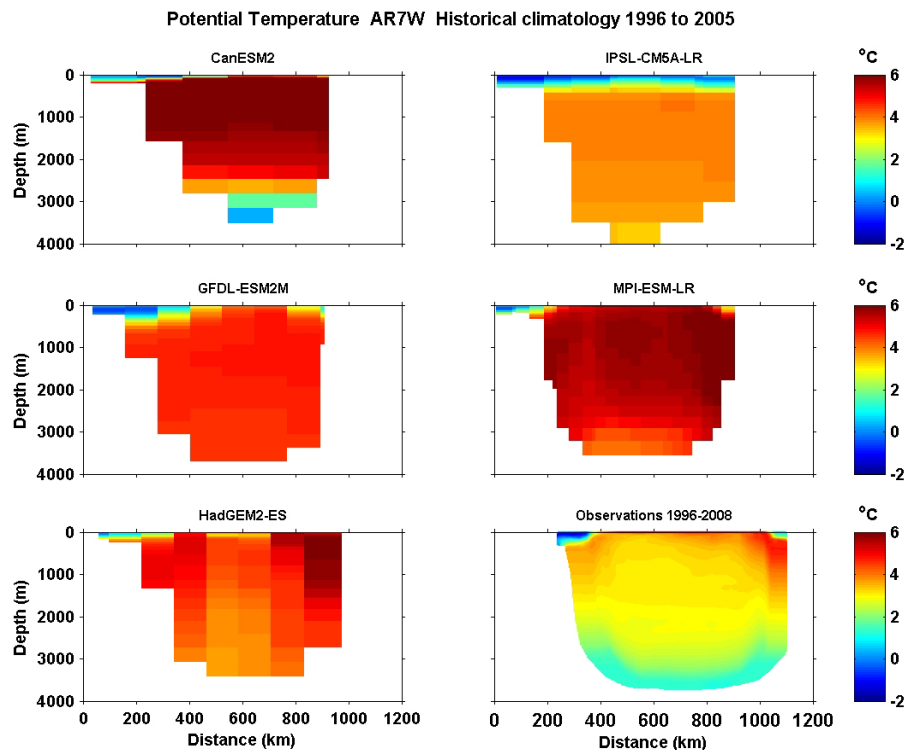


**Figure 7-1** Comparison of decadal-mean (1996-2005) ocean temperature across the LSSS section from five ESMs, with observations from the AR7W line (courtesy of I. Yashayaev).

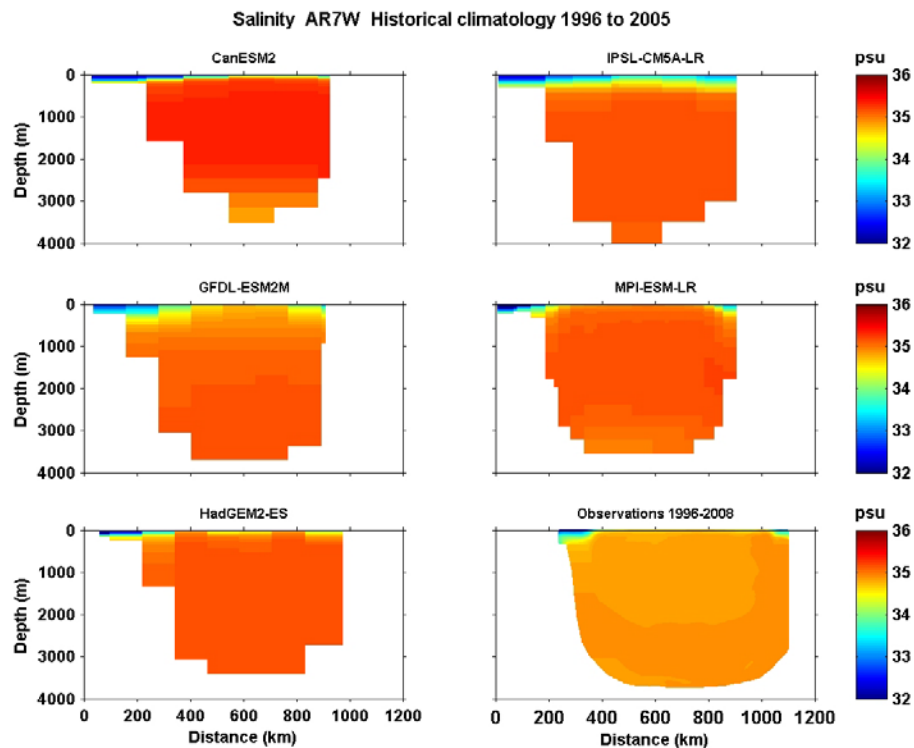


**Figure 7-2** Comparison of decadal mean (1996-2005) ocean salinity across the LSSS section from five ESMs, with observations on the AR7W line (courtesy of I. Yashayaev).



## 7b Projected Climate Changes

The projected changes of bi-decadal mean temperature from 1986-2005 to 2046-2065 in the five ESMs on the three sections are displayed in Figure 7-3, and those of bi-decadal mean salinity in Figure 7-4. The corresponding bi-decadal mean fields for the past and future periods for the five models across the three sections are shown in Figures E-1 to E-6 (Appendix E).

Perhaps the most striking feature of the 1986-2005 Historical fields is that, while CanESM2 has the warmest freshest intermediate layer in the Labrador Sea (Figure E-2), it has the coldest and saltiest subsurface water in Baffin Bay (Figure E-1). The origin of this is unclear. There is much warmer and saltier water in the upper ocean on the SSSR section in all the models (Figure E-3), consistent with the subtropical gyre influence.

Warming by differing amounts and with somewhat different spatial patterns is apparent in the temperature change fields in Figure 7-3. The greatest warming in Baffin Bay is in the 100-400m depth range in CanESM2, that in the Labrador Sea is in the upper 800m in CanESM2, and that on the SSSR section is on the shelf in HadGEM2 and in the upper 600m over the shelf and extending offshore in CanESM2. The smallest increases in Baffin Bay are at depth in HadGEM2, those in the Labrador Sea are in the offshore near-surface waters in GFDL-ESM2M, and those on the SSSR are in the deep waters in CanESM2, with there also being some areas with decreases in these areas.

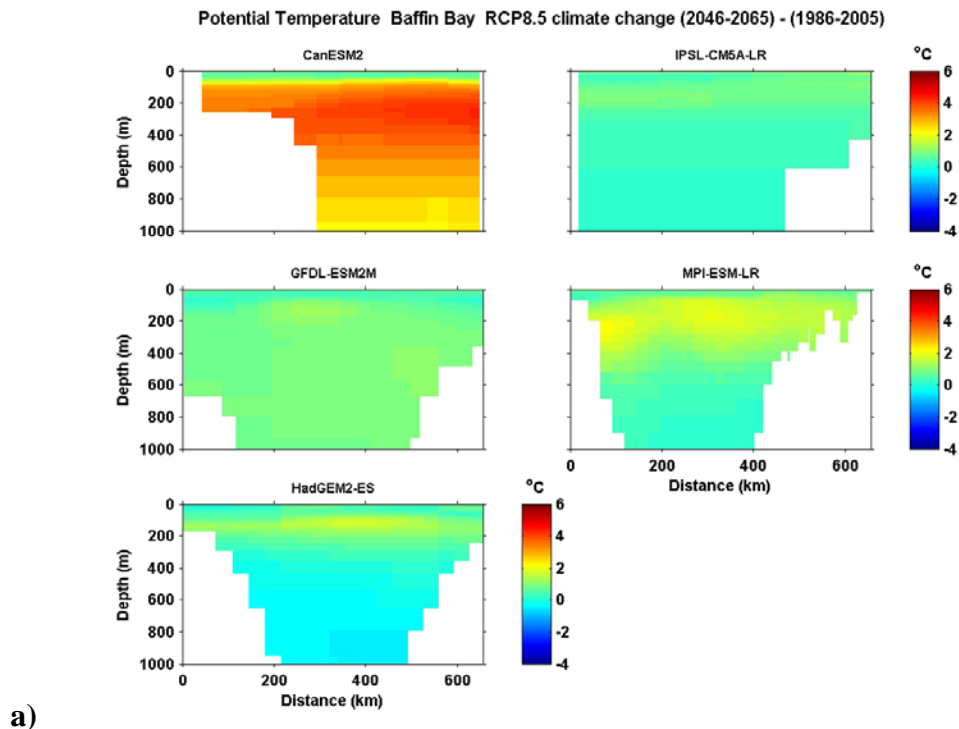
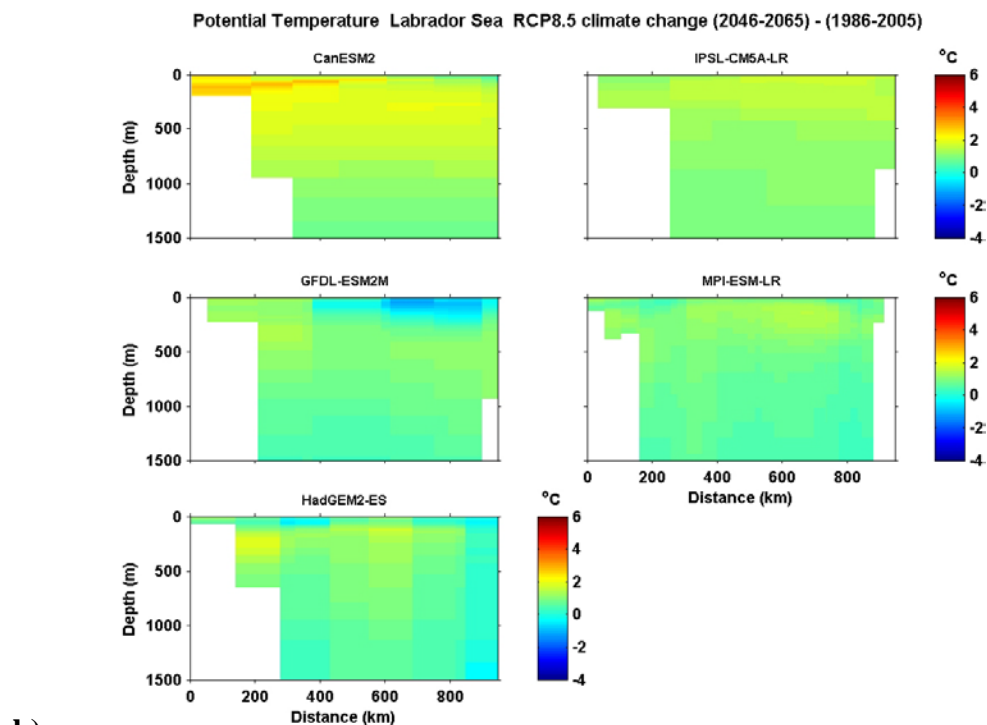
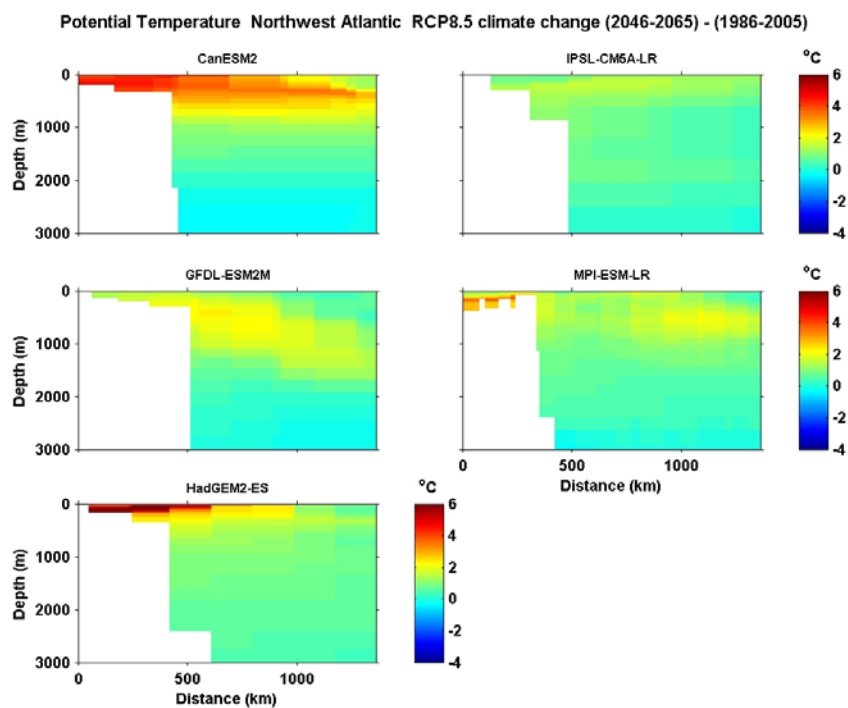


**Figure 7-3** Changes in bi-decadal mean potential temperature from 1986-2005 in the Historical simulations to 2046-2065 in the RCP8.5 simulations of five ESMs, on sections across **a)** Baffin Bay, **b)** the LSSS and **c)** the SSSR (NW Atlantic).



b)



c)

**Figure 7-3** Changes in bi-decadal mean potential temperature from 1986-2005 in the Historical simulations to 2046-2065 in the RCP8.5 simulations of five ESMs, on sections across a) Baffin Bay, b) the LSSS and c) the SSSR (NW Atlantic).

There is a general pattern of greatest warming in Baffin Bay in a subsurface layer (but with different magnitudes and extents among the models). There is no general pattern to the subsurface temperature changes on the LSSS section, while there is a general pattern of greatest warming over the shelf or in a subsurface layer extending offshore in the upper ocean on the SSSR section.

Similarly, there is decreasing or increasing salinity by differing amounts in the different models and on the different sections (Figure 7-4), but with greater similarities among the models in the patterns than for temperature. The largest salinity decreases occur in the near-surface waters in CanESM2 and HadGEM-ES on the Baffin Bay and LSSS sections, while the largest salinity increases occur in the upper 1000-2000m on the SSSR section. There are general patterns across the models of greater freshening in the upper 200-600m in Baffin Bay and the Labrador Sea (but with different magnitudes and vertical extents), and largest salinity increases at depth over the shelf or in the upper 1000-2000m over the slope and rise on the SSSR section. Notable inter-model differences include a layer of higher salinity increase at 400-600m in CanESM2 and MPI-ESM-LR in Baffin Bay, a layer of small salinity increase in the 200-1000m depth range in the Labrador Sea, and salinity increases extending to 3000m depth over the Scotian Rise. While the origin of these spatial structures and model differences are unclear, there are clear suggestions of substantial differences amongst the models, superimposed on the broad-scale pattern of surface-intensified freshening in the north and an enhanced upper-ocean increase in temperature and salinity in the south (as in previous studies, e.g. Meehl et al. 2007; Palmer et al. 2009; Capotondi et al. 2012).

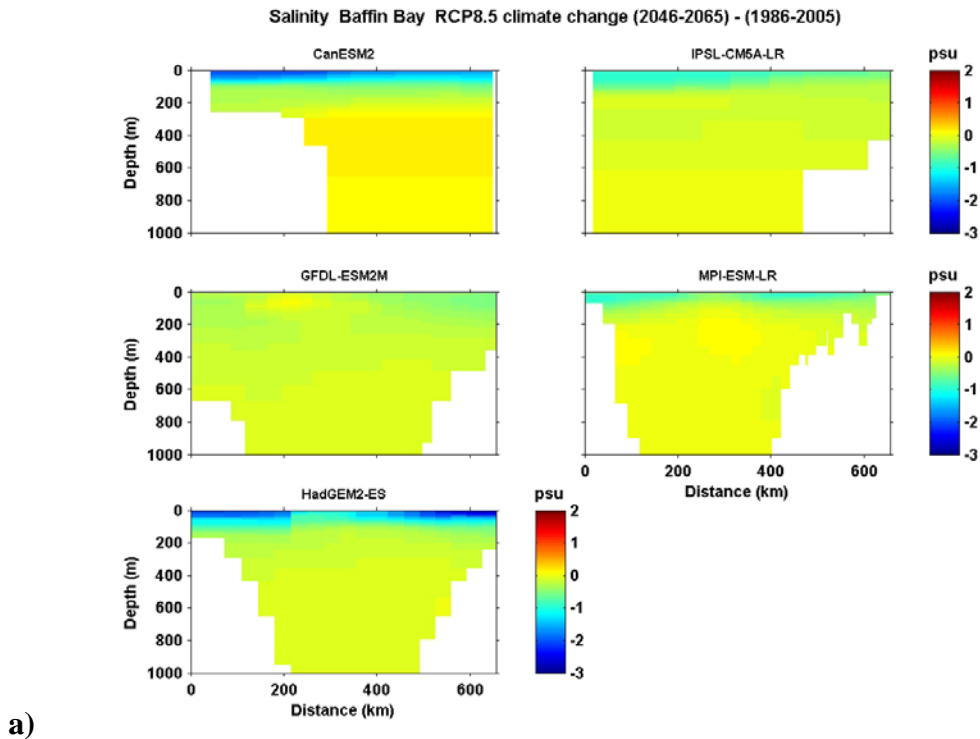
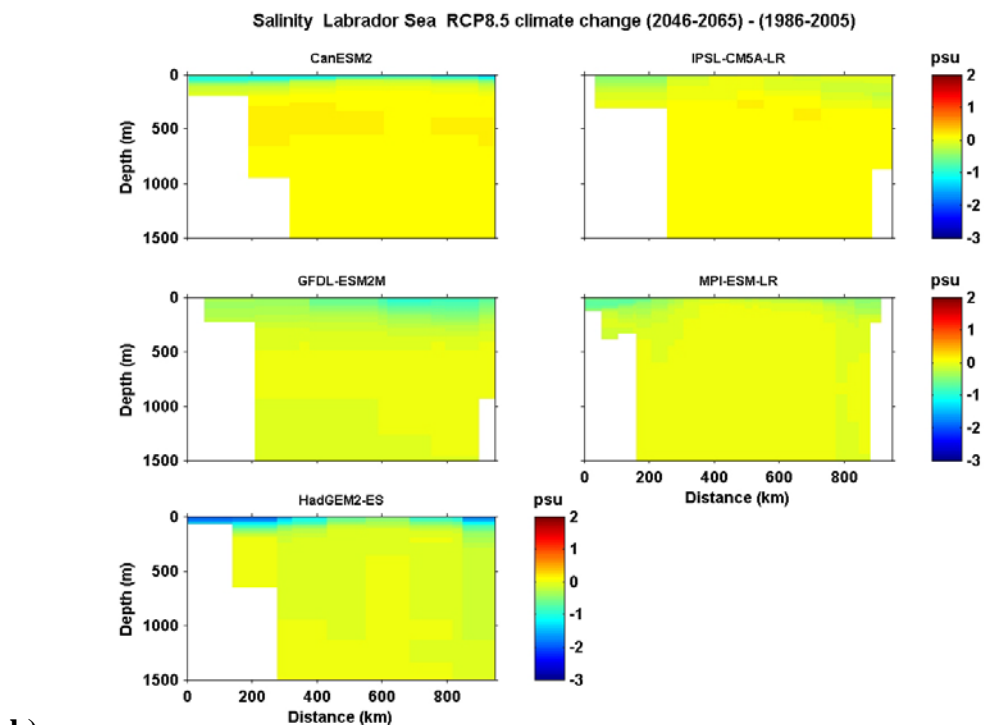
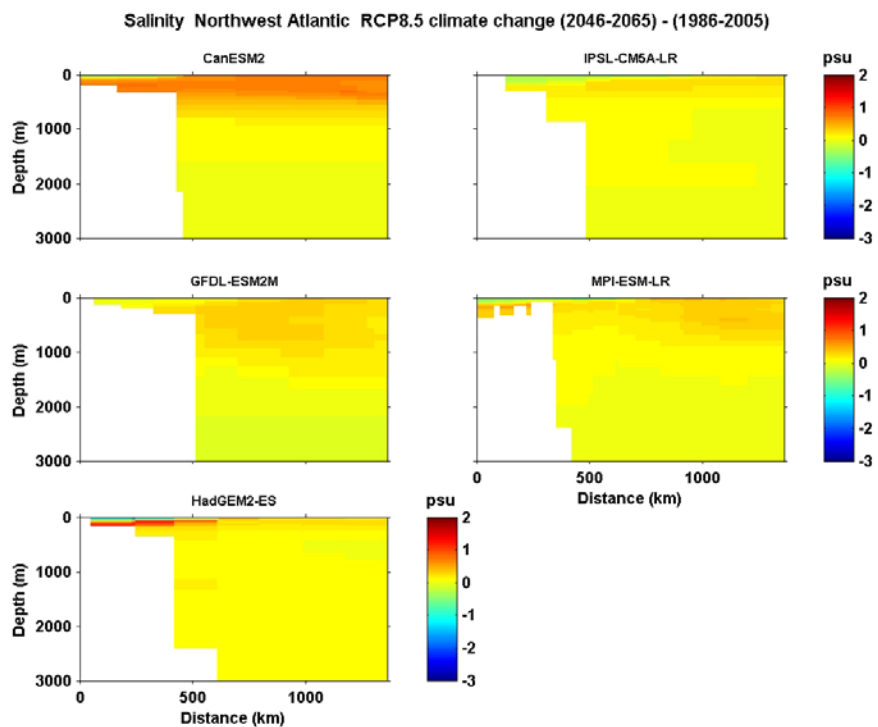


**Figure 7-4** Changes in bi-decadal mean salinity from 1986-2005 in the Historical simulations to 2046-2065 in the RCP8.5 simulations of five ESMs, on sections across a) Baffin Bay, b) the LSSS and c) the SSSR (NW Atlantic) sections.



b)



c)

**Figure 7-4** Changes in bi-decadal mean salinity from 1986-2005 in the Historical simulations to 2046-2065 in the RCP8.5 simulations of five ESMs, on sections across a) Baffin Bay, b) the LSSS and c) the SSSR (NW Atlantic) sections.

## 8 Ocean Mixed Layer Depth (OML-max)

In this section we examine the maximum depth of the Ocean Mixed Layer (OML-max) in the four ESMs from which data (interpolated to a common grid) for this variable were available. We choose February as a representative month for winter considering deep convection and the observed occurrence of maximum mixed layer depths in the NWA in late winter (e.g. Petrie et al. 1991; Umoh and Thompson 1994; Yashayaev and Loder 2009). OML-max is specified in CMIP5 as the “Monthly Maximum Ocean Mixed Layer Thickness defined by mixing scheme” (Taylor, 2012) such that, with the bi-decadal means used here, the displays are of the average over each bi-decade of the maximum OML depth in February in each year of the simulation.

Figure 8-1 presents the spatial distribution of OML-max in February for 1986-2005 from the Historical simulations and for 2046-2065 from the RCP8.5 simulations. There is a common coarse-scale pattern across the models in the Historical simulations (Figure 8-1a), with a band of enhanced mixed layer depths in a mid-latitude band extending eastward from Capes Cod-Hatteras in the Gulf Stream region (possibly related to observed “Eighteen Degree Water”; Talley and Raymer 1982), and with much larger enhancements in local areas of the subpolar region (consistent with deep convection; Yashayaev 2007). This pattern has some similarity to the observed climatology of de Boyer Montégut et al. (2004), but there is a notable difference in three of the models in that the mid-latitude and subpolar areas with deep mixed layers are not connected whereas they are in the observed climatology (and in GFDL-ESM2M).

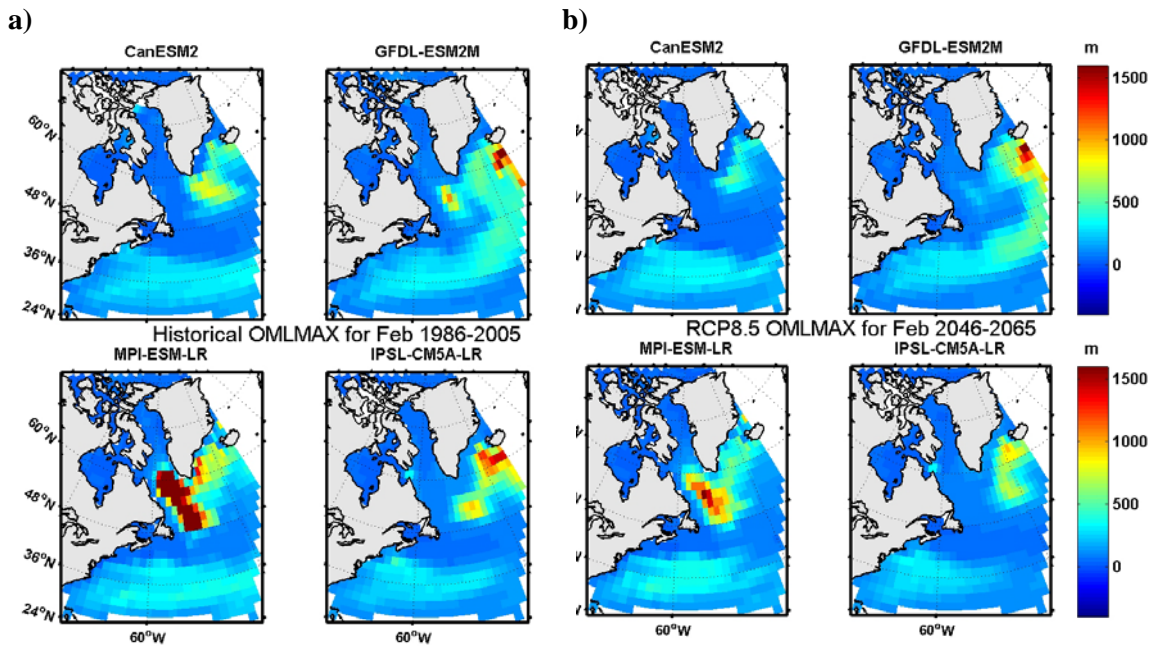


**Figure 8-1** Bi-decadal mean fields of OML-max in February from interpolated data from four ESMs for a) 1986-2005 from their Historical simulations and b) 2046-2065 from their RCP8.5 simulations.

There are also large inter-model differences in the magnitudes and detailed spatial structure of the enhanced subpolar mixed layer depths (Figure 8-1a). There is little deep convection in the

Labrador Sea in CanESM2 and IPSL-CM5A-LR, and only a small area of convection to 1000m in the southern Labrador Sea in GFDL-ESM2M, such that intermediate-depth water mass modification is less than observed in this area in these three ESMs (reminiscent of that in earlier versions of these models (de Jong et al. 2009). In contrast, there is a large area of deep mixed layers in MPI-ESM-LR that extend to the bottom (2800m) in some locations, which is much broader and deeper than observed.

The OML-max fields for February 2046-2065 (Figure 8-1b) show similar patterns to those for 1986-2005, with a reduction in the magnitude and extent of the large values in the subpolar region apparent. The climate changes in OML-max are better seen in the change fields between these periods shown in Figure 8-2. There are substantial (by >200m) reductions in OML-max in the subpolar areas with deep mixed layers, as well as patches with substantial increases in OML-max at the fringes of these areas. The former is expected with surface warming and freshening, while the latter probably reflects changes in ocean circulation of uncertain reliability (and slight horizontal shifts of the water with deep mixed layers). There is also a broad area with small (10-60m) increases in OML-max in the area of the enhanced depths extending eastward from Capes Cod-Hatteras to beyond the GB, especially in three of the models. These increases are probably related to some combination of changes in the position and structure of the Gulf Stream, Eighteen Degree Water and subpolar-subtropical gyre boundary, but this has not been examined in detail. Considering the discrepancies between the model and observed distributions of OML-max discussed in relation to Figure 8-1a, the projected changes from the models should be interpreted with caution, except perhaps for the reduced mixed layer depths in the subpolar deep convection areas which are consistent with expectations (e.g. Solomon et al. 2007).

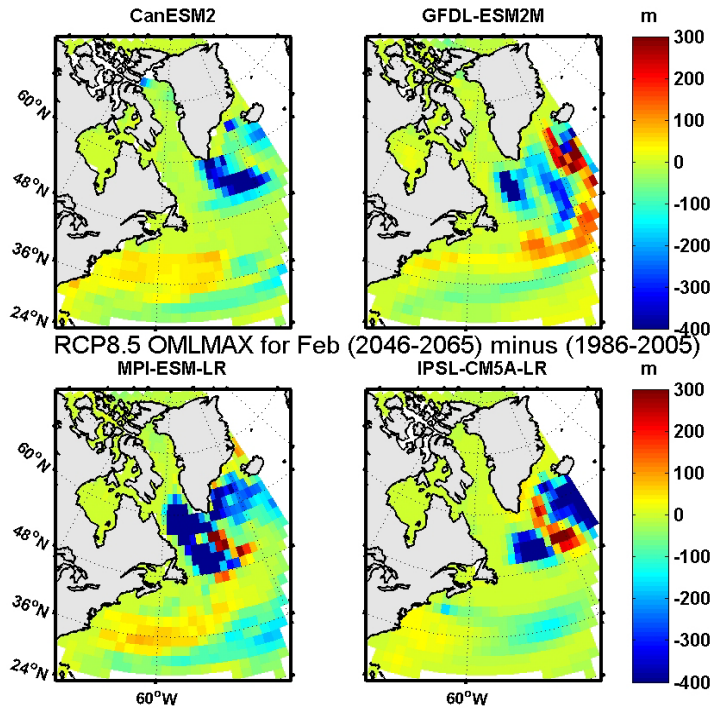


**Figure 8-2** Projected change in bi-decadal mean OML-max in February from four ESMs from 1986-2005 (Historical simulations) to 2046-2065 (RCP8.5 simulations).

## 9 Sea Surface Height (SSH)

In this section we examine changes in Sea Surface Height (SSH) in CanESM2 and GFDL-ESM2M, using data on their native grids. We use two output variables from these CMIP5 models (Taylor 2012):

- Sea Surface Height Above the Geoid referred to as “zos”, and
- Global Average Sea Level Change referred to as “zosga”.

zos varies with time and horizontal position, with the time variation being relative to the global average geoid height such that zos has a global average of zero. zosga varies only with time. As an approximation to the spatially- and temporally-varying SSH in the ESMs, we present displays of an “adjusted zos” taken as the sum of zos and zosga. This variable does not represent the total (relative to the coastline) sea level change expected from climate change since contributions from important factors such as Greenland and Antarctic ice sheet melting, gravitational interactions between the ice sheets and oceans, and regional vertical land movement associated with Glacial Isostatic Adjustment are not included (e.g. Slangen et al. 2011; Han et al. 2013).

Sea level rise projections from thirty-four CMIP5 models have recently been published by Yin (2012) including the two models that we use. Yin (2012) examined the contributions to sea level rise from “dynamic sea level” for which only zos was used (Jianjun Yin, personal communication, 2013) and global-ocean thermal expansion for which another CMIP5 variable called Global Average Thermosteric Sea Level Change (zostoga) was used. We have compared zosga and zostoga from CanESM2 and found close similarity in the long-term variation. GFDL-ESM2M did not have output available for zostoga

Figure 9-1 shows the bi-decadal mean distribution of adjusted zos (an indication of SSH relative to the geoid) around Canada from the Historical (1986-2005) and RCP8.5 (2046-2065) simulations of CanESM2 and GFDL-ESM2M for February and August. For a particular model, there is close similarity of the patterns and magnitudes in February and August, indicating limited seasonal variations. There is also similarity in the patterns for the past and future periods in a particular model, although a general increase in SSH is apparent. The largest difference in these SSH fields occurs between the two models. While there are similarities in the patterns within a particular ocean basin, there are substantial differences in the magnitudes in the two models in the Northeast Pacific Ocean and in Hudson Bay, in particular. For the western North Atlantic, both models show the known signature patterns of SSH in the subpolar (depression) and subtropical (dome) gyres, and the tail of depressed sea level extending equatorward over the western Atlantic continental shelf and slope associated with the extension of the subpolar gyre west of the Grand Bank (e.g. Yin et al. 2009). Note that the SSH difference between the centers of the subpolar and subtropical gyres is about 1.5m and that from the Gulf Stream to the Scotian Shelf nearly 1m which are comparable to, although slightly smaller than, observational estimates (Thompson et al. 2009).



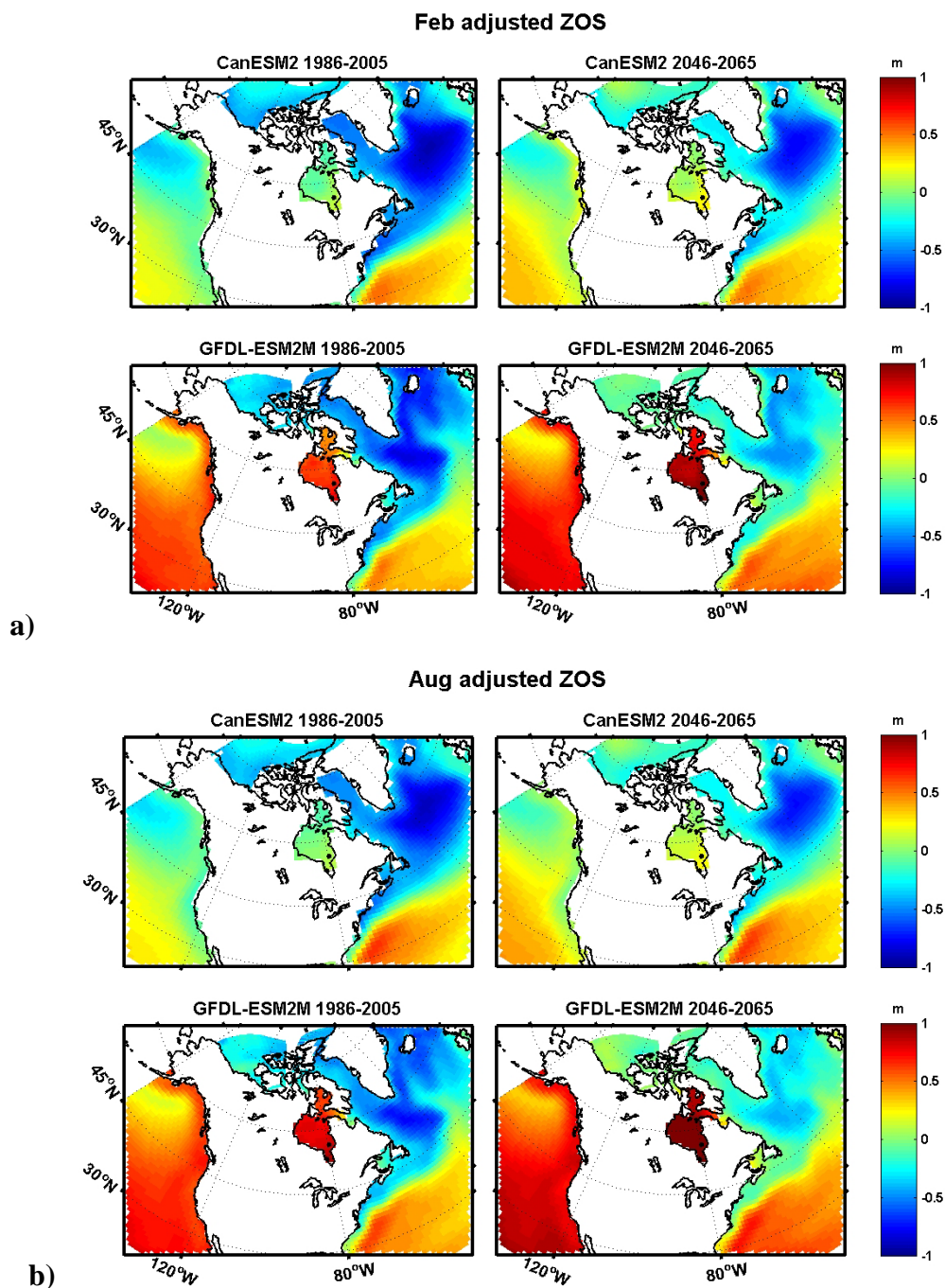


**Figure 9-1** Bi-decadal monthly mean adjusted SSH ( $zos + zosga$ ) for Canada for a) February and b) August, from CanESM2 and GFDL-ESM2M for 1986-2005 from their Historical simulations (left panels) and for 2046-2065 from their RCP8.5 simulations (right panels).

The projected climate changes in adjusted zos (SSH) around Canada for RCP8.5 are shown in Figure 9-2. While there is greater similarity in the change patterns in the Northeast Pacific from the two different models than in the bi-decadal mean SSH patterns, there are still significant differences in the patterns, particularly in the NWA. These patterns bear close resemblance to those (for the same models) in Supplementary Figure 5 of Yin (2012). The largest SSH increases occur in the subpolar NWA and parts of the Arctic, while there are small SSH decreases in the subtropical NWA and, in GFDL-ESM2M, in the northeastward extension of the subtropical gyre past the Grand Bank in the area of the North Atlantic Current. The detailed pattern of the SSH changes east of the Grand Bank is strikingly different in CanESM2 than in GFDL-ESM2M, reflecting differing changes (discussed above) in upper-ocean circulation which is undoubtedly a contributor to the different patterns in the TOS, SOS and OML-max changes in these models in this region. There is also a notable difference between the two models in the change patterns for the eastern Arctic and waters around Greenland. GFDL-ESM2M shows a broad area with an overall SSH increase with magnitudes nearly as large as the peak ones in the offshore North Atlantic, and CanESM2 has smaller increases in the eastern Arctic and NWA, particularly in Hudson Bay. The smaller increases may be related to the latter being largely land-locked in CanESM2.

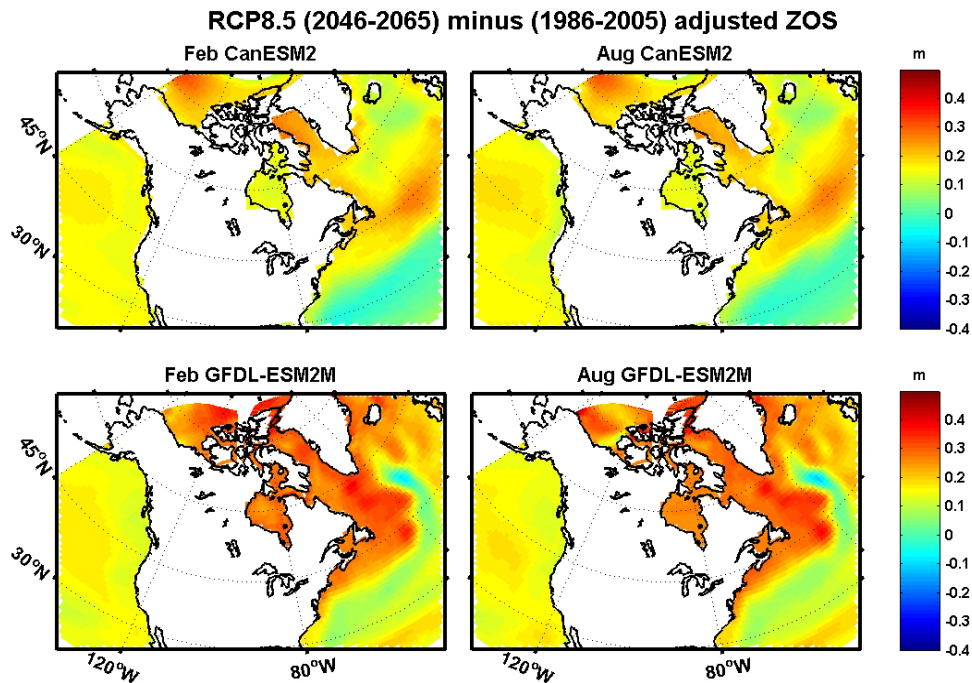


**Figure 9-2** Changes in bi-decadal mean adjusted SSH (zos + zosga) for Canada for February (left) and August (right) from CanESM2 (upper) and GFDL-ESM2M (lower), from 1986-2005 using the models' Historical simulations to 2046-2065 using their RCP8.5 simulations.

Figure 9-3 shows the projected changes in adjusted zos in the NW Atlantic and eastern Arctic for both RCP4.5 and RCP8.5. The change patterns for RCP4.5 in each of the models are very similar to those for RCP8.5, with the RCP4.5 magnitudes approximately 70% of those from RCP8.5.

Information on the origin of the different patterns is provided by the displays of bi-decadal mean zos and of changes in zos in the Appendix F. Recall that zos contributes the spatial patterns to adjusted zos.

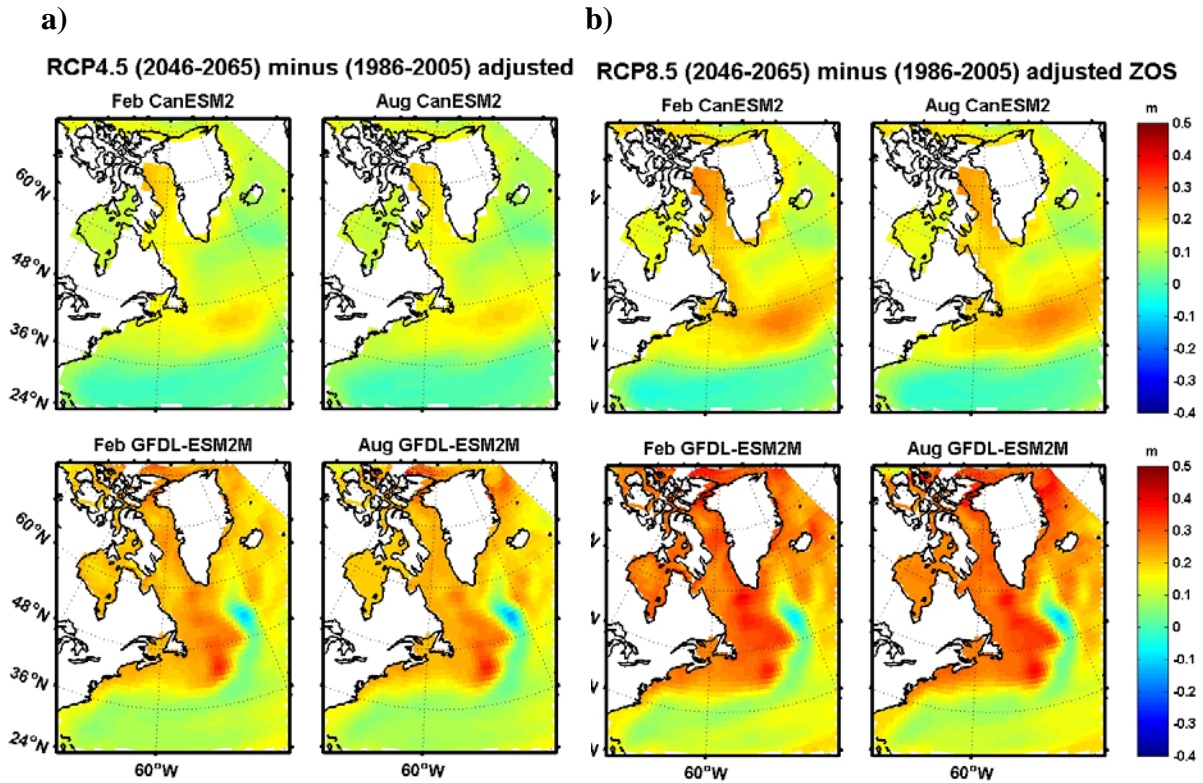


**Figure 9-3** Changes in bi-decadal mean adjusted SSH (zos + zosga) from 1986-2005 to 2046-2065 in February (left) and August (right), for the NWA from CanESM2 (upper row) and GFDL-ESM2M (lower row), for a) RCP4.5 and b) RCP8.5.

## 10 Summary, Discussion and Conclusions

The spatial and temporal variability of six variables has been examined in the Historical and future (RCP4.5 and RCP8.5) simulations of six Earth System Models (ESMs) being assessed in CMIP5 for IPCC AR5 (Taylor et al. 2012; Rogelj et al. 2012). A set of observational comparisons and projected changes for four variables (Surface Air Temperature or TAS, Sea Ice Concentration or SIC, Surface Ocean Temperature or TOS, and Surface Ocean Salinity or SOS) using interpolated monthly-mean data from a six-member ensemble of run 1 from all six ESMs has been presented, and variability in TAS, TOS and SOS among the runs of a particular model has been examined using 5 runs of CanESM2. Subsurface temperature and salinity, and maximum ocean mixed layer depth (OML-max) have been examined in five and four of the ESMs, respectively, and Sea Surface Height (SSH) and long-term variability in TAS, TOS and SOS have been examined in two ESMs. Attention has been focussed on eastern Canada and the NW Atlantic (NWA) which are of primary relevance to the Atlantic Large Aquatic Basin (LAB) being assessed in ACCASP, but some consideration of the Canada-wide distributions has been given for key variables (for input to assessments for other LABs). Attention has also been focussed on monthly climate changes from the 1986-2005 bi-decade in the Historical simulations to the 2046-2065 bi-decade in the future simulations, as an approximation to the potential changes on the ACCASP 50-Year time scale.

The climatological means and annual cycles of TAS are approximately reproduced at most sites in most (but not all) of the models, but past interannual-to-decadal-scale regional variability is not reproduced. These results are as expected for coarse-resolution global climate models.

For TOS and SOS, agreement between the model and observed means and annual cycles is reduced (compared to that for TAS), particularly for SOS. The large-scale TOS and SOS structures of the NWA's subpolar and subtropical gyres are approximately reproduced in the models, but there are significant differences in the location and structure of the boundary between the gyres. In particular, the subtropical gyre is too far north (Gulf Stream) in the Gulf of Maine (GoM) and Scotian Shelf (SS) region in the models, and not far enough north (North Atlantic Current) east of Flemish Cap. Alternatively expressed, subpolar water does not extend far enough equatorward along the shelf (e.g. SS-GoM) in the models, and there is too much subpolar water turning eastward north of the Grand Bank (GB). Probably related to the gyre structure in the models, seasonal ice cover in most of the models does not extend as far equatorward along the coast as observed but extends too far south in the offshore Labrador Sea. And probably related to the latter, the OML-max distributions and the vertical temperature and salinity distributions across the Labrador Sea indicate that there is much less deep convection there than observed. Further, observed decadal-scale TOS and SOS variability in the region is not reproduced by the models, again as expected for coarse-resolution models.

Collectively, the comparison of the model and observed distributions and annual cycles of these key variables indicates that there are substantial differences in the representation of coupled ice-ocean variability in the NWA among the models, and in the detailed spatial and temporal patterns between the models and observations. It is doubtful whether any of the models have an adequate representation of regional ocean dynamics to reliably simulate ocean climate variability

and change, but it is unclear whether any of the models examined are worse than the others to the point that they should be rejected from an ensemble approach to climate change projections.

The common approach (e.g. in IPCC AR4 and AR5) to obtaining useful climate change projections (from models which are not able to resolve natural decadal- and regional-scale climate variability) is to consider the ensemble statistics of the models' simulations. This approach has been used here for run 1 from the six ESMs, using bi-decadal monthly mean fields interpolated to a common grid and provided by J. Christian of DFO-IOs. The observational annual-cycle comparisons for TAS, TOS and SOS for 1986-2005 at selected observation sites (Figures 3-2b, 5-3b, 6-3b), indicating that the observed bi-decadal monthly means are generally within the inter-model standard deviations of the ensemble-mean monthly values from the models' Historical simulations, provide some encouragement for the utility of this approach and the ESM fields. However, it should be cautioned that limitations are expected for features with space scales not resolved by the ice and ocean components of the ESMs.

The projected ensemble-mean climate changes in TAS show the previously-identified (e.g. Meehl et al. 2007) Arctic amplification in winter, and the weaker mid-latitude continental amplification in summer, with both having apparent extensions across part of the Atlantic LAB. As a result, the winter TAS climate changes are largest in the northern part of the LAB and smallest in the southern part, while there is no clear seasonal variation in the southern part. However, the inter-model spread of the projected changes is of comparable magnitude to the ensemble-mean changes (except for the northern sites in winter), such that there is uncertainty regarding the magnitude of the changes. The projected ensemble-mean climate changes in SIC show seasonal reductions in the areas of the Atlantic LAB that are near the limit of seasonal ice cover in the Historical simulations, consistent with expectations for atmospheric warming. It is noteworthy that, in the different models, the offshore extent of the winter area of amplified TAS increase approximates that of the winter offshore extent of sea ice in the Labrador Sea, suggesting an inter-relation that may have implications for the reliability of detailed projections of both the TAS and SIC for the region.

The projected ensemble-mean TOS changes over the Atlantic LAB are largest in a mid-latitude zonal band of warming extending eastward from the GoM-SS-GB and Gulf of St. Lawrence (GSL) region, with largest magnitudes and extent in summer. This feature bears some similarity to the zonal band of amplified TAS increases that extends offshore across the southern part of the LAB in summer, pointing to the likelihood of an inter-relation between the TAS and TOS changes although the origin (atmospheric versus oceanic) is unclear. The presence of a weaker version of this feature in the winter TOS changes, together with the evidence from the SOS and SSH changes of a northward expansion of the subtropical gyre in the region, suggest a strong oceanic influence in this band of amplified TAS and TOS warming. If this is the case, there is the possibility that the poor representation of the regional ocean in the ESMs is affecting the TAS patterns (as well as those of other atmospheric variables).

In the northern part of the LAB, the ensemble-mean TOS climate changes are smaller (than in the southern part), except in coastal and the Baffin Bay regions in summer where there is notable warming. In winter, there is an area of cooling south of Greenland similar to that in previous model projections and sometimes attributed to a projected reduction in the Atlantic Meridional



Overturning Circulation (AMOC) in the models (e.g. Meehl et al. 2007). This feature extends into the southeastern Labrador Sea in some of the ESMs, resulting in little (ensemble-mean) warming in the offshore Labrador Sea in winter and only weak warming in summer. There is also no winter warming in the northern parts of the LAB (e.g. Baffin Bay) that remain ice-covered in winter in the model projections, in stark contrast to the amplified warming of the overlying atmosphere (due to the insulating effect of the sea ice and the TAS remaining below freezing).

On the quantitative side for the Atlantic LAB's shelf, the ESMs indicate that the winter (February) increases in TOS on the 50-Year time scale will be in the range of 0-1 °C for the Northern Labrador Shelf, 0-2 °C from the Central Labrador Shelf to Flemish Cap, 1-3 °C for the GB and Southern Newfoundland Shelf, and 1-4 °C for the GSL, SS and west. They indicate that the summer (August) changes will be in the 0-4 °C range on the Labrador and Newfoundland Shelves, and in the 1-5 °C range for Flemish Cap, GSL, SS, and GoM. The ranges are similar for off-shelf areas in the LAB, with the exceptions that some models project cooling in the Labrador Sea and waters south of Greenland (particularly in winter) and some project localized areas of greater warming near the boundary of the subpolar and subtropical gyres.

The projected ensemble-mean SOS changes indicate a general pattern of year-round freshening over most of the Atlantic LAB as expected in subpolar waters, and a slight increase in SOS in the subtropical waters that encroach on the southern part of the LAB, again as expected. The transition zone (little change in SOS) varies from model to model, and lies in the 40-42°N latitude range in the ensemble-mean pattern. However, the spread in the magnitude of the projected changes in both the six-member ESM ensemble and the five-member CanESM2 ensemble generally exceeds the magnitude of the ensemble-mean change, and there are qualitative inconsistencies among the annual cycles from some of the models in some areas, such that the magnitudes and detailed spatial structure of the SOS changes remain uncertain.

The projected climate changes in the vertical distribution of annual-mean ocean temperature and salinity on three cross-basin sections in five of the ESMs indicate that the TOS and SOS changes are representative of widely-varying upper-layer depths in the various models and areas covered. The peak warming is below the surface in many areas (e.g. Baffin Bay) and near the surface in other areas (e.g. Scotian Shelf and Slope). The largest changes in salinity are generally at or near the surface. Considering the differences among the models in the temperatures and salinities on these sections in the 1986-2005 historical periods, it is difficult to interpret the vertical structure of the changes as well as to assess their reliability.

The differing patterns of OML-max among the models, and the poor agreement of these patterns with the subpolar areas of observed deep convection, raise further questions about the reliability of the projected subsurface temperature and salinity changes. Nevertheless, the projected climate changes in OML-max in the four ESMs examined point to reduced depths of deep convection in the subpolar areas where it occurs, consistent with expectations. The models also show consistency in a band of increased OML-max values extending eastward from Capes Cod-Hatteras, possibly related to changes in the position and structure of the Gulf Stream or the subtropical-subpolar gyre boundary, or an increased depth of newly-formed "Eighteen Degree Water". However, this needs further investigation.

The projected climate changes in SSH in both CanESM2 and GFDL-ESM2M show amplified increases in the NW Atlantic, although there are differences in the detailed patterns and in the magnitudes of the changes in Baffin and Hudson Bays. The different patterns in the models provide a further indication of the differences in the two models' representation of the interaction of the subpolar and subtropical gyres, although both show lower increases in the subtropical gyre dome than elsewhere pointing to a relaxation (and northward expansion of the gyre). The magnitudes of the projected 50-Year changes in this component of sea level rise along the Atlantic LAB's coast are in the 0.15-0.35m range for the two models and RCPs. Together with the amplified increases in the NW Atlantic found by Yin (2012) for a much larger ensemble of CMIP5 models, and observational trends (e.g. Sallenger et al. 2012), there is a strong basis for projecting SSH increases in the Atlantic LAB. It should also be noted that there are other expected contributions to relative (to the land) sea level rise in the region, such as the contribution from land vertical motion associated with Glacial Isostatic Adjustment (GIA) which is expected to contribute an additional 0.1m to relative rise in the southern part of the LAB (e.g. Han et al. 2013). On the other hand, there is rising (uplifting) land due to GIA some parts (e.g. northern GSL and Baffin Bay) of the Atlantic LAB which will at least partly offset the ocean climate contributions to relative sea level rise. Further, in the longer term, the reduced gravitational attraction of a melting Greenland ice sheet is expected to make a contribution towards sea level fall in the northern part of the Atlantic LAB (e.g. Slangen et al. 2011).

In conclusion, it should be emphasized that the six ESMs examined here are just a subset of the CMIP5 AOGCMs being examined in IPCC AR5, and the CMIP5 models are only one of a number of information sources that need to be considered in developing projections and assessing their reliability for use in planning and decision-making. With the limited number of models and information sources considered here, it is difficult to provide firm quantitative estimates of the projected changes and to quantify their uncertainty. However, it is clear from the discrepancies between their Historical simulations and observations for a number of key variables in the Atlantic LAB that the present generation of AOGCMs continue to have problems with resolving important features (e.g. sea ice, ocean gyres, Arctic outflows, annual cycles) of the coupled atmosphere-ice-ocean system in the NW Atlantic. There are also indications from the ESMs examined here that some of these inadequacies may be degrading the simulations of regional atmospheric variability in the models. Thus, caution needs to be used in the application and interpretation of projected regional changes from these (and previous) AOGCMs, whether in using their outputs directly for impacts assessments and adaptation planning, or indirectly through inputs to regional dynamical or statistical down-scaling.



## 11 **Acknowledgements**

This examination of ESMs was carried out as part of the climate trends and projections activities in DFO's Aquatic Climate Change Adaptation Service Program (ACCASP), with the objective of providing input to ACCASP risk assessments for the Atlantic and Arctic Large Aquatic Basins (LABs). Model data were obtained directly or indirectly from the Climate Model Intercomparison Project Phase 5 (CMIP5) of the Program for Climate Model Diagnosis and Intercomparison (PCMDI; <http://www.pcmdi.llnl.gov/>). The organizations that contributed the model data to CMIP5 are gratefully acknowledged for their immense and important work in the development and running of the models, and in the availability of the data.

A key contribution to this study was the availability of surface fields for TAS, SIC, TOS, SOS and OML-max from the six ESMs on a common grid, generously provided by Jim Christian of DFO-IOS to whom we are grateful. We also thank Diane Lavoie of DFO-IOS and colleagues at the Canadian Centre for Climate Modelling and Analysis (CCCMA) for sharing model fields.

We thank Igor Yashayaev of DFO-BIO for invaluable contributions through the provision of climatological fields for observed ocean temperature and salinity in the NW Atlantic and for time series from the Labrador Sea. We also thank Roger Pettipas of DFO-BIO for providing observational time series from AZMP.

Finally, we thank the following for other inputs to the study and/or comments on the report: David Brickman, Jim Christian, Brendan DeTracey, Guoqi Han, Diane Lavoie, Warren Lee, Bill Merryfield, and Ingrid Peterson.

## 12 References

- Andrews, T., J. M. Gregory, M. J. Webb, and K. E. Taylor (2012). Forcing, feedbacks and climate sensitivity in CMIP5 coupled atmosphere-ocean climate models, *Geophys. Res. Lett.*, 39, L09712, doi:10.1029/2012GL051607.
- Arora, V. K., J. F. Scinocca, G. J. Boer, J. R. Christian, K. L. Denman, G. M. Flato, V. V. Kharin, W. G. Lee, and W. J. Merryfield (2011). Carbon emission limits required to satisfy future representative concentration pathways of greenhouse gases, *Geophys. Res. Lett.*, 38(5), L05805, doi:10.1029/2010GL046270.
- Bindoff, N. L., J. Willebrand, V. Artale, A. Cazenave, J. Gregory, S. Gulev, K. Hanawa, C. Le Quéré, S. Levitus, Y. Nojiri, C. K. Shum, L. D. Talley, and A. Unnikrishnan (2007). Observations: Oceanic Climate Change and Sea Level, In: *Climate Change 2007: The Physical Science Basis. Contribution of Working Group I to the Fourth Assessment Report of the Intergovernmental Panel on Climate Change* [Solomon, S., D. Qin, M. Manning, Z. Chen, M. Marquis, K. B. Averyt, M. Tignor, and H. L. Miller (Eds.)], Cambridge University Press, Cambridge, United Kingdom and New York, NY, USA.
- Booth, B. B. B., N. J. Dunstone, P. R. Halloran, T. Andrews, and N. Bellouin (2012). Aerosols implicated as a prime driver of twentieth-century North Atlantic climate variability, *Nature*, 484(7393): 228-232, doi: 10.1038/nature10946.
- Brovkin, V., L. Boysen, T. Raddatz, V. Gayler, A. Loew, and M. Claussen (2012). Evaluation of vegetation cover and land-surface albedo in MPI-ESM CMIP5 simulations, *J. Adv. Model. Earth Syst.*, 5: 48-57, doi:10.1029/2012MS000169.
- Bryan, F. O., M. W. Hecht, and R. D. Smith (2007). Resolution convergence and stability studies with North Atlantic circulation models. Part I: The western boundary current system, *Ocean Modell.*, 16(3-4): 141-159.
- Bukovsky, M. S. (2012). Temperature trends in the NARCCAP regional climate models, *J. Clim.*, 25(11): 3985–3991.
- Capotondi, A., M. A. Alexander, N. A. Bond, E. N. Curchitser, and J. D. Scott (2012). Enhanced upper ocean stratification with climate change in the CMIP3 models, *J. Geophys. Res.*, 117(C4), C04031, doi: 10.1029/2011JC007409.
- Cavalieri, D. J. and C. L. Parkinson (2012). Arctic sea ice variability and trends, 1979-2010, *The Cryosphere*, 6: 881-889, doi:10.5194/tc-6-881-2012.
- Chassé, J., W. Perrie, Z. Long, D. Brickman, L. Guo, and N. Lambert (2013). Regional atmosphere-ocean-ice climate downscaling results for the Gulf of St. Lawrence using the DFO Regional Climate Downscaling System, Can. Tech. Rep. Hydrogr. Ocean Sci. (under revision).

- Cheng, W., J. C. H. Chiang, and D. Zhang (2013). Atlantic Meridional Overturning Circulation (AMOC) in CMIP5 models: RCP and historical simulations, *J. Clim.*, doi.org/10.1175/JCLI-D-12-00496.1.
- Christian, J. R., and M. G. G. Foreman (Eds.) (2013). Climate trends and projections for the Pacific Aquatic Basin, Can. Tech. Rep. Fish. Aquat. Sci. 3032: xi + 112 p.
- Colbourne, E., J. Craig, C. Fitzpatrick, D. Senciall, P. Stead, and W. Bailey (2012). An assessment of the physical oceanographic environment on the Newfoundland and Labrador Shelf during 2011. Fisheries and Oceans Canada, Can. Sci. Advis. Sec. Res. Doc. 2012/044. iv + 33 p. [http://www.dfo-mpo.gc.ca/csas-sccs/Publications/ResDocs-DocRech/2012/2012\\_044-eng.html](http://www.dfo-mpo.gc.ca/csas-sccs/Publications/ResDocs-DocRech/2012/2012_044-eng.html)
- de Boyer Montégut, C., G. Madec, A.S. Fischer, A. Lazar, and D. Iudicone (2004). Mixed layer depth over the global ocean: an examination of profile data and a profile-based climatology, *J. Geophys. Res.*, 109(C12), C12003, doi:10.1029/2004JC002378.
- de Jong, M. F., S. S. Drijfhout, W. Hazeleger, H. M. van Aken, and C. A. Severijns (2009). Simulations of hydrographic properties in the northwestern North Atlantic Ocean in coupled climate models, *J. Clim.*, 22: 1767–1786, doi:10.1175/2008JCLI2448.1.
- DFO (2013a). Risk-based assessment of climate change impacts and risks on the biological resources and infrastructure within Fisheries and Oceans Canada’s mandate – Atlantic Large Aquatic Basin. Fisheries and Oceans Canada, Can. Sci. Sec. Sci. Resp. 2012/044. 40 p. [http://www.dfo-mpo.gc.ca/csas-sccs/Publications/ScR-RS/2012/2012\\_044-eng.html](http://www.dfo-mpo.gc.ca/csas-sccs/Publications/ScR-RS/2012/2012_044-eng.html)
- DFO (2013b). Risk-based assessment of climate change impacts and risks on the biological resources and infrastructure within Fisheries and Oceans Canada’s mandate – Arctic Large Aquatic Basin, Fisheries and Oceans Canada, Can. Sci. Sec. Sci. Resp. 2012/042, 39 p. [http://www.dfo-mpo.gc.ca/csas-sccs/Publications/ScR-RS/2012/2012\\_042-eng.html](http://www.dfo-mpo.gc.ca/csas-sccs/Publications/ScR-RS/2012/2012_042-eng.html)
- Diffenbaugh, N. S. and F. Giorgi (2012). Climate change hotspots in the CMIP5 global climate model ensemble, *Climatic Change*, 114: 813-822, doi:10.1007/s10584-012-0570-x.
- Drijfhout, S., G. J. van Oldenborgh, and A. Cimadoribus (2012). Is a decline of AMOC causing the warming hole above the North Atlantic in observed and modeled warming patterns? *J. Clim.*, 25: 8373-8379, doi:10.1175/JCLI-D-12-00490.1.
- Dufresne, J.-L., M.-A. Foujols, S. Denvil, A. Caubel, O. Marti and 56 others (2013). Climate change projections using the PSL-CM5 Earth System Model: from CMIP3 to CMIP5, *Clim. Dyn.*, 40(9-10): 2123-2165, doi:10.1007/s00382-0S. 12-1636-1.
- Dunne, J. P., J. G. John, A. J. Adcroft, S. M. Griffies, R. W. Hallberg, E. Shevliakova, R. J. Stouffer, W. Cooke, K. A. Dunne, M. J. Harrison, J. P. Krasting, S. L. Malyshev, P. C. D. Milly, P. J. Phillipps, L. T. Sentman, B. L. Samuels, M. J. Spelman, M. Winton, A. T. Wittenberg, and N. Zadeh (2012). GFDL’s ESM2 Global Coupled Climate–Carbon Earth System Models. Part I: Physical formulation and baseline simulation characteristics, *J. Clim.*, 25: 6646–6665, doi:10.1175/JCLI-D-11-00560.

- Durack, P. J. and S. E. Wijffels (2010). Fifty-year trends in global ocean salinities and their relationship to broad-scale warming, *J. Clim.*, 23: 4342-4362, doi:10.1175/2010JCLI3377.1.
- Durack, P. J., S. E. Wijffels, and R. J. Matear (2012). Ocean salinities reveal strong global water cycle intensification during 1950 to 2000, *Science*, 336(6080): 455-458.
- Han, G., Z. Ma, J. Loder, H. Z. Bao and A. van der Baaren (2013). Mean sea level trends in the Northwest Atlantic: Historical estimates and future projections, *In: Aspects of Climate Change in the Northwest Atlantic off Canada* [Loder, J. W., A. van der Baaren, G. Han, P. S. Galbraith and J. Chassé (Eds.)], Can. Tech. Rep. Fish. Aquat. 3045 (in press).
- Harvey, B. J., L. C. Shaffrey, T. J. Woolings, G. Zappa, and K. I. Hodges (2012). How large are projected 21<sup>st</sup> century storm track changes? *Geophys. Res. Lett.*, 39(18), L18707, doi:10.1029/2012GL052873.
- Henry, M. (2011). Sea ice trends in Canada, pp. 3-13 *In: Envirostats Service Bulletin, Winter 2011*, Statistics Canada Catalogue No. 16-002-X <http://www.statcan.gc.ca/pub/16-002-x/2011004/part-partie3-eng.htm>
- Ishizaki, Y., H. Shiogama, S. Emori, T. Yokohata, T. Nozawa, T. Ogura, M. Abe, M. Yoshimori, and K. Takahashi (2012). Temperature scaling pattern dependence on representative concentration pathway emission scenarios, *Climatic Change*, 112(2): 535-546, doi:10.1007/s10584-012-0430-8.
- Lavoie, D., N. Lambert, S. ben Mustafa, and A. van der Baaren (2013a). Projections of future physical and biogeochemical conditions in the Northwest Atlantic from CMIP5 Global Climate Models, Can. Tech. Rep. Hydrog. Ocean. Sci. 285: xiv + 156 p.
- Lavoie, D. and N. Lambert (2013b). Projections of future physical and biogeochemical conditions in Hudson and Baffin Bays CMIP5 Global Climate Models, Can. Tech. Rep. Hydrog. Ocean. Sci. 289: xiii + 129 p.
- Li, W., L. Li, M. Ying, and Y. Liu (2012a). Intensification of Northern Hemisphere subtropical highs in a warming climate, *Nature Geosci.*, 5: 830-834, doi:10.1038/ngeo1590.
- Li, G., X. Zhang, F. Zwiers, and Q. H. Wen (2012b). Quantification of uncertainty in high-resolution temperature scenarios for North America, *J. Clim.*, 25,:3373-3389.
- Loder, J. W., A. van der Baaren, and I. Yashayaev (2011). Ocean climate change in the NW Atlantic, 45<sup>th</sup> Congress of the Canadian Meteorological and Oceanographic Society, June 5-9, Victoria, B.C. <http://www.cmos.ca/CongressAbstracts/cong4511.pdf>
- Loder, J. W., J. Chassé, P. Galbraith, G. Han, D. Lavoie and others (2013). Summary of climate change trends and projections for the Atlantic Large Aquatic Basin off Canada, Can Tech Rep Fish Aquat. Sci. 3051 (under revision)
- Loder, J. W., Z. Wang, A. van der Baaren and R. Pettipas (2013). Trends and variability of sea surface temperature in the North Atlantic, from the HadISST, ERSST, and COBE datasets, Can. Tech. Rep. Hydrogr. Ocean Sci. 290 (in press).

- Marti, O., P. Braconnot, J.-L. Dufresne, J. Bellier, R. Benshila, S. Bony, P. Brockmann, P. Cadule, A. Caubel, F. Codron, N. de Noblet, S. Denvil, L. Fairhead, T. Fichefet, M.-A. Foujols, P. Friedlingstein, H. Goosse, J.-Y. Grandpeix, E. Guilyardi, F. Hourdin, A. Idelkadi, M. Kageyama, G. Krinner, C. Lévy, G. Madec, J. Mignot, I. Musat, D. Swingedouw, and C. Talandier (2010). Key features of the IPSL ocean atmosphere model and its sensitivity to atmospheric resolution, *Clim. Dyn.*, 34(1): 1-26, doi:10.1007/s00382-009-0640-6.
- Meehl, G. A., T. F. Stocker, W. D. Collins, P. Friedlingstein, A. T. Gaye, J. M. Gregory, A. Kitoh, R. Knutti, J. M. Murphy, A. Noda, S. C. B. Raper, I. G. Watterson, A. J. Weaver, and Z.-C. Zhao (2007). Global Climate Projections. In: *Climate Change 2007: The Physical Science Basis. Contribution of Working Group I to the Fourth Assessment Report of the Intergovernmental Panel on Climate Change* [Solomon, S., D. Qin, M. Manning, Z. Chen, M. Marquis, K. B. Averyt, M. Tignor and H. L. Miller (Eds.)]. Cambridge University Press, Cambridge, United Kingdom and New York, NY, USA.
- Mizuta, R. (2012). Intensification of extratropical cyclones associated with the polar jet change in the CMIP5 global warming projections, *Geophys. Res. Lett.*, 39, L19707, doi:10.1029/2012GL053032.
- Moss, R. H., J. A. Edmonds, K. A. Hibbard, M. R. Manning, S. K. Rose, D. P. van Vuuren, T. R. Carter, S. Emori, M. Kainuma, T. Kram, G. A. Meehl, J. F. B. Mitchell, N. Nakicenovic, K. Riahi, S. J. Smith, R. J. Stouffer, A. M. Thomson, J. P. Weyant, and T. J. Wilbanks (2010). The next generation of scenarios for climate change research and assessment, *Nature*, 463: 747-756, doi:10.1038/nature08823.
- Nakićenović, N., J. Alcamo, G. Davis, B. de Vries, J. Fenhann, S. Gaffin, K. Gregory, A. Grubler, T. Y. Jung, T. Kram, E. L. La Rovere, L. Michaelis, S. Mori, T. Morita, W. Pepper, H. Pitcher, L. Price, K. Riahi, A. Roehrl, H.-H. Rogner, A. Sankovski, M. Schlesinger, P. Shukla, S. Smith, R. Swart, S. van Rooijen, N. Victor, and Z. Dadi (2000). *IPCC Special Report on Emissions Scenarios*, Cambridge, U. K. and New York: Cambridge University Press. [http://www.grida.no/publications/other/ipcc\\_sr/](http://www.grida.no/publications/other/ipcc_sr/)
- Overland, J. E. and M. Wang (2013). When will the summer Arctic be nearly ice free? *Geophys. Res. Lett.*, 40(10): 2097-2101, doi: 10.1002/grl.50316.
- Palmer, M. D., S. A. Good, K. Haines, N. A. Rayner, and P. A. Stott (2009). A new perspective on warming of the global oceans, *Geophys. Res. Lett.*, 36, L20709, doi:10.1029/2009GL039491.
- Peters, G. P., R. M. Andrew, T. Boden, J. G. Canadell, P. Ciais, C. Le Quéré, G. Marland, M. R. Raupach, and C. Wilson (2013). The challenge to keep global warming below 2° C. *Nature Climate Change*, 3: 4-6, doi:10.1038/nclimate1783.
- Peterson, I. K. and R. Pettipas (2013). Trends in air temperature and sea ice in the Atlantic Large Aquatic Basin and adjoining areas, *Can. Tech. Rep. Hydrogr. Ocean Sci.* 290: v + 59 p.
- Petrie, B. and K. D. Drinkwater (1993). Temperature and salinity variability on the Scotian Shelf and Gulf of Maine 1945-1990, *J. Geophys. Res.*, 98(C11): 20079-20089.

- Petrie, B., J. W. Loder, S. Akenhead, and J. Lazier (1991). Temperature and salinity variability on the eastern Newfoundland Shelf: The annual harmonic, *Atmos.-Ocean*, 29: 14-36, doi: 10.1080/07055900.1991.9649390.
- Rayner, N. A., D. E. Parker, E. B. Horton, C. K. Folland, L. V. Alexander, D. P. Rowell, E. C. Kent, and A. Kaplan (2003). Global analyses of sea surface temperature, sea ice, and night marine air temperature since the late nineteenth century, *J. Geophys. Res.*, 108(D14), doi:10.1029/2002JD002670.
- Rogelj, J., M. Meinshausen, and R. Knutti (2012). Global warming under old and new scenarios using IPCC climate sensitivity range estimates, *Nature Climate Change*, 2: 248-253, doi:10.1038/nclimate1385.
- Sallenger, A. H., K. S. Doran, and P. A. Howd (2012). Hotspot of accelerated sea-level rise on the Atlantic coast of North America, *Nature Climate Change*, 2: 884-888, doi:10.1038/nclimate1597.
- Serreze, M. C. and R. G. Barry (2011). Processes and impacts of Arctic amplification: A research synthesis, *Global Planet. Change*, 77: 85–96, doi:10.1016/j.gloplacha.2011.03.004.
- Sillmann, J., V. V. Kharin, X. Zhang, F. W. Zwiers, and D. Bronaugh (2013a). Climate extremes indices in the CMIP5 multimodel ensemble: Part 1. Model evaluation in the present climate, *J. Geophys. Res. Atmos.*, 118(4):1716-1733, doi:10.1002/jgrd.50203.
- Sillmann, J., V. V. Kharin, X. Zhang, F. W. Zwiers, and D. Bronaugh (2013b). Climate extremes indices in the CMIP5 multimodel ensemble: Part 2. Future climate projections, *J. Geophys. Res. Atmos.*, 118(6): 2473–2493, doi:10.1002/jgrd.50188.
- Slangen, A. B. A., C. A. Katsman, R. S. W. van de Wal, L. L. A. Vermeersen, and R. E. M. Riva (2011). Towards regional projections of twenty-first century sea-level change based on IPCC SEES scenarios, *Clim. Dyn.*, 38(5-6): 1191-1209, doi:10.1007/s00382-011-1057-6.
- Solomon, S., D. Qin, M. Manning, R. B. Alley, T. Berntsen, N. L. Bindoff, Z. Chen, A. Chidthaisong, J. M. Gregory, G. C. Hegerl, M. Heimann, B. Hewitson, B. J. Hoskins, F. Joos, J. Jouzel, V. Kattsov, U. Lohmann, T. Matsuno, M. Molina, N. Nicholls, J. Overpeck, G. Raga, V. Ramaswamy, J. Ren, M. Rusticucci, R. Somerville, T. F. Stocker, P. Whetton, R. A. Wood, and D. Wratt (2007). Technical Summary. In: *Climate Change 2007: The Physical Science Basis. Contribution of Working Group I to the Fourth Assessment Report of the Intergovernmental Panel on Climate Change* [Solomon, S., D. Qin, M. Manning, Z. Chen, M. Marquis, K. B. Averyt, M. Tignor, and H. L. Miller (Eds.)]. Cambridge University Press, Cambridge, United Kingdom and New York, NY, USA.
- Steiner, N., K. A. Azetsu-Scott, P. Galbraith, J. Hamilton, K. Hedges, X. Hu, M.Y. Janjua, N. Lambert, P. Larouche, D. Lavoie, J. Loder, H. Melling, A. Merzouk, P. Myers, W. Perrie, I. Peterson, R. Pettipas, M. Scarratt, T. Sou, M. Starr, R.F. Tallmann and A. van der Baaren (2013). Climate change trends and projections assessment in the Arctic basin – a contribution to the Aquatic Climate Change Adaptation Services Program. Can. Tech. Rep. Fish. Aquat. Sci. 3042: xv + 163 p.



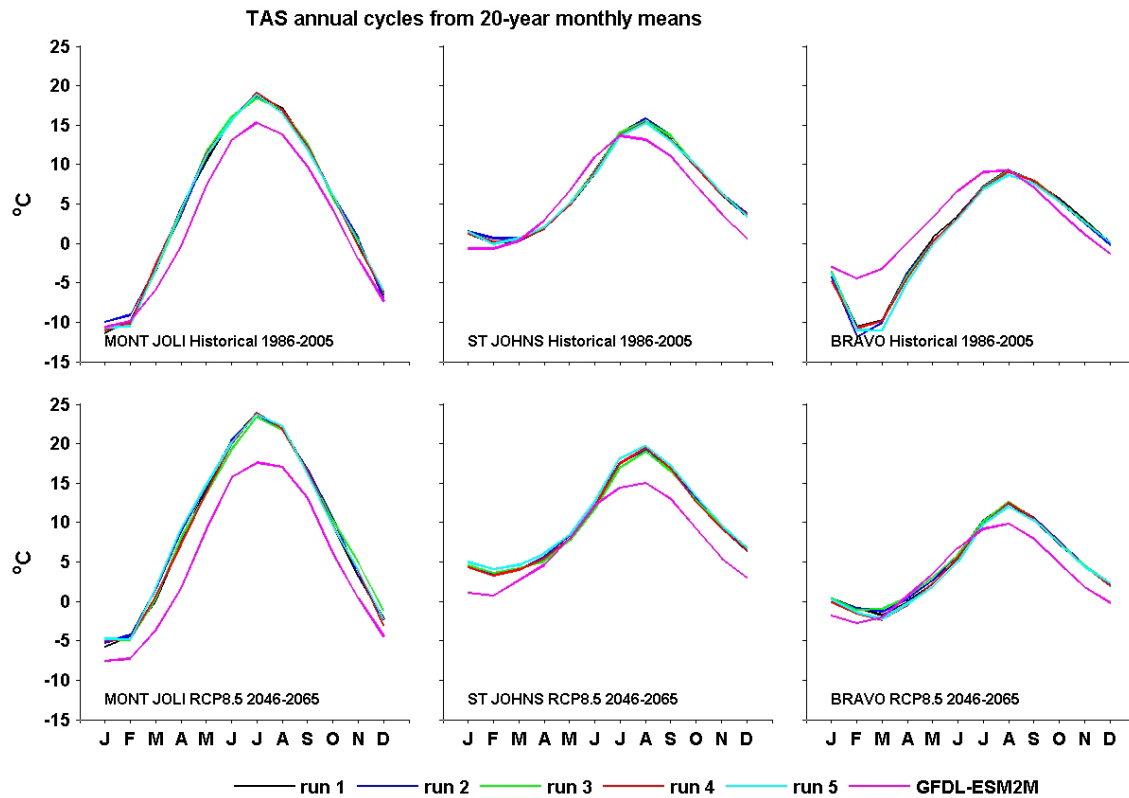
- Stroeve, J. C., V. Kattsov, A. Barrett, M. Serreze, T. Pavlova, M. Holland, and W. N. Meier (2012). Trends in Arctic sea ice extent from CMIP5, CMIP3, and observations, *Geophys. Res. Lett.*, 39(16), L16502. doi [10.1029/2012GL052676](https://doi.org/10.1029/2012GL052676).
- Sutcliffe, W. H., R. H. Loucks, and K. F. Drinkwater (1976). Coastal circulation and physical oceanography of the Scotian Shelf and Gulf of Maine, *J. Fish. Res. Bd. Can.*, 33(1): 98-115, doi: 10.1139/f76-012.
- Talley, L. D. and M. E. Raymer (1982). Eighteen Degree water variability, *J. Mar. Res.*, 40(52): 757-775.
- Taylor, K. (2012). CMIP5 standard\_output (12 March 2012). [http://cmip-pcmdi.llnl.gov/cmip5/docs/standard\\_output.pdf](http://cmip-pcmdi.llnl.gov/cmip5/docs/standard_output.pdf)
- Taylor, K. E., R. J. Stouffer, and G. A. Meehl (2011). A summary of the CMIP5 experiment design (12 January 2011). [http://cmip-pcmdi.llnl.gov/cmip5/docs/Taylor\\_CMIP5\\_design.pdf](http://cmip-pcmdi.llnl.gov/cmip5/docs/Taylor_CMIP5_design.pdf)
- Taylor, K. E., R. J. Stouffer, and G. A. Meehl (2012). An overview of CMIP5 and the experiment design, *Bull. Amer. Meteor. Soc.*, 93: 485-498, doi:[10.1175/BAMS-D-11-00094.1](https://doi.org/10.1175/BAMS-D-11-00094.1).
- Thompson, K. R., J. Huang, M. Véronneau, D. G. Wright, and Y. Lu (2009). Mean surface topography of the northwest Atlantic: Comparison of estimates based on satellite, terrestrial gravity, and oceanographic observations, *J. Geophys. Res.*, 114 (C7), C07015, doi:10.1029/2008JC004859.
- Tivy, A., S. E. L. Howell, B. Alt, S. McCourt, R. Chagnon, G. Crocker, T. Carrieres, and J. J. Yackel (2011). Trends and variability in the Canadian Arctic based on the Canadian Ice Service Digital Archive, 1960-2008 and 1968-2008, *J. Geophys. Res.*, 116(C3), C03007, doi:10.1029/2009JC005855.
- Trenberth, K. E., P. D. Jones, P. Ambenje, R. Bojariu, D. Easterling, A. Klein Tank, D. Parker, F. Rahimzadeh, J. A. Renwick, M. Rusticucci, B. Soden, and P. Zhai (2007) Observations: Surface and Atmospheric Climate Change. In: *Climate Change 2007: The Physical Science Basis: Contribution of Working Group I to the Fourth Assessment Report of the Intergovernmental Panel on Climate Change* [Solomon, S., D. Qin, M. Manning, Z. Chen, M. Marquis, K. B. Averyt, M. Tignor, and H. L. Miller (Eds.)]. Cambridge University Press, Cambridge, United Kingdom and New York, NY, USA.
- Umoh, J. U. and Thompson, K. R. (1994). Surface heat flux, horizontal advection, and the seasonal evolution of water temperature on the Scotian Shelf, *J. Geophys. Res.*, 99, doi:10.1029/94JC01620.
- Vincent, L. A., X. L. Wang, E. J. Milewska, H. Wan, F. Yang, and V. Swail (2012). A second generation of homogenized Canadian monthly surface air temperature for climate trend analysis, *J. Geophys. Res.*, 117, D18110, doi:10.1029/2012JD017859.
- Wang, M. and J. E. Overland (2012). A sea ice free summer Arctic within 30 years - an update from CMIP5 models. *Geophys. Res. Lett.*, 39, L18501, doi:10.1029/2012GL052868.

- Watanabe, S., T. Hajima, K. Sudo, T. Nagashima, T. Takemura, H. Okajima, T. Nozawa, H. Kawase, M. Abe, T. Yokohata, T. Ise, H. Sato, E. Kato, K. Takata, S. Emori, and M. Kawamiya (2011). MIROC-ESM 2010: model description and basic results of CMIP5-20c3m experiments, *Geosci. Model Dev.*, 4: 845-872, doi:10.5194/gmd-4-845-2011.
- Wu, L., W. Cai, L. Zhang, H. Nakamura, A. Timmerman, T. Joyce, M. J. McPhaden, M. Alexander, B. Qiu, M. Visbeck, P. Chang, and B. Giese (2012). Enhanced warming over the global subtropical western boundary currents, *Nature Climate Change*, 2: 161-166, doi:10.1038/nclimate1353.
- Yashayaev, I. (2007). Hydrographic changes in the Labrador sea, 1960-2005. *Prog. in Oceanogr.*, 73 (3-4): 242-276.
- Yashayaev, I., N. P. Halliday, M. Bersch, and H. M. van Aken (2008). The history of the Labrador Sea Water: production, spreading, transformation and loss. pp. 569-612 *In: Arctic-SubArctic Ocean Fluxes* [R.R. Dickson, J. Meincke and P. Rhines (Eds.)], Springer, Dordrecht, Netherlands.
- Yashayaev, I. and J. W. Loder (2009). Enhanced production of Labrador Sea Water in 2008. *Geophys. Res. Lett.*, 36, L01606, doi:10.1029/2008GL036162.
- Yin, J. (2012). Century to multi-century sea level rise projections from CMIP5 models. *Geophys. Res. Lett.*, 39(17), L17709, doi:10.1029/2012GL052947.
- Yin, J., M. E. Schlesinger, and R. J. Stouffer (2009). Model projections of rapid sea-level rise on the northeast coast of the United States, *Nature Geoscience*, 2: 262-266, doi:10.1038/ngeo462.

## Appendix A: Additional Displays of Surface Air Temperature (TAS)

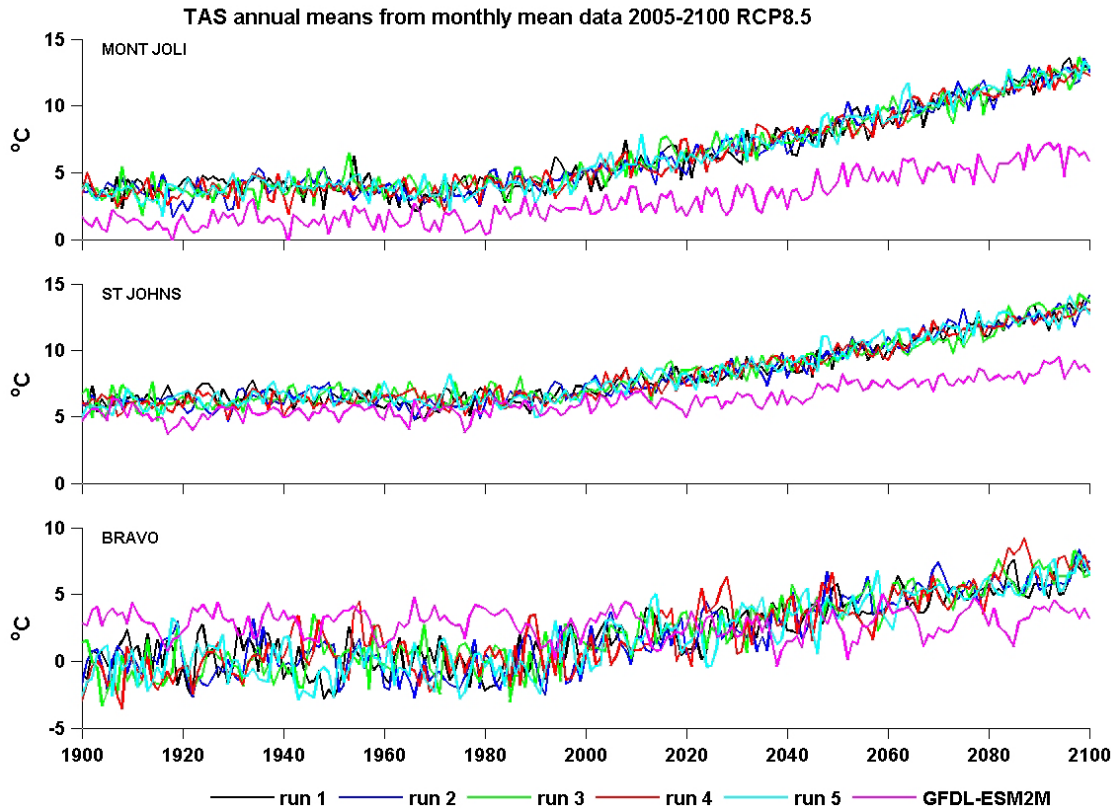
The displays presented in this appendix provide further details of the TAS variability described in Section 3.

Figure A-1 shows the means and annual cycles of bi-decadal monthly TAS at three stations at which time variability is examined in Figures 3-1 and 3-5, for the Historical 1986-2005 and RCP8.5 2046-2065 periods from the CanESM2 and GFDL-ESM2M simulations. The means and annual cycles from all five CanESM2 runs are shown, indicating little difference among the five runs, especially compared to the difference between the two models.



**Figure A-1** Annual cycles computed from bi-decadal monthly means for TAS from Historical (1986-2005; row 1) and RCP8.5 (2046-2065; row 2) data for Mont-Joli, St. John's and Bravo, for five runs from CanESM2 and run 1 from GFDL-ESM2M (see Fig. 2-3 for site locations).

Figure A-2 shows the time series of the annual means of TAS at the same three stations from the same model runs as in Figure A-1, covering the period 1900 to 2100. There is a more noticeable difference in the interannual-to-decadal scale variability among the five CanESM2 runs (than in the annual cycles). Nevertheless, Figure A-2 indicates that the differences in the long-term evolution and interannual-decadal variability between these two ESMs shown in Figures 3-3 and 3-9 are larger than those among the different CanESM2 members.



**Figure A-2** Time series of annual means of TAS for Historical and RCP8.5 data for 1900-2100 at the same three sites as in Figure A-1 for five runs of CanESM2 and run 1 of GFDL-ESM2M.

Figures A-3 and A-4 show the bi-decadal monthly distributions of TAS in the six ESMs for representative winter (February) and summer (August) months, respectively. In each case, the distributions are shown for the Historical (1986-2005) and future (2046-2065 from RCP8.5) periods. Some differences among the distributions from the different models and the different periods (e.g. the overall warming) are apparent but, because of the large TAS range ( $80^{\circ}\text{C}$ ) in these displays, the differences are more obvious in the corresponding TAS change fields (Figure 3-4).

To further demonstrate the large scatter/range in the projected climate changes from the different ESMs and to compare these differences with those between the two RCPs, Figure A-5 shows the ensemble mean, minimum, and maximum of the TAS change fields for each of the monthly RCP ensembles of the 6 models (6 models for each month for each RCP). The differences in the projected changes for the two RCPs are substantially smaller than the extremes among the six models. If one considers the two RCPs and six models to provide an indication of the potential range/uncertainty of the changes, then comparison of the RCP4.5 Min and RCP8.5 Max distributions suggests that this could be as much as  $5\text{-}10^{\circ}\text{C}$ . While this is probably an overestimate due to the potential regional deficiencies of particular models, it does indicate the potential pitfalls of using only one or two models in regional downscaling or in climate change impacts assessments.

Finally, to provide more information on the projected climate changes in the annual cycles at the 9 selected sites discussed in Section 3-3, Figure A-6 shows the bi-decadal monthly means for 1986-2005 from the Historical simulation and for 2046-2065 from the RCP8.5 simulation, for each of the CanESM2 ensemble mean and run 1 from GFDL-ESM2M. The future bi-decadal means are larger than the Historical ones at all sites and in all months, in each of the models. There is little difference in the changes in the bi-decadal monthly means among the different CanESM2 runs (Figure A-7), but there are substantial differences between the changes in the different models.

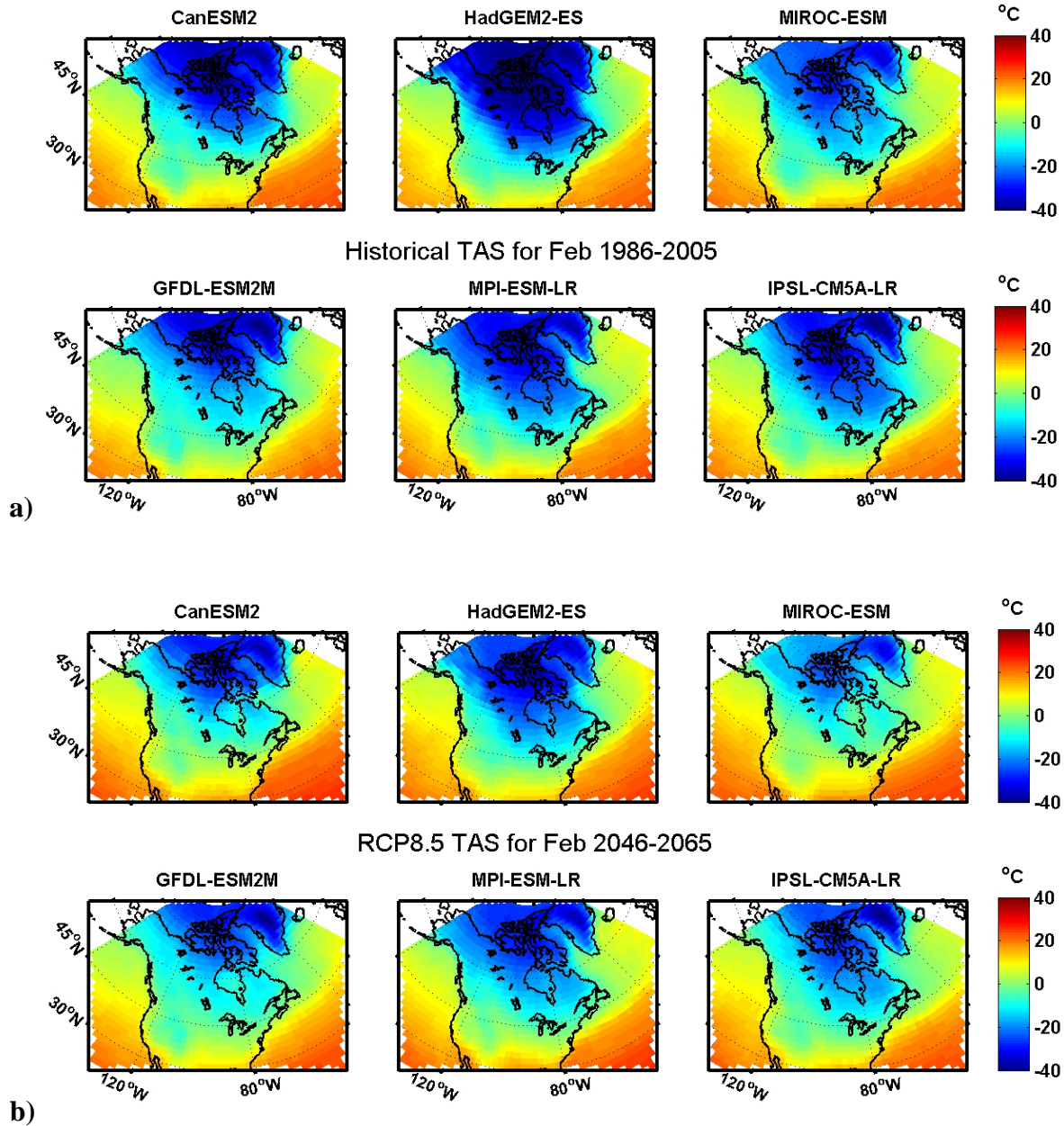


**Figure A-3** Bi-decadal February TAS means for Canada using interpolated data from six ESMs for a) 1986-2005 from their Historical simulations and b) 2046-2065 from their simulations for RCP8.5.



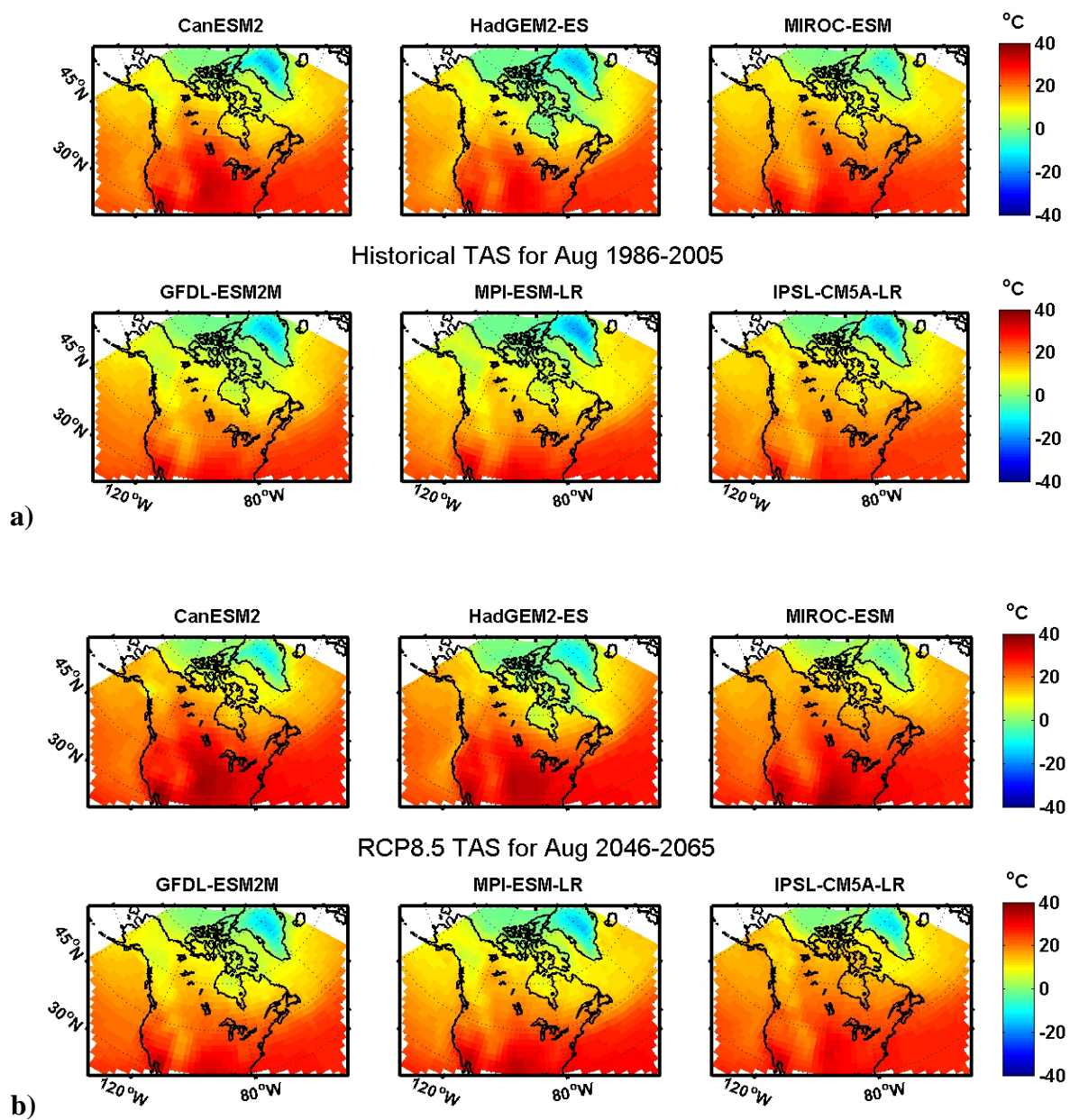


**Figure A-4** Bi-decadal August TAS means for Canada using interpolated data from six ESMs for a) 1986-2005 from their Historical simulations and b) 2046-2065 from their simulations for RCP8.5.



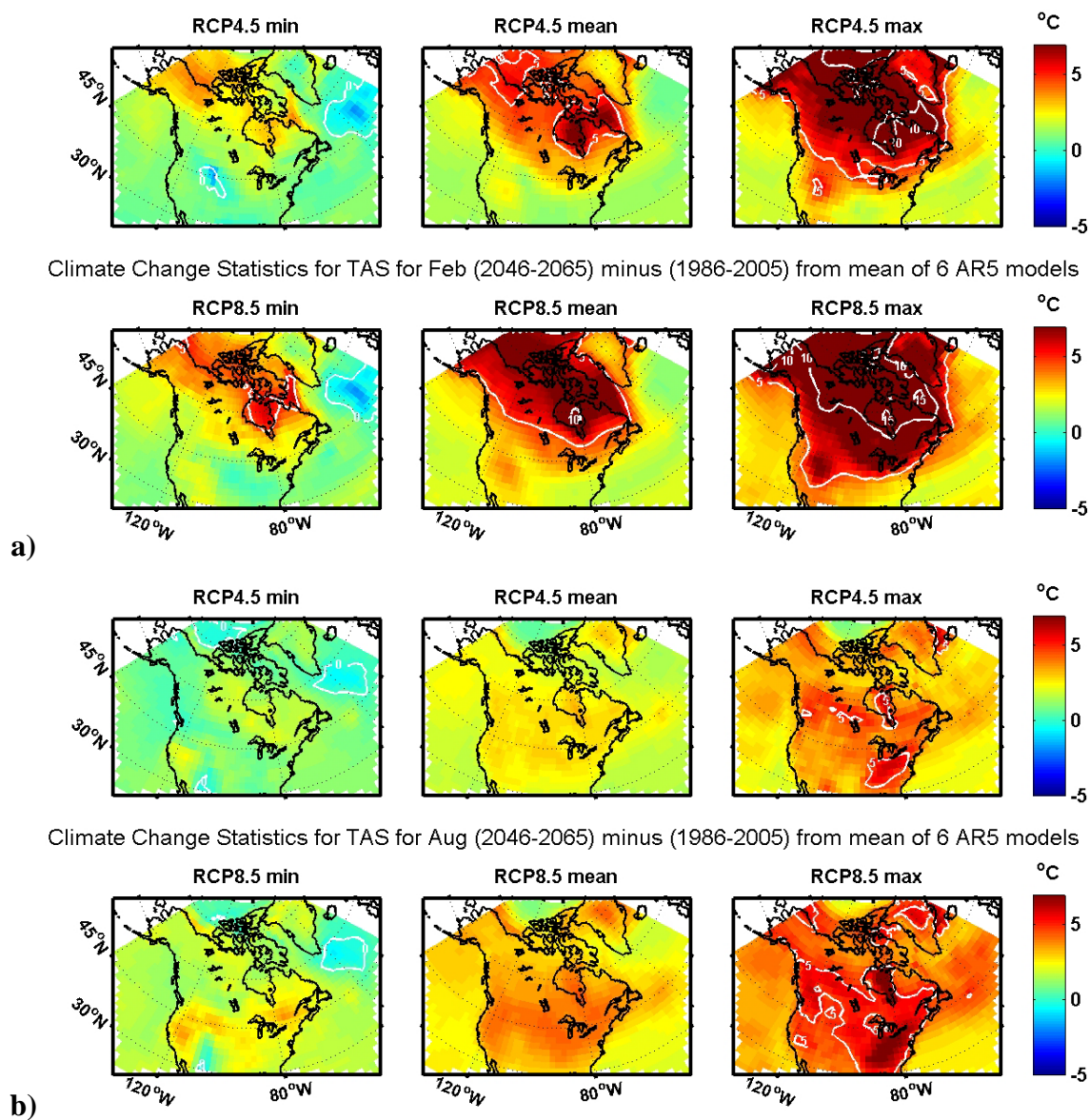


**Figure A-5** Minimum (left), mean (middle), and maximum (right) TAS changes for Canada from 1986-2005 to 2046-2065 in a) February and b) August, from the ensemble of six ESMs for each of RCP4.5 and RCP8.5. The white contours are the 0, 5 and 10 °C isotherms.

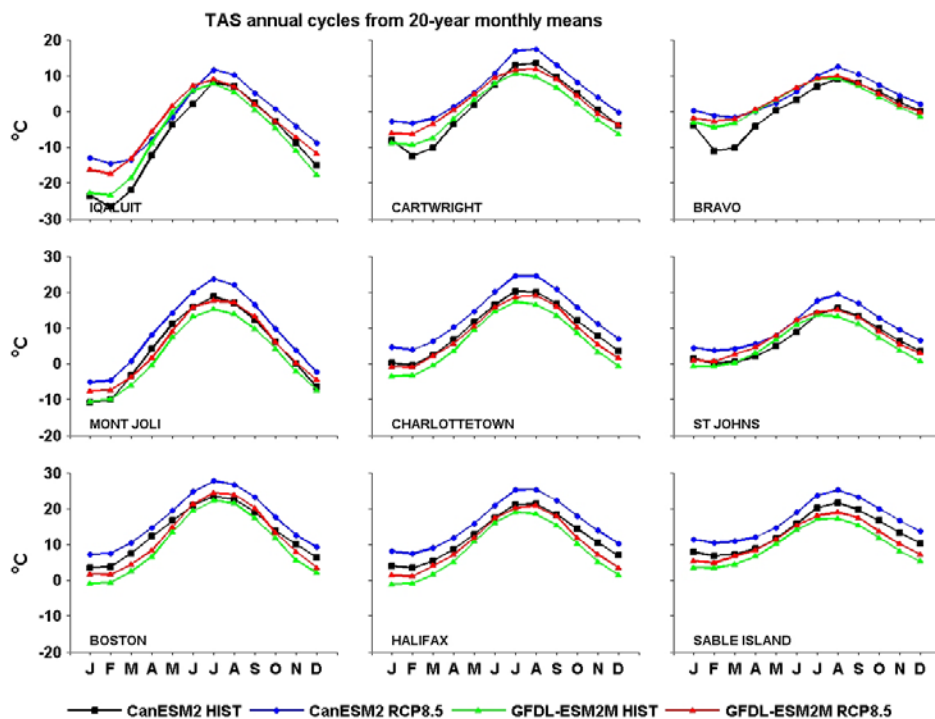


**Figure A-6** Bi-decadal annual cycles of TAS at same nine stations as in Figure 3-7, for Historical (1986-2005) and RCP8.5 (2046-2065) from the CanESM2 ensemble of five runs and run 1 from GFDL-ESM2M (see Fig. 2-3 for locations).

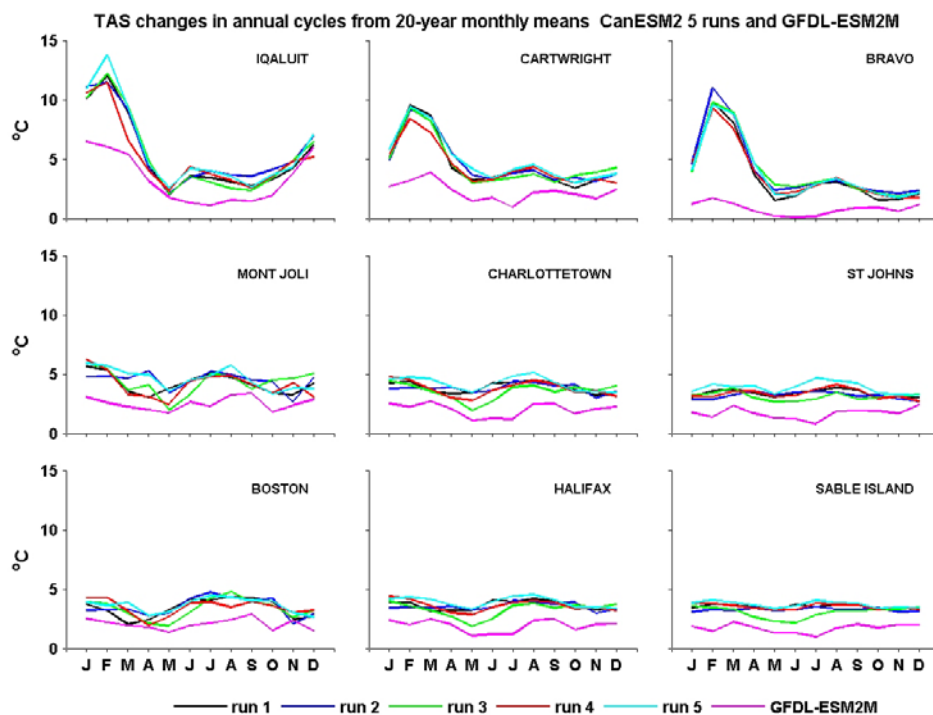


**Figure A-7** Annual cycle of climate changes in bi-decadal monthly TAS from 1986-2005 to 2046-2065 at the same nine locations as in Figure A-6, for five runs of CanESM2 and run 1 of GFDL-ESM2M for RCP8.5.

## Appendix B: Additional Displays of Sea Ice Concentration (SIC)

Figure B-1 compares the bi-decadal mean SIC fields for January and May of 1986-2005 from the Historical ESM simulations with those observed from HadISST1, complementing the corresponding displays for March and September in Figure 4-1.

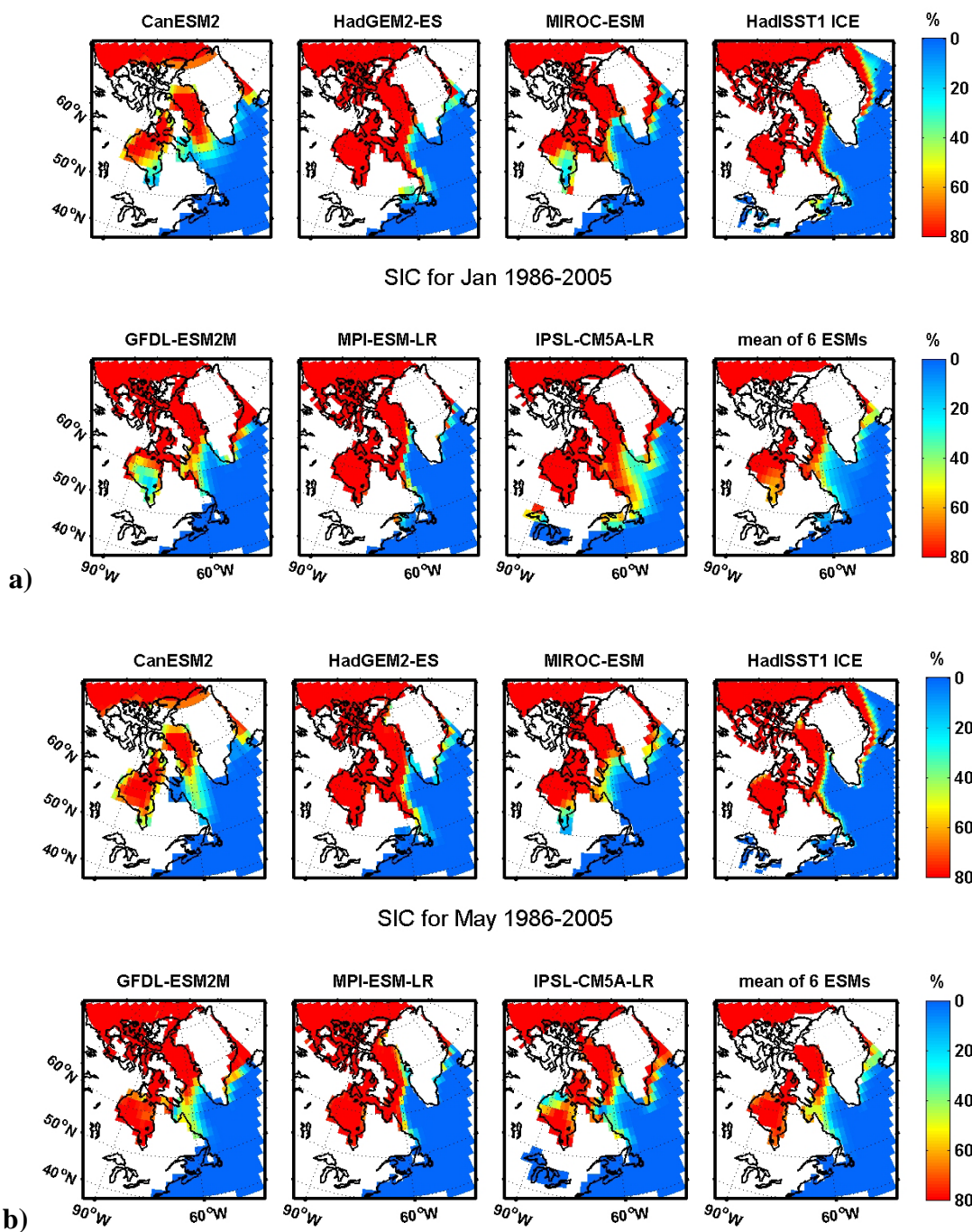


**Figure B-1** Bi-decadal mean SIC in a) January and b) May for 1986-2005, from the Historical simulations with the six ESMs, the observational HadISST1 dataset (upper right panels), and the ensemble mean of the ESMs (lower right panels).

## **Appendix C: Additional Displays of Surface Ocean Temperature (TOS)**

The displays presented in this appendix provide further detail on the TOS variability described in Section 5, specifically on the spatial structure of TOS in the six ESMs.

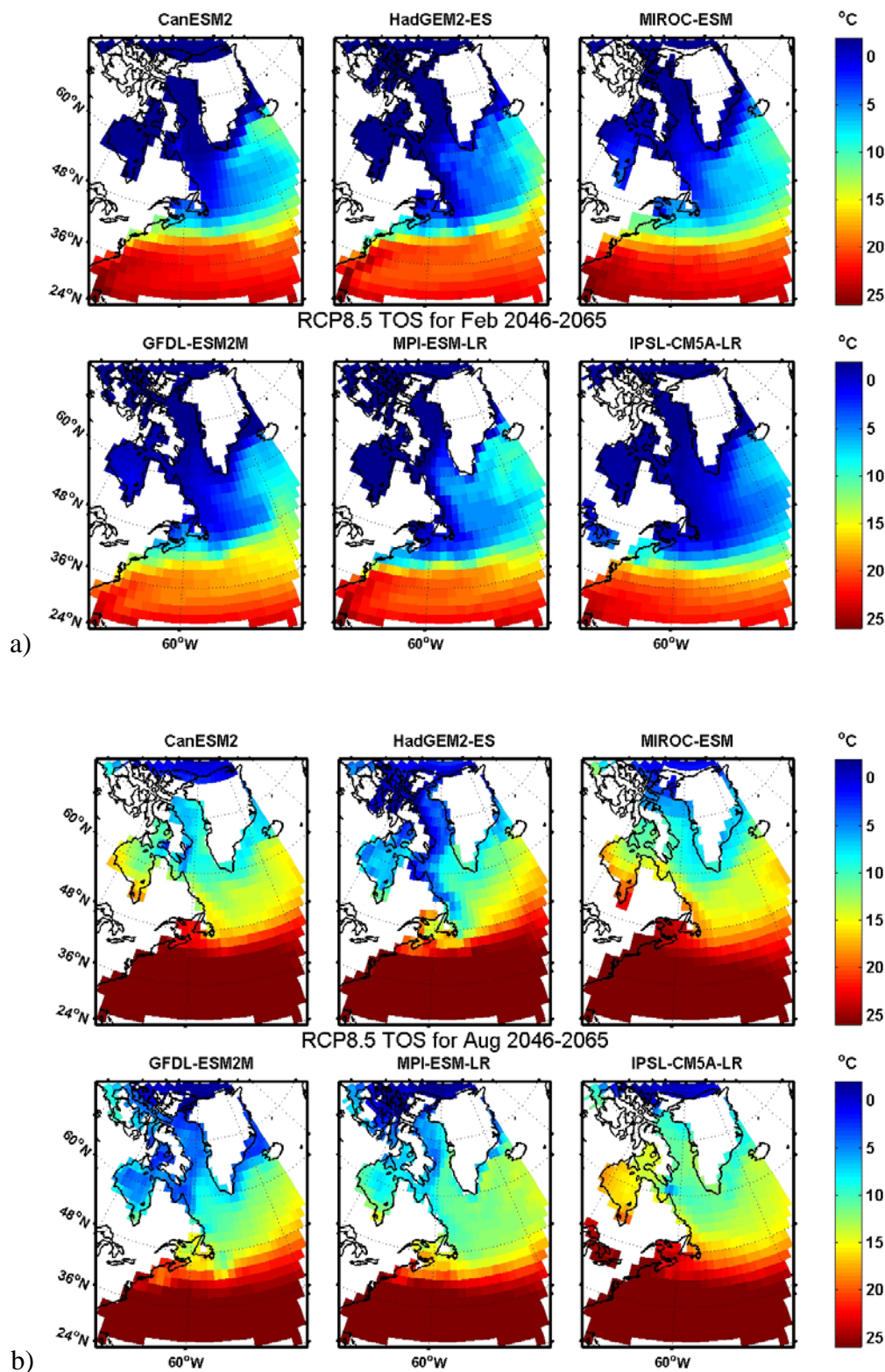
Figure C-1 shows the projected monthly distributions of TOS for the NW Atlantic (NWA) during 2046-2065, from the RCP8.5 simulations of the six ESMs for winter (February) and summer (August). These distributions can be compared with those for 1986-2005 from the Historical simulations shown in Figure 5-1.

Figure C-2 shows the projected climate changes in TOS for February and August from 1986-2005 of the Historical simulations to 2046-2065 of the RCP8.5 simulations for the six ESMs, shown on a Canada-wide domain in order to help put the change distributions shown in Figure 5-5 in a broader geographic perspective. Substantial spatial and inter-model differences are apparent in all three LABs (see Section 5-2 for a brief discussion.)

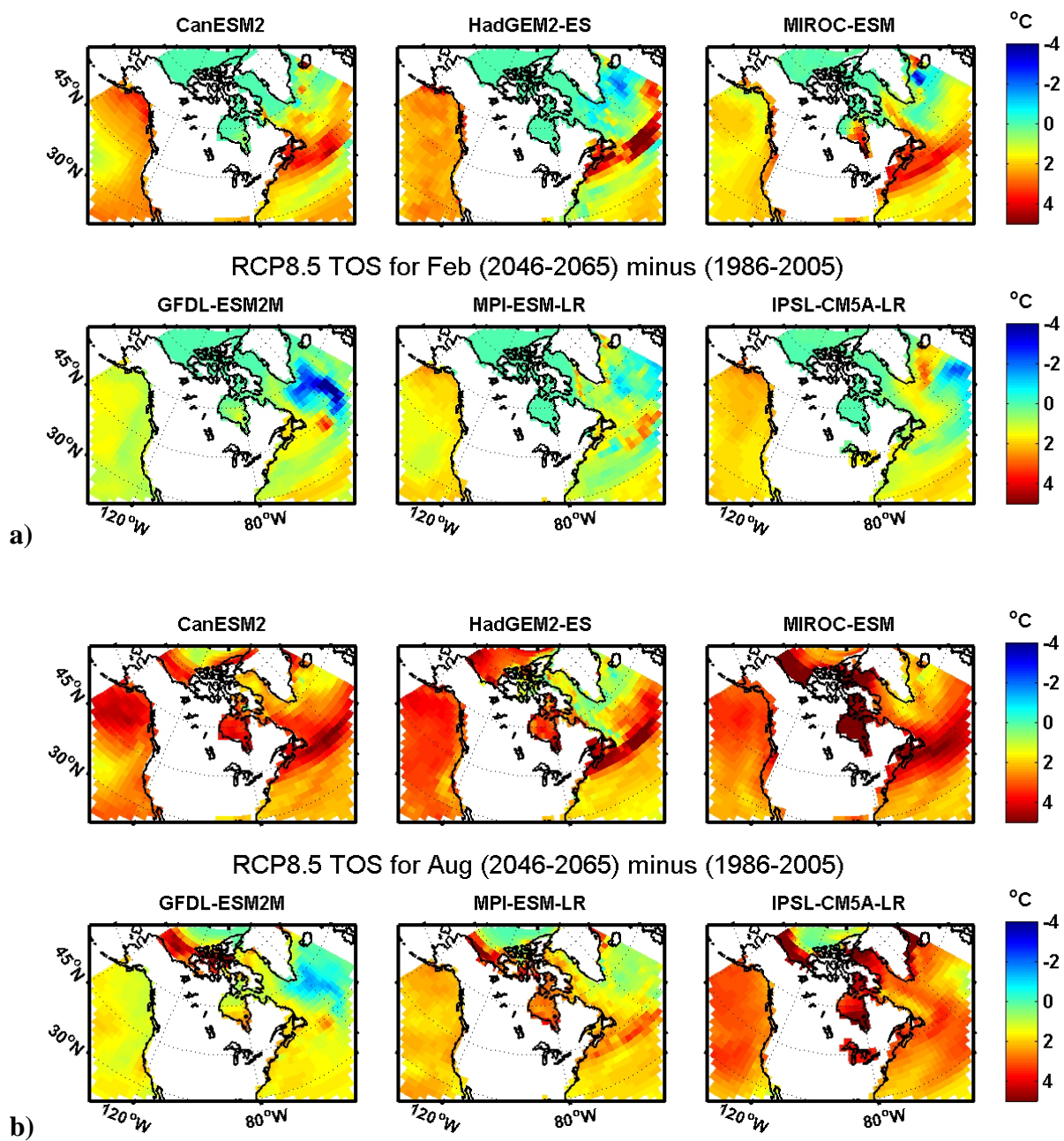
The statistics of the climate change fields for the Canada domain are shown in Figure C-3, for both months, and for both RCPs 4.5 and 8.5 to show the dependence on the RCP. These statistics complement those shown in Figure 5-6 for the NWA.

Figure C-4 further illustrates the inter-model, seasonal, and inter-RCP differences by showing the ensemble's mean, minimum, and maximum climate changes in TOS at each point, for various six-member ESM ensembles.





**Figure C-1** Bi-decadal mean TOS for the NWA in a) February and b) August in 2046-2065 from the six ESMs for RCP8.5, using data interpolated to the common grid.



**Figure C-2** Climate changes in bi-decadal mean TOS in a) February and b) August from 1986-2005 to 2046-2065 for the waters surrounding Canada for RCP8.5, using interpolated data from the six ESMs.



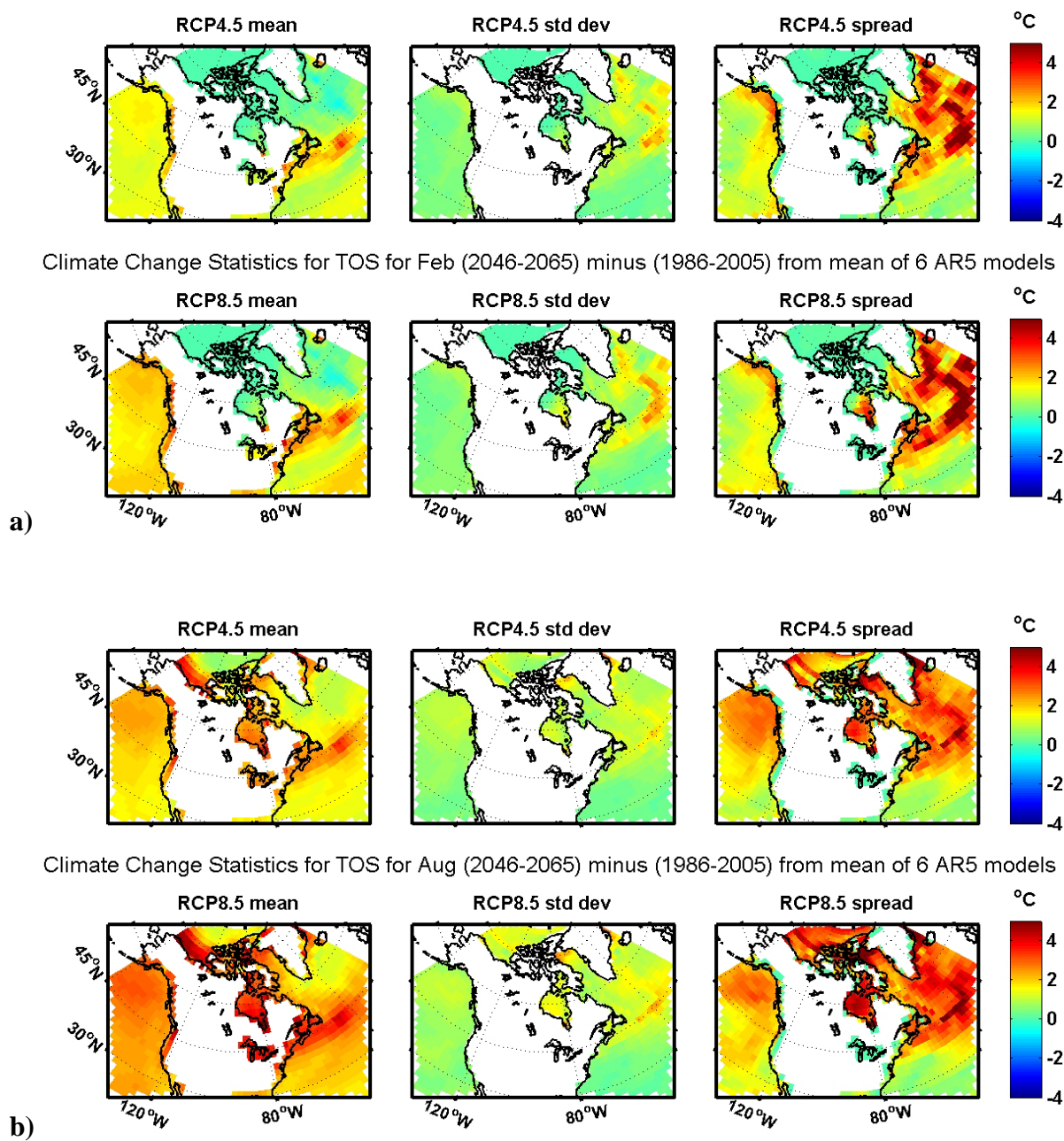


**Figure C-3** Statistics (ensemble mean, standard deviation, and spread) of climate changes in bi-decadal mean TOS from 1986-2005 to 2046-2065 for the waters surrounding Canada in a) February and b) August, for RCP4.5 (upper rows) and RCP8.5 (lower rows) using interpolated data from the six ESMs.

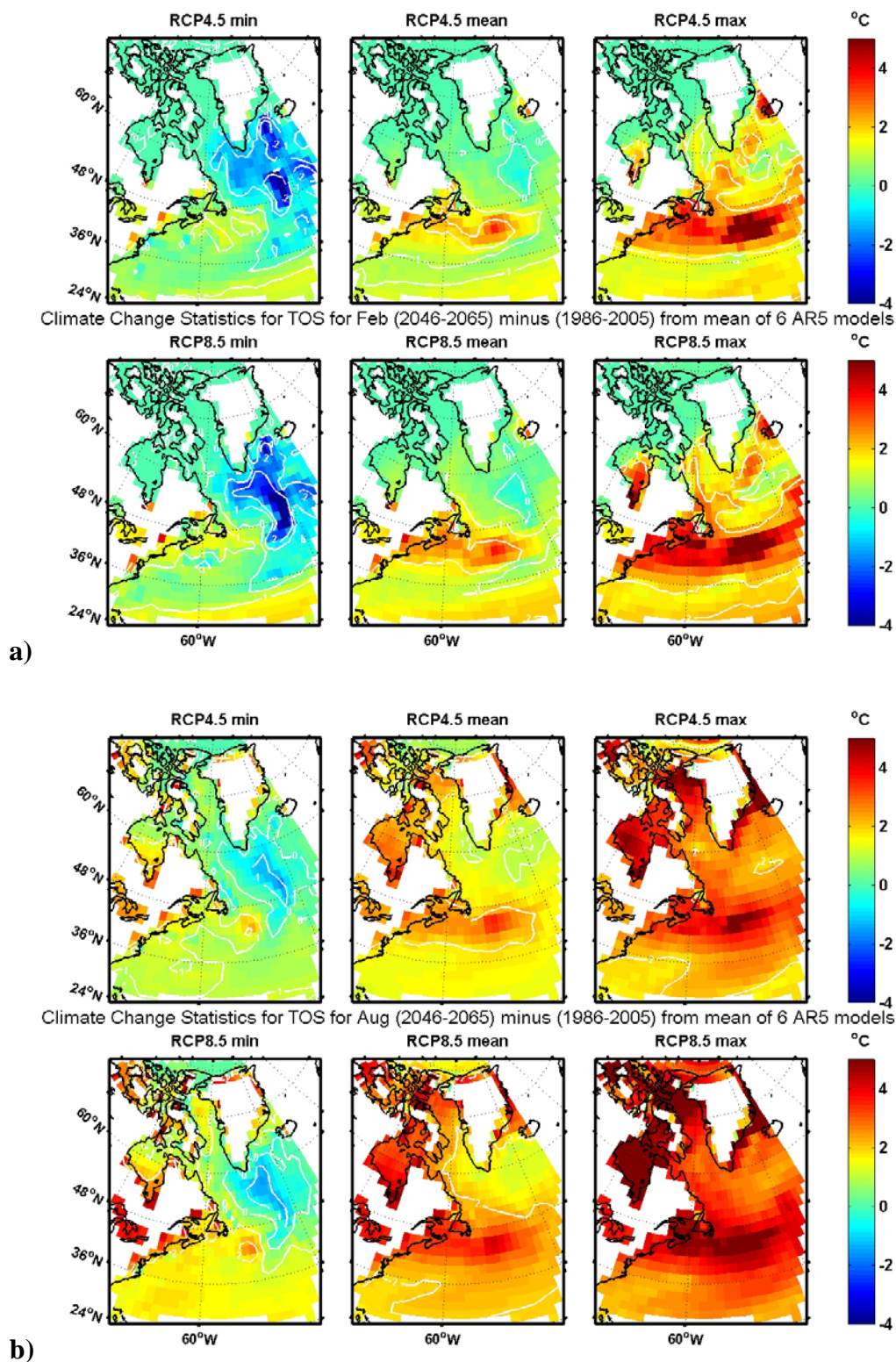


**Figure C-4** Statistics (ensemble minimum, mean and maximum) of climate changes in bi-decadal monthly TOS from 1986-2005 to 2046-2065 for the NWA in a) February and b) August, for RCP4.5 (upper rows) and RCP8.5 (lower rows) using interpolated data from the six ESMs. The white contours are the -2, -1, 0, +1 and +2 °C isotherms.

## **Appendix D: Additional Displays of Surface Ocean Salinity (SOS)**

The displays presented in this appendix provide further detail on the SOS variability described in Section 6, specifically on the spatial structure in the six ESMs. These displays are analogous to those for TOS in Appendix C.

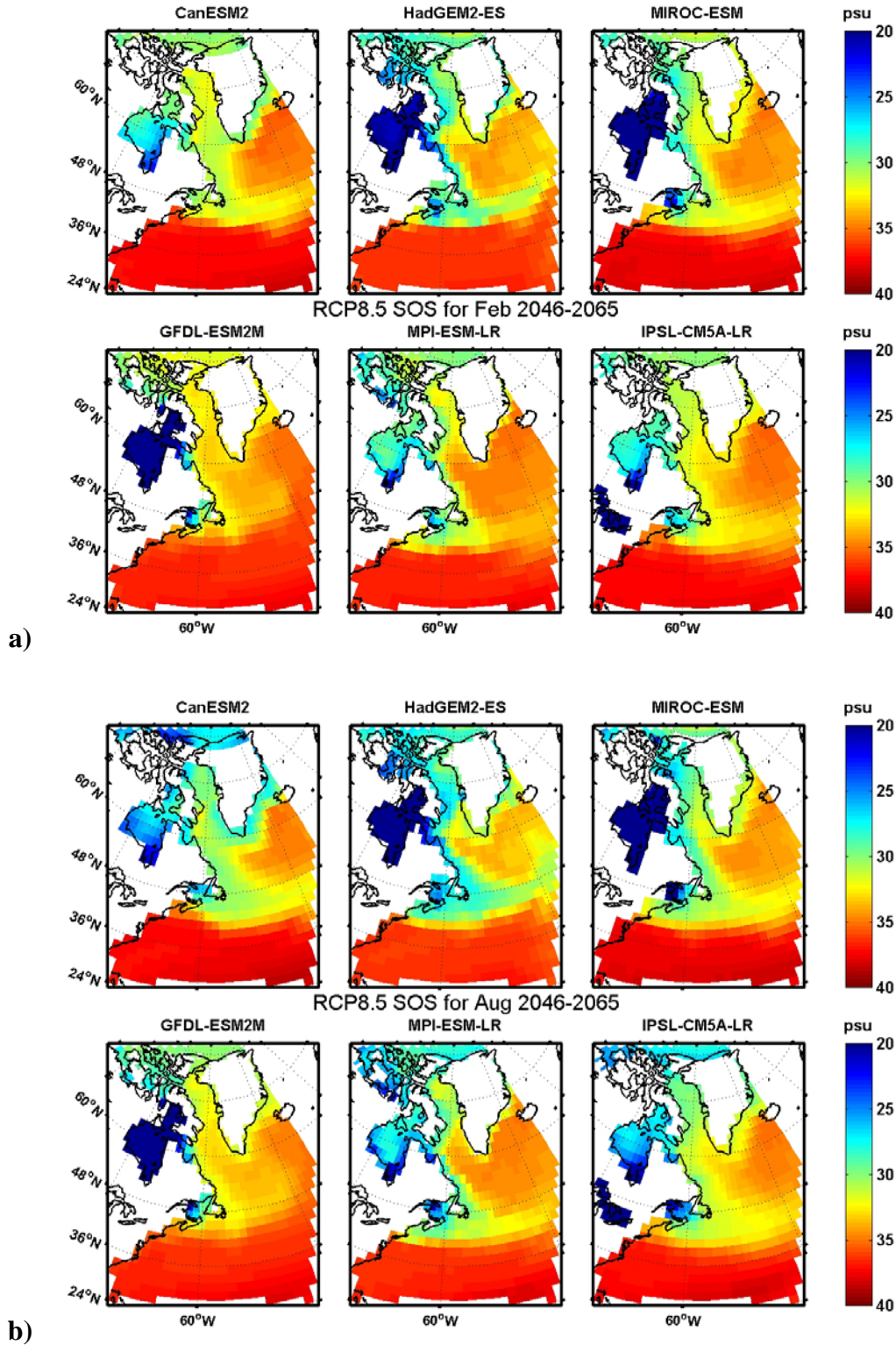
Figure D-1 shows the projected bi-decadal monthly distributions of SOS for the NW Atlantic during 2046-2065, from the RCP8.5 simulations of the six ESMs for winter (February) and summer (August). These distributions can be compared with those for 1986-2005 from the Historical simulations with the ESMs (Figure 6-1).

Figure D-2 shows the projected climate changes in SOS for February and August between 1986-2005 of the Historical simulations and 2046-2065 of the RCP8.5 simulations for a Canada-wide domain, using interpolated data from the six ESMs. This puts the change distributions shown in Figure 6-5 in a broader geographic perspective.

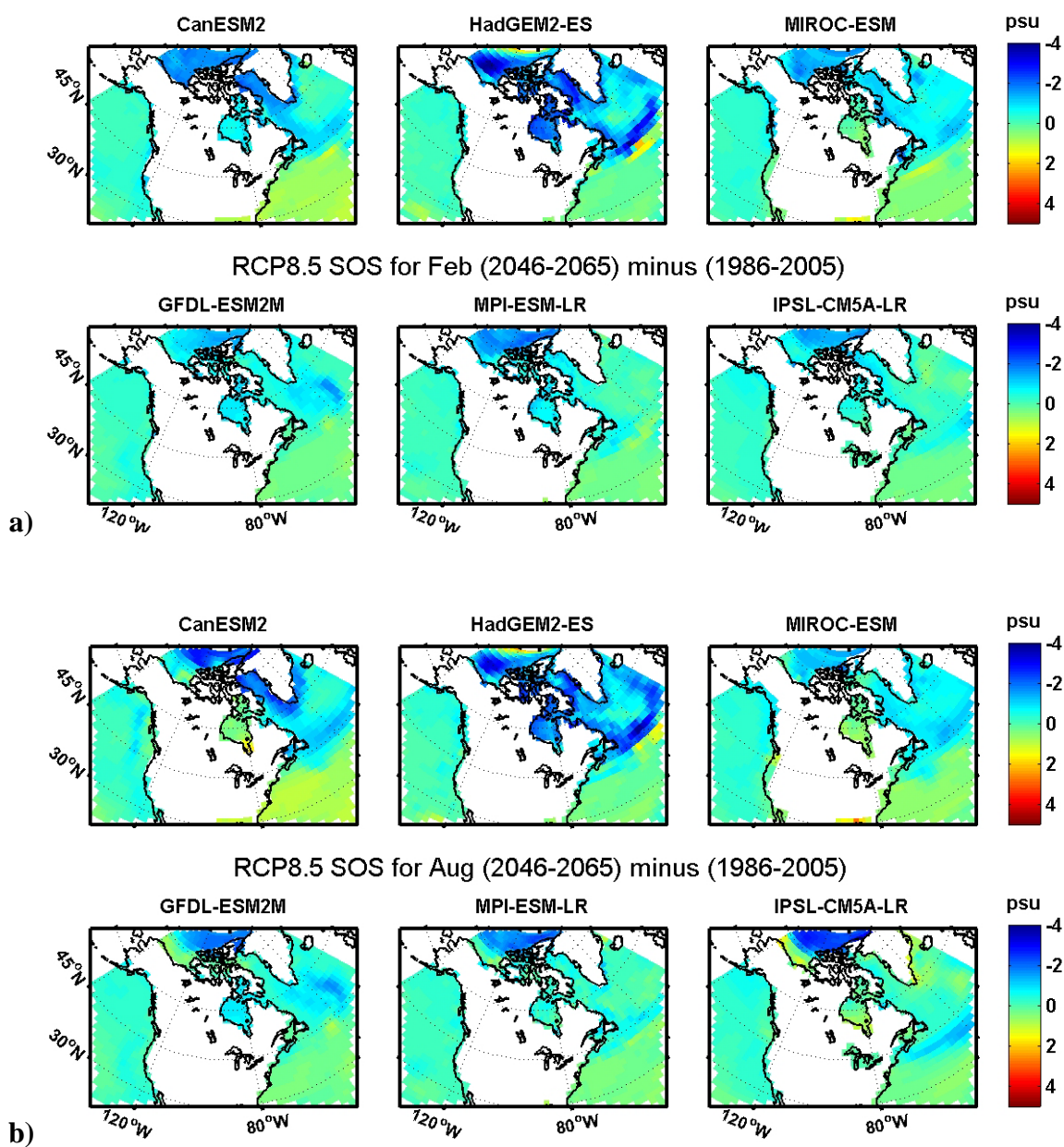
The statistics of the climate change fields in SOS on the Canada domain are shown in Figure D-3 for both winter and summer months, and for both RCPs 4.5 and 8.5 to show the dependence on each RCP. These statistical fields complement those shown in Figure 6-6 for the NWA.

Figure D-4 further illustrates the inter-model, seasonal and inter-RCP differences in the SOS climate changes by showing the ensemble mean, minimum, and maximum changes at each point, for various 6-member ESM ensembles.





**Figure D-1** Bi-decadal mean SOS for the NWA in a) February and b) August in 2046-2065 from the six ESMs for RCP8.5, using data interpolated to the common grid.



**Figure D-2** Climate changes in bi-decadal mean SOS in a) February and b) August from 1986-2005 to 2046-2065 for the waters surrounding Canada for RCP8.5, using interpolated data from the six ESMs.

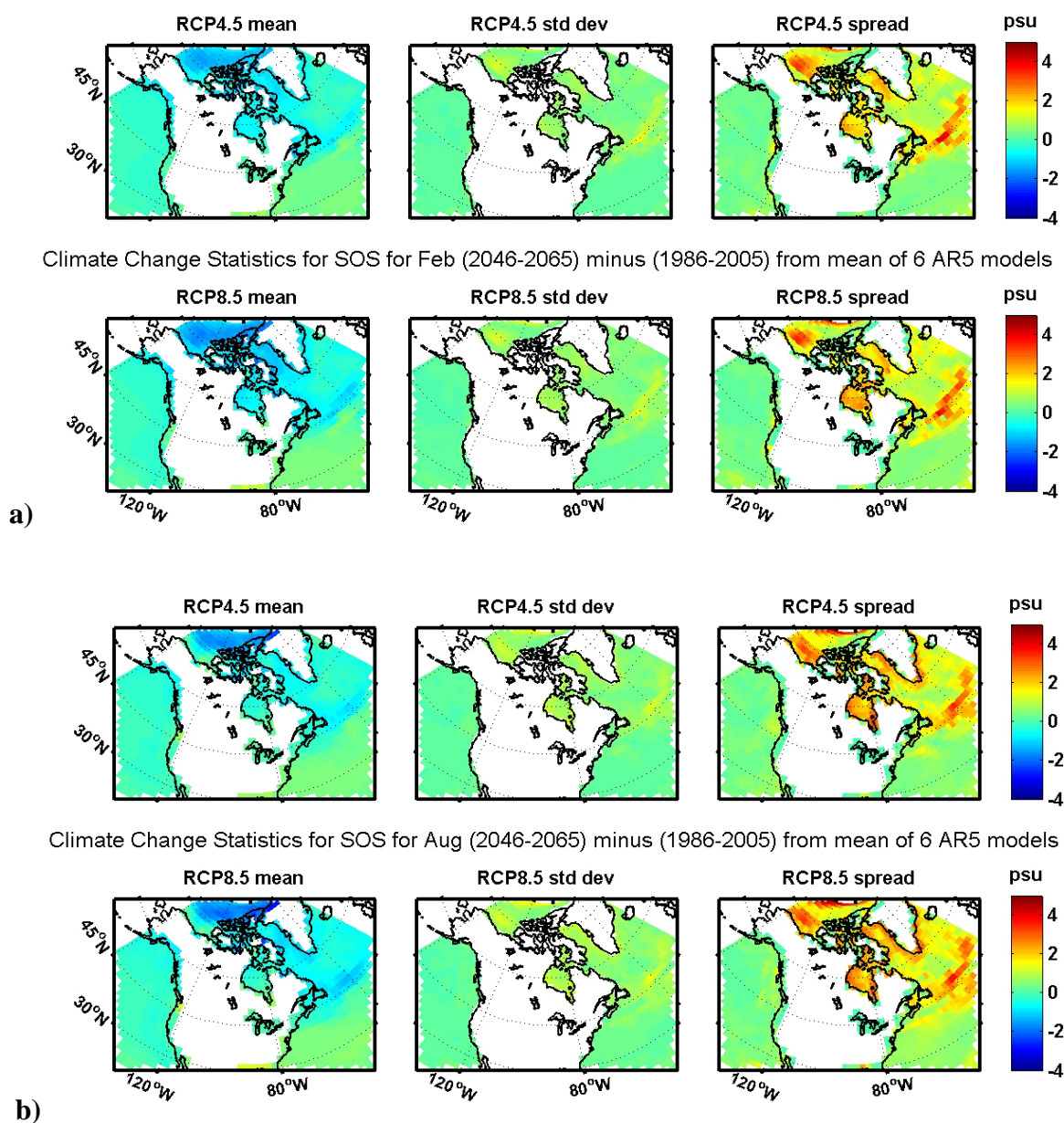


**Figure D-3** Statistics (ensemble mean, standard deviation, and spread) of climate changes in bi-decadal mean SOS from 1986-2005 to 2046-2065 for the waters surrounding Canada in a) February and b) August, for RCP4.5 (upper rows) and RCP8.5 (lower rows) using interpolated data from the six ESMs.



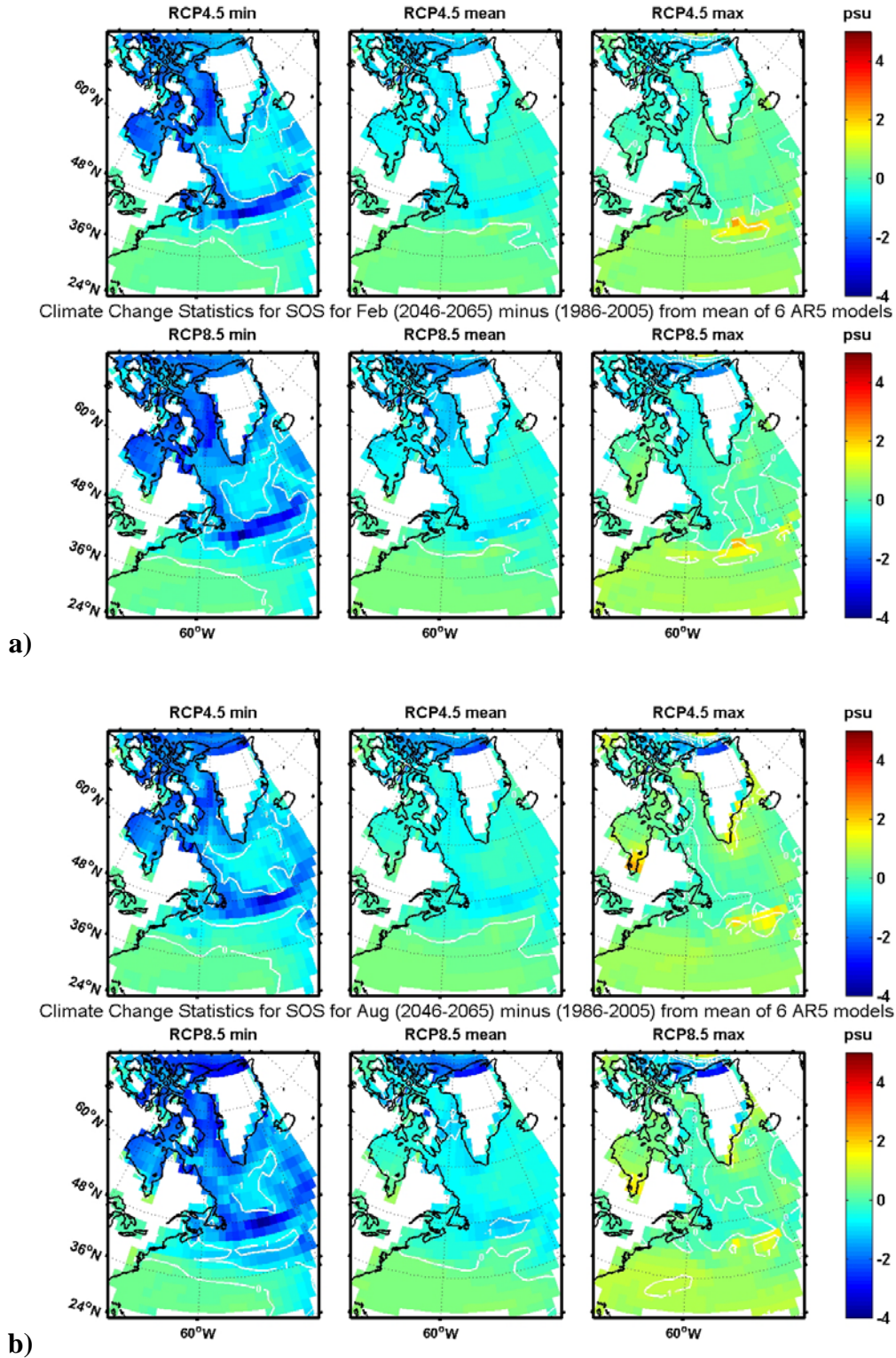


**Figure D-4** Statistics (ensemble minimum, mean and maximum) of climate changes in bi-decadal monthly SOS from 1986-2005 to 2046-2065 for the NWA in a) February and b) August, for RCP4.5 (upper rows) and RCP8.5 (lower rows) using interpolated data from the six ESMs. The white contours are the -1, 0 and +1 isohalines.

## **Appendix E: Additional Displays of Subsurface Ocean Temperature and Salinity**

This appendix presents displays of the bi-decadal means of the annual temperature and salinity fields on three cross-basin sections in five ESMs, for 1986-2005 from their Historical simulations and for 2046-2065 from the RCP8.5 simulations. These displays are complementary to those in Section 7.

Figures E-1, E-2, and E-3 present the bi-decadal temperature fields for the two periods on sections across Baffin Bay, the Labrador Shelf/Slope/Sea (LSSS), and the Scotian Shelf/Slope/Rise (SSSR), respectively, and Figures E-4, E-5 and E-6 present the corresponding salinity fields.

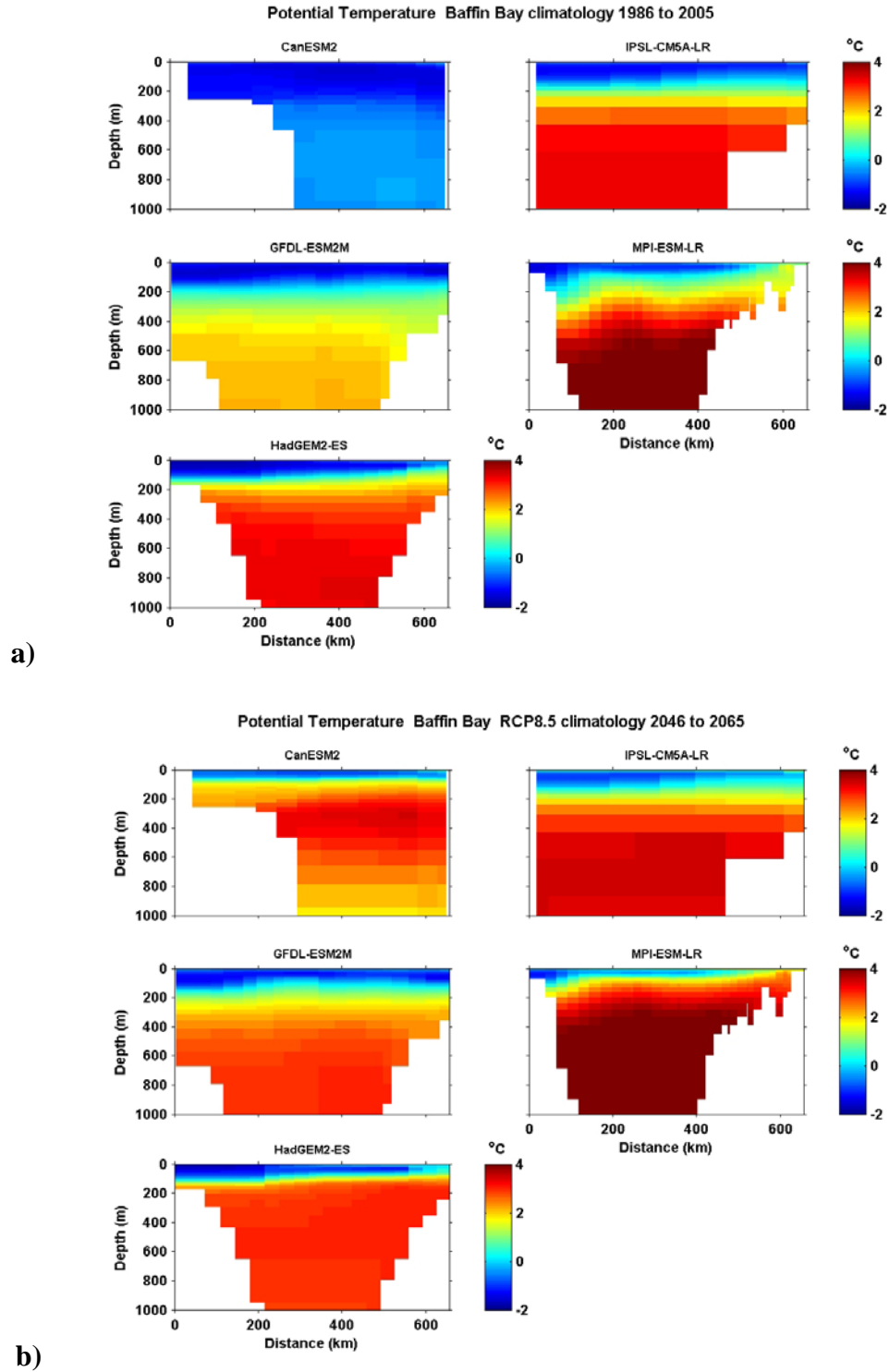


**Figure E-1** Bi-decadal mean temperature across the Baffin Bay section from five AR5 models for a) 1986-2005 from their Historical simulations and b) 2046-2065 from their RCP8.5 simulations.

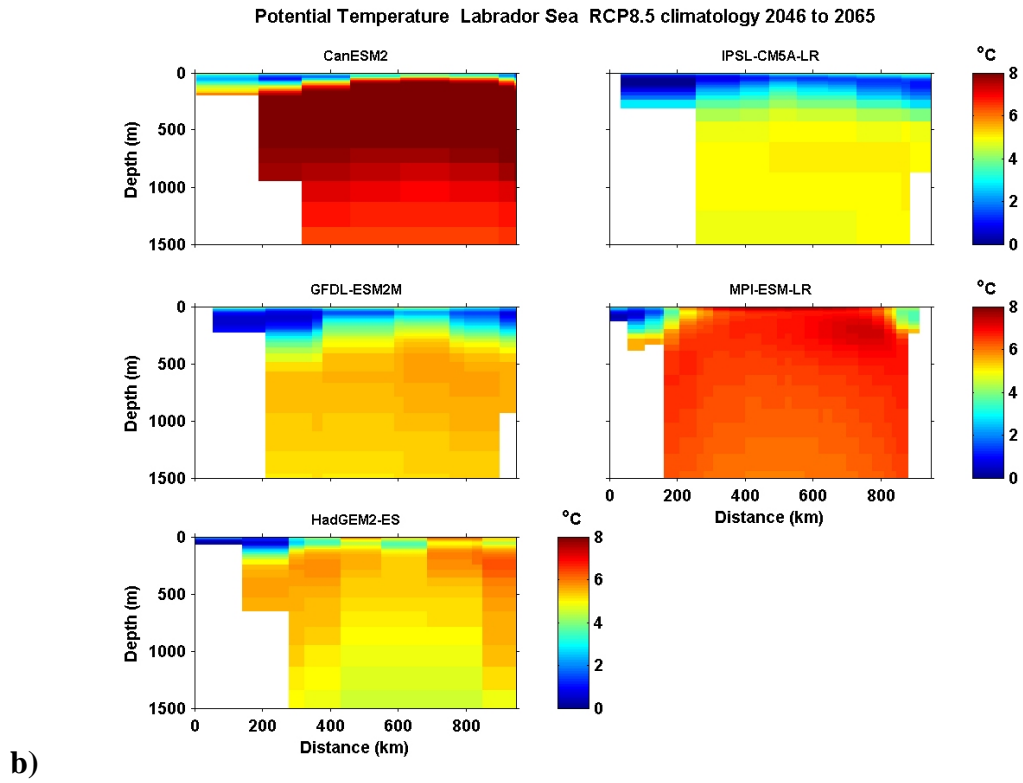
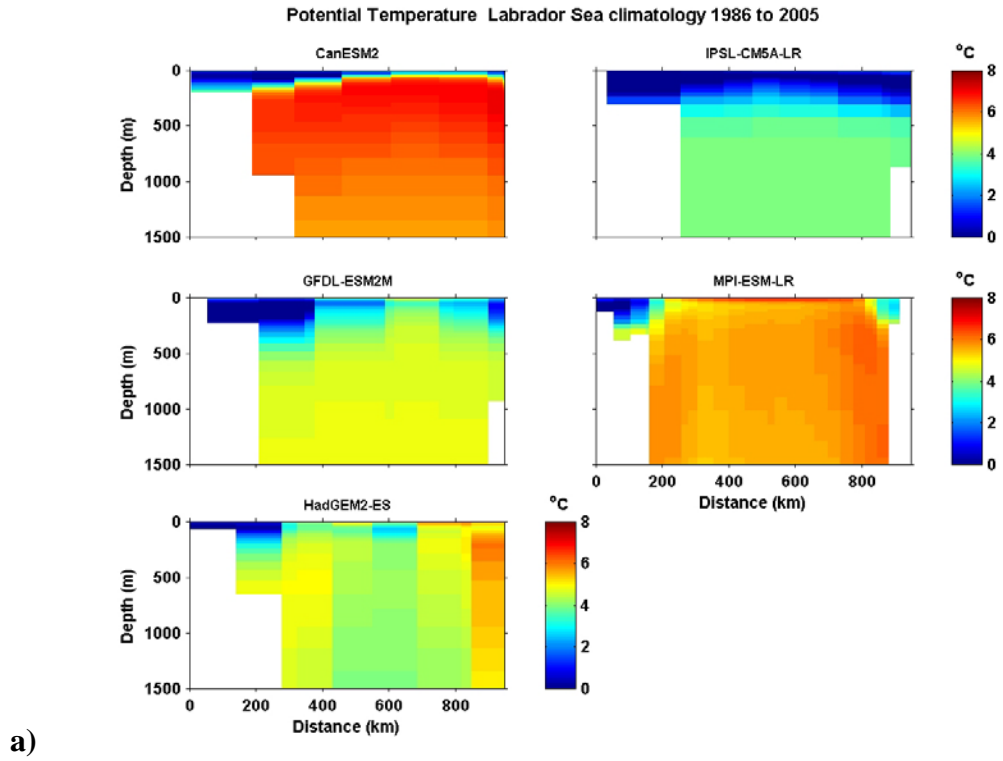


**Figure E-2** Bi-decadal mean temperature across the LSSS section from five AR5 models for a) 1986-2005 from their Historical simulations and b) 2046-2065 from their RCP8.5 simulations.

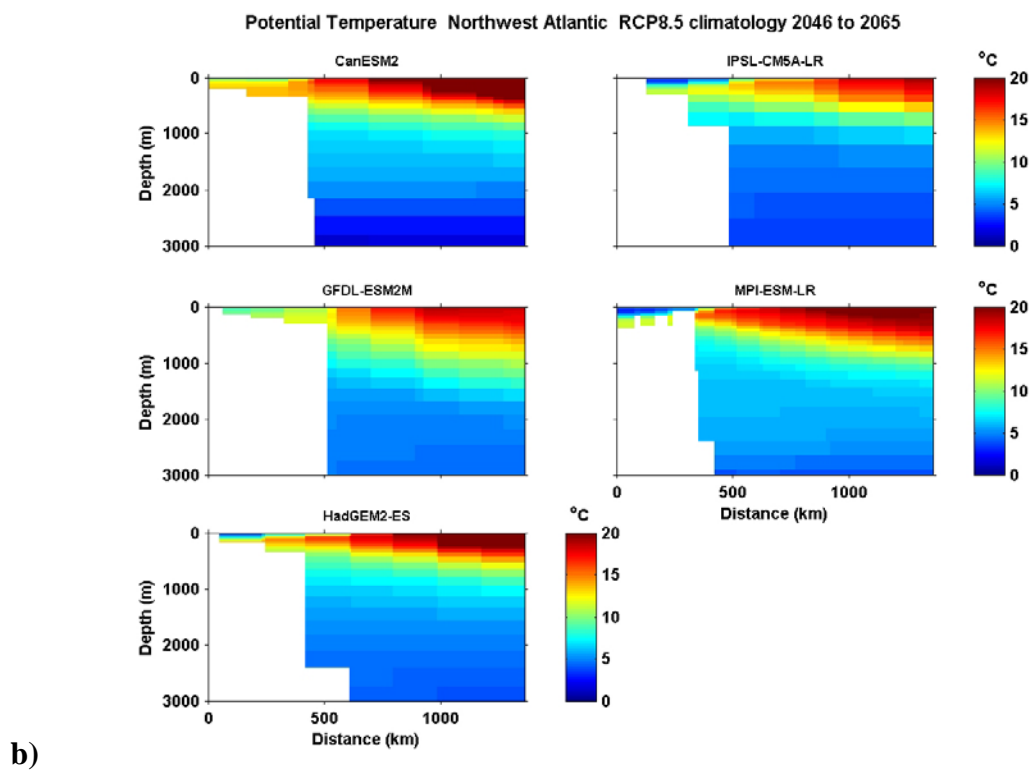
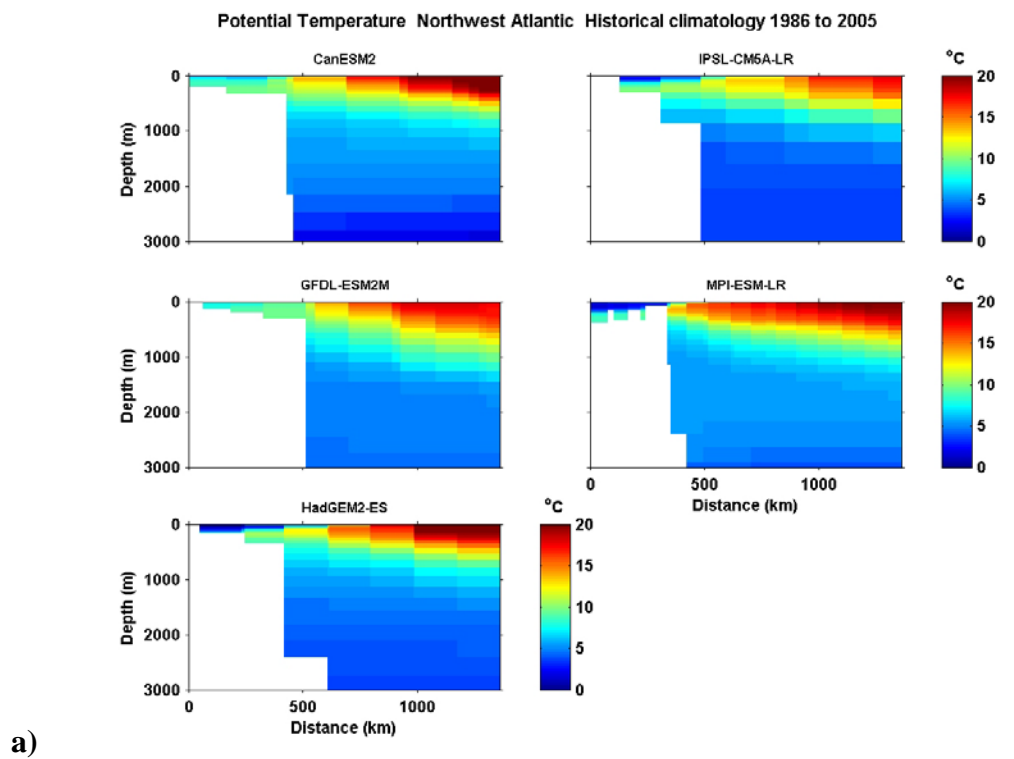
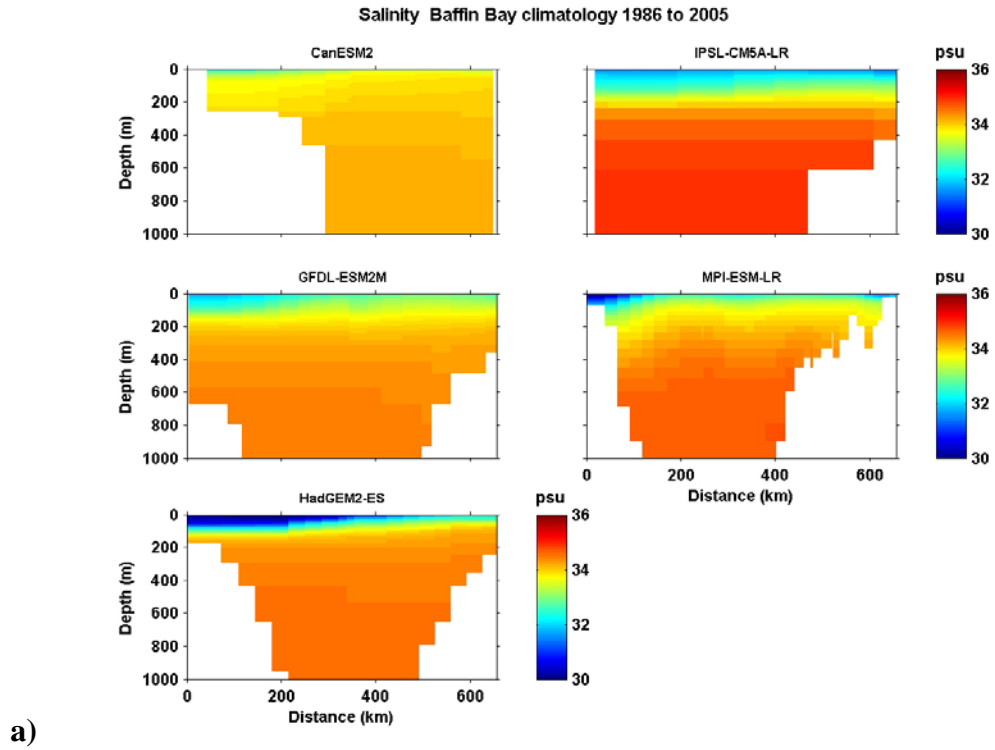
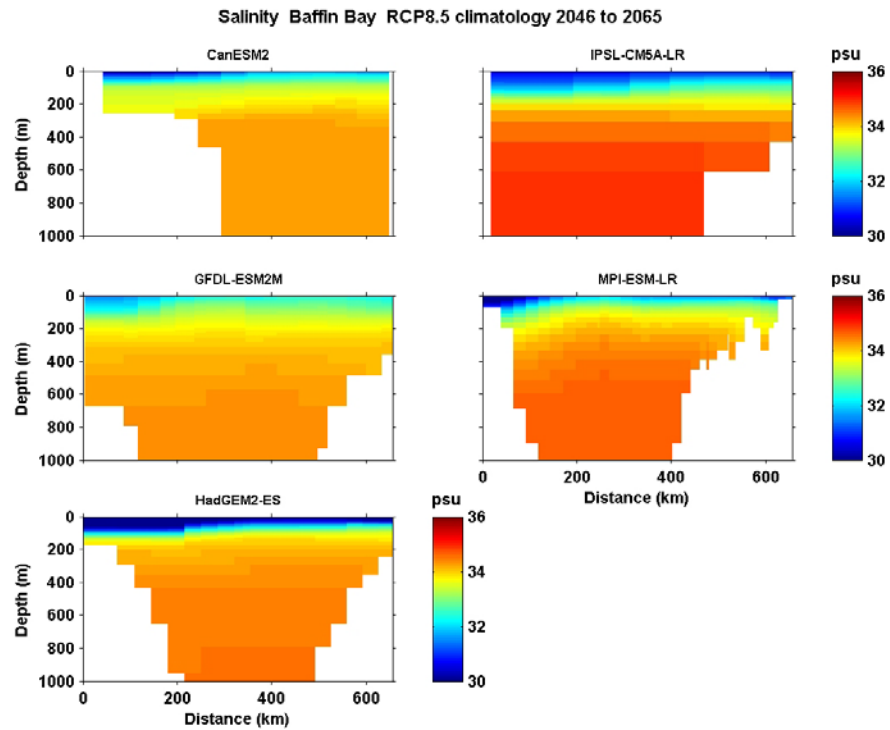


**Figure E-3** Bi-decadal mean temperature across the SSSR section from five AR5 models for a) 1986-2005 from their Historical simulations and b) 2046-2065 from their RCP8.5 simulations.



a)



b)

**Figure E-4** Bi-decadal mean salinity across the Baffin Bay section from five AR5 models for a) 1986-2005 from their Historical simulations and b) 2046-2065 from their RCP8.5 simulations.



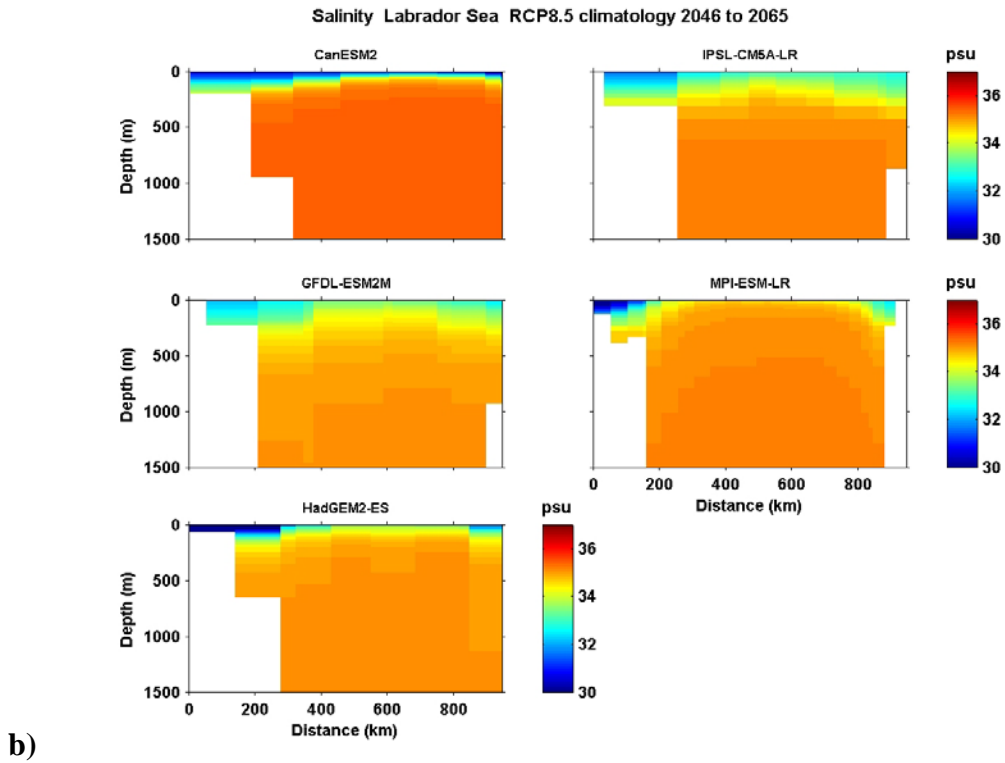
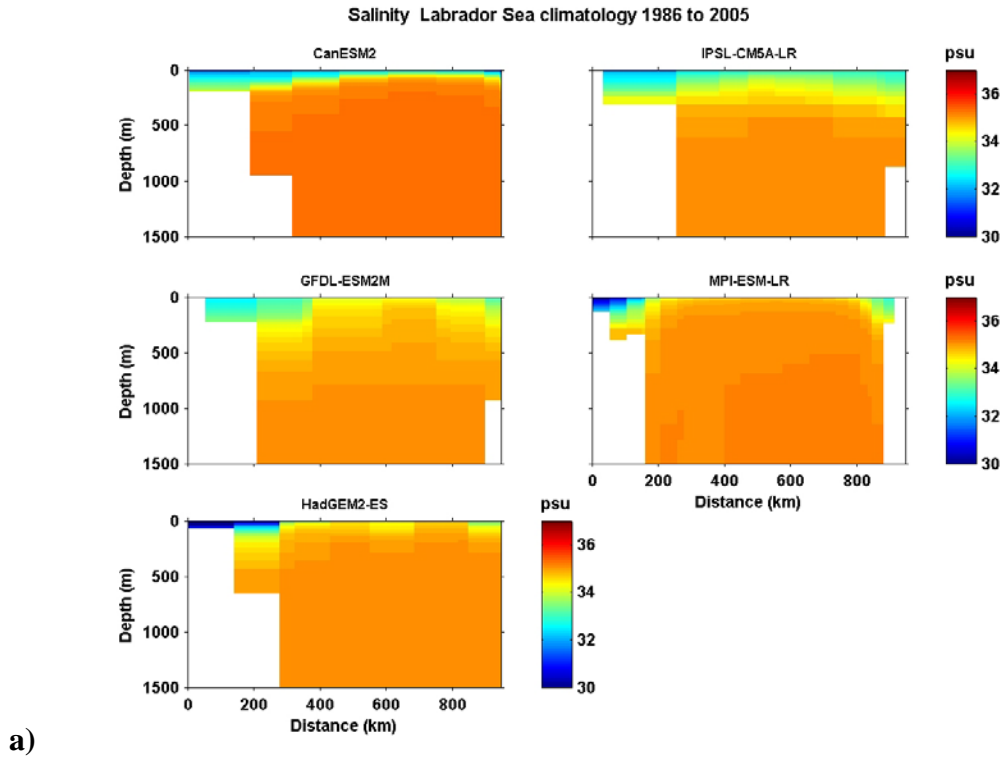


**Figure E-5** Bi-decadal mean salinity across the LSSS section from 5 AR5 models for a) 1986-2005 from their Historical simulations and b) 2046-2065 from their RCP8.5 simulations.

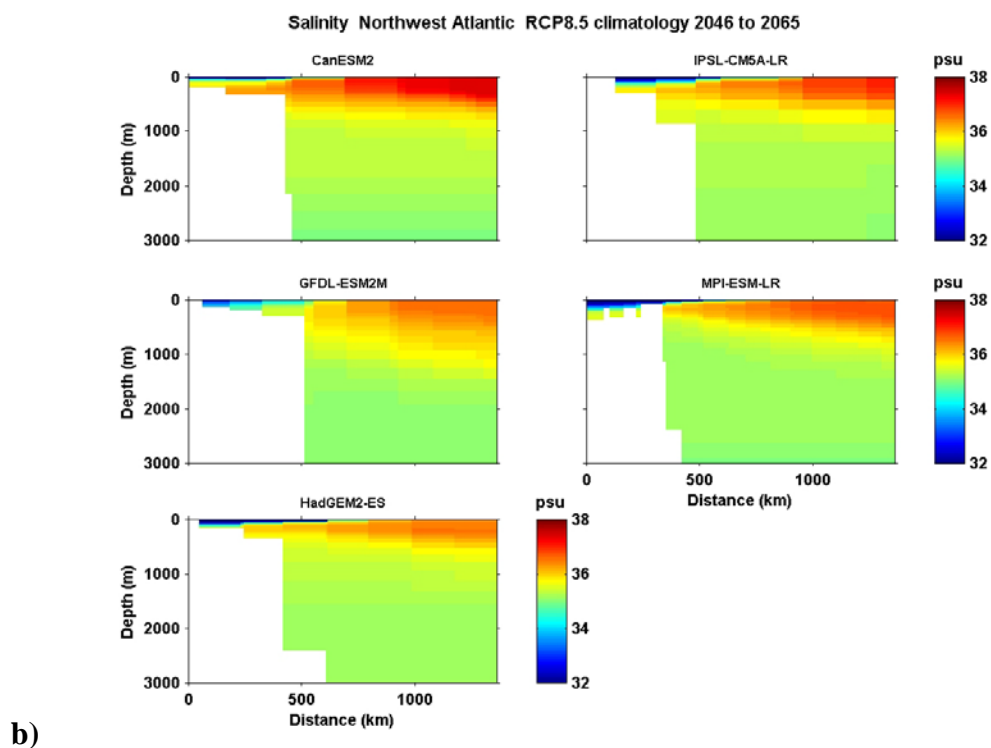
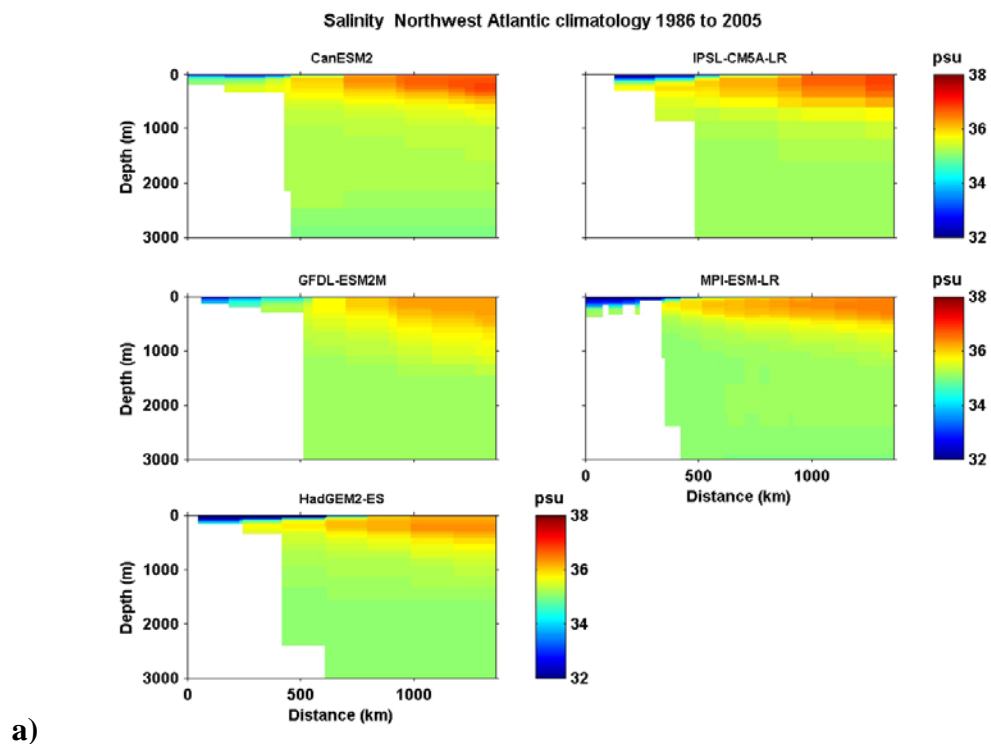


**Figure E-6** Bi-decadal mean salinity across the SSSR section from five AR5 models for a) 1986-2005 from their Historical simulations and b) 2046-2065 from their RCP8.5 simulations.

## Appendix F: Additional Displays of Sea Surface Height (SSH)

This appendix presents displays of zos to complement those of “adjusted zos” (zos + zosga) presented in Section 9.

Figure F-1 shows the bi-decadal monthly means of adjusted zos for February and August in past and future periods from CanESM2 and GFDL-ESM2M data. The broad-scale pattern of the depression in the subpolar gyre and the dome in the subtropical gyre is apparent in all cases, but there are differences in the detailed structure, particularly between the two models. The most noticeable is in Hudson Bay but this may be an artifact of its land-locked representation in CanESM2 (note the white land separating Hudson Bay from Baffin Bay in Figure F-1). It can be seen that the projected climate change involves a reduction in the magnitudes of the SSH maxima and minima in the subtropical and subpolar gyres, respectively. This indicates that there is a relaxation of these major features. There is also an indication of an extension of the subtropical gyre east of the Grand Bank toward the northeast in GFDL-ESM2M (as observed), but not in CanESM2 where the subpolar gyre extends eastward in this region. The latter has some similarity to the excessive eastward extension of relatively cold and fresh subpolar water in this region in CanESM2 that is seen in Figures 5-1 and 6-1.

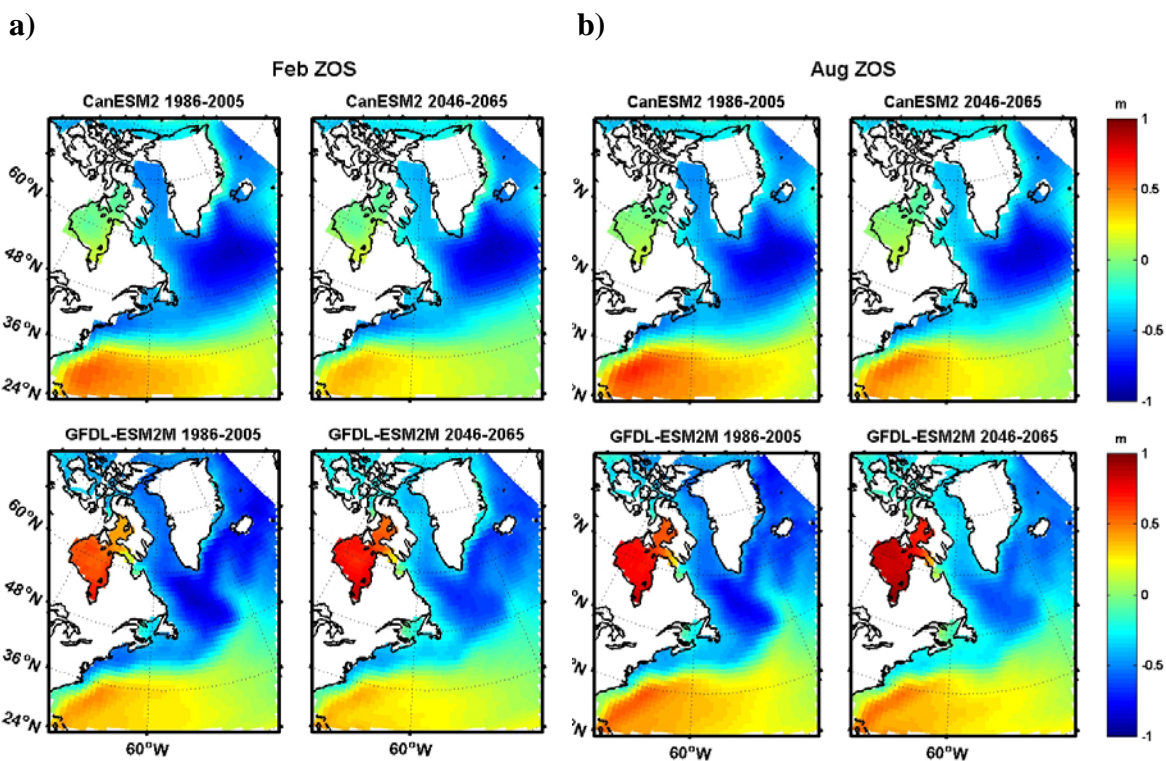


**Figure F-1:** Bi-decadal monthly mean zos in the NWA from CanESM2 (top row) and GFDL-ESM2M (bottom row) for 1986-2005 from their Historical simulations and 2046-2065 from their RCP8.5 simulations for a) February and b) August.

Figure F-2 shows the projected changes in bi-decadal zos in each model and season. Distinct differences between the models are apparent, along the lines discussed in Section 9 for adjusted zos. In both models there are indications of a northward shift or broadening of the Gulf Stream west of the Grand Bank, but the interpretation of the changes in terms of circulation features is less clear north and east of the Grand Bank.

In both models, the reduced eastward extension of the subtropical dome (related to the Gulf Stream) and the reduced equatorward extent of the subpolar depression (related to the Labrador Current) are apparent in the bi-decadal mean zos patterns (Figure F-1). However, there are major differences in the climate change patterns between the models. In GFDL-ESM2M, the mid-latitude band of reduced zos turns northward east of the GB, while the zone of increased zos in the subpolar NWA extends southward through the Labrador Basin and around the GB to Cape Hatteras. In contrast, there is a larger decrease of the subtropical dome south of 40°N in CanESM2, but it does not extend northward east of the GB; instead a zonal band of increased zos extends eastward over and beyond the GB. The latter's dynamical interpretation is unclear, with potential contributions from both the AMOC and upper-ocean gyres.

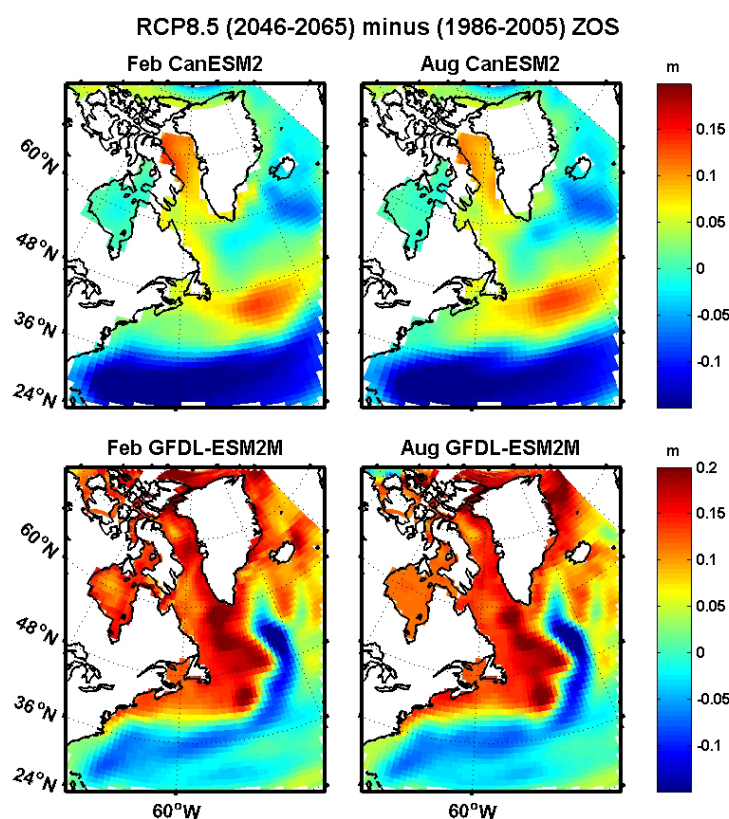


**Figure F-2** Climate changes in bi-decadal monthly zos in the NWA from CanESM2 (top row) and GFDL-ESM2M (bottom row) from Historical 1986-2005 to RCP8.5 2046-2065 simulation data, for February (left column) and August (right column).